



Technische Universität München

Fakultät für Medizin

Non-invasive in vivo monitoring of human T cells via  
immunoPET to evaluate response patterns of cancer  
immunotherapies

Dario Gosmann

Vollständiger Abdruck der von der Fakultät für Medizin der Technischen Universität München zur Erlangung des akademischen Grades eines Doktors der Naturwissenschaften (Dr.rer.nat.) genehmigten Dissertation.

Vorsitz: Prof. Dr. Percy A. Knolle

Prüfende der Dissertation: 1. Prof. Dr. Angela Krackhardt  
2. apl. Prof. Dr. Robert Oostendorp

Die Dissertation wurde am 09.08.2022 bei der Technischen Universität München eingereicht und durch die Fakultät für Medizin am 03.01.2023 angenommen.

## Table of contents

Table of contents .....	1
Preface .....	5
Summary.....	6
Zusammenfassung .....	7
<b>1 Introduction .....</b>	<b>8</b>
1.1 Cancer Immunotherapies .....	8
1.1.1 Vaccination therapy .....	9
1.1.2 Tumor-targeting monoclonal antibodies .....	11
1.1.3 Immune Checkpoint Inhibitors .....	12
1.1.4 Adoptive T-cell therapy .....	14
1.2 Conventional non-invasive imaging strategies and limitations .....	17
1.3 Non-invasive T-cell imaging .....	20
1.3.1 Indirect T-cell imaging via reporter genes .....	21
1.3.2 Ex vivo direct radiolabeling of T cells .....	22
1.3.3 ImmunoPET .....	23
1.4 Pan T-cell marker.....	28
1.4.1 CD2 .....	29
1.4.2 CD7 .....	30
<b>2 Aim of this study .....</b>	<b>32</b>
<b>3 Material .....</b>	<b>33</b>
3.1 Technical Equipment .....	33
3.2 Consumables .....	36
3.3 Reagents and chemicals .....	37
3.4 Kits.....	39
3.5 Buffer .....	40
3.6 Media .....	41
3.7 Cytokines .....	41
3.8 Antibodies .....	42
3.9 Vectors .....	43
3.10 CRISPR RNAs (crRNA).....	43
3.11 Primers .....	44

3.12 Cell lines and primary cells.....	45
3.13 Mouse model.....	46
3.14 Software .....	46
<b>4 Methods .....</b>	<b>47</b>
4.1 Cell culture methods .....	47
4.1.1 Freezing and thawing of cells	47
4.1.2 Counting of cells	47
4.1.3 Cultivation of cell lines	47
4.1.4 Cloning of cells by limited dilution	48
4.1.5 Isolation of PBMCs from whole peripheral blood	48
4.1.6 Purification of human CD8 <sup>+</sup> T cells	48
4.1.7 Activation of CD8 <sup>+</sup> T cells	49
4.2 Retroviral transduction.....	49
4.2.1 Production of virus particles for retroviral transduction	49
4.2.2 Transduction of CD8 <sup>+</sup> T cells and tumor cell lines	49
4.3 CRISPR/Cas9 knockout.....	50
4.3.1 Generation of the ribonucleoproteins (RNPs) complex for CRISPR/Cas9 knockout	50
4.3.2 Lipofection of target cells for CRISPR/Cas9 transfection	51
4.4 Flow cytometry analysis .....	52
4.4.1 Flow cytometry staining of surface markers	52
4.4.2 Flow cytometry staining CD2 and CD7 using sdAb	52
4.4.3 Evaluation of the dissociation constant of sdAbs	52
4.4.4 Thermal stability of sdAbs	52
4.5 Functional assessment of CD8 <sup>+</sup> T cells.....	53
4.5.1 Coincubation of CD8 <sup>+</sup> T cells and tumor cells	53
4.5.2 Cytokine secretion evaluation via ELISA	53
4.5.3 XCELLigence Assay	54
4.6 Recloning of sdAb genes from pMECS in pHEN6c vector.....	54
4.6.1 Plasmid isolation	54
4.6.2 PCR to amplify sdAb genes	55
4.6.3 Restriction digest	56
4.6.4 Gel electrophoresis and purification	56
4.6.5 Ligation of sdAb genes and pHEN6c vector	57
4.6.6 Transformation of chemically competent E. coli	57
4.6.7 Generation of electrocompetent E. coli WK6	58
4.6.8 Transformation of electrocompetent E. coli	58
4.7 Production and purification of sdAbs .....	59
4.7.1 Production of sdAbs in bacterial culture	59

4.7.2 His-Tag purification	59
4.7.3 SDS-PAGE	60
4.7.4 Concentration and buffer exchange	60
4.8 In vivo experiments.....	60
4.8.1 ML2 tumor model in NSG mice	61
4.8.2 Adoptive T-cell transfer	61
4.8.3 PET/MRI Imaging	61
4.9 Ex vivo analyses.....	62
4.9.1 Biodistribution	62
4.9.2 Flow cytometry analysis of murine tissue	62
4.10 Statistical analysis .....	62
<b>3 Results .....</b>	<b>63</b>
3.1 Production and purification of CD2- and CD7-sdAb .....	63
3.1.1 Recloning of sdAb genes to pHEN6 vector and transformation in <i>E.coli</i> WK6 strain	64
3.1.2 Determination of purity and mass of generated CD2- and CD7-sdAb	64
3.2 Binding characteristics of CD2- and CD7-sdAb.....	66
3.2.1 Binding of CD2- and CD7-sdAb on human CD8 <sup>+</sup> T cells	66
3.2.2 Specific binding on target-antigen transduced tumor cell line U698M	68
3.2.3 Specific binding on T cell leukemia cell line Jurkat E6.1 after CRISPR/Cas9 knockout of CD2 and CD7 respectively	70
3.2.4 Dissociation constant and binding affinity of CD2- and CD7-sdAb	74
3.2.5 Evaluation of thermal stability of CD2- and CD7-sdAb	75
3.3 Impact of CD2- and CD7-sdAb binding on CD8 <sup>+</sup> T cells in vitro .....	77
3.3.1 Effects of CD2- and CD7-sdAb binding on the dynamic cytotoxic activity of CD8 <sup>+</sup> T cells in vitro	77
3.3.2 Effects of CD2- and CD7-sdAb on cytokine-production of CD8 <sup>+</sup> T cells in vitro	84
3.4 Impact of CD2- and CD7-sdAb binding on cytotoxicity of CD8 <sup>+</sup> T cells in vivo .....	87
3.4.1 Effect of CD2- and CD7-sdAb on cytotoxicity of TCR-transgenic CD8 <sup>+</sup> T cells in vivo	87
3.5 Using CD2- and CD7-sdAb to monitor tumor reactive TCR-transgenic CD8 <sup>+</sup> T cells in vivo .....	91
3.5.1 Intratumoral injections and PET/MRI-monitoring of CD8 <sup>+</sup> T cells in vivo	91
3.5.2 Evaluation of image-acquisition time point for PET/MRI imaging using CD2- and CD7-sdAb	93
3.5.3 Monitoring of intravenously injected human CD8 <sup>+</sup> T cells at the tumor site using <sup>68</sup> Ga-NOTA-CD2- and <sup>68</sup> Ga-NOTA-CD7-sdAb	96

4	Discussion .....	101
4.1	Evaluation of CD2 and CD7 as target antigens for immunoPET imaging .....	101
4.1.1	CD2 .....	102
4.1.2	CD7 .....	103
4.2	Specific binding site of CD2-sdAb and implications.....	103
4.3	Impact of CD2- and CD7-sdAb binding on T-cell functionality .....	105
4.4	Tracer-characteristics of CD2- and CD7-sdAb.....	107
4.4.1	Target-antigen specificity .....	107
4.4.2	Binding affinity .....	108
4.4.3	Thermal stability .....	110
4.5	Suitability of sdAb for immunoPET imaging .....	110
4.6	CD2- and CD7-sdAb as immunoPET imaging tracers .....	113
5	Conclusion and outlook.....	115
6	References .....	117
7	Appendix .....	144
7.1	List of figures .....	144
7.2	List of tables.....	146
7.3	Abbreviations .....	147
8	Danksagung .....	151

## Preface

Parts of this dissertation are based on joint work together with the doctoral candidates Theresa Käsbauer (TK) and Sandro Bissenberger (SB), who have been partly supervised by the author of this dissertation.

## Summary

Due to the ever-increasing advancement of novel immunotherapeutic approaches such as immune checkpoint modulation, CAR-T cell therapy and adoptive T-cell transfer, reliable and universally applicable surrogate markers to monitor and assess the wide variety of immunotherapeutic responses are still missing. This lack of in-depth insight can result in delayed assessment of non-responders or the misinterpretation of tumor pseudoprogression, which consequently can lead to premature termination of appropriate treatment and initiation of alternative, possibly more harmful alternatives. Therefore, a non-invasive imaging method to screen and validate a patient's immune response, irrespective of the used immunotherapeutic approach, is essential and indispensable to improve patient outcome.

To address this problem, two single-domain antibodies (sdAbs) were developed, targeting the pan T-cell markers CD2 and CD7 respectively. Preclinical experiments demonstrated ideal properties in terms of binding affinity, thermostability and specificity for CD2- and CD7-sdAb. Binding specificity was illustrated by transduction of the CD2- and CD7-negative B cell lymphoma tumor cell line U698M with both target antigens respectively and knockout of each target antigen on the naturally CD2- and CD7 positive T cell leukemia cell line Jurkat E6.1.

Furthermore, binding of CD2- and CD7-sdAb to human CD8<sup>+</sup> T cells did not result in altered cytokine secretion, nor did it impair T-cell functionality in vitro. In addition, utilizing a xenogenic myeloid sarcoma mouse model, the cytotoxic ability of transferred TCR-transduced human CD8<sup>+</sup> T cells was not compromised upon intravenous (i.v.) application of CD2- and CD7-sdAb.

Ultimately, using the same xenograft mouse model, intravenously injected <sup>68</sup>Ga-NOTA-CD2-sdAb and <sup>68</sup>Ga-NOTA-CD7-sdAb were able to clearly depict and visualize previously administered TCR-transduced CD8<sup>+</sup> T cells at the tumor site by positron emission tomography/magnetic resonance imaging (PET/MRI) imaging.

Application of the developed constructs, CD2- and CD7-sdAb, enables direct non-invasive monitoring and visualization of both endogenously stimulated as well as genetically modified T cells in the context of any form of immunotherapy. The comprehensive preclinical analysis of CD2-sdAb and CD7-sdAb as well as their advantageous properties compared to currently used assessment methods for immunotherapies makes both tracers especially attractive for clinical translation.

## Zusammenfassung

Aufgrund der immer weiter fortschreitenden Entwicklung neuartiger immuntherapeutischer Ansätze wie der Immun-Checkpoint-Modulation und der CAR-T-Zelltherapie, fehlt eine zuverlässige und universell einsetzbare Methode zur Überwachung und Evaluation der vielfältigen Immunantworten im Kontext der Immuntherapien. Dieser Mangel an Informationen kann zu einer verzögerten Beurteilung von Non-Respondern oder zur Fehlinterpretation von Pseudoprogression des Tumors führen, was in der Folge zu einem vorzeitigen Abbruch einer geeigneten Behandlung und der Einleitung alternativer, möglicherweise schädlicherer Therapien führen kann. Daher ist ein nicht-invasives bildgebendes Verfahren zum Screening und zur Validierung der Immunantwort eines Patienten, unabhängig vom immuntherapeutischen Ansatz, essentiell.

Um dieses Problem zu lösen, wurden zwei Single-Domain-Antikörper (sdAbs) entwickelt, die die Pan-T-Zell-Marker CD2 bzw. CD7 binden. In präklinischen Versuchen wurden ideale Eigenschaften beider Konstrukte hinsichtlich Bindungsaffinität, Thermostabilität und Spezifität nachgewiesen. Die Spezifität wurde durch Transduktion der negativen B-Zell-Lymphom-Tumorzelllinie U698M mit beiden Zielantigenen und durch Knockout der Zielantigenen auf der ursprünglich CD2- und CD7-positiven T-Zell-Leukämiezelllinie Jurkat E6.1 nachgewiesen. Darüber hinaus führte die Bindung von CD2- und CD7-sdAb an menschliche CD8<sup>+</sup> T-Zellen weder zu einer veränderten Zytokinsekretion noch zu einer Beeinträchtigung der T-Zell-Funktionalität *in vitro*. Darüber hinaus wurde in einem xenogenen myeloischen Sarkom-Mausmodell die zytotoxische Fähigkeit von transferierten TCR-transduzierten humanen CD8<sup>+</sup> T-Zellen nach intravenöser (i.v.) Applikation von CD2- und CD7-sdAb nicht beeinträchtigt. In demselben Mausmodell konnten intravenös injizierte <sup>68</sup>Ga-NOTA-CD2-sdAb und <sup>68</sup>Ga-NOTA-CD7-sdAb die zuvor verabreichten TCR-transduzierten CD8<sup>+</sup> T-Zellen an der Tumorstelle mittels Positronen-Emissions-Tomographie/Magnetresonanztomographie (PET/MRT) deutlich darstellen und sichtbar machen.

Die Anwendung von CD2- und CD7-sdAb ermöglicht die direkte, nicht-invasive Überwachung und Visualisierung von endogen stimulierten als auch von genetisch veränderten T-Zellen im Rahmen jeder Form von Immuntherapie. Die umfassende präklinische Analyse von CD2- und CD7-sdAb sowie ihre vorteilhaften Eigenschaften gegenüber derzeit verwendeten Bewertungsmethoden für Immuntherapien machen beide Tracer besonders attraktiv für die klinische Umsetzung.

# 1 Introduction

## 1.1 Cancer Immunotherapies

Cancer remains one of the leading causes of death worldwide, with an estimated 19.3 million new cases and 9.9 million cancer deaths in 2020 (Sung et al., 2021). While conventional therapies such as chemotherapy, surgery and radiotherapy have seen great success over the past years, these treatment options carry with them a variety of intrinsic limitations in regards to safety and efficiency (Dranitsaris et al., 2017; Poon et al., 2015; R. Sullivan et al., 2015). To overcome these restraints and provide more specific and effective cancer treatments, new treatment approaches such as a diversity of immunotherapies have been developed. Cancer immunotherapy can be defined as the sensitization of the body’s immune system, which leads to increased sensitivity and reduced side effects (Oldham, 2017). The idea to utilize the patient’s immune system to generate an anti-tumor effect dates back a century ago, when Busch (Busch, 1868) and Fehleisen (Fehleisen, 1882) first noticed an association between the immune status and cancer. Since then, various breakthrough immunotherapeutic strategies in cancer treatment have been developed and will be outlined with examples below.

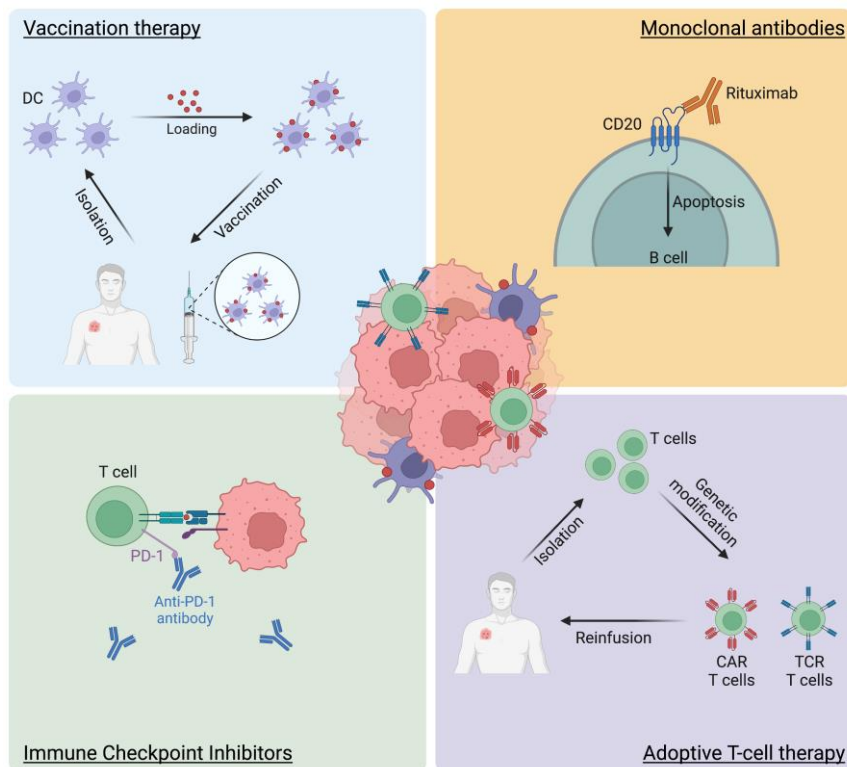


**Figure 1: Overview of immunotherapeutic approaches. (Created with BioRender.com)**

### 1.1.1 Vaccination therapy

Therapeutic cancer vaccination aims to utilize tumor-specific antigens to induce T-cell mediated tumor-reactive immune responses, resulting in tumor regression (Sahin & Tureci, 2018). Due to inherently different mechanism of achieving that goal, cancer vaccines can be separated into two platforms, namely cellular- or molecular (DNA, RNA, virus, peptide) vaccines (Pardi, Hogan, Porter, & Weissman, 2018).

Development of cellular vaccines is based on attaining tumor antigens either via autologous patient-derived tumor cells (Le, Pardoll, & Jaffee, 2010) or cells that are derived from an allogeneic tumor cell line (Harari, Graciotti, Bassani-Sternberg, & Kandalaft, 2020). In order to utilize tumor antigens to elicit anti-tumor immunity, these antigens are taken up and processed by antigen-presenting cells (APCs) (Banchereau & Steinman, 1998). Of the different cells that make up the APCs, dendritic cells (DCs) are best equipped to develop cellular cancer vaccines due to their ability to engulf, process and subsequently present the processed tumor antigens to induce an immune response from cytotoxic T lymphocytes (CTLs) (Harari et al., 2020). Cancer patients often suffer from malfunctioning DC maturation (Gabrilovich, Chen, et al., 1996), which can lead to defective antigen presentation and subsequent poor induction of T-cell responses (Gabrilovich, Ciernik, & Carbone, 1996).

To utilize DCs in terms of cancer vaccination, isolated DCs are ex vivo pulsed with either tumor antigens or tumor-cell lysates and stimulated with a specific cocktail to induce maturation (Mastelic-Gavillet, Balint, Boudousquie, Gannon, & Kandalaft, 2019). Currently, the only DC-based vaccination to receive FDA and EMA approval is Sipuleucel-T (Provenge, Dendreon Corporation), which is used to treat advanced prostate cancer (Kantoff et al., 2010). For this, the patients' monocytes were pulsed ex vivo by granulocyte macrophage colony-stimulating factor (GM-CSF) and prostatic acid phosphatase (PAP), resulting in the detection of tumor-specific CD8<sup>+</sup> T cells as soon as seven days after DC-infusion (Butterfield et al., 2003). However, even though Sipuleucel-T showed promise in preclinical efficacy and safety, widespread adoption and clinical use remain limited (Rinde, 2019), reflecting insufficient clinical efficacy (Small et al., 2006) as well as the disadvantageous work- and cost-intensive preparation of the therapy (Sharma, Wagner, Wolchok, & Allison, 2011). Nonetheless, various other vaccines derived from ex vivo DCs are currently investigated in clinical studies, such as a vaccine that uses yeast cell wall particles (YCWP) to load autologous DCs with autologous tumor lysate in order to treat melanoma and solid tumors (Chick et al., 2020; Herbert et al., 2018; Hickerson et al., 2019). The YCWP based vaccine prolonged disease-free survival of

resected melanoma patients compared to unloaded controls (Chick et al., 2020). Overall, the overarching disadvantages of these approaches, such as the unfavorable cost-benefit ratio and the intricacy in obtaining suitable patient-derived tumor cells, limit their feasibility and versatility.

As part of the molecular vaccines, peptide-based vaccines are generally based on epitopes derived from either tumor-associated or tumor-specific antigens (TSAs or TAA respectively) (Wagner, Mullins, & Linnebacher, 2018). While TAAs are proteins expressed by unmutated genes, they can be found on both healthy and cancer cells, but are significantly over-expressed on cancer cells (Zamora, Crawford, & Thomas, 2018). Since TAAs are part of the patients normal host proteome, they can be subject to central as well as peripheral tolerance mechanisms (Yarchoan, Johnson, Lutz, Laheru, & Jaffee, 2017) and can lead to autoimmune toxicity (Nagasaki et al., 2020). Vaccines against TAAs have been studied in clinical trials for cancer entities such as melanoma (Butts et al., 2014) or lung cancer (Vansteenkiste et al., 2013), but with dissatisfying results.

TSAs, or neoantigens, on the other hand are often based on somatic mutations and are therefore only expressed in tumor cells (Sahin & Tureci, 2018). Because of this, neoantigens are unaffected by tolerance mechanisms, may have higher major histocompatibility complex (MHC) affinity (Peng et al., 2019) and do not induce autoimmune toxicity (Nagasaki et al., 2020), making neoantigens ideal targets for therapeutic cancer vaccines. To identify neoantigens and subsequently characterize their potential as immunogenic targets, next-generation sequencing (NGS) is utilized in combination with algorithms for the prediction of MHC-binding epitopes (Jurtz et al., 2017; Peters, Nielsen, & Sette, 2020; Sarkizova et al., 2020).

Neoantigen-based cancer vaccines have seen numerous successful studies in clinical translation. For example, GEN-009 is a personalized solid-tumor cancer vaccine that consists of neoantigens which have previously been identified using the ATLAS epitope-discovery platform (Cohen et al., 2019; Long et al., 2014). GEN-009 is targeting neoantigens which were pre-confirmed to induce autologous T-cell responses *ex vivo*, thereby using epitopes that the patients' immune system is already primed for (Cohen et al., 2019). In a recently completed multi-center phase I/IIa study, safety as well as initial treatment results were positive (Cohen et al., 2019; Lopez et al., 2020), with patients all patients showing peripheral CD4<sup>+</sup> as well as CD8<sup>+</sup> T-cell responses against at least one of the used neoantigens. Furthermore, T-cell specific responses were sustained in numerous patients for more than twelve months post treatment (Cohen et al., 2019).

Taken together, cancer vaccines can provide a platform that is easily combined with existing therapies and greatly profit from technological advances, with overall minimal toxicities and several promising candidates currently in clinical trials.

### 1.1.2 Tumor-targeting monoclonal antibodies

The foundation of modern monoclonal-antibody therapies was laid by Kohler and Milstein in 1975, when they first described the use of hybridoma technology to produce monoclonal antibodies (mAb), which were able to bind to a single epitope (Kohler & Milstein, 1975). To date, more than 100 mAb have been approved by the US Food and Drug Administration (FDA) for a variety of diseases such as asthma (Padilla-Galo et al., 2021), Alzheimer's disease (Cummings et al., 2021) and most prominently, cancer (Mullard, 2021). In cancer immunotherapy, mAbs are able to bind tumor surface antigens and subsequently induce cytotoxicity through various modes of action, such as inhibiting key signaling pathway (Weiner et al., 2008), antibody-dependent cellular cytotoxicity (ADCC) (Hubert & Amigorena, 2012; Weiner, Surana, & Wang, 2010), complement-dependent cytotoxicity (CDC) (Di Gaetano et al., 2003) and/or antibody-dependent cellular phagocytosis (ADCP) (Weiskopf et al., 2013).

One prominent example of a mAb that acts both via induced CDC and ADCC is the chimeric mouse-human mAb rituximab (Golay et al., 2000). Rituximab targets the B-cell lineage marker CD20, which is expressed on 95 % of both normal and malignant B cells, but is lost following its differentiation into plasma cells (Nadler et al., 1984; Stashenko, Nadler, Hardy, & Schlossman, 1980). Rituximab was the first FDA-approved mAb for the treatment of non-Hodgkin lymphoma (S. D. Scott, 1998) and has since then also been part of the standard of care for treatment of chronic lymphocytic leukemia (CLL) and Non-Hodgkin lymphoma (NHL) (Brown et al., 2018).

While mAb-therapy using rituximab utilizes its effects regarding CDC and ADCC, antibodies targeting oncogenes from the group of human epidermal growth factor receptor 2 (HER2) act by directly impairing the ability of HER2-positive cells to proliferate by blocking downstream PI3K signaling (Capelan et al., 2013; Junttila et al., 2009). HER2 is an ideal target for mAb therapy, since it overexpressed in various cancers, primarily in ovarian- and breast carcinomas (Schechter et al., 1984; Slamon et al., 1989) and is associated with adverse survival outcome (Slamon et al., 1987). While the previously described mAb against HER2 and CD20 have seen great success due to their direct effect on anti-tumor activity, these targets are the exception rather than the norm.

However, because of the specificity and safety of mAb (Kimby, 2005), they serve as ideal candidates to directly deliver cytotoxic components to the tumor site. Therefore, the anti-tumor efficacy of an mAb can be highly improved by linking a cytotoxic small molecule to the mAb, resulting in an antibody-drug conjugate (ADC) (Chau, Steeg, & Figg, 2019).

ADCs are comprised of three distinct components, a mAb that is specifically binding to a cancer-antigen while not impacting healthy cells (A. M. Scott, Wolchok, & Old, 2012), a cytotoxic small-molecule agent to induce cell death after internalization (Chari et al., 1992) and a linker to control the release of the ADC (Ducry & Stump, 2010). Beyond small-molecule drugs, mAbs can also be conjugated to oligonucleotides (Mullard, 2022a), protein toxins (Rogers et al., 2021) or radionuclides (Steiner & Neri, 2011). As of this writing, a total of ten ADCs have been approved by the FDA (Mullard, 2021) and more than 100 candidate-ADCs are currently investigated in clinical trials (Z. Fu, Li, Han, Shi, & Zhang, 2022).

One example of an FDA-approved ADCs is Sacituzumab govitecan (SG), which received FDA-approval in April 2021 as a treatment for adults suffering from metastatic triple-negative breast cancer (mTNBC) and who had undergone two prior systematic therapies (Carey et al., 2022). SG is composed of a humanized IgG1 mAb targeting Trop-2, a transmembrane glycoprotein that is overexpressed in various cancers, including TNBC (Stepan et al., 2011; J. Wang, Day, Dong, Weintraub, & Michel, 2008), a hydrolysable linker (CL2A) and its cytotoxic payload, SN-38, a topoisomerase I inhibitor (Cardillo et al., 2015). The effectiveness of SG was evaluated in a pivotal phase III ASCENT study (NCT02574455), which showed an increase in both progression-free and overall survival in mTNBC patients treated with SG compared to a single-agent chemotherapy (Bardia et al., 2021). Even despite their recent success, ADCs are not without specific drawbacks. One major challenge for ADCs is their potential for off-target toxicity (Polakis, 2016), which is caused by premature release of the cytotoxic payload into the blood circulation, leading to systematic exposure (Drago, Modi, & Chandarlapaty, 2021; Rossin et al., 2018).

While mAbs are widely used for ADCs, they are also part of another aspect of immunotherapy, namely immune checkpoint inhibitors (ICIs).

### 1.1.3 Immune Checkpoint Inhibitors

The expectation and concomitant promise of the discovery of ICIs has been the reason why *Science Magazine* named immunotherapy as the Breakthrough of the Year 2013 (Couzin-Frankel, 2013). The namesake for ICI-therapies are immune checkpoints, which are molecules

belonging to the coinhibitory signaling pathways, thereby effectively regulating the immune system (Pardoll, 2012). However, since immune checkpoints are useful in maintaining immune tolerance, cancer cells are often utilizing and exploiting this trait to evade the patients' own immunosurveillance (Chen & Flies, 2013). Therefore, the purpose of ICIs is to inhibit the targeted coinhibitory signaling pathways, thereby facilitating immune-mediated elimination of cancer cells and reinstating the patients' antitumor response (Sharma & Allison, 2015).

The first immune checkpoint molecule to be discovered in 1987 was the cytotoxic T-lymphocyte antigen number 4 (CTLA-4) (Brunet et al., 1987), whose function and potential as an immune checkpoint molecule was described in 1995 (Krummel & Allison, 1995; Leach, Krummel, & Allison, 1996). CTLA-4 then became the target molecule for ipilimumab, the first mAb to receive FDA approval in 2011 for the treatment of advanced melanoma (Ledford, 2011). By binding and inhibiting CTLA-4, ipilimumab promotes enhanced T-cell activation, induces durable antitumor responses and ultimately conferred a short-term survival improvement of 3.6 months (Hodi et al., 2010). Furthermore, long-term survival analysis showed that 22 % of patients treated with ipilimumab gained an additional 3 years or more of life (Schadendorf et al., 2015) and over 20 % of patients enrolled in the initial clinical trials are still alive as of today (Oiseth & Aziz, 2017). As of today, ipilimumab is part of an established immunotherapeutic treatment for patients suffering from advanced melanoma (Spain, Larkin, & Turajlic, 2020), renal cell carcinoma (RCC) and non-small cell lung cancer (NSCLC) where it is used in combination with nivolumab, an ICI targeting PD-1, resulting in improved patient-outcomes compared to each treatment individually (Hellmann et al., 2018; Larkin et al., 2015; Motzer et al., 2018).

PD-1 is an immune checkpoint molecule on the surface of T cells (Ishida, Agata, Shibahara, & Honjo, 1992), with a similar function compared to CTLA-4, in that it restrains continuous activation of the immune system through negative regulation (Agata et al., 1996; Nishimura, Nose, Hiai, Minato, & Honjo, 1999) in conjunction with its ligand, PD-L1 (Dong, Zhu, Tamada, & Chen, 1999). However, tumor cells can express and upregulate PD-L1, thereby induce T-cell overactivation (Wherry & Kurachi, 2015) and escape the PD-1 regulated immune response (Iwai et al., 2002). Conversely, inhibition of both PD-1 and PD-L1 inhibition can result in reinstated cytotoxicity of T cells and subsequent tumor regression (Hirano et al., 2005), indicating that both molecules can serve as targets for mAb in ICI-therapy. As a result, the humanized PD-1 targeting mAb nivolumab was approved by the FDA in 2014 for the treatment of melanoma (Johnson, Peng, & Sosman, 2015) and the clinical use of nivolumab has since then been extended to various tumor entities such as Hodgkin lymphoma (Ansell et al., 2015),

renal cell carcinoma (Motzer et al., 2015) and head and neck squamous cell carcinoma (Ferris et al., 2016). Additionally, further PD-1 targeting mAb have seen clinical translation (Gandhi et al., 2018) as well as therapeutic mAb targeting the PD-1 ligand PD-L1, such as atezolizumab (J. E. Rosenberg et al., 2016).

Besides PD-1, PD-L1 and CTLA-4, various other newly discovered T-cell activation regulators are currently being investigated for their potential as novel immune-checkpoint targets (Burugu, Dancsok, & Nielsen, 2018), such as the lymphocyte activation gene 3 (LAG3) (Maruhashi, Sugiura, Okazaki, & Okazaki, 2020) which received FDA approval for the treatment of untreated advanced melanoma in 2022 (Tawbi et al., 2022) and T cell immunoglobulin 3 (TIM-3) (Friedlaender, Addeo, & Banna, 2019). As a member of the TIM family of genes, TIM-3 was originally described as a cell surface marker of CD4<sup>+</sup> T helper- and CD8<sup>+</sup> cytotoxic T cells (Monney et al., 2002). Since then, it has been discovered as a receptor on effector T cells, regulatory T cells, B cells, NK cells, DCs and macrophages (Y. He et al., 2018), and high levels of TIM-3 expression have been correlated with poor prognosis in tumor entities such as prostate- and colon cancer (Das, Zhu, & Kuchroo, 2017). Currently, more than ten TIM-3 targeting mAb-candidates are being investigated in the context of clinical trials (Tian & Li, 2021), mostly in combination with mAbs against PD-1 (Wolf, Anderson, & Kuchroo, 2020). One of the currently active trials is using a TIM-3 targeted mAb (sabatolimab) with and without conjunction of spartalizumab, a PD-1 inhibitor for advanced solid tumors (NCT02608268). Of the patients receiving combination therapy, ORR was at 5 %, DCR at 44 % and in four patients the combination therapy resulted in partial response (PR) (Curigliano et al., 2019). Preliminary results of this study indicate that TIM-3 targeted immune-checkpoint therapy may be a beneficial adjunct therapy to PD-1 (Marin-Acevedo, Kimbrough, & Lou, 2021).

Even though the discovery and clinical use of ICIs have been a revolutionary advance in immunotherapy, the overall response rates are still insufficient and, especially for cancers with low mutational burden (X. He & Xu, 2020).

#### 1.1.4 Adoptive T-cell therapy

As previously mentioned, the development of ICIs were one of the reasons why *Science Magazine* termed immunotherapy as the Breakthrough of the Year 2013 (Couzin-Frankel, 2013), the other being the development of patient-derived chimeric antigen receptor (CAR) T cells. At their core, CAR T cells are lymphocytes that are genetically modified with a synthetic receptor to specifically target tumor antigens (Imai et al., 2004). They are comprised of four

main elements: an extracellular domain to bind the target-antigen, a spacer, a transmembrane domain and intracellular signaling domains (Jayaraman et al., 2020). So-called first-generation CAR T cells were dependent solely on one intracellular domain, the CD3-zeta-chain, to provide T cells with an activation signal and stimulate TCR-signaling (Kuwana et al., 1987). However, this design proved to be ineffective as no sufficient T-cell responses were generated and the durability of these CAR T cells was persistent in vitro (Brocker & Karjalainen, 1995). This was confirmed by initial clinical studies that showed only limited T-cell proliferation and cytokine production, resulting in limited efficacy of the treatment (Brocker, 2000; Till et al., 2008). Therefore, following generations of CAR T cells were designed to rely on multiple intracellular signaling-domains such as CD28 (Maher, Brentjens, Gunset, Riviere, & Sadelain, 2002), CD40 (Kuhn et al., 2019) or 4-1BB (CD137) (Finney, Akbar, & Lawson, 2004).

As a result of continuous improvements in engineering, CD-19 targeting CAR T cells have seen great success in the treatment of chronic lymphocytic leukemia (CLL) (Porter, Levine, Kalos, Bagg, & June, 2011) and B-cell acute lymphoblastic leukemia (B-ALL), where all treated patients achieved complete remission (Brentjens et al., 2013), leading to FDA approval of the first CAR T cell therapy for the treatment of acute lymphoblastic leukemia (ALL) in children and young adults in 2017 (Mullard, 2017). Part of the clinical success in treatment of various B-cell malignancies is the CD19 target antigen, since it is uniformly expressed by the vast majority of B-cell malignancies (Nadler et al., 1983) and limited to the B-cell lineage (Uckun et al., 1988).

For the treatment of solid tumors however, CAR T cells face a variety of specific challenges such as high efficient trafficking to and subsequent infiltration of tumor tissue (Rafiq, Hackett, & Brentjens, 2020), a highly immunosuppressive tumor microenvironment (TME) (Nagarsheth, Wicha, & Zou, 2017) and crucially, antigen escape (Gardner et al., 2016; Jacoby et al., 2016; Sotillo et al., 2015). Antigen escape describes a mechanism by which the tumor either completely or partially loses or downregulates the target antigen (Singh et al., 2020) via selection of antigen-negative cells (Grupp et al., 2013) or the use of lineage switches (Gardner et al., 2016; Jacoby et al., 2016). While clinical trials using CD19-CAR T-cell treatment also suffered from relapse of CD19-negative tumors in more than 20 % of initial responders (Curran et al., 2015), the issue of antigen escape is even more substantial in solid tumors due to their more prominent antigen heterogeneity (Alexandrov et al., 2013; Rafiq et al., 2020). To overcome this aspect and allow for a more sustained approach to target solid tumors, recent advantages have been made in engineering bispecific CAR T-cells with specificities for multiple target antigens (Bailey & Maus, 2019). An indication on the possible effectiveness of

such an approach was seen in a successful clinical study where patients were sequentially treated with different CAR T-cells, each targeting a different antigen (Pan et al., 2019). Bispecific CAR T-cell treatment in a multiple myeloma mouse model, where the CAR was bispecific for the B-cell maturation antigen (BCMA) and SLAM family member 7 (SLAMF7), was able to overcome antigen escape and show a robust and continuous tumor-control (Zah et al., 2020). Further engineering to minimize the impact of antigen escape while simultaneously decreasing the chance for enhanced on-target, off-tumor toxicity is needed to translate the success of CAR T-cell therapy from lymphomas and leukemias to solid tumors (Hou, Chen, & Chen, 2021).

While CAR T-cell therapy relies on naturally occurring antigens on the surface of tumor cells to be effective (Jackson, Rafiq, & Brentjens, 2016), T-cell receptor (TCR) engineered T-cell therapy is reliant on the interaction between TCR and antigen presentation via the MHC complex (Xu et al., 2018; Zinkernagel & Doherty, 1974). This allows TCR therapy to target not just surface-expressed antigens, but also recognize intracellular antigens presented by MHC molecules (Harris & Kranz, 2016), which constitute 85 % of whole cell protein population and therefore allows for greater application potential (Weekes et al., 2010).

Yet, TCR therapy also faces unique challenges due to its very specific but restrictive nature, with one of these challenges being the optimization of TCR-affinity (Labrecque et al., 2001; Thaxton & Li, 2014). TCR-affinity directly correlates with T-cell avidity (Derby, Alexander-Miller, Tse, & Berzofsky, 2001) and therefore also with its function (Tan et al., 2015; Zeh, Perry-Lalley, Dudley, Rosenberg, & Yang, 1999). The importance of TCR-affinity is also evidenced by the preclinical analysis of tebentafusp, an immune-mobilizing monoclonal TCRs against cancer (ImmTAC) targeting glycoprotein 100 (gp100), and the first FDA-approved TCR-therapeutic (Urquhart, 2022). Utilizing seven TCRs against gp100, with various affinities spanning the physiological range, it was shown that in vitro and in vivo lysis of tumor cells plateaued at 10  $\mu$ M and any higher affinities did not result in increased anti-tumor activity (Zhong et al., 2013).

These results contributed to further development of tebentafusp until it was successfully tested in an open-label phase I/II trial (Middleton et al., 2020). Tebentafusp is a bispecific construct comprised of a TCR arm against gp100 and a single-chain variable fragment (scFv) targeted against CD3, to recruit CD3-positive cells (Damato, Dukes, Goodall, & Carvajal, 2019). In an open-label, randomized phase III clinical trial, 378 patients suffering from HLA-A\*02:01-positive uveal melanoma were assigned either tebentafusp treatment or, as a control, the investigator's choice of either the PD1-inhibiting pembrolizumab, CTLA4-inhibiting

ipilimumab or the chemotherapy dacarbazine (Nathan et al., 2021). Patients treated with tebentafusp achieved an overall survival (OS) of 21.7 months compared to 16 months in the control group, similarly, tebentafusp-treated patients experienced longer progression-free survival (PFS) with 3.3 months compared to 2.9 months in the control group. Taken together, the 1-year OS in the tebentafusp-treated group was 73 % and 59 % in the control arm of the study (Nathan et al., 2021). Based on the success of this study, tebentafusp was approved as the first TCR-based therapy for the treatment of HLA-A\*02:01-positive uveal melanoma. (Mullard, 2022b).

With the ever-increasing progress and development of previously discussed immunotherapeutic approaches such as cancer vaccines, immune checkpoint inhibitors, CAR-T cell therapy and TCR T-cell therapy, reliable and specific techniques to monitor and evaluate the wide variety of therapeutic responses are still missing, immunotherapies need to be evaluated and there are several approaches to characterize and visualize therapeutic outcomes, more specifically to monitor the key components of immune responses, T cells.

## 1.2 Conventional non-invasive imaging strategies and limitations

Cancer immunotherapies have changed the way various solid and hematologic malignancies can be treated. Particularly immune checkpoint blockage (ICB) targeting PD-1/PD-L1 (Sezer et al., 2021) and CTLA-4 (Cascone et al., 2021) as well as anti-CD19 CAR-T cells (Ying et al., 2019) have seen resounding success over the past years. However, while immunotherapies are highly specific in terms of their target structures and mechanism of action, both their

progression and response patterns differ widely from conventional anticancer treatments (Borcoman et al., 2019) and therefore require specific care to be correctly evaluated.

One of the most challenging problems relating to immunotherapy assessment is the differentiation between progression and so called pseudoprogression (Aide et al., 2019). Pseudoprogression describes an increase in size of the primary tumor, tumor-lesions or the appearance of new lesions, followed by a delayed tumor shrinkage (Reardon & Weller, 2018) and was first described in a phase II clinical trial of the previously discussed CTLA-4 mAb ipilimumab, where a patient suffering from advanced melanoma saw an initial increase of tumors lesions with subsequent, delayed partial response (Di Giacomo et al., 2009).

Since then, pseudoprogression has been described in various tumor entities, primarily in melanoma (Pires da Silva et al., 2020), but also tumor entities such as renal-cell carcinoma (Zhang et al., 2021), HNSCC (Haddad et al., 2019) and NSCLC (Ayati et al., 2021; Gettinger et al., 2015; Tazdait et al., 2018). Even though there are various studies on pseudoprogression and its incidence, there is no unifying consensus on all underlying molecular mechanisms (Nishino et al., 2017). However, the major mechanism of pseudoprogression and the seeming tumor-growth after immunotherapy is mainly attributed to a recruitment and an influx of immune cells such as CD8<sup>+</sup>- and CD4<sup>+</sup> T cells (Di Giacomo et al., 2009; Tanizaki et al., 2016). For example, one case report showed that a patient, who was suffering from non-small cell lung cancer (NSCLC) and was treated with nivolumab, underwent histological evaluation of a metastatic liver lesion to reveal that the fibrotic tissue contained no viable tumor cells but infiltrated lymphocytes positive for CD3, CD4 and CD8 (Tanizaki et al., 2016).

The significant risk that can result from failure to correctly identify pseudoprogression is the premature discontinuation of an otherwise effective treatment (Chiou & Burotto, 2015; Okada et al., 2015). Clinical ramifications of pseudoprogression are highlighted by the incidence in various cancer entities. For instance, reports showed an incidence rate for pseudoprogression of 10 – 15 % malignant melanoma (Hodi et al., 2016), 5 – 7 % in NSCLC (Borghaei et al., 2015) and 9 – 30 % in GBM (Thust, van den Bent, & Smits, 2018). The severity of pseudoprogression and the increase of immunotherapeutic treatments have led to the development of iRECIST, an updated version of the RECIST guidelines that includes specific categories for response assessment to immunotherapy (Seymour et al., 2017).

The development of new assessment guidelines has to be accompanied by advances in equally specific imaging techniques to correctly identify pseudoprogression in affected patients. Current medical imaging techniques such as computed tomography (CT), magnetic resonance imaging (MRI) and metabolic imaging such as 2-deoxy-2-[fluorine-18]fluoro-D-glucose (<sup>18</sup>F-

FDG) combined with positron emission tomography (PET) all suffer from drawbacks in terms of their inability to specifically distinguish true tumor-progression from pseudoprogression (Hegi-Johnson et al., 2022).

As anatomical imaging modalities, both CT and MRI imaging techniques are based on monitoring structural changes within the tumor (Reddy & Robinson, 2010) and therefore primarily rely on tumor-growth as a readout of therapeutic success (D. C. Sullivan, Schwartz, & Zhao, 2013). Hence, even though both techniques offer high spatial and temporal resolution and are routinely used for diagnosis and staging of tumors (Heusch et al., 2015; Spick, Herrmann, & Czernin, 2016), they are incapable of providing the specificity needed to assess unique immunotherapeutic response patterns, which was highlighted in a meta-analysis of pseudoprogression in GBM patients. Based on MRI assessment, true tumor-progression occurred in 2603 patients, however, subsequent histological confirmation or imaging follow-up revealed that 36 % of patients demonstrated falsely identified pseudoprogression (Abbasi et al., 2018).

$^{18}\text{F}$ -FDG -PET is based on the principle that the glucose-analogue FDG is combined with the radioisotope fluorine-18 ( $^{18}\text{F}$ ), which decays over time, thereby releasing positive charged positrons that can be detected using PET (Rege et al., 1994). While  $^{18}\text{F}$  is necessary for the visualization through PET, FDG is utilized and processed by highly glycolic cells such as brain cells, lymph nodes, kidneys and cancer cells (Niiranen et al., 2021). Therefore,  $^{18}\text{F}$ -FDG is widely used as a sensitive marker for changes in glucose metabolism and, since cancer cells consume large amounts of glucose due to increased glycolysis, to diagnose and monitor malignant tumors (Hess, Blomberg, Zhu, Hoiland-Carlsen, & Alavi, 2014). Yet there is a major disadvantage of  $^{18}\text{F}$ -FDG in the context of immunotherapies, namely that activated immune cells upregulate the expression of glucose transporters (GLUT) (Jones & Thompson, 2007), leading to an increase in glycolysis and a distinct  $^{18}\text{F}$ -FDG from immune cells (Aide et al., 2019; Laing, Nair-Gill, Witte, & Radu, 2010). Therefore, the pivotal role of glycolysis in both immune- and cancer cells can lead to misinterpretation of pseudoprogression, false evaluation of treatment responses and subsequent premature discontinuation of the given therapy (Sachpekidis et al., 2015; Tumei, Radu, & Ribas, 2008).

Taken together, the data strongly indicates that there is an urgent need for a novel imaging technique to screen and validate immune response during immunotherapy and ultimately is improving patient outcome. To circumvent the disadvantages that come with indirectly monitoring treatment-response based on tumor-growth or -metabolic activity, directly

visualizing the most significant immune cells involved in antitumor-immunity would be an ideal readout of treatment efficacy.

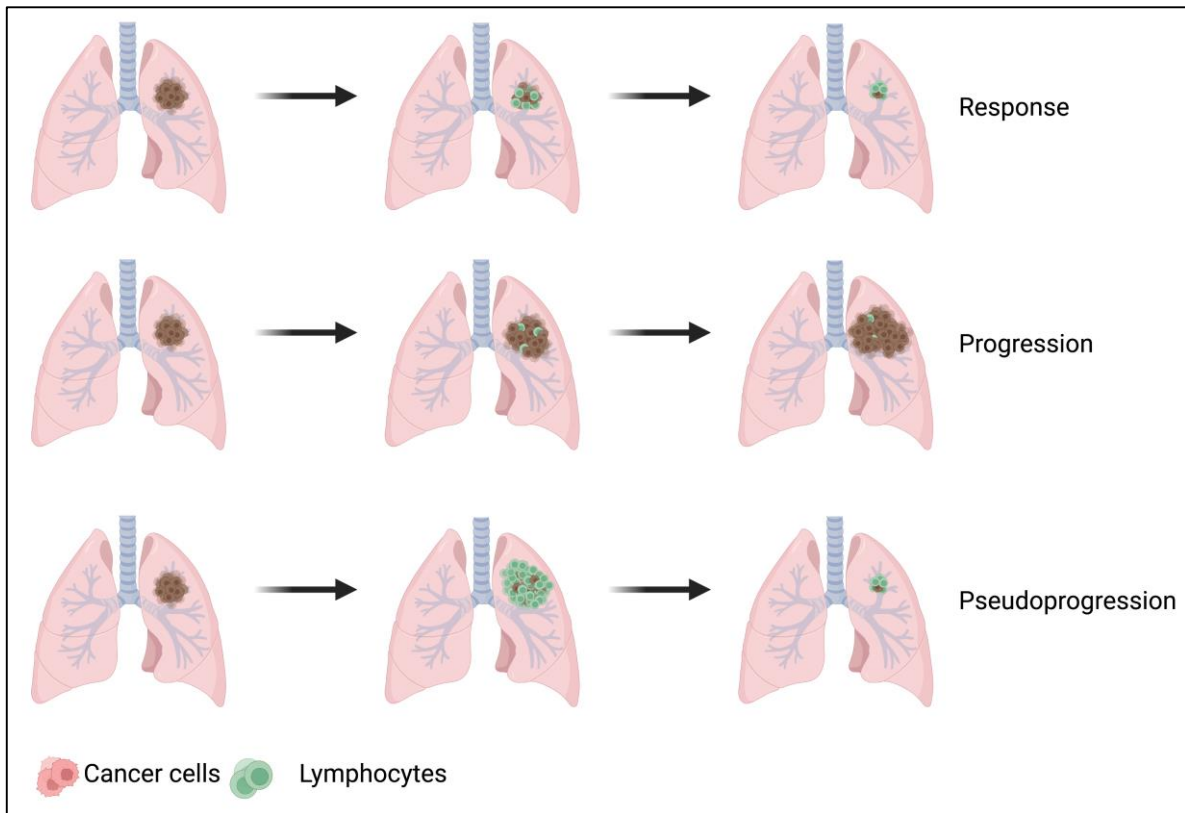


**Figure 2: Schematic overview of response-patterns for immunotherapies.**

**(Created with BioRender.com)**

### 1.3 Non-invasive T-cell imaging

As previously described, assessing treatment-responses based on changes in structure and size of monitored tumors proved to be insufficient in the context of immunotherapeutic approaches. Visualizing the key components of the immune-response themselves, however, would allow for a direct evaluation of the patients' specific immune-response. As the key components in immune checkpoint inhibition (Hui et al., 2017), cancer vaccines (Kreiter et al., 2015) and,

evidently, adoptive T-cell therapy (S. A. Rosenberg et al., 2011), T cells represent the ideal target-cell population in terms of immunotherapy-specificity.

On the one hand, T-cell monitoring would therefore facilitate a clear assessment of unique immunotherapy response patterns such as pseudoprogession (Krekorian et al., 2019), but it would also enable the use of T cells as surrogate markers in immunotherapy (Tumeh et al., 2014), which will be discussed later on. Visualization of T cells can be achieved in various ways; however, most approaches utilize PET as a non-invasive method to depict T cells in vivo. A selection of promising approaches will be outlined hereinafter.

### 1.3.1 Indirect T-cell imaging via reporter genes

Generally, there are two main approaches when it comes to T-cell imaging: direct and indirect labeling of T cells (Kircher, Gambhir, & Grimm, 2011). Indirect labeling is based on the principle that the targeted cells are genetically modified to express a reporter gene (Jefferson, Burgess, & Hirsh, 1986), which can code for either an enzyme, a transport protein or a cell surface protein (Ashmore-Harris, Iafrate, Saleem, & Fruhwirth, 2020). To image the cells and monitor them in vivo, the specific features of the reporter genes are utilized by administering a radiolabeled reporter probe (Tjuvajev et al., 2002). Depending on the type of reporter gene, these reporter probes will then specifically accumulate either on the surface (cell surface protein) or inside (enzyme & transport protein) the targeted cells and mark them for PET-detection (Yaghoubi, Campbell, Radu, & Czernin, 2012).

Since indirect imaging is dependent on the ex vivo gene-transfer of the suitable reporter gene into the desired cells (Gambhir et al., 1999), immunotherapeutic approaches such as CAR T-cell therapy and TCR therapy are well suited for reporter-gene imaging (Chung, Kang, & Kang, 2010). One example of a reporter gene that is used in synergy with an ICAM-1 targeting CAR T-cell therapy is the human somatostatin receptor subtype 2 (SSTR2). To ensure the visualization of CAR T cells specifically, SSTR2 was concurrently expressed with the CAR via the use of P2A (Vedvyas et al., 2019). In a preclinical gastric cancer NSG mouse model, PET/CT imaging of CAR T-cell treated mice showed a distinct PET signal and therefore accumulation of CAR T-cells at the subcutaneous tumor site compared to the control group (Yang et al., 2021). While SSTR2 was able to specifically visualize CAR T cells in a human immunocompromised mouse model, it also has inherent drawback due to its expression profile. Since SSTR2 is also endogenously expressed on a variety of tissues such as the kidneys and the gastrointestinal tract (Yamada et al., 1992), it is most importantly also expressed on immune

cells such as T cells, B cells and macrophages (Elliott et al., 1999). While there are major advantages and applications for imaging a wider array of the immune response, it is counterproductive when the goal is to only monitor one immune cell subtype or genetically modified cells, since major background activity is expected,

Another indirect-labeling approach to monitor T cells uses the herpes simplex virus type-1 thymidine kinase (HSV1-tk) as a reporter gene (Koehne et al., 2003). The benefit of this approach is that HSV1-tk is not endogenously expressed in healthy humans (Ashmore-Harris et al., 2020), thereby enabling a more specific monitoring of genetically modified T cells. After successful in vivo testing (Tjuvajev et al., 2002), HSV1-tk radiolabeled 9-[4-[<sup>18</sup>F]fluoro-3-(hydroxymethyl)butyl]guanine ([<sup>18</sup>F]FHBG has since been translated into the clinic to monitor CAR T cells in patients suffering from recurrent glioma (Keu et al., 2017) or to track ex vivo expanded cytolytic CD8<sup>+</sup> T cells in glioma patients (Yaghoubi et al., 2009). Both approaches proved to be simultaneously safe and effective in monitoring adoptively transferred T cells, and yet, reporter-gene based T-cell imaging has overarching limitations. The genetic modification of the target cells by a non-human protein, in addition to the insertion of CARs or TCRs, can increase the risk of immunogenicity (Li, Wang, Liu, & Lan, 2018). Furthermore, reporter genes can internalize upon ligand binding, leading to a decrease in sensitivity and signal intensity (Cescato et al., 2006).

### 1.3.2 Ex vivo direct radiolabeling of T cells

Another approach to be able to visualize the T cells of interest, instead of relying on the expression and functionality of reporter genes, is to directly label T cells with an appropriate radionuclide (Meidenbauer et al., 2003). Direct radiolabeling of cells is done ex vivo, coupling cells of interest to a radiation-emitting radionuclide, which should have no significant effect on cell functionality, viability and trafficking (Maxwell et al., 2008), with subsequent injection back into the subject (Lu et al., 2021).

While there are a number of radionuclides that have been successfully used in the generation of direct cell-labeling agents such as  $^{64}\text{Cu}$  (Gawne et al., 2018),  $^{99\text{m}}\text{Tc}$  (Demaimay et al., 1997) and  $^{111}\text{In}$  (Fisher et al., 1989),  $^{89}\text{Zr}$  has recently emerged as a promising radionuclide to trace T cells, because, due to its long half-life (78 h),  $^{89}\text{Zr}$  is well suited for longitudinal cell imaging applications (Holland, Sheh, & Lewis, 2009). However, the usage of long-lived radionuclides such as  $^{89}\text{Zr}$  comes with major drawbacks, which will be discussed later. As a tool for direct ex vivo radiolabeling of immune cells, [ $^{89}\text{Zr}$ ]oxinate<sub>4</sub> was first synthesized in 2015 (Charoenphun et al., 2015) and has since been utilized in long-term monitoring of NK cells (Sato et al., 2020),  $\gamma\delta$ -T cells (Man et al., 2019) and CAR T cells (Weist et al., 2018) in mice. As of this writing, one clinical trial to investigate the potential of [ $^{89}\text{Zr}$ ]oxinate<sub>4</sub> in immune-cell tracking is being investigated, where ex vivo labeled leukocytes are tracked in the context of neuroinflammation (NCT03807973).

While this approach has the major advantage that there is no need to genetically modify the T cells for imaging (Iafate & Fruhwirth, 2020), it has its own set of limitations. One such disadvantage is the fact that due to cell-division and proliferation, the radiolabeling agent will be diluted over time, leading to a decreased concentration of radionuclide per cell, resulting in strongly reduced sensitivity (Hong et al., 2020; S. H. Lee et al., 2020). Furthermore, direct radiolabeling does not enable a differentiation between radionuclide-signal coming from alive or dead cells, which can then also result in accumulation of the radionuclide in unwanted tissues, such as a strong signal in bone due to bone-seeking properties of leaked Zirconium-89 (Lechermann et al., 2020).

### 1.3.3 ImmunoPET

Even though both indirect reporter-gene labeling as well as direct T-cell labeling have specific advantages and fields of application, over the past decade, the importance of immuno-positron emission tomography (immunoPET) has drastically increased in association with immunotherapy (Ehlerding, England, McNeel, & Cai, 2016). ImmunoPET utilizes probes such as antibodies, antibody-fragments ( $\text{F}(\text{ab}')_2$ , scFv, sdAb) or engineered antibody-derived constructs (diabody, minibody) that are coupled to positron-emitting radionuclides, which are

then injected to bind and visualize their specific target antigen (Tavare et al., 2016). Due to its unique approach, immunoPET combines the high affinity and specificity of antibodies with the sensitivity of PET imaging. The potential and possible applications of immunoPET are therefore dependent on three main aspects, which need to complement each other: the probe, the radionuclide and the target antigen.

	mAb	Fab'(ab') <sub>2</sub>	Minibody	Fab	Cys-diabody	Single-domain antibody
<b>Molecular weight</b>	150kDa	110 kDa	75 kDa	55 kDa	50 kDa	13 kDa
<b>Serum half-life</b>	> 10 days	8 - 10 h	5 - 10 h	12 - 20 h	2 - 4 h	15 - 30 min
<b>Clearance route</b>	Hepatic	Hepatic	Hepatic	Renal	Renal	Renal
<b>Size</b>						Tissue penetration

**Figure 3: Key characteristics of antibody-based constructs with regards to immunoPET based imaging.**

(Created with BioRender.com)

Full-size mAb were the first constructs to be characterized and investigated in terms of their capability as immunoPET-probes (van Dongen, Visser, Lub-de Hooge, de Vries, & Perk, 2007). However, while the pharmacokinetics of mAb often provide the basis for excellent drugs (Ovacik & Lin, 2018), their long circulatory half-lives ( $t_{1/2}$  of days to weeks, depending on the mAb) necessitate the use of equally long-lived radionuclides for useful imaging and their circulation time becomes a liability (R. Fu, Carroll, Yahioğlu, Aboagye, & Miller, 2018). The use of such long-lived radionuclides leads to significant drawbacks in terms of clinical applicability and patient safety, because not only does it result in longer wait between tracer-injection and imaging, but it also increases the radiation exposure of key organs such as kidney, bone marrow and liver of patients (Phan et al., 2008). Furthermore, the relatively large molecular weight of a mAb (~150 kDa) also negatively affects its diffusion and tissue penetration (Thurber, Schmidt, & Wittrup, 2008), thereby further increasing time until image-acquisition and hindering image-quality.

Taken together, this highlights one of the key aspects in terms of tracer-engineering for immunoPET applications, namely that characteristics of probe and radionuclide are mutually

dependent on one another. Yet, full-size mAb have seen success in preclinical models. One example is a CD3-targeted mAb that was radiolabeled with  $^{89}\text{Zr}$  and used to monitor cytotoxic T-cell infiltration in a xenograft mouse model of colorectal cancer after CTLA-4 therapy (Larimer, Wehrenberg-Klee, Caraballo, & Mahmood, 2016). This approach showed a strong correlation between accumulation of the radiotracer, the number of T cells at the tumor site and an enhanced therapeutic response to CTLA-4 therapy. The study also showed tracer uptake in lymphoid organs such as spleen, thymus and lymph nodes, which was confirmed by a different group using a syngeneic bladder cancer model (Beckford Vera et al., 2018).

With a molecular weight of 110 kDa,  $\text{F(ab')}_2$  fragments, which can be generated via enzymatic digestion of full-size mAb (Mariani, Camagna, Tarditi, & Seccamani, 1991), are the largest antibody-fragments used in immunoPET. Due to their large size, however,  $\text{F(ab')}_2$  fragments prove no major advantage over full-size mAb and are restricted by the same limitations. Still,  $^{89}\text{Zr}$ -labeled  $\text{F(ab')}_2$ -based radiotracers targeting CD4 and CD8 respectively were developed to monitor T cells in a colon carcinoma syngeneic mouse model and quantitative region-of-interest (ROI) analysis of PET images showed tumor-to-heart ratios of  $8.9 \pm 0.5$  for both  $^{89}\text{Zr}$ -DFO-CD4 and  $9.25 \pm 0.98$  for  $^{89}\text{Zr}$ -DFO-CD8 (Kristensen et al., 2019). Importantly, application of both  $\text{F(ab')}_2$  fragments did not interfere with the simultaneous PD-1 targeted treatment in any impairing way.

In an effort to improve pharmacokinetic traits of immunoPET-probes, the engineered antibody fragments called bivalent cys-diabodies (cDb), with a molecular weight of approximately 50 kDa and a circulatory half-life of 2 – 4 hours, were adapted for tracer development (M Rashidian & Ploegh, 2020). Advantages due to the small size of cDbs compared to full-size mAbs and  $\text{F(ab')}_2$  fragments include a rapid renal clearance, leading to increased target-to-background ratios, the feasibility of utilizing shorter-lived radionuclides such as  $^{18}\text{F}$  ( $t_{1/2}$  110 min) or  $^{68}\text{Ga}$  ( $t_{1/2}$  68 min) and reduced time between injection and image-acquisition (Olafsen & Wu, 2010; A. M. Wu, 2014). However, even though cDb allow for radiolabeling with more favorable radionuclides, cDbs currently investigated for preclinical T-cell imaging have so far been radiolabeled with either  $^{89}\text{Zr}$  ( $t_{1/2}$  78.4 h) (Tavare et al., 2014) or  $^{64}\text{Cu}$  ( $t_{1/2}$  12.7 h) (Seo et al., 2018), thereby not fully utilizing the beneficial properties of the cDb-probe. Furthermore, one limitation that all protein scaffolds with a molecular weight above 40 kDa face, however, is an aspect termed enhanced permeability and retention (EPR), which can negatively impact tracer-binding and therefore result in false-positive results (D'Huyvetter, Xavier, et al., 2014; Fang, Nakamura, & Maeda, 2011).

An  $^{89}\text{Zr}$ -labeled anti-CD8 cDb was used in a syngeneic colon carcinoma mouse model to track CD8<sup>+</sup> T-cells after antigen-specific adoptive T-cell transfer or PD-L1 immunotherapy (Tavare et al., 2016). Acquired PET-signals based on  $^{89}\text{Zr}$ -CD8-cDb showed a clear differentiation between control tumors and antigen-specific tumors, with off-target accumulation of the tracer in the kidneys, due to the renal clearance of the cDb and in the bones, due to the bone-seeking properties of  $^{89}\text{Zr}$  (Abou, Ku, & Smith-Jones, 2011). Compared with a previously engineered  $^{64}\text{Cu}$ -radiolabeled anti-CD8 minibody (molecular weight ~ 80 kDa) of the same group, the cDb showed slower blood clearance and less aggregation, while also exhibiting a higher renal accumulation due to the lower molecular weight and the residual characteristics of the used radionuclide  $^{89}\text{Zr}$  (Tavare et al., 2014).

Nonetheless, the described minibody, called  $^{89}\text{Zr}$ -IAB22M2C, was used in a first-in-humans dose escalation phase clinical trial, where it was studied in six patients suffering from solid malignancies such as melanoma, small cell-or non-small cell lung cancer and hepatocellular carcinoma (Pandit-Taskar et al., 2020). The study was able to show the safety of  $^{89}\text{Zr}$ -IAB22M2C application, with no immediate or delayed side effects following the injection. Tracer uptake was observed mostly in the spleen, bone marrow and the liver, with a relatively low kidney-uptake. Importantly, while tracer-uptake was visible as early as two hours post injection in some tumor lesions, most  $^{89}\text{Zr}$ -IAB22M2C-positive lesions were not detectable until 24 hours post initial injection, which can be attributed to the size of the construct and the consequential drawbacks in terms of blood circulation and tissue penetration (Pandit-Taskar et al., 2020).

In an effort to overcome these limitations and use a construct for T-cell imaging that would allow fast tissue penetration and accelerated image-acquisition, single-domain antibodies (sdAb), alternatively also named nanobodies, were developed (Dumoulin et al., 2002). Derived from camelid heavy chain-only antibodies, sdAb are small antigen-binding fragments with molecular weight of around 15 kDa (Wesolowski et al., 2009). Compared to conventional mAbs and their recombinant fragments, sdAb come with a variety of beneficial characteristics. Because the type 3 VH domain (VH3) of sdAbs is highly homologous to human VH3, sdAbs exhibit very low immunogenicity and good biocompatibility (Steeland et al., 2015). Furthermore, due to their small size and high solubility, their capability for strong and fast tissue penetration is highly increased, allowing them to quickly enter dense tissues such as solid tumors (Zottel et al., 2020) and even cross the blood-brain barrier (Muruganandam, Tanha, Narang, & Stanimirovic, 2002).

Their small size also enables sdAbs to rapidly bind their target-antigen with a high degree of affinity (Mitchell & Colwell, 2018) and specificity (Hassanzadeh-Ghassabeh, Devoogdt, De Pauw, Vincke, & Muyldermans, 2013), while also allowing unbound sdAb to be quickly cleared via renal elimination (Xenaki et al., 2021). Lastly, sdAbs exhibit unique properties in terms of their antigen-binding site. While conventional mAbs and antibody fragments typically have a planar- or concave antigen-binding site (MacCallum, Martin, & Thornton, 1996), the complementarity determination region-3 (CDR3) of the sdAb is able to form loops (Desmyter, Decanniere, Muyldermans, & Wyns, 2001) that facilitate binding to otherwise inaccessible epitopes by conventional mAb-constructs, such as epitopes in protein clefts (Hu, Liu, & Muyldermans, 2017; Huen et al., 2019).

Taken together, this makes sdAbs promising candidates for immunoPET that would allow for highly specific antigen-binding and subsequent monitoring of T cells with high-tumor-to-background ratios already at one hour post injection (Chakravarty, Goel, & Cai, 2014). Due to all their favorable characteristics, sdAbs have extensively been studied in terms of their imaging-capabilities over the past years, also in the context of T-cell imaging.

One approach was using an  $^{89}\text{Zr}$ -radiolabeled PEGylated-sdAb to monitor the presence and infiltration of  $\text{CD8}^+$  T cells in a syngeneic melanoma mouse model after CTLA-4 immunotherapy (M. Rashidian et al., 2017). The CD8-sdAb was able to depict CD8-presence in thymus and secondary lymphoid structures as well as intratumoral  $\text{CD8}^+$  T cells at 24 hours post injection. Additionally, longitudinal PET-monitoring over the course of four CTLA-4 treatments, 9, 16, 23, and 30 days post tumor-inoculation, revealed that a response to CTLA-4 correlated with a distinctly homogenous distribution of  $^{89}\text{Zr}$ -CD8-sdAb signal compared to a more heterogeneous distribution of  $^{89}\text{Zr}$ -CD8-sdAb in non-responders (M. Rashidian et al., 2017).

These promising results were further solidified from the same group by additionally using breast cancer- and colorectal cancer models which showed comparable tracer-accumulation and distribution (M. Rashidian et al., 2019). All PET-images were acquired 24 hours post injection of the tracer, which allowed for a very specific signal of CD8-bound sdAb because at this point in time, most unbound tracer was already cleared via the kidneys. However, this was only possible due to  $^{89}\text{Zr}$ -radiolabelling and therefore encompassed the previously discussed disadvantageous aspects of  $^{89}\text{Zr}$ -radiolabelling for clinical translation.

Therefore, in a more recent study, anti-CD8 sdAbs were labeled using  $^{68}\text{Ga}$ , thereby utilizing the beneficial characteristics of sdAb in terms of eventual clinical translation (Zhao et al., 2021). Though in this study, the  $^{68}\text{Ga}$ -CD8-sdAb tracer was not used to monitor and track  $\text{CD8}^+$  T cells

in the context of immunotherapy, but to visualize murine colon cancer tumors MC38, which have been modified to express human CD8. Yet, this study showed that a  $^{68}\text{Ga}$ -radiolabelled immune-cell targeting sdAb was able to infiltrate tumor tissue and bind its target antigen in a timely manner that allowed image-acquisition only one hour post injection (Zhao et al., 2021). In summary, the development of sdAb has opened a new chapter in the aspect of monitoring immunotherapeutic responses using immunoPET and so far has not been utilized to its full potential.

#### 1.4 Pan T-cell marker

As previously described, CD8 has been a major focus of T-cell imaging over the past decade, with numerous different approaches to visualize  $\text{CD8}^+$  T cells in the context of immunotherapy. The reasoning behind the focus on  $\text{CD8}^+$  T cells is the well-described fact that tumor-infiltrating  $\text{CD8}^+$  T cells have been shown to predict patient survival and response to immunotherapy in a variety of tumor entities like colorectal cancer (Pages et al., 2005), melanoma (Azimi et al., 2012), TNBC (Savas et al., 2018) and other (Herbst et al., 2014).

However, by restricting T-cell monitoring to narrowly defined  $\text{CD8}^+$ -populations, the versatile aspect of T-cell responses during immunotherapy cannot be assessed to its full extent. For example, while it has long been known that  $\text{CD4}^+$  T cells are necessary in supporting the differentiation and effector function of  $\text{CD8}^+$  T cells (Keene & Forman, 1982), recent studies have emphasized the crucial role of  $\text{CD4}^+$  T cells in the context of anti-tumor immune responses (Ahmadzadeh et al., 2019; Tran et al., 2014).

For example, two separate studies in 2017 were able to show that personalized neoantigen-vaccines in melanoma mouse models induced anti-tumor responses primarily in  $\text{CD4}^+$  T rather than  $\text{CD8}^+$  T cells (Ott et al., 2017; Sahin et al., 2017), with one of the groups showing that 57 % of induced immune responses was due to  $\text{CD4}^+$  T cells, 26 % due to  $\text{CD8}^+$ - and  $\text{CD4}^+$  T cells combined and just 17 % because of  $\text{CD8}^+$  T cells alone (Sahin et al., 2017). Beyond cancer vaccination,  $\text{CD4}^+$  T cells have also seen a newfound role in adjuvant therapy. In a preclinical study where breast cancer- and colon carcinoma- mouse models received treatment consisting of CD40-mAb and  $\text{IFN}\gamma$ , analysis of the T-cell subset that drove tumor-eradication showed that  $\text{CD4}^+$  T cells were more vital to achieve an effective immune response compared to  $\text{CD8}^+$  T cells (Spitzer et al., 2017).

As for immune checkpoint inhibition, in a study that analysed 85 patients suffering from classic Hodgkin Lymphoma (cHL) it was shown that  $\text{CD4}^+$  T-cell infiltration, but not  $\text{CD8}^+$  T-cell

infiltration, served as a good prognostic marker for PD-1 therapy (Nagasaki et al., 2020). Lastly, CAR T-cell therapy has also seen success in the development and use of CD4<sup>+</sup> CAR T-cells in glioblastoma- (D. Wang et al., 2018) and leukemia patients (Yang et al., 2017). In patients suffering from leukemia, the treatment with CD4<sup>+</sup> CAR T-cells demonstrated equal cytotoxicity compared to CD8<sup>+</sup> CAR T-cells, but only CD4<sup>+</sup> CAR T-cell therapy resulted in long-term tumor eradication (Yang et al., 2017).

Taken together, these studies highlight the importance of encapsulating and monitoring the whole spectrum of T-cell responses during immunotherapy, since limiting the scope to a restricted population might detrimentally effect therapy-evaluation and consequently patient outcome. A way to achieve a more complete picture of the T-cell based immune response via immunoPET is by utilizing a pan T-cell marker, which is a surface antigen that is found on all T-cell subsets. These markers include CD2, CD3 and CD7, with the primary focus of this dissertation being CD2 and CD7, since work by Mayer & Mall et al. has shown detrimental effects of CD3-based pan T-cell tracers on T-cell viability. (Mayer et al., 2018).

#### 1.4.1 CD2

Human CD2 was first described in 1981 as a member of the immunoglobulin superfamily (Howard et al., 1981). Further research characterized it as a transmembrane glycoprotein (Sayre, Hussey, Chang, Ciardelli, & Reinherz, 1989) that is expressed on the surface of all T-cell subsets (Selvaraj et al., 1987), NK cells (Timonen, Gahmberg, & Patarroyo, 1990), dendritic cells (Matsui et al., 2009) and thymocytes (Reinherz, 1985). CD2 has a molecular weight of around 40 kDa (UniProt, 2019) and its corresponding binding partners are lymphocyte-associated antigen 3 (LFA3), also known as CD58 (Krensky et al., 1983) and CD48 (McArdel, Terhorst, & Sharpe, 2016), both of which are expressed on antigen-presenting cells. Binding between CD2 and its ligands leads to cell-cell-adhesion, subsequent co-stimulatory signaling and T-cell activation (Hahn & Bierer, 1993; Moingeon et al., 1992).

The structure of CD2 has been described to be based on three distinct epitopes, named T11.1, T11.2 and T11.3 (Meuer et al., 1984). While T11.1 and T11.2 are part of the adhesion domain and involved in the binding of LFA3 (Vollger, Tuck, Springer, Haynes, & Singer, 1987), T11.3 belongs to the membrane-proximal domain and, due to conformational changes of CD2 upon T-cell activation, it is increasingly exposed and accessible on activated T cells (Jing Li, Alex Smolyar, Raute Sunder-Plassmann, & Ellis L Reinherz, 1996). Targeting CD2 via mAbs has repeatedly shown to induce apoptosis (Dumont et al., 1998; Hammond et al., 2006; Mayer et

al., 2018) or, if the anti-CD2-mAb was given during T-cell priming, result in a reduced T-cell response (Gücel et al., 1991).

Expression levels of CD2 vary between the different T-cell subsets, with its highest expression on memory T cells (Sanders et al., 1988). Furthermore, compared to resting T cells, CD2-expression is upregulated on activated T cells (Denise J Lo et al., 2011), which has been confirmed by various groups (Demetriou et al., 2019; Mayer et al., 2018). These features make CD2 an attractive target not just to visualize all T cells involved in the individual immune-response, but also to simultaneously highlight specifically activated T cells.

Therefore, Mayer & Mall et al. have investigated an approach to target CD2 for immunoPET imaging in a preclinical mouse model by utilizing a  $^{89}\text{Zr}$ -labelled  $\text{F(ab')}_2$  (Mayer et al., 2018). In vitro analysis showed that CD2- $\text{F(ab')}_2$  binding did not impair proliferation or functional anti-tumor efficacy of bound T cells, which led to further characterization of the tracer in a myeloid sarcoma model of adoptive T-cell transfer. Imaging via PET/CT of adoptively transferred T cells resulted in a distinct tracer accumulation at the tumor site and high contrast images of T-cell distribution. However, while there was no major T-cell impairment visible in vitro, application of the CD2- $\text{F(ab')}_2$  did impact T-cell functionality in vivo and resulted in T-cell depletion and failure to reject the targeted tumor (Mayer et al., 2018).

#### 1.4.2 CD7

CD7 is a transmembrane glycoprotein with a molecular weight of 40 kDa that is expressed by all T cells, NK cells and thymocytes (Haynes, Eisenbarth, & Fauci, 1979; Hannah Rabinowich, Luminita Pricop, Ronald B Herberman, & Theresa L Whiteside, 1994). Additionally, it is also expressed in over 95 % of lymphoblastic T-cell leukemias and T-cell lymphomas, as well as in peripheral T-cell lymphomas (Campana et al., 1991). Expression levels of CD7 vary depending on the T-cell subtype, with naïve- and memory T cells exhibiting the highest levels of expressed CD7, while CD7-low expressing cells are typically effector T-cells (Aandahl et al., 2003).

Similar to CD3, CD7 plays an important costimulatory role in T-cell activation due to binding to its ligand SECTM1 (K12) (Chan, Mobley, Fields, & Shimizu, 1997; Ward et al., 1995). However, unlike CD3, CD7 does not seem to play a central role in T-cell development, since genomic disruption of CD7 in murine T-cell progenitors did not impair T-cell development, – homeostasis and -protective functions while only slightly affecting effector functions (D. M. Lee et al., 1998).

Targeting CD7 by using an  $^{89}\text{Zr}$ -labelled  $\text{F(ab')}_2$  has already shown preclinical success in monitoring adoptively transferred T cells (Mayer et al., 2018). Mayer & Mall et al. have evaluated the potential of CD2- and CD7- $^{89}\text{Zr}$ -labelled  $\text{F(ab')}_2$  simultaneously, and while application of CD2-  $\text{F(ab')}_2$ , as previously described, led to T-cell depletion and failed tumor rejection in vivo, CD2-  $\text{F(ab')}_2$  showed no impairment of T-cell functionality in the same mouse model. Additionally, PET/CT images showed a strong signal at the subcutaneous injected HLA-relevant tumor site with no significant accumulation in the control tumor.

Taken together, intravenous injection of  $^{89}\text{Zr}$ -CD2-  $\text{F(ab')}_2$  did not affect T-cell functionality and subsequent therapeutic success in vivo, while at the same time allowing precise T-cell monitoring.

## 2 Aim of this study

While immunotherapies are highly specific in terms of their target structures and mechanism of action, both their progression and response patterns can differ substantially from conventional anticancer treatments and therefore necessitate appropriate tools to be correctly evaluated. As a consequence, sensitive methods that facilitate timely evaluation of immunotherapeutic response patterns and allow more insight into their pharmacodynamics and-kinetics are still missing, yet necessary to improve patient outcome.

In order to resolve this issue, direct and specific monitoring of the most relevant immune cells involved in antitumor immunity would be ideal. The majority of research on this topic is focused on imaging individual T-cell subsets, such as CD8<sup>+</sup> T cells, rather than the overall population of T cells. However, focusing on narrowly defined populations can result in failure to depict the versatile aspect of T-cell responses during immunotherapy to its full extent.

Therefore, the need to monitor and evaluate the whole spectrum of immunotherapeutic responses during therapy using a universally applicable non-invasive imaging method is rapidly growing.

Utilizing a pan T-cell tracer in order to comprehensively visualize CD4<sup>+</sup> as well as CD8<sup>+</sup> T cells in patients during immunotherapy would constitute a promising novel approach in immunotherapeutic response assessment. In order to bridge the gap between preclinical research and clinical translation, extensive and in-depth analysis of the evaluated CD2<sup>+</sup> and CD7<sup>+</sup>-sdAb tracers in terms of purity, binding stability and binding specificity is necessary. Furthermore, ensuring that the tracer can be used to monitor T cells in the context of immunotherapies without interfering in the therapy itself by impairing T-cell functionality is crucial for a thorough safety-assessment.

Besides evaluation of CD2<sup>+</sup> and CD7<sup>+</sup>-sdAb binding characteristics and their respective impact on T-cell functionality, detailed analysis in terms of in vivo PET-imaging is crucial to demonstrate the beneficial impact of such a technology.

### 3 Material

#### 3.1 Technical Equipment

**Table 1: Technical Equipment**

<b>Device</b>	<b>Company</b>
Analytical balance SI-64	Denver Instrument, Göttingen, Germany
Autoclave Systec V75, V150	Systec GmbH, Linden, Germany
BD FACSCanto II	BD Biosciences, Franklin Lakes, USA
BD LSR II	BD Biosciences, Franklin Lakes, USA
BioDocAnalyze	Biometra GmbH, Göttingen, Germany
Centrifuge 5417R	Eppendorf AG, Hamburg, Germany
Centrifuge 5810R	Eppendorf AG, Hamburg, Germany
Centrifuge 7-0040	neoLab Migge GmbH, Heidelberg, Germany
MTS 2/4 microtiter shaker	IKA-Werke, Staufen, Germany
MPC-L Magnetic Particle Concentrator	Invitrogen Dynal AS, Oslo, Norway
EcoVac Vacuum Pump	Schuett-biotec GmbH, Göttingen, Germany
ENVAIR eco safe Comfort laminar flow	CARLO ERBA Reagents GmbH, Emmendingen, Germany
Fume cupboard 2-453-DXNN	Köttermann GmbH & Co KG, Uetze/Hänigsen, Germany
GABI Star $\gamma$ detector	Elysia-raytest GmbH, Straubenhardt, Germany
Gamma counter 2480Wizard2	PerkinElmer, Waltham, USA
GEL iX20 Imager	Intas Science Imaging Instruments GmbH, Göttingen, Germany
Gene Pulser Xcell Electroporation System	Bio-Rad Laboratories, Inc., Hercules, USA
Glomax Discover Microplate Reader	Promega GmbH, Walldorf, Germany
Growth chamber WTC	BINDER GmbH, Tuttlingen, Germany

Incubator BBD 6220	Heraeus Holding GmbH, Hanau, Germany
Incubator CB 150	BINDER GmbH, Tuttlingen, Germany
Infors HT shaker	Infors AG, Bottmingen, Switzerland
Innova 40 shaker	Eppendorf AG, Hamburg, Germany
LS6000 sample container	Tec-lab GmbH, Taunusstein, Germany
MACSmix Tube Rotator	Miltenyi Biotec GmbH, Bergisch Gladbach, Germany
Magnetic stirrer RH basic 2	IKA®-Werke GmbH & CO. KG, Staufen, Germany
Megafuge 1.0R	DJB Labcare Ltd, Buckinghamshire, UK
Microscope Axiovert 40 C	Carl Zeiss AG, Feldbach, Schweiz
Mini-PROTEAN Tetra Vertical Electrophoresis Cell	Bio-Rad Laboratories, Inc., Hercules, USA
Minishaker MS2	IKA®-Werke GmbH & CO. KG, Staufen, Germany
Multichannel pipets	Eppendorf AG, Hamburg, Germany
Multifuge 3 S-R	Heraeus Holding GmbH, Hanau, Germany
NALGENE Cryo 1°C Freezing Container	Thermo Fisher scientific, Waltham, USA
NanoDrop Spectrophotometer ND1000	PeqLab/VWR International GmbH, Darmstadt, Germany
Nanophotometer	Implen GmbH, Munich, Germany
nanoScan PET/MRI	Mediso GmbH, Münster, Germany
Neubauer improved counting chamber	Karl Hecht GmbH & Co KG, Sondheim/Röhn, Deutschland
Pipets	Eppendorf AG, Hamburg, Germany
Pipette controller	INTEGRA Biosciences GmbH, Biebertal, Germany
PowerPac Universal Power Supply	Bio-Rad Laboratories, Inc., Hercules, USA
Precision balance 440	KERN & SOHN GmbH, Balingen, Germany

Premium -20°C Freezer	Liebherr-International Deutschland GmbH, Biberach an der Riß, Germany
Prominence HPLC system with a Photo Diode Array detector	Shimadzu, Kyoto, Japan
Refrigerator Profi line	Liebherr-International Deutschland GmbH, Biberach an der Riß, Germany
Rotina 420R	Andreas Hettich GmbH & Co.KG, Tuttlingen, Germany
SEC column Yarra 3µm SEC-3000	Phenomenex, Aschaffenburg, Germany
Sub-Cell GT horizontal gel electrophoresis cell	Bio-Rad Laboratories, Inc., Hercules, USA
TGradient	Biometra GmbH, Göttingen, Germany
Thermomixer Compact	Eppendorf AG, Hamburg, Germany
TProfessional Thermocycler	Biometra GmbH, Göttingen, Germany
Vortex Mixer 7-2020	neoLab Migge GmbH, Heidelberg, Germany
Vortexer Reax top	Heidolph Instruments GmbH & Co.KG, Schwabach, Germany
Vortex-Genie 2	Scientific Industries, Inc., New York, USA
VWR Power Source 300V	VWR International GmbH, Darmstadt, Germany
Waterbath	Memmert GmbH + Co. KG, Schwabach, Germany
Ziegra Ice machine	ZIEGRA Eismaschinen GmbH, Isernhagen, Germany

### 3.2 Consumables

**Table 2: Consumables**

<b>Consumable</b>	<b>Company</b>
Amicon Ultra – 0,5 Centrifugal Filter Device	Merck KGaA, Darmstadt, Germany
Amicon Ultra – 15 Centrifugal Filter Device	Merck KGaA, Darmstadt, Germany
Cell culture flask (T25, T75, T175)	Greiner Bio-One GmbH, Frickenhausen, Germany
Cell strainer (40, 70, 100 µm)	BD bioscience, Franklin Lakes, USA
Cryopure tubes	Sarstedt AG & Co., Nümbrecht, Germany
EIA/RIA plates	Corning, New York, USA
E-Plate 96-well plate	ACEA Biosciences, Inc., San Diego, USA
Erlenmeyer baffled cell culture flasks – 1 l	Corning, New York, USA
Erlenmeyer baffled cell culture flasks – 2 l	Corning, New York, USA
Falcons (15 ml, 50 ml)	BD Biosciences, Franklin Lakes, USA
Gene PulserR Electroporation Cuvettes 0.2 cm gap	Bio-Rad Laboratories, Inc., Hercules, USA
Gloves Dermatril P	KCL GmbH, Eichenzell, Germany
Inoculating loops	VWR, Darmstadt, Germany
Microtubes (1.2 ml)	Alpha Laboratories, Hampshire, UK
Nitrile gloves	Abena A/Sm Aabenraa, Denmark
Non-tissue culture treated plates (6-/24-well)	BD Biosciences, Franklin Lakes, USA
NuPAGE Bis-Tris Mini Gel	Thermo Fisher Scientific, Waltham, USA
Parafilm MR laboratory film	Pechiney Plastic Packaging, Chicago, USA
PCR reaction tubes (0.5 ml)	VWR International GmbH, Darmstadt, Germany
Petri dishes	Greiner Bio-One, Frickenhausen, Germany
Pipet tips (10/20/300/1250 µl)	Sarstedt AG & Co., Nümbrecht, Germany
Reaction tubes (1.5, 2 ml)	Sarstedt AG & Co., Nümbrecht, Germany
Round-bottom polystyrene test tubes (1.2 ml)	Falcon, Corning Brand, Glendale, USA

Round-bottom polystyrene test tubes (5 ml)	Falcon, Corning Brand, Glendale, USA
Screw Cap Micro Tubes	Sarstedt AG & Co., Nümbrecht, Germany
Sealing foil (ELISA)	Alpha Laboratories, Hampshire, UK
Serological Pipets (5 ml, 10 ml, 25 ml, 50 ml)	Sarstedt AG & Co., Nümbrecht, Germany
Stericup/Steritop 0.22 µm filters	Merck KGaA, Darmstadt, Germany
Sub-Q syringes (1 ml)	BD bioscience, Franklin Lakes, USA
Syringe filters (0.2, 0.45 µm)	TPP Techno Plastic Products AG, Trasadingen, Switzerland
Syringes (2 ml, 5 ml, 10 ml, 50 ml)	BD Bioscience, Franklin Lakes, USA
Tissue culture-treated plates (48-well)	BD Biosciences, Franklin Lakes, USA
Tissue culture-treated plates (6-/12-/24-well, round/flat bottom 96-well)	TPP Techno Plastic Products AG, Trasadingen, Schweiz

### 3.3 Reagents and chemicals

**Table 3: Reagents and chemicals**

Reagent / chemical	Company
100 bp DNA ladder	Thermo Fisher scientific, Waltham, USA
1 kb DNA ladder	Thermo Fisher scientific, Waltham, USA
4x Laemmli protein sample buffer	Bio-Rad Laboratories, Inc., Hercules, USA
6X loading buffer	Thermo Fisher scientific, Waltham, USA
7-Aminoactinomycin D (7-AAD)	Merck KGaA, Darmstadt, Germany
AccuCheck Counting beads	Thermo Fisher scientific, Waltham, USA
Acetic acid	Roth, Karlsruhe, Germany
ACK Lysis buffer	Thermo Fisher Scientific, Waltham, USA
Agar-Agar	Roth, Karlsruhe, Germany
Agarose	Roth, Karlsruhe, Germany
Ampicillin	Merck KGaA, Darmstadt, Germany
Bacto Tryptone	BD Biosciences, Franklin Lakes, USA
Bacto Yeast Extract	BD Biosciences, Franklin Lakes, USA
Bovine serum albumin	Merck KGaA, Darmstadt, Germany
Brilliant blue R 250	Roth, Karlsruhe, Germany
Coomassie Brilliant Blue G-250 Dye	Thermo Fisher Scientific, Waltham, USA
DEPC-H <sub>2</sub> O	Thermo Fisher scientific, Waltham, USA

Desferrioxamine	Macrocyclics, Inc, Dallas, USA
DMEM	Thermo Fisher scientific, Waltham, USA
DMSO	Merck, KGaA, Darmstadt, Germany
EDTA	Thermo Fisher scientific, Waltham, USA
Ethanol	Merck KGaA, Darmstadt, Germany
Fetal calf serum (FCS)	Thermo Fisher scientific, Waltham, USA
Ficoll-Paque	Cytiva, Marlborough, USA
Gentamycin	Thermo Fisher scientific, Waltham, USA
Glucose	Roth, Karlsruhe, Germany
Glycerol	Merck KGaA, Darmstadt, Germany
HEPES	Thermo Fisher scientific, Waltham, USA
Human serum (HS)	Technische Universität München, Germany
Isofluran	CP Pharma, Burgendorf, Germany
Isopropanol	Merck KGaA, Darmstadt, Germany
LDS Sample Buffer (4X)	Thermo Fisher scientific, Waltham, USA
L-Glutamine	Thermo Fisher scientific, Waltham, USA
Lipofectamine CRISPRMAX	Thermo Fisher scientific, Waltham, USA
Methanol	Roth, Karlsruhe, Germany
MgCl <sub>2</sub>	Roth, Karlsruhe, Germany
NaCl	Roth, Karlsruhe, Germany
Non-essential amino acids	Thermo Fisher scientific, Waltham, USA
Opti-MEM I	Thermo Fisher scientific, Waltham, USA
PageRuler Prestained Protein Ladder	Thermo Fisher scientific, Waltham, USA
Paraformaldehyde (PFA)	Merck KGaA, Darmstadt, Germany
PBS	Thermo Fisher scientific, Waltham, USA
PBS powder	Merck KGaA, Darmstadt, Germany
Penicilline/Streptomycine	Thermo Fisher scientific, Waltham, USA
Protamine sulfate	MP Biomedicals, Illkirch, France
Restriction enzymes	New England Biolabs, Ipswich, UK
RetroNectin	Takara Bio, Japan
RPMI 1640	Thermo Fisher scientific, Waltham, USA
S.O.C. Medium	New England Biolabs, Ipswich, UK
Skim milk powder	Merck KGaA, Darmstadt, Germany
Sodium carbonate (Na <sub>2</sub> CO <sub>3</sub> )	Merck KGaA, Darmstadt, Germany
Sodium hydrogen carbonate (Na <sub>2</sub> HCO <sub>3</sub> )	Merck KGaA, Darmstadt, Germany
Sodium pyruvate	Thermo Fisher scientific, Waltham, USA
Sucrose	Roth, Karlsruhe, Germany

Sulfuric acid (1M)	Roth, Karlsruhe, Germany
SYBR Safe	Thermo Fisher scientific, Waltham, USA
Terrific Broth medium	Thermo Fisher scientific, Waltham, USA
TransIT transfection reagent	Mirus Bio LLC, Madison, USA
Trypane blue	Thermo Fisher scientific, Waltham, USA
Trypsine EDTA (0.5 %)	Thermo Fisher scientific, Waltham, USA
Tween 20	Merck KGaA, Darmstadt, Germany

### 3.4 Kits

**Table 4: Kits**

Kit	Company
Alt-R Genome Editing Detection Kit	Integrated DNA Technologies, Coralville, USA
Alt-R HPRT PCR Primer Mix, Human, 2nmol	Integrated DNA Technologies, Coralville, USA
BD OptEIA Human GM-GSF ELISA Set	BD Biosciences, Franklin Lakes, USA
BD OptEIA Human IL-2 ELISA Set	BD Biosciences, Franklin Lakes, USA
BD OptEIA Human IL-6 ELISA Set	BD Biosciences, Franklin Lakes, USA
BD OptEIA Human INF $\gamma$ ELISA Set	BD Biosciences, Franklin Lakes, USA
BD OptEIA TMB Substrate Reagent Set	BD Biosciences, Franklin Lakes, USA
DNA blood and tissue kit - QIAwave	QIAGEN GmbH, Hilden, Germany
DreamTaq Green Hot Start PCR Mastermix (2X)	Thermo Fisher Scientific, Waltham, USA
DreamTaq Hot Start PCR Mastermix (2X)	Thermo Fisher Scientific, Waltham, USA
Dynabeads™ Human T-Activator CD3/CD28	Thermo Fisher scientific, Waltham, USA
Dynabeads™ Untouched Human CD8 T Cells Kit	Thermo Fisher scientific, Waltham, USA
HisPur™ Ni-NTA Spin Purification Kit, 3 ml	Thermo Fisher scientific, Waltham, USA
NAb™ Protein A Plus Spin column (1 ml)	Thermo Fisher Scientific, Waltham, USA
NEB® 5-alpha competent <i>E. coli</i>	New England BioLabs Inc., Ipswich, USA
NucleoBond® Xtra Maxi EF	MACHERY-NAGEL GmbH & Co. KG, Düren, Deutschland
NucleoSpin® Gel and PCR Clean-up	MACHERY-NAGEL GmbH & Co. KG, Düren, Deutschland
NucleoSpin® Plasmid EasyPure	MACHERY-NAGEL GmbH & Co. KG, Düren, Deutschland
Pierce™ F(ab') <sub>2</sub> Preparation Kit	Thermo Fisher Scientific, Waltham, USA
Quick Ligation™ Kit	New England Biolabs, Ipswich, UK

### 3.5 Buffer

**Table 5: Buffers**

<b>Buffer</b>	<b>Application</b>	<b>Ingredients</b>
25 mM wash buffer	sdAb production	PBS + 25 mM imidazole
50 mM wash buffer	sdAb production	PBS + 50 mM imidazole
Blocking buffer	ELISA	PBS + 1 % (w/v) skim milk powder
Coating buffer	ELISA	100 mM NaHCO <sub>3</sub> and 30 mM Na <sub>2</sub> CO <sub>3</sub> in H <sub>2</sub> O, pH 9.5
Coomassie solution	SDS-PAGE	1 g/l Brilliant blue, 50 % ethanol, 10 % acetic acid in H <sub>2</sub> O
Destain buffer	SDS-PAGE	50 % methanol, 10 % acetic acid in H <sub>2</sub> O
Elution buffer	sdAb production	PBS + 250 mM imidazole
Equilibration buffer	sdAb production	PBS + 10 mM imidazole
FACS buffer	Flow cytometry	PBS + 1 % ΔFCS
Fix solution	Intracellular staining	PBS + 25 % FOXP3 Fix/Perm buffer (4X)
IDTE buffer	RNP production	10 mM Tris, 0.1 mM EDTA in H <sub>2</sub> O
Isolation buffer	T-cell isolation	PBS + 2 % ΔFCS, 2 mM EDTA
MES buffer (1X)	SDS-PAGE	H <sub>2</sub> O + 5 % MES SDS Running Buffer (20X) (Thermo Fisher scientific)
Permeabilization buffer	Intracellular staining	PBS + 10 % FOXP3 Perm buffer 10X (BioLegend)
SDS-PAGE buffer	SDS-PAGE	50ml 20x NuPAGE MES Puffer und 950ml H <sub>2</sub> O
TAE buffer (1X)	Gel electrophoresis	H <sub>2</sub> O + 10 % TAE buffer 10X (Thermo Fisher scientific)
TES buffer	sdAb production	0.2 M Tris, 0.5 mM EDTA, 0.5 M sucrose in H <sub>2</sub> O, pH 8.0
Tris buffer (1 M, pH = 8.0)	sdAb production	121,14 g Tris in H <sub>2</sub> O, adjusted to pH 8.0 with HCl
Washing buffer	ELISA	PBS + 0.05 % (v/v) Tween 20
ΔFCS	Multiple applications	FCS, heat inactivated for 20 min at 58°C
ΔHS	Multiple applications	HS, heat inactivated for 20 min at 58°C

### 3.6 Media

**Table 6: Media**

<b>Medium</b>	<b>Ingredients</b>
cDMEM	DMEM supplemented with 10 % $\Delta$ FCS, 10 mM non-essential amino acids, 1 mM sodium pyruvate, 2 mM L-Glutamine, 100 U/ml Penicillin and 100 $\mu$ g/ml Streptomycin
cRPMI	RPMI supplemented with 10 % $\Delta$ FCS, 10 mM non-essential amino acids, 1 mM sodium pyruvate, 2 mM L-Glutamine, 100 U/ml Penicillin and 100 $\mu$ g/ml Streptomycin
cMEM	MEM supplemented with 10 % $\Delta$ FCS, 10 mM non-essential amino acids, 1 mM sodium pyruvate, 2 mM L-Glutamine, 100 U/ml Penicillin and 100 $\mu$ g/ml Streptomycin
Freezing medium	90 % $\Delta$ FCS + 10 % DMSO
LB medium	10 g Bacto-Tryptone, 5 g Bacto-Yeast extract and 10 g NaCl dissolved in 1 l H <sub>2</sub> O, autoclaved after preparation
OptiMEM	OptiMEM (Thermo Fisher Scientific, Waltham, USA), no supplements
Terrific broth medium (TB medium)	Terrific broth medium (Thermo Fisher Scientific, Waltham, USA) supplemented with 2 mM MgCl <sub>2</sub> and 0.1 % Glucose
T-cell medium (TCM)	RPMI 1640 supplemented with 5 % $\Delta$ FCS, 5 % $\Delta$ HIS, 10 mM non essential amino acids, 1 mM sodium pyruvate, 2 mM L-Glutamine, 100 U/ml Penicillin, 100 $\mu$ g/ml Streptomycin, 10 mM HEPES buffer and 16.6 $\mu$ g/ml Gentamycin

### 3.7 Cytokines

**Table 7: Cytokines**

<b>Cytokine</b>	<b>Company</b>
Human IL-2	PeptoTech, London, UK
Human IL-7	PeptoTech, London, UK
Human IL-15	PeptoTech, London, UK

### 3.8 Antibodies

**Table 8: Antibodies for flow cytometry**

<b>Antibody</b>	<b>Clone</b>	<b>Conjugation</b>	<b>Company</b>
anti-human CD2	RPA-2.10	APC, PE and unconjugated	Thermo Fisher Scientific, Waltham, USA
anti-human CD2	OKT11	APC, PE and unconjugated	BioLegend, San Diego, USA
anti-human CD2	OKT11	unconjugated	Caprico Biotechnologies, Norcross, USA
anti-human CD2	CD2-sdAb	unconjugated	VIB Nanobody Core, Brussels, Belgium
anti-human CD3	UCHT1	V450, APC, PE	BD Biosciences, Franklin Lakes, USA
anti-human CD4	RPA-T4	APC-Cy7, FITC	BD Biosciences, Franklin Lakes, USA
anti-human CD45RA	HI100	APC	BD Biosciences, Franklin Lakes, USA
anti-human CD45RO	UCHL1	PE	BD Biosciences, Franklin Lakes, USA
anti-human CD62L	DREG-56	PE	BD Biosciences, Franklin Lakes, USA
anti-human CD7	124-1D1	APC	Thermo Fisher Scientific, Waltham, USA
anti-human CD7	CD7-sdAb	unconjugated	VIB Nanobody Core, Brussels, Belgium
anti-human CD8	RPA-T8	APC	BD Biosciences, Franklin Lakes, USA
anti-human CD8	HIT8a	FITC	BD Biosciences, Franklin Lakes, USA
anti-human HA-Tag	912426	AF488	R&D Systems, Inc., Minneapolis, USA
anti-human HIS-Tag	AD1.1.10	AF647	Bio-Rad Laboratories, Inc., Hercules, USA
anti-human HLA-B7	BB7.1	APC	Novus Biologicals, Centennial, USA
anti-murine TCR (TCR $\mu$ )	H57-597	FITC and unconjugated	BD Biosciences, Franklin Lakes, USA
Control-sdAb	R3b23-sdAb	unconjugated	VIB Nanobody Core, Brussels, Belgium
Isotype control	MOPC-21	FITC, PE, APC, AF700, V450, APC-CyTM7	BD Biosciences, Franklin Lakes, USA
MPO <sub>5</sub>	5B8	FITC	BD Biosciences, Franklin Lakes, USA

### 3.9 Vectors

**Table 9: Vectors**

Vector	Characteristics	Resistance	Origin
pMECS-GG	If sdAb are produced from pMECS vector, the His.Tag at C-terminus is cleaved off after storage at 4°C or several freeze/thaw cycles	Ampicillin	VIB Nanobody Core, Brussels, Belgium
pHEN6c	C-terminal His-Tag remains intact through storage at 4°C or several freeze/thaw cycles	Ampicillin	VIB Nanobody Core, Brussels, Belgium
pMP71-P2A-dsRed	pMP71GPRE with P2A element upstream of dsRed	Ampicillin	Generated by Richard Klar

### 3.10 CRISPR RNAs (crRNA)

Sequences are depicted in 5' → 3' direction.

**Table 10: crRNA sequences**

crRNA	Sequence	Application
CD2-C	UUACGAAUGCCUUGGAAACCGUUUUAGAGCUAUGCU	Knockout of CD2
CD2-H	AAGCUGGCUACAAAUUUACAGUUUUAGAGCUAUGCU	Knockout of CD2
CD2-M	CAAGGCAUUCGUAAUCUCUUGUUUUAGAGCUAUGCU	Knockout of CD2
CD2-N	CUUGGGUCAGGACAUCAACUGUUUUAGAGCUAUGCU	Knockout of CD2
CD2-O	ACGAAUGCCUUGGAAACCGUUUUAGAGCUAUGCU	Knockout of CD2
CD7.AA	CACUACGGACAGACGGUUCGUUUUAGAGCUAUGCU	Knockout of CD7
CD7.AB	AUGCUCGGACGCCCCACCAAGUUUUAGAGCAUAGCU	Knockout of CD7
CD7.AC	CAUCAUUUACUACGAGGACGGUUUUAGAGCUAUGCU	Knockout of CD7
CD7.AJ	GAUGCUCGGACGCCCCACCAGUUUUAGAGCUAUGCU	Knockout of CD7

### 3.11 Primers

Primers were dissolved in DEPC-H<sub>2</sub>O to a stock concentration of 100 µM. Sequences are depicted in 5' → 3' direction.

**Table 11: Primers**

Primer	Sequence	Application
A6E	GATGTGCAGCTGCAGGAGTCTGGGGGAGG	sdAb recloning
PMCF	CTAGTGCGGCCGCTGAGGAGACGGTGACCTGGGT	sdAb recloning
sdAb_fwd	CGCCAGGGTTTTCCCAGTACAGAC	Sequencing of recloned sdAb
sdAb_rev	TCACACAGGAAACAGCTATGAC	Sequencing of recloned sdAb
MP057	TTATGCTTCCGGCTCGTATG	Sequencing of recloned sdAb
CD2_col_fwd	TCCAAAGGTGCAGTCTCAA	Colony-PCR of recloned CD2-sdAb
CD2_col_rev	AGAAGTTCGTGGCATTAGAGGA	Colony-PCR of recloned CD2-sdAb
CD7_col_fwd	CCACAGCCCCAAGACATCAT	Colony-PCR of recloned CD7-sdAb
CD7_col_rev	GAGAAGTTCGTGGCCTGGTA	Colony-PCR of recloned CD7-sdAb
MP71_fwd	TGAAAATTAGCTCGACAAAG	Sequencing of recloned CD2- and CD7-sdAb in pMP71 vector
MP71_rev	GTAAATGATTGCCCCACCA	Sequencing of recloned CD2- and CD7-sdAb in pMP71 vector

## 3.12 Cell lines and primary cells

Table 12: Cell lines and primary cells

Cell line	Medium	Characteristics	Origin
293Vec-RD114	cMEM	Retroviral packaging cell line based on HEK 293	BioVec Pharma inc., Québec, Canada
624.38 Mel	cDMEM	Human melanoma cell line	Kindly provided by E. Noessner, Munich, Germany
CD8 <sup>+</sup> T cells	TCM	Generated from PBMCs of healthy donors	Healthy donors
HL60-B7	cRPMI	APL cell line HL60, transduced with HLA-B*15:01-P2A-GFP	Generated by former lab members
HL60-B15	cRPMI	APL cell line HL60, transduced with HLA-B*07:02-P2A-eGFP	Generated by former lab members
Jurkat E6.1	cRPMI	Human acute T-cell leukemia cell line	Kindly provided by AG Ruland, Munich, Germany
ML2-B15	cRPMI	AML cell lines ML2, transduced with HLA-B*15:01-P2A-GFP	Generated by former lab members
ML2-B7	cRPMI	AML cell lines ML2, transduced with HLA-B*07:02-P2A-eGFP	Generated by former lab members
NB4-B15	cRPMI	APL cell line NB4, transduced with HLA-B*15:01-P2A-GFP	Generated by former lab members
NB4-B7	cRPMI	APL cell line NB4, transduced with HLA-B*07:02-P2A-eGFP	Generated by former lab members
U698M	cRPMI	Human B cell lymphoma	DSMZ, Braunschweig, Germany
U698M-CD2	cRPMI	U698M, transduced with human CD2-P2A-DsRed	Self-generated
U698M-CD7	cRPMI	U698M, transduced with human CD7-P2A-DsRed	Self-generated

### 3.13 Mouse model

**Table 13: Mouse model**

Mouse strain	Genetic background	Company
NOD <i>scid</i> gamma (NSG®)	NOD.Cg- <i>Prkdc</i> <sup><i>scid</i></sup> <i>Il2rg</i> <sup><i>tm1Wjl</i></sup> /SzJ	The Jackson Laboratory, Bar Harbor, Maine, USA

### 3.14 Software

**Table 14: Software**

Software	Application	Origin
CHOPCHOP	crRNA design	<a href="https://chopchop.cbu.uib.no/">https://chopchop.cbu.uib.no/</a> (Labun et al., 2019)
BioDocAnalyze	SDS-PAGE gel visualization	Biometra GmbH, Göttingen, Germany
EndNote™ X5	Citation management	Clarivate Analytics, London, UK
FlowJo™	Flow cytometry analysis	BD Bioscience, Franklin Lakes, USA
Graphpad Prism v10	Data processing and analysis	GraphPad Software, Inc., La Jolla, USA
Human Protein Atlas	Protein expression analysis	<a href="https://www.proteinatlas.org">https://www.proteinatlas.org</a>
Inveon Research Workplace	PET/MRI image analysis	Siemens, Knoxville, USA
Magellan	ELISA-plate reader software	Tecan Group Ltd., Maennedorf, Switzerland
Microsoft Office (Word, Excel, Powerpoint), 2010	Data processing and presentation	Microsoft Corporation, Redmond, USA
NCBI Basic Local Alignment Search Tool (BLAST)	Sequence alignments	<a href="https://www.blast.ncbi.nlm.nih.gov/Blast.cgi">https://www.blast.ncbi.nlm.nih.gov/Blast.cgi</a>
NEBcutter V2.0	In-silico cloning	New England Biolabs, Ipswich, UK
Sequencher v5.0	DNA sequence analysis	Gene Codes Corporation, Ann Arbor, USA
SerialCloner 2.6.1	In-silico cloning	Freeware ( <a href="http://serialbasics.free.fr/Serial_Cloner.html">http://serialbasics.free.fr/Serial_Cloner.html</a> )

## 4 Methods

### 4.1 Cell culture methods

Cell culture methods were performed under sterile conditions and work with human blood samples and retroviruses was performed according to S2 safety guidelines.

#### 4.1.1 Freezing and thawing of cells

To freeze cells, they were centrifuged, resuspended in 1 ml freezing medium and placed in cryotubes. The cryotubes were then transferred into a freezing container which itself contains 80% isopropanol, and frozen at -80 °C overnight before being transferred to liquid nitrogen for long-term storage.

To thaw cells, the cryotubes were quickly warmed in a water bath and the cells were taken up in 10ml of appropriate medium and centrifuged. After centrifugation at 500 g for 5 min, the supernatant was discarded and the cell-pellet was resuspended in appropriate medium and cultivated in the desired cell culture flask or plate.

#### 4.1.2 Counting of cells

To determine the concentration of cultured cells, a small, well-mixed volume of the cell suspension was diluted with 4 % trypan blue solution to differentiate between dead and live cells. To evaluate the concentration of 20 µl cell suspension, 80 µl of trypan blue solution was added and carefully placed in a Neubauer chamber, carefully counted and the concentration was calculated using the following formula:

$$C_{cells} \left( \frac{\text{cells}}{\text{ml}} \right) = \frac{\text{number of alive cells in each square}}{\text{number of counted squares}} \times \text{dilution factor} \times 10000$$

#### 4.1.3 Cultivation of cell lines

Suspension cell lines as well as adherent cell lines were cultured in appropriate medium at a concentration of 0.5 to 1x10<sup>6</sup> cells per ml and split every two to four days. For this purpose, suspension cells were centrifuged and resuspended in new medium. Semi-adherent RD114 cells

were mechanically detached by gentle clapping of the flask and subsequently split equal to suspension cells. To split adherent cells, the culture medium was removed and the cells were washed with PBS. Subsequently, Trypsin/EDTA was added to the cells and they were incubated for 3 – 5 min at 37 °C, after which detachment of the cells was verified under the microscope and medium was again added. Cells were then transferred to a 50 ml Falcon, centrifuged and resuspended in new appropriate medium.

#### 4.1.4 Cloning of cells by limited dilution

Cells were cloned by limiting dilution to create a stable cell line carrying either the retrovirally transduced design or the CRISPR/Cas9 knockout of interest. Cells were counted and 200 µl of cells in respective medium were seeded in 96-well U-bottom plates at a concentration of 2.5 – 5 cells/ml, to achieve 0.5 – 1.0 cells per well. Cells were grown and regularly checked until day seven after seeding, at which time point cells were analyzed for their respective transgene by flow cytometry.

#### 4.1.5 Isolation of PBMCs from whole peripheral blood

Blood from healthy donors was collected after informed consent following requirements of the local ethical board. PBMCs were isolated from whole blood by using density-gradient centrifugation. To that end, blood was diluted 1:1 with RPMI medium and 35 ml of this mixture was carefully layered on 15 ml Ficoll/Hypaque (Biochrom, Berlin, Germany) in a 50 ml tube. After centrifugation at room temperature for 20 min at 880 g with reduced acceleration and no brake, the leukocyte layer in the interface was carefully harvested with a 10 ml serological pipette. Leukocyte cell suspensions were washed twice with RPMI, counted and then used for further downstream applications or stored in liquid nitrogen.

#### 4.1.6 Purification of human CD8<sup>+</sup> T cells

CD8<sup>+</sup> T cells were isolated via negative selection by using the Dynabeads™ Untouched™ Human CD8 T Cells Kit (Thermo Fisher Scientific) according to the manufacturer's instructions. Of the previously isolated PBMCs,  $1 \times 10^8$  cells were used at a concentration of  $1 \times 10^8$  cells per ml and resuspended in isolation buffer. Addition of 200 µl of heat-inactivated FCS and 200 µl of the antibody mix was followed by incubation for 20 min at 4°C. The cells were then washed with 4 ml isolation buffer and centrifuged at 350 g for 8 min at 4°C, after which

the supernatant was discarded. Cells were resuspended in 1 ml of isolation buffer and 1 ml of Depletion Dynabeads and incubated using a rotator for 15 min at room temperature. Next, cells were mixed with 8 ml isolation buffer, thoroughly resuspended and placed in the magnet for 2 min. After all Depletion Dynabeads were attached to the magnet, the supernatant containing CD8<sup>+</sup> cells was carefully removed and transferred to a new tube. The remaining Depletion Dynabeads were resuspended in 4 ml isolation buffer and again placed in the magnet for an additional separation. Afterwards, supernatant was removed as described before and both supernatants containing CD8<sup>+</sup> cells were pooled.

#### 4.1.7 Activation of CD8<sup>+</sup> T cells

Previously isolated T cells were taken up at a concentration of  $1 \times 10^6$  cells per ml in T cell medium, seeded in a 24-well plate. T cells were then stimulated with 30 U/ml human IL-2 and 25  $\mu$ l CD3/CD28 beads that were washed according to manufacturer's instructions (Thermo Fisher Scientific). After two days of incubation at 37 °C the cell suspension was mixed thoroughly, cells were collected and placed in a tube on magnet to separate the beads via magnetic separation. Isolated activated CD8<sup>+</sup> T cells were then used for further assays.

## 4.2 Retroviral transduction

### 4.2.1 Production of virus particles for retroviral transduction

For production of retroviral particles, RD114 cells were used as a viral packaging cell line.  $7.5 \times 10^5$  cells were seeded in 3 ml/well cDMEM on a tissue-culture treated six-well plate to adhere for at least eight hours before transfection. Afterwards, confluency was assessed using a light microscope and a confluency of 60 % of the six-well plate was aimed for. Then, the transfection solution was prepared by mixing 200  $\mu$ l DMEM with 3  $\mu$ l of the transfection reagent TransIT, followed by vortexing and incubation for 20 min at room temperature. Afterwards, 1  $\mu$ g of retroviral plasmid was added, carefully mixed and incubated for 30 min at room temperature. The mixture was then added dropwise to the cells, the plate was gently panned and incubated for 48 hours at 37 °C.

### 4.2.2 Transduction of CD8<sup>+</sup> T cells and tumor cell lines

Untreated 24-well plates were coated with 400  $\mu$ l RetroNectin solution (12.5  $\mu$ g/ml in PBS) per well, covered with Parafilm and incubated overnight at 4 °C. After removal of the RetroNectin

solution, the wells were blocked with 500  $\mu$ l of sterile filtered 2 % BSA in PBS at 37 °C for 30 min. Subsequently, each well was washed twice with 1 ml of PBS with 2.5 % HEPES and stored at 4 °C until the start of transduction. Next, three approaches are described to prepare cells for transduction with retroviral supernatant. The sections describe the preparation of CD8<sup>+</sup> T cells, suspension cell lines and adherent cell lines respectively.

CD8<sup>+</sup> T cells were isolated and activated as described above. Then,  $1 \times 10^6$  CD8<sup>+</sup> T cells were plated on RetroNectin-coated and blocked 24-well plates in 1ml TCM per well and supplemented with IL-2 ( $c_{END} = 100$  U/ml), HEPES ( $c_{END} = 5$  mM) and Protamine sulfate ( $c_{END} = 4$   $\mu$ g/ml) with all end concentrations calculated in relation to  $V_{END} = 2$  ml/well.

Suspension cell lines were washed with PBS and  $0.5 \times 10^6$  cells were seeded in 1 ml cRPMI on RetroNectin-coated and blocked 24-well plates, with the supplementation of HEPES and Protamine sulfate as described above.

Adherent cell lines were plated the evening before on tissue-culture treated 6-well plates to a density of  $0.3 \times 10^6$  cells/well. The next day, cells were checked for adherence and confluency and 1 ml/well of medium was added, supplemented with HEPES and Protamine sulfate as described above.

Independent of the used cell line, treatment of retroviral supernatant was done equally with 1 ml of retroviral supernatant used for each previously prepared RetroNectin-coated well. The remaining supernatant was kept for the second transduction. Retroviral supernatant was harvested, filtered through a 0.45  $\mu$ m filter and added to each well containing the cell suspension or adherent cells. Supplementation of each condition with IL-2, Protaminsulfat and HEPES was done as described above and the second transduction was done in the same way as the first. After incubation overnight, cells were washed and resuspended in their respective culture medium. CD8<sup>+</sup> T cells were expanded in TCM supplemented with 5 ng/ml of IL-7 and 5 ng/ml of IL-15.

## 4.3 CRISPR/Cas9 knockout

### 4.3.1 Generation of the ribonucleoproteins (RNPs) complex for CRISPR/Cas9 knockout

The methods used for preparation of the RNP complex is based on instructions by the manufacturer. In order to achieve a final concentration of 200  $\mu$ M, crRNA and tracrRNA were

resuspended and diluted in IDTE buffer. CrRNA and TracrRNA were combined in an equimolar ratio to a duplex concentration of 100  $\mu\text{M}$  to produce the gRNA. The mixture was heated to 95  $^{\circ}\text{C}$  for 5 min and then allowed to cool to room temperature. The previously prepared gRNA and the supplied Cas9 enzyme were combined in PBS to form the ribonucleoprotein complex according to the table below. The complex was incubated for 20 min at room temperature, after which it was kept on ice until further use.

**Table 15: Preparation of RNP complex**

Component	Concentration	Volume
gRNA	100 $\mu\text{M}$	12 $\mu\text{l}$
Cas9 enzyme	62 $\mu\text{M}$	17 $\mu\text{l}$
PBS	/	Fill up to 50 $\mu\text{l}$

#### 4.3.2 Lipofection of target cells for CRISPR/Cas9 transfection

Thermo Fisher Scientific's CRISPRMAX Cas9 Transfection Reagent was utilized for lipofection of target cells. Previously generated RNP complexes were diluted to a ratio of 1:20 with supplied IDTE buffer and subsequently mixed according to the table below for lipofection.

**Table 16: Lipofection mix**

Component	Volume
RNP complex	1.5 $\mu\text{l}$
Cas9 PLUS Reagent	0.6 $\mu\text{l}$
Opti-MEM	Fill up to 20 $\mu\text{l}$

The mix was incubated at room temperature for 5 min and afterwards supplemented with 1.2  $\mu\text{l}$  of CRISPRMAX transfection reagent and 23.8  $\mu\text{l}$  Opti-MEM. After incubating the lipofection mix for 20 min at room temperature, 50  $\mu\text{l}$  was added to each well of a 96-well plate. Afterwards, target cells were diluted to achieve a concentration of  $0.4 \times 10^6$  cells per ml and 100  $\mu\text{l}$  of the cell suspension was added to the previously prepared lipofection mix in a 96-well plate. The knockout rates of the cells were examined after two days of incubation.

## 4.4 Flow cytometry analysis

### 4.4.1 Flow cytometry staining of surface markers

Cells were washed using FACS buffer and afterwards blocked with 100 %  $\Delta$ HS for 10 min at 4 °C. After an additional washing step with FACS buffer, 1.5  $\mu$ l of each antibody as well as 1  $\mu$ l of 7-AAD ( $c_{\text{END}} = 0.5$  mg/ml) were added to the sample and the cells were incubated for 60 min at 4 °C in the dark. Afterwards, cells were washed with 1 ml FACS buffer and stored at 4 °C in the dark until measurement. Analysis of the samples was performed on a LSR II (BD Biosciences) and results were analyzed using FlowJo v7.6.5 software (BD Bioscience).

### 4.4.2 Flow cytometry staining CD2 and CD7 using sdAb

For sdAb-based flow cytometry staining, all steps were performed on ice.  $0.5 \times 10^6$  cells were washed three times with FACS buffer. The respective sdAb was added to a final concentration of 10  $\mu$ g/ml per sample and the cells were incubated for 60 min at 4 °C in the dark. Afterwards, cells were washed three times with FACS buffer, 1  $\mu$ l of anti-His-Tag antibody was added and the cells were again incubated for 60 min at 4 °C in the dark. Then, cells were washed again with FACS buffer and stored at 4 °C in the dark until measurement. Analysis of the samples was performed on a LSR II (BD Biosciences) and results were analyzed using FlowJo v7.6.5 software (BD Bioscience).

### 4.4.3 Evaluation of the dissociation constant of sdAbs

Cells were stained using sdAbs as previously described. Concentrations of used sdAbs ranged from  $1 \times 10^{-11}$  M to  $1 \times 10^{-3}$  M and were achieved through a series of sequential dilutions at a rate of 1:10. Binding of sdAb at their respective concentrations were performed on a LSR II (BD Biosciences) and results were analyzed using FlowJo v7.6.5 software (BD Bioscience), by analysing Mean Fluorescence Intensity (MFI) of each condition.

### 4.4.4 Thermal stability of sdAbs

Different samples of tested sdAbs were incubated at 37 °C, 60 °C or 90 °C for 0.5 h, 1 h, 2 h, 4 h and 6 h, with a control sample that was kept at 4 °C. Jurkat E6.1 cells were used as target cells and  $0.2 \times 10^6$  cells were washed with FACS buffer and then seeded in a 96-well plate. The respective sdAb was added to the sample at a concentration of 5 nM and the cells were incubated for 60 min at 4 °C. Afterwards, cells were washed three times with FACS buffer and 1  $\mu$ l of

anti-His-Tag antibody was added per well and the samples were again incubated for 60 min at 4 °C. Cells were washed with FACS buffer and analysis of the samples was performed on a LSRII (BD Biosciences) and results were analyzed using FlowJo v7.6.5 software (BD Bioscience).

## 4.5 Functional assessment of CD8<sup>+</sup> T cells

### 4.5.1 Coincubation of CD8<sup>+</sup> T cells and tumor cells

Previously isolated and retrovirally transduced CD8<sup>+</sup> T cells were used for coincubation assays with tumor cells in a 96-well U-bottom plate using an effector to target ratio (E:T) from 1:1 to 1:10 in 200 µl of TCM. After 4 h to 24 h of incubation at 37 °C, the supernatants were carefully removed and either used immediately or stored at -20 °C for later use.

### 4.5.2 Cytokine secretion evaluation via ELISA

Supernatants of previous coincubation were used to analyse the cytokine levels of IFN $\gamma$ , GM-CSF, IL2, and TNF $\alpha$  by using the respective BD OptEIA ELISA set (BD Bioscience). ELISA plates were coated with respective capture antibody diluted 1:250 in coating buffer, sealed and incubated over night at 4 °C. Afterwards, the plates were washed three times with washing buffer and unspecific binding was blocked by addition of ELISA blocking buffer for 1 h at room temperature. Plates were washed three times and 50 µl of serial 1:2 dilutions of standards for each cytokine were added in duplicates to each plate (1000 pg/ml to 31.25 ng/ml). 50 µl of sample supernatant was diluted appropriately and added to each plate in triplicates, followed by incubation for 1 h at room temperature. Plates were then washed five times and detection solution, consisting of 1 % milk powder in PBS with biotinylated detection antibody (1:250) and Streptavidin-horseradish peroxidase (HRP) conjugate (1:250), was added to each well and incubated for 1 h at room temperature in the dark. Afterwards, plates were washed seven times before 100 µl of substrate solution (TMB substrate Reagent Set, BD) was added per well and the plates were incubated at room temperature in the dark. The reaction was stopped after 10 – 20 min by adding 50 µl of sulfuric acid (H<sub>2</sub>SO<sub>4</sub>; 1 M). Absorbance was measured at a wavelength of 450 nm with 560 nm as a reference wavelength, using an ELISA reader (Glomax Discover Microplate Reader, Promega).

### 4.5.3 XCELLigence Assay

TCM and cDMEM were mixed in a 1:1 ratio and 200  $\mu\text{l}$  of the mix were added to a 96-well xCELLigence plate. After 30 min incubation at room temperature, a background measurement of the plate was performed on the xCELLigence RTCA MP instrument. Then, 100  $\mu\text{l}$  of medium was carefully removed from each well and  $7.5 \times 10^4$  tumor cells, resuspended in the same TCM and cDMEM mix, were added per well. The plate was then incubated at 37 °C for 24 h in the xCELLigence RTCA MP instrument and the cell index was determined every 30 min. After 24 h, 100  $\mu\text{l}$  of medium was carefully removed and  $7.5 \times 10^4$  transduced CD8<sup>+</sup> T cells as well as sdAbs ( $c_{\text{END}} = 100 \text{ nM}$  or  $500 \text{ nM}$ ) were added in 100  $\mu\text{l}$  of TCM and cDMEM mix. Each condition was evaluated in triplicates. After another 24 h incubation at 37 °C with a cell index analysis every 30 min, the coincubation was stopped and the data was analyzed using RTCA software 2.0. The cell index was normalized at the time of T-cell addition.

## 4.6 Recloning of sdAb genes from pMECS in pHEN6c vector

The generated CD2- and CD7-sdAb from VIB were supplied in *E. coli* TG1, harboring the recombinant vector pMECS, containing the genes encoding for sdAb. To circumvent the loss of His-Tag if sdAb are produced in pMECS vectors, the His-Tags are likely to be cleaved off upon storage at 4° C. Therefore, sdAb were recloned into pHEN6c vectors, facilitating stable storage of the expressed sdAb.

### 4.6.1 Plasmid isolation

*E. coli* TG1 with pMECS vector encoding for each sdAb were spread on an LB agar plate with 100  $\mu\text{g}/\text{ml}$  ampicillin and 1 % glucose and incubated over night at 37 °C. A colony was picked and shaken in 3 ml LB medium containing 100  $\mu\text{g}/\text{ml}$  ampicillin and 1 % glucose at 250 rpm and 37 °C overnight. The plasmid was then purified using the NucleoSpin Plasmid EasyPure Kit (Machery-Nagel) according to the manufacturer's instructions. For this, 2 ml of the culture was transferred to a 2 ml reaction tube, centrifuged at 500 g for 5 min and the cell pellet was taken up in 150  $\mu\text{l}$  resuspension buffer. Then, 250  $\mu\text{l}$  of blue stained lysis buffer was added, the tube was inverted five times and incubated for 2 min at room temperature. Afterwards, the reaction was stopped by adding 350  $\mu\text{l}$  neutralization buffer, the tube was inverted until the lysate became colorless and subsequently centrifuged at 20000 g for 3 min. The supernatant was added to an enclosed column and centrifuged at 1500 g for 30 s. Then, 450  $\mu\text{l}$  wash buffer

was added to the column and it was centrifuged at 20000 g for 1 min and remaining wash buffer was removed during a second centrifugation that was done equally.

Subsequently, DNA was eluted with 25  $\mu$ l elution buffer by incubation at room temperature for 1 min followed by centrifugation at 20000 g for 1 min. This step was repeated and the concentration of the purified plasmid was measured using the NanoDrop ND-1000 (PeqLab).

#### 4.6.2 PCR to amplify sdAb genes

To amplify the sdAb genes of the previously isolated plasmids, a PCR was performed using the DreamTaq Hot Start PCR Mastermix (2X) (Thermo Fisher Scientific). The reaction was set up as described in the table below.

**Table 17: PCR reaction mix**

Component	Amount
DramTaq Hot Start PCR MasterMix (2X)	25 $\mu$ l
Primer A6E (100 $\mu$ M)	0.5 $\mu$ l
Primer PMCF (100 $\mu$ M)	0.5 $\mu$ l
Plasmid	100 ng
DEPC H <sub>2</sub> O	Fill up to 50 $\mu$ l

The components were mixed in a 1.5 ml tube and incubated according to the following table.

**Table 18: PCR reaction program**

Step	Temperature	Time
1	94 °C	30 s
2	55 °C	30 s
3	72 °C	45 s (30 cycles starting from step 1)
4	72 °C	10 min
5	4 °C	$\infty$

The PCR product was then purified using the NucleoSpin Gel and PCR Clean-up Kit (Machery-Nagel) according to the manufacturer's instructions. The sample was mixed with double the amount of binding buffer, then added onto an enclosed column and centrifuged at 11000 g for 30 s. This was followed by two wash steps with 700  $\mu$ l wash buffer and centrifugation at 11000 g for 30 s. To remove excess wash buffer from the column, the column was centrifuged again at 11000 g for 1 min, after which the DNA was eluted. Therefore, 20  $\mu$ l of elution buffer was

added to the column, incubated at room temperature for 1 min and then centrifuged at 11000 g for 1 min. Subsequently, the concentration of the eluted DNA was measured on the NanoDrop ND-1000 (PeqLab).

#### 4.6.3 Restriction digest

The purified PCR products and the vector pHEN6c were digested using the restriction enzymes PstI-HF and BstEII-HF for 1 h at 37 °C. The composition of the reaction mixtures for the digestion of amplified sdAb genes and pHEN6c are respectively shown below.

After the respective reactions, the digested PCR products of the sdAb genes were purified again using the NucleoSpin Gel and PCR Clean-up Kit (Machery-Nagel), and the digested vector pHEN6c was purified using agarose gel electrophoresis.

**Table 19: Reaction mixture for the digestion of amplified sdAb genes**

Component	Amount
PCR-Product	2 µg
PstI-HF	2 µl
BstEII-HF	2 µl
NeBuffer 10 x	5 µl
DEPC H <sub>2</sub> O	Fill up to 50 µl

**Table 20: Reaction mixture for the digestion of pHEN6c vector**

Component	Amount
Vector pHEN6c	9 µg
PstI-HF	9 µl
BstEII-HF	9 µl
NEBuffer 10 x	15 µl
DEPC H <sub>2</sub> O	Fill up to 150 µl

#### 4.6.4 Gel electrophoresis and purification

For the analysis of the DNA fragments as well as for the inactivation of the restriction enzymes, agarose gel electrophoresis with 1 % agarose gel was performed. For this, 1 g of agarose was completely dissolved in 100 ml of 1xTAE buffer by heating, after which ethidium bromide was added (C<sub>END</sub> 0.6 µg/ml). The respective samples were mixed with 20 µl of 6x loading buffer and loaded into the pockets. For subsequent interpretation of sample size, an additional 6 µl of

1 kb or 100 bp ladder was loaded to an additional well. Electrophoresis was performed at 110 V for 30 – 45 min in a Compact M Horizontal Gel Electrophoresis Apparatus (Biometra) and the results were analyzed and documented using the BioDocAnalyze gel documentation system (Biometra). Desired PCR products were cut out and purified using the Nucleospin Gel and PCR Cleanup kit (Macherey-Nagel) according to the manufacturer's instructions. Then, PCR products were eluted using 20 µl DEPC H<sub>2</sub>O and the concentration was measured using NanoDrop ND-1000 (PeqLab).

#### 4.6.5 Ligation of sdAb genes and pHEN6c vector

A molar ratio (n) of 1:3 was chosen for ligation of the nanobody genes with vector pHEN6c (vector:insert). The used amounts of sdAb-inserts and pHEN6c-vector were calculated with regard to their length according to the following formula:

$$m_{insert} = n \times \left( \frac{C_{insert}}{C_{vector}} \right) \times \left( \frac{length (bp)_{insert}}{length (bp)_{vector}} \right)$$

The reaction mix was set up according to table 21 and ligation was performed at room temperature for 5min, followed by storage on ice.

**Table 21: Reaction mix for ligation**

<b>Component</b>	<b>Amount</b>
DNA Vector	50 ng
Insert	variable
Quick Ligase	1 µl
Quick Ligase Buffer	10 µl
DEPC H <sub>2</sub> O	Fill up to 150 µl

#### 4.6.6 Transformation of chemically competent E. coli

Chemically competent E.coli bacteria (NEB5α) were quickly thawed on ice, after which 5 µl of previously prepared ligation product was added to 50 µl of bacterial suspension, carefully mixed and incubated for 30 min on ice. Heat-shock was performed for 30 sec at 42 °C and followed by incubation for 2 min on ice. Then, 950 µl S.O.C medium was added to the mix and the bacteria were shaken for 60 min at 300 rpm and 37 °C in a Thermomixer. Afterwards, 50 – 100 µl of suspension were dispersed on LB-agar plates supplemented with Ampicillin (100

µg/ml) and grown over night at 37 °C. A single colony was picked and incubated in 3 ml LB medium (+ 100 µg/ml Ampicillin) over night at 37 °C at 250 rpm, after which it was used for DNA purification.

#### 4.6.7 Generation of electrocompetent *E. coli* WK6

*E. coli* WK6 were spread on an LB agar plate and incubated overnight at 37 °C. The next day, a single colony was picked and shaken in 5 ml of LB medium at 250 rpm and 37 °C overnight. 3 ml of culture was then added to 300 ml of 2xTY medium and cultured at 37 °C and 250 rpm until an OD600 of 0.80 was reached. The bacterial culture was then distributed to six 50 ml centrifuge tubes and chilled on ice for one hour before centrifugation at 3300 rpm and 4 °C for 7 min. All further steps were done at 4 °C. Supernatant was discarded and after resuspension of each pellet with 25 ml of 1 mM HEPES, centrifugation was repeated at 3200 rpm for 7 min. Each pellet was then taken up in 25 ml of 10 % glycerol and centrifuged at 3200 rpm for 7 min. Subsequently, all bacteria were resuspended in a total volume of 40 ml of 10 % glycerol, centrifuged at 3200 rpm for 6 min and resuspended up in 2.5 ml of 10 % glycerol. These electrocompetent *E. coli* WK6 were then stored in small volumes at -80 °C.

#### 4.6.8 Transformation of electrocompetent *E. coli*

25 µl of electrocompetent *E. coli* WK6 were mixed with 1 µl of purified plasmid in a GenePulser cuvette and subsequently electroporated at 1800V with a time constant of approximately 5.0 ms. Afterwards, the mixture was rapidly resuspended in 500 µl of LB medium and shaken at 37 °C and 250 rpm for 1 h. Then, 100 µl of culture was spread on an LB agar plate containing 100 µg/ml ampicillin and incubated at 37 °C overnight. The next day, a colony was carefully picked and shaken in 3 ml LB medium supplemented with 100 µg/ml ampicillin at 250 rpm and 37 °C overnight. Afterwards, 500 µl of this culture was mixed with 500 µl of 50 % glycerol and stored at -80° C.

## 4.7 Production and purification of sdAbs

The production of CD2- and CD7-sdab was done according to instructions provided by VIB after previous recloning in pHEN6c vector and transformation of electrocompetent *E. coli* WK6 with CD2- and CD7-sdAb.

### 4.7.1 Production of sdAbs in bacterial culture

*E. coli* WK6 glycerol stocks were scraped using a pipette tip and carefully spread on an agar plate supplemented with ampicillin ( $c_{\text{END}} = 100 \mu\text{g/ml}$ ) and 1 % glucose. After the plates were incubated over night at 37 °C, a single colony was carefully picked and transferred to 10 ml LB medium supplemented with ampicillin ( $c_{\text{END}} = 100 \mu\text{g/ml}$ ) 1 % glucose. The bacteria were shaken over night at 37 °C and 250 rpm and afterwards, 2 ml of this suspension was added to a 2 l baffled shaker flask and mixed with 660 ml of TB medium supplemented with ampicillin ( $c_{\text{END}} = 100 \mu\text{g/ml}$ ). The culture was then shaken at 37 °C and 250 rpm until an OD600 of 0.6 – 0.9 was reached, which is when IPTG ( $c_{\text{END}} = 1 \text{ mM}$ ) was added to induce sdAb-expression and the culture was shaken over night at 28 °C and 250 rpm until an OD600 of 25 – 30 was reached. Then, the culture was centrifuged at 8000 g for 8 min and the pellet was resuspended in 8 ml of TES buffer. This was followed by incubation on ice at 250 rpm for one hour before 12 ml of TES/4 were added to the suspension and shaken for an additional hour on ice at 250 rpm. Afterwards, the bacterial lysate was centrifuged at 8000 g and 4 °C for 30 min and the transparent supernatant was carefully transferred to a new Falcon for subsequent His-Tag purification or stored at -20 °C.

### 4.7.2 His-Tag purification

His-Tag purification of produced sdAbs was performed using the HisPur™ Ni-NTA Spin Purification Kit (3 ml) (Thermo Fisher Scientific) with a slightly modified protocol. All steps were performed at room temperature and each centrifugation was conducted at 700 g for 2 min. After each centrifugation, the flow-through was kept for later analysis via SDS-PAGE.

After initial centrifugation of the columns to remove storage buffer, equilibration of the columns was performed by adding 6 ml of equilibration buffer (10 mM imidazole) to the column, which was then centrifuged again. Afterwards, 15 ml of previously in bacteria produced extracted supernatant was mixed with 5 ml of equilibration buffer and added to the column. The column was incubated at 4 °C for 30 min on a rotator, after which it was

centrifuged again and washed twice with 6 ml wash buffer (25 mM imidazole in PBS) and subsequent centrifugation. After a third wash with 6 ml wash buffer (50 mM imidazole in PBS), the column was eluted four times with 3 ml elution buffer (250 mM imidazole in PBS) each. Purity of the purified sdAbs was assessed via SDS-PAGE or via SE-HPLC and Mass Spectroscopy by Lisa Russelli from the nuclear medicine department.

#### 4.7.3 SDS-PAGE

30 µl of each HIS-Tag purification step was mixed with 10 µl of 4X LAEMMLI buffer and incubated for 5 min at 95 °C. Then, 20 µl of each sample and 7 µl of a prestained protein ladder were applied to the pockets of a NuPAGE Bis-Tris Mini gel and run for 35 min at a constant voltage of 200 V. The gel was then stained in a Coomassie Brilliant Blue solution for one hour on a plate shaker and then panned in a destaining solution overnight. Afterwards, when the protein bands were clearly visible, the gel was scanned using BioDocAnalyze (Biometra).

#### 4.7.4 Concentration and buffer exchange

Concentration and buffer exchange of the sdAbs was performed using Amicon Ultra-15 centrifuge filter units (3K) (Merck). For this, the column was first rinsed with sterile PBS before the pooled elution steps of the His-Tag purification were added to the column and it was centrifuged for 60 min at 4000 g and 8 °C. The flow-through was discarded and 15 ml of sterile PBS was added to the column for buffer exchange and it was then centrifuged again for 60 min at 4000 g and 8 °C. The remaining solution in the column contained the concentrated sdAb in PBS and was carefully removed. The concentration of the sdAb was then measured on the NanoDrop ND-1000 (PeqLab), after which the sdAb was stored at -80°C or used for further applications.

### 4.8 In vivo experiments

NSG mice aged 6 to 12 weeks were used to study the influence of nanobodies on T cell cytotoxicity in vivo. The experimental animals were kept at the Center for Preclinical Research of the Technical University of Munich at TranslaTUM according to the institute guidelines and after approval of the local authorities.

#### 4.8.1 ML2 tumor model in NSG mice

ML2-B7 or ML2-B15 tumor cells were washed twice, resuspended in PBS at a concentration of  $5 \times 10^7$  cells/ml and kept on ice until injection. 200  $\mu$ l of cell suspension were subcutaneously (s.c.) injected either into the left and right flank of the mice for the tumor-rejection studies or above the left and right shoulder blades, with ML2-B7 cells injected on the right side and ML2-B15 cells on the left side. Tumor-growth kinetics were assessed by caliper measurement and indicated as tumor size calculated by length x width of the.

#### 4.8.2 Adoptive T-cell transfer

Transfer of retrovirally transduced T cells was performed either intratumorally (i.t.) or intravenously (i.v.). T cells were washed twice, resuspended in PBS at a concentration of  $1 \times 10^8$  cells/ml and kept on ice until injection. For intratumoral and intravenous injection, 200  $\mu$ l of cell suspension containing  $2 \times 10^7$  T cells were injected either directly into the tumor or into the tail vein of tumor bearing mice.

#### 4.8.3 PET/MRI Imaging

All the imaging studies were performed using a nanoScan 3T PET/MRI scanner (Mediso). PET/MRI imaging of mice was performed in cooperation with the preclinical imaging team (Sybille Reeder, Markus Mittelhäuser, Hannes Rolbieski) from the department of nuclear medicine, Klinikum rechts der Isar in Munich. Mice were anesthetized using 1.5 % isoflurane and subsequently injected with the tracer into the tail vein. Right before image acquisition, mice were placed in the device in prone position under constant anesthesia with 1.5 % isoflurane. The initial MRI scan of 10 min was followed by acquisition of static PET emission images for 20 min, after which the mice were sacrificed for further ex vivo analyses. The obtained PET/MRI images were reconstructed, fused and further processed using the Nucline software (Mediso). Tracer uptake was displayed as standardized uptake value (SUV) and images were shown.

## 4.9 Ex vivo analyses

Following the respective in vivo experiments, mice were euthanized using isoflurane and cervical dislocation to minimize distress for the animals.

### 4.9.1 Biodistribution

Biodistribution studies were performed after animals were sacrificed to examine the in vivo distribution of tracer. Therefore, blood, heart, lung, spleen, liver, pancreas, kidney, stomach, small intestine, large intestine, bladder, muscle, femur, tail and brain were collected, weighted and the respective activity was quantified using a gamma-counter. The tracer accumulation for each sample was expressed as percentage of injected dose per gram of tissue (%ID/g).

### 4.9.2 Flow cytometry analysis of murine tissue

Blood was collected via cardiac puncture of the sacrificed animal, mixed with 10 ml of ACK buffer and incubated at room temperature for 5 min. Then, 5 ml of FACS buffer was added, the mix was centrifuged for 5 min at 500 g and afterwards stained as previously described.

Murine organs and tumors were mashed and mechanically filtered through 40  $\mu$ m filters in PBS, after which they were stained as previously described.

Mechanically filtered spleen suspensions were centrifuged for 5 min at 500 g and then resuspended in 2 ml ACK buffer and incubated for 5 min at room temperature for erythrocyte lysis. Lysis was then stopped by addition of 10 ml FACS buffer, the cell suspension was centrifuged for 5 min at 500g and the cells were subsequently stained as previously described.

## 4.10 Statistical analysis

Data are presented as mean  $\pm$  standard deviations (SD). Statistical analysis of results was performed using GraphPad Prism software version V.8.0.2 using a two tailed non-parametric test (Mann-Whitney test) as indicated in Figure legends.

### 3 Results

#### 3.1 Production and purification of CD2- and CD7-sdAb

In cooperation with the VIB Nanobody Core facility of the Vrije Universiteit Brussel (VUB), single-domain antibodies were generated against the human surface proteins CD2 (CD2-sdAb) and CD7 (CD7-sdAb) respectively. For this purpose, llamas were immunized weekly with the carrier-free recombinant extracellular domains of human CD2 and CD7 for up to five weeks. Afterwards, llama lymphocytes were used to generate a phage library to screen for antigen-specific sdAb (Figure 4). Panning of the phage-library and subsequent ELISA against either CD2 or CD7 revealed 19 sdAb specific for CD2 and 63 sdAb specific for CD7. The 19 CD2-specific sdAb are comprised of sdAb from four different CDR3-subgroups, while six CDR3 subgroups are found in the 63 CD7-specific sdAb.

Of the 19 CD2-specific sdAb, only one clone, #ID 10563, showed consistent and repeatable binding and was the focus of the CD2-specific sdAb. Similarly, of the 63 generated CD7-specific sdAb, clone #ID 10215 exhibited consistently strong binding and was subsequently characterized (Table 22).

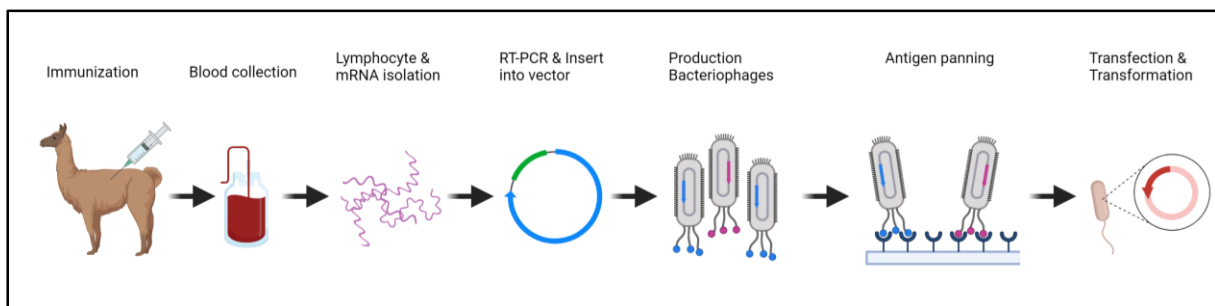


**Figure 4: Scheme of the generation and identification of sdAb specific for CD2 and CD7.**

Llamas were immunized against the human T-cell surface proteins CD2 and CD7 respectively, with subsequent blood collection and isolation of Lymphocytes. Extracted mRNA from these lymphocytes were used to amplify sdAb gene regions and clone them into phage display vectors for construction of a phage display library. This library was then used for antigen panning against immobilized CD2 or CD7 respectively, where bound sdAb clones were selected and transformed into *E.coli* for further use. (Created with BioRender.com)

### 3.1.1 Recloning of sdAb genes to pHEN6 vector and transformation in *E. coli* WK6 strain

The generated CD2- and CD7-sdAb from VIB were supplied in *E. coli* TG1, harboring the recombinant vector pMECS, which contains the genes encoding for sdAb. Sequences for the sdAb are followed by a HA- and His-Tag, which can be used for purification and subsequent screening. However, once sdAb are expressed and purified in pMECS vectors, the His-Tags are likely to be cleaved off upon storage at 4 °C. To circumvent this, sdAb were recloned into pHEN6c vectors, which simultaneously removed the HA-Tag and allowed for stable storage of the expressed sdAb. Furthermore, in order to increase expression yields of sdAb, the newly recloned pHEN6c vectors were used to transform a non-suppressor *E. coli* strain (WK6) with the sdAb-genes.

As a result, CD2- and CD7-sdAb could be expressed in a non-suppressor *E. coli* strain by utilizing a vector that allows for stable storage and downstream applications via His-Tag. Subsequent production and purification of CD2- and CD7-sdAb was done according to instructions provided by VIB. In short, *E. coli* bacteria harboring sdAb-genes were inoculated overnight, after which Isopropyl- $\beta$ -D-thiogalactopyranosid (IPTG) was added to induce Lac-operon dependent expression of sdAb. After overnight incubation, sdAb were extracted from the *E. coli* periplasm and purified using Immobilized metal affinity chromatography (IMAC). This allowed for stable and high-yielding production as well as isolation of CD2-sdAb and CD7-sdAb as a foundation for further analysis.

**Table 22: Protein sequences and CDR3 allocation of CD2- and CD7-sdAb**

Clone	CDR3 group	Protein sequence
CD2 - 10563	4	QVQLQESGGGLVQAGGSLVSVCTASGRTFSNYAVGWFRQAPGKEREFVATIHGSDTTTAYA DSVKGRFTISRDNKNTVFLQMNSLKPEDTAVYYCAATWSSGYLFRSPTQYDYWGQGTQVT VSSAAAYPYDVPDYGSHHHHHH
CD7 - 10215	2	QVQLQESGGGLVQAGGSLRLSCAASGRTFSDYLMGWFRQTPGKEREFVAAYIWNAGSTYYA DSVKGRFTISRDNKNTMYLQMNSLKPEDTAVYYCAAG---QR--- GLAYARTYDYDYWGQGTQVTVSSAAAYPYDVPDYGSHHHHHH

### 3.1.2 Determination of purity and mass of generated CD2- and CD7-sdAb

After production in *E. coli* and isolation via IMAC, both an SDS-PAGE and a high-performance liquid chromatography (HPLC) analysis were performed to determine the purity of the examined sdAb. SDS-PAGE gel electrophoresis showed a high degree of purity with neither visible agglomeration nor isoforms for anti-CD2-sdAb and anti-CD7-sdAb respectively (Figure 5A). The size-exclusion chromatography (Figure 5B) for anti-CD2-sdAb (top) and anti-CD7-

sdAb (bottom) were able to confirm the results by displaying a single sharp elution profile for each sdAb. Additionally, mass spectrometry (MS) analysis combined with high-performance liquid chromatography (HPLC) of either sdAb further supported the purity of the generated sdAb by revealing no contaminants or aggregates (Figure 5C). Mass spectrometry also revealed the precise masses of each sdAb, with CD2-sdAb's mass being 14.2 kDa (Figure 5C, top) and CD7-sdAb's mass being 14.6 kDa (Figure 5C, bottom). The in-depth validation and characterization of both the purity and mass of the produced sdAb allowed for ensuing first analyses to evaluate the binding properties of CD2-sdAb and CD7-sdAb.

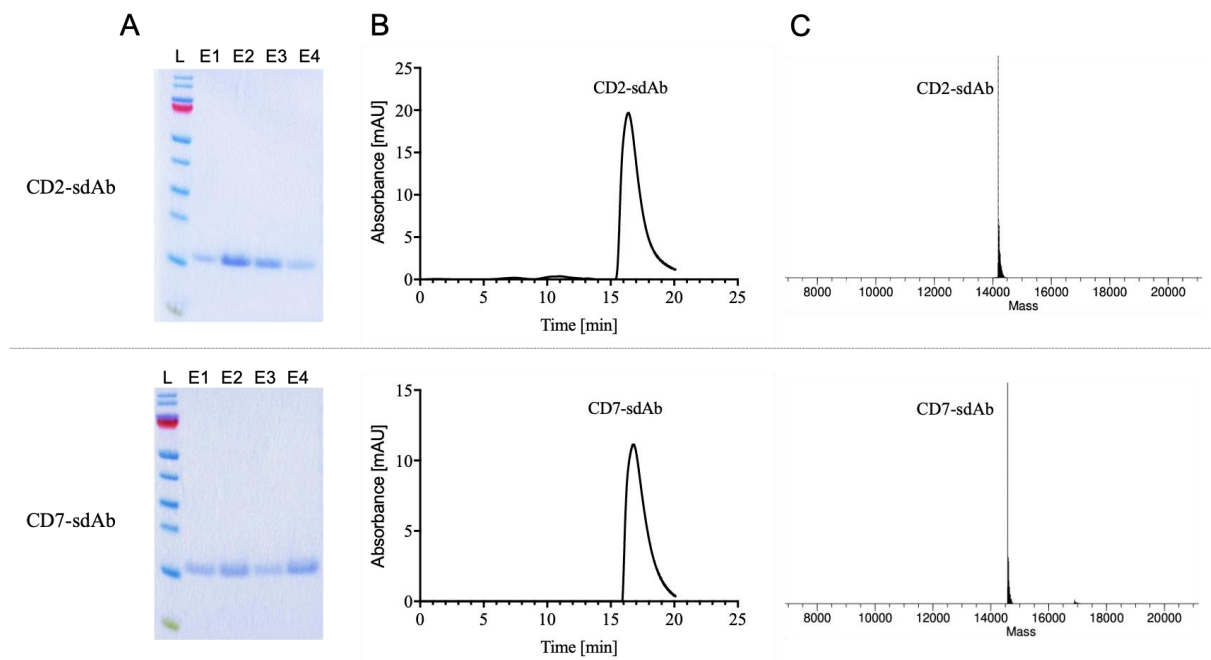


**Figure 5: Size-validation and -characterization of CD2- and CD7-sdAb after His-Tag based purification.**

Assessment of size-characteristics for CD2-sdAb (top) and CD7-sdAb (bottom). (A) SDS-PAGE gel electrophoresis of eluted CD2-sdAb and CD7-sdAb after His-Tag purification (L: Ladder Size marker, E1 – E4: elution steps) (B) Size-exclusion chromatography analysis of CD2-sdAb and CD7-sdAb. (C) HPLC-MS analysis of CD2-sdAb and CD7-sdAb. (In cooperation with SB)

## 3.2 Binding characteristics of CD2- and CD7-sdAb

To ensure that CD2-sdAb and CD7-sdAb can reliably and selectively depict T cells as key players during immunotherapy, both a highly specific as well as stable binding of CD2-sdAb and CD7-sdAb to T cells is vital. For the purpose of specificity, both sdAb were analyzed in regards to their binding to human CD8<sup>+</sup> T cells, tumor cells that were retrovirally transduced with the respective target antigen as well as target-antigen knockout leukemia cells. Stable and resilient binding was tested in a thermal binding assay spanning six hours.

### 3.2.1 Binding of CD2- and CD7-sdAb on human CD8<sup>+</sup> T cells

As a pan T-cell marker, CD2-sdAb and CD7-sdAb have to exhibit consistent and strong binding to human T cells. To verify this, human CD8<sup>+</sup> T cells were isolated from whole blood and used as target cells for flow cytometry based binding analysis of both sdAb. As a control, a non-targeting irrelevant sdAb (R3b23-sdAb) served as a reference for non-specific binding during the experiment. The control sdAb features the same basic structure as the CD2- and CD7-specific sdAb, but with a binding site that does not target any structure present in humans. Therefore, inclusion of the control sdAb is used to exclude any unspecific binding of the sdAb basic framework-structure. To verify CD2- and CD7-presence on the target cells and serve as a positive control for the sdAb, full monoclonal antibodies targeting CD2 (CD2-mAb) and CD7 (CD7-mAb) respectively were used.

The control R3b23-sdAb did not exhibit binding to CD8<sup>+</sup> T cells throughout the experiment, thereby indicating that unspecific binding due to the overall sdAb-structure is nonexistent (Figure 6, grey). Use of the CD2-mAb (Figure 6A) and CD7-mAb (Figure 6B) resulted in distinct binding to CD8<sup>+</sup> T cells and confirmed the presence and accessibility of both target antigens. Similarly, both CD2-sdAb (Figure 6A) and CD7-sdAB (Figure 6B) were shown to distinctively bind to CD8<sup>+</sup> target cells compared to the internal control R3b23-sdAb. This confirmed the aptness of both sdAb to target human CD8<sup>+</sup> T cells efficiently. However, to rule out the possibility of unspecific binding not just based on the sdAb-structure, but also to surface molecules other than CD2 and CD7 on CD8<sup>+</sup> T cells, further verification of binding specificity was necessary and subsequently performed.

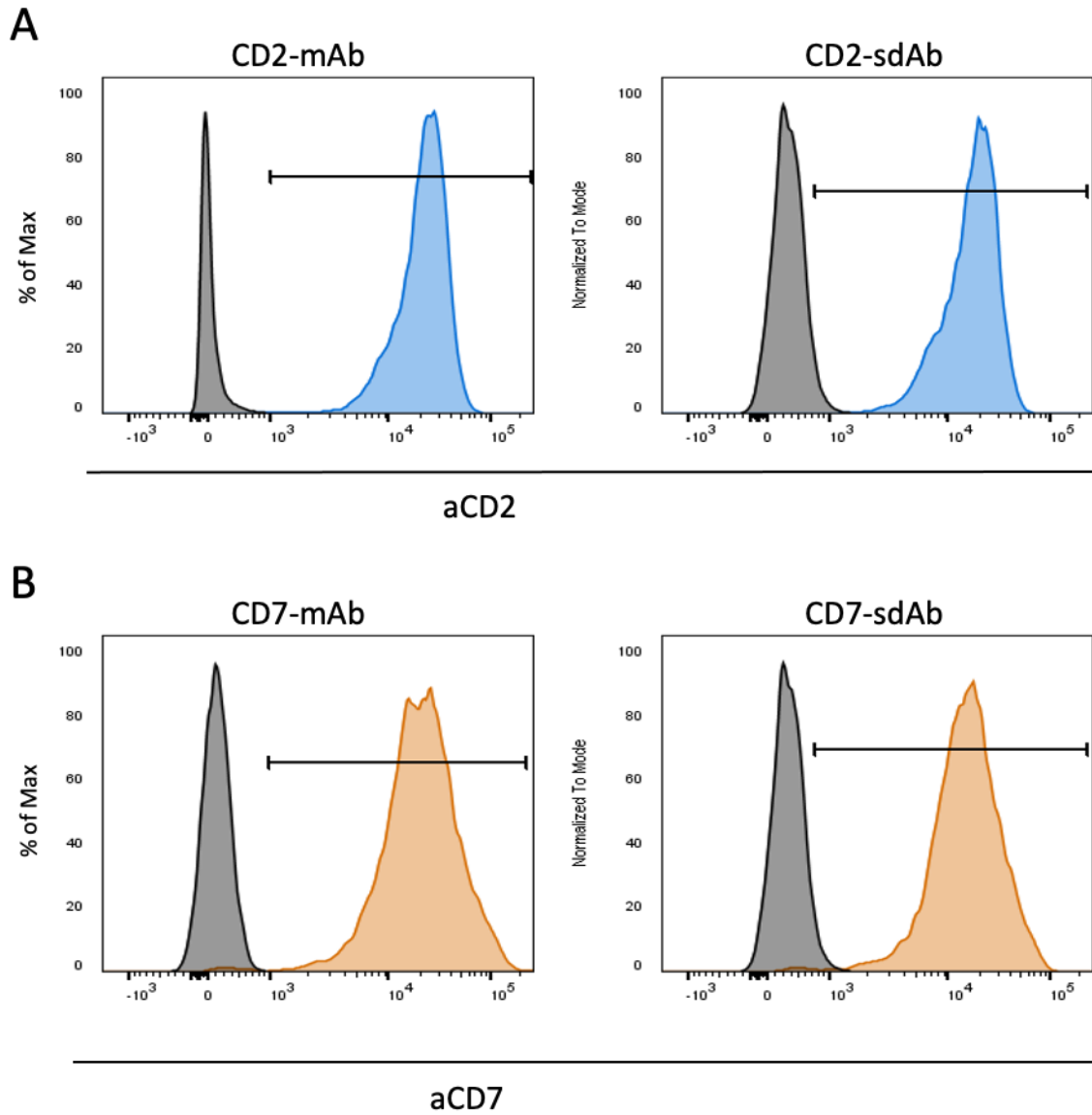


**Figure 6: Analysis of the capability of CD2-sdAb and CD7-sdAb to bind human CD8<sup>+</sup> T cells.**

Flow cytometry-based determination of binding specificity to human CD8<sup>+</sup> T cells of CD2-sdAb (A) and CD7-sdAb (B). A non-targeting irrelevant sdAb (R3b23-sdAb) was used as a control to exclude unspecific binding of the sdAb basic framework-structure (grey histogram). Monoclonal antibodies against CD2 (A) and CD7 (B) were used as a positive control to verify possible binding of respective target antigens.

### 3.2.2 Specific binding on target-antigen transduced tumor cell line U698M

While the binding assay of CD2-sdAb and CD7-sdAb to human CD8<sup>+</sup> T cells was successful, it did not undoubtedly proof CD2- and CD7-specificity. Therefore, the CD2- and CD7-negative B cell lymphoma tumor cell line U698M was transduced with both target antigens respectively. The target cell line U698M was transduced using CD2 and CD7 coupled to the red fluorescent protein DsRed, which served as a marker for transduction efficiency. Flow cytometry analysis of U698M after retroviral transduction with CD2 revealed a transduction efficiency of 38 % of alive single cells (Figure 7A), while CD7-transduction resulted in 27 % of alive U698M cells positive for CD7 (Figure 7B). The consequent partially CD2- or CD7-positive U698M cell lines were subsequently used for single-cell cloning to create a homogenous population of cells that are positive for CD2 or CD7, allowing for a distinct analysis of CD2- and CD7-specificity.

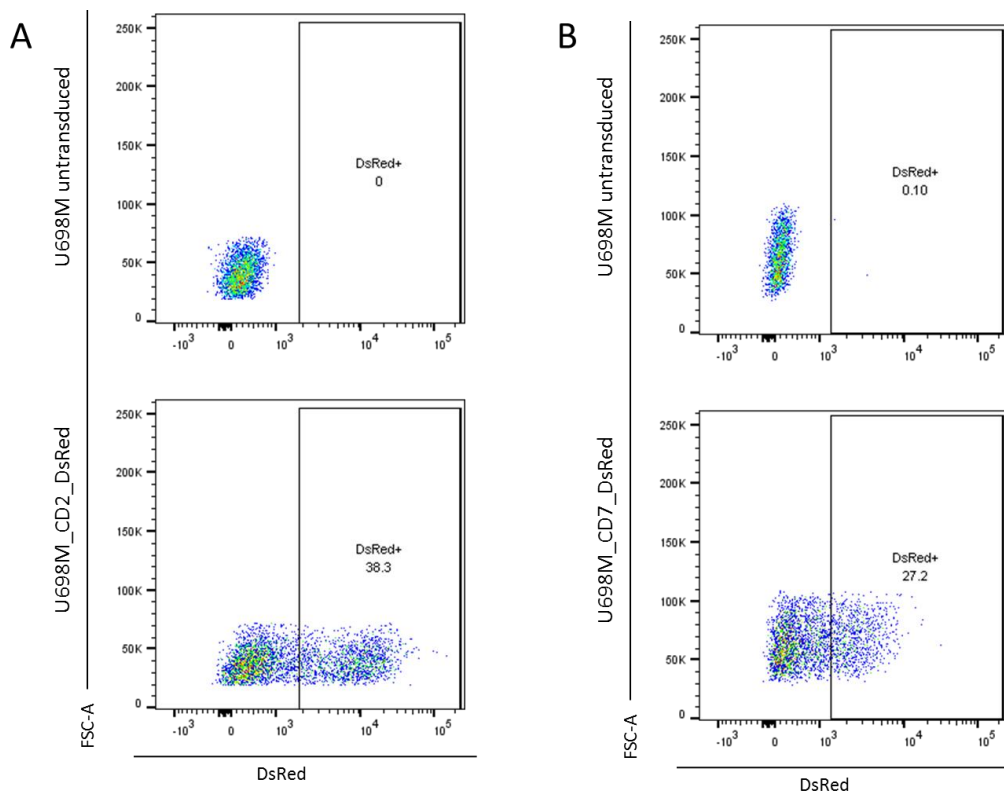


**Figure 7: Transductions of B cell lymphoma tumor cell line U698M with human CD2 or CD7.**

Flow cytometry analysis of U698M cells after retroviral transduction with CD2 (A) and CD7 (B). For each transduction, untransduced U698M cells were used as a negative control (top) and efficiency of transduced U698M cells was examined using DsRed as a fluorescent marker (bottom). (In cooperation with TK)

The thereby generated cell lines were used for flow cytometry analysis to examine if CD2-sdAb and CD7-sdAb are specifically recognizing and binding to their target antigens (Figure 8). R3b23-sdAb was used as a control to rule out unspecific binding. Both the CD2-sdAb and the CD7-sdAb showed no binding to untransduced U698M cells (Figure 8A, B, grey), while a clear and specific binding was observed for the target-antigen transduced cell lines cells (Figure 8A, B, blue). This confirms that both sdAb specifically recognize and bind to transduced human CD2 and CD7 respectively on the surface of otherwise CD2- and CD7-negative tumor cells.

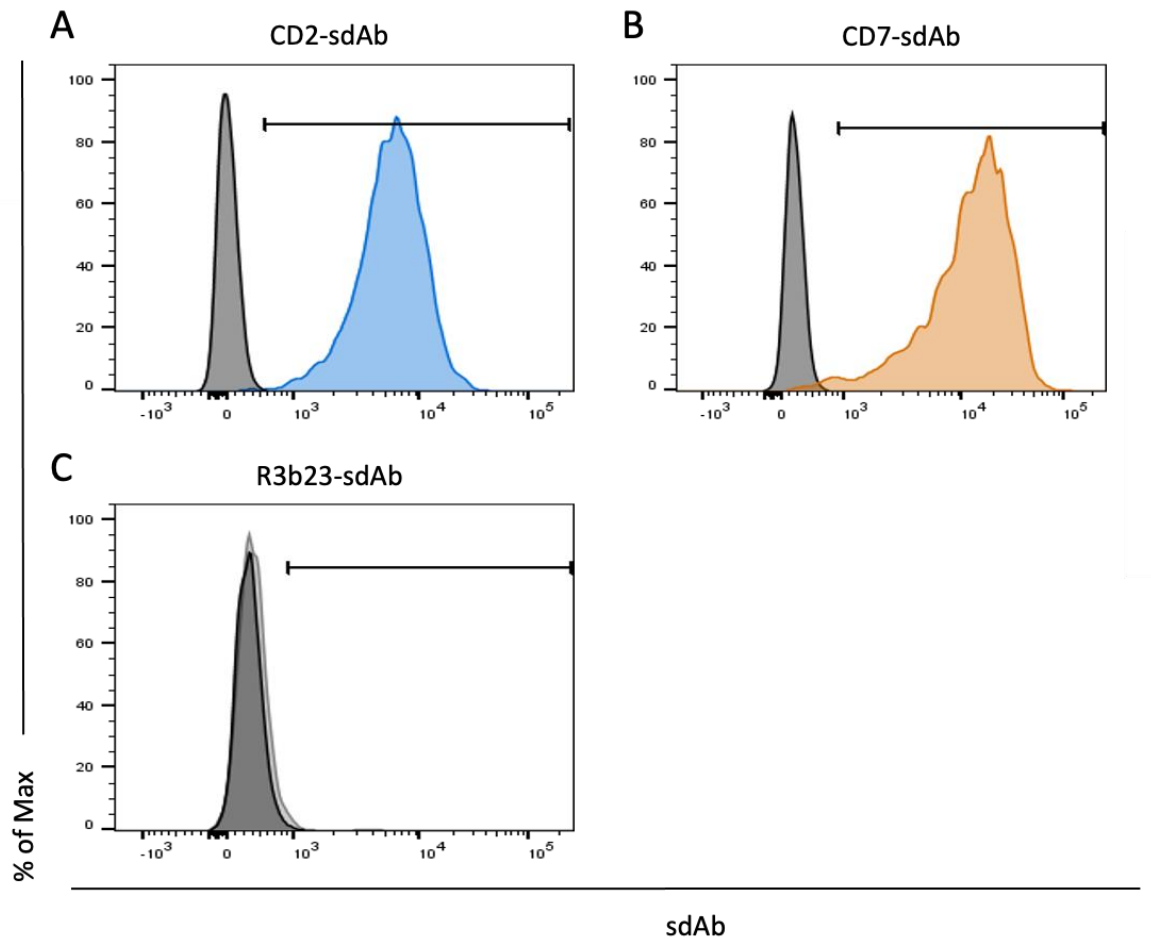


**Figure 8: Analysis of CD2- and CD7-sdAb binding to retrovirally transduced U698M cells.**

Flow cytometry-based determination of binding specificity to retrovirally transduced B cell lymphoma tumor cell line U698M with respective target antigens. (A) CD2-sdAb binding to CD2-transduced U698M cells, with wild type U698M used as a negative control. (B) CD7-sdAb binding to CD7-transduced U698M cells, with wild type U698M used as a negative control. (C) Exemplary binding of R3b23 to CD2-transduced U698M cells, with wild type U698M used as a negative control.

### 3.2.3 Specific binding on T cell leukemia cell line Jurkat E6.1 after CRISPR/Cas9 knockout of CD2 and CD7 respectively

Since target-antigen specificity of CD2-sdAb and CD7-sdAb is crucial for future clinical translation, an additional approach was used. In addition to generating an artificially CD2- and CD7-positive B cell lymphoma tumor cell line with U698M, the naturally CD2- and CD7 positive T cell leukemia cell line Jurkat E6.1 was used to knockout both target antigens. Thus, proving that only naturally occurring CD2 or CD7 are responsible for the respective sdAb binding on a T-cell based cell line.

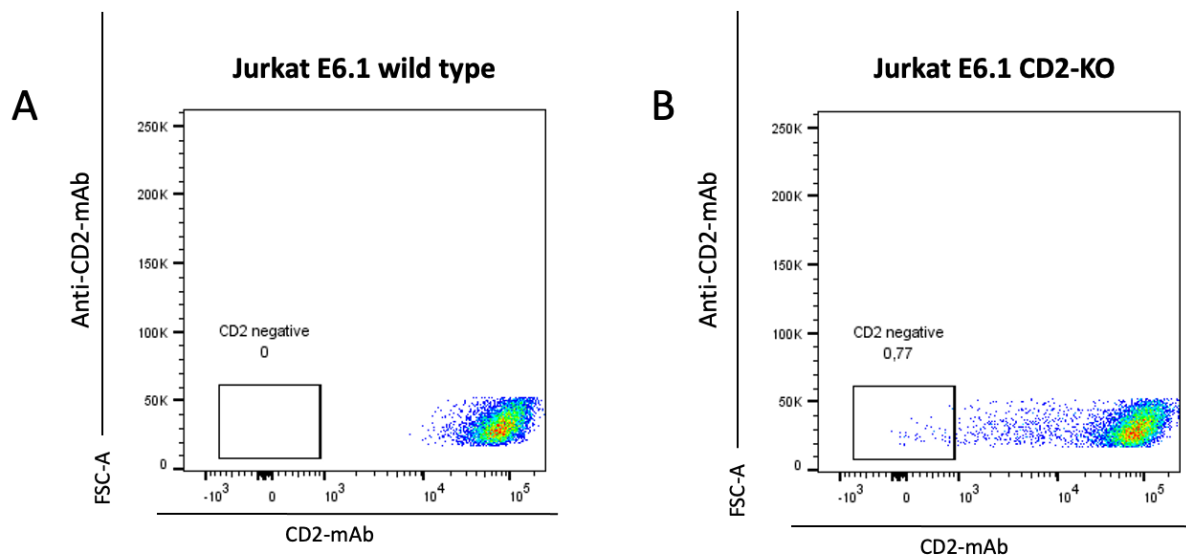


**Figure 9: CRISPR/Cas9-generated CD2-negative Jurkat E6.1 cells after lipofection.**

Flow cytometry analysis of Jurkat E6.1 cells before and after lipofection with RNPs to knockout CD2. (A) Wild type CD2-positive Jurkat E6.1 cells were stained using a CD2-mAb and served as a negative control. (B) Jurkat E6.1 cells after lipofection (Jurkat E6.1 CD2-KO) were equally stained with CD2-mAb and showed a CD2-negative population of 0.77 %. Gates for a successful knockout were set based on unstained wild type Jurkat E6.1 cells. (In cooperation with SB)

Using the CRISPR/Cas9 system, different crispr RNAs (crRNA) were designed to specifically target the first exon of the CD2- or CD7-gene in Jurkat E6.1 cells, leading to frameshift mutations due to non-homologous end joining (NHEJ). In short, combining the specifically designed crRNA with trans-activating crRNA (tracrRNA) led to the formation of guide RNA (gRNA). This gRNA was mixed with Cas9 nuclease to form a ribonucleoprotein (RNP) complex, which was then delivered into the cytoplasm of the target cells by lipofection. Following the lipofection, Jurkat E6.1 cells were analyzed via flow cytometry in regard to their target antigen expression. Wild type Jurkat E6.1 cells were used as a positive control and

exhibited a strong expression of both CD2 and CD7 on its surface, as shown by staining with anti-CD2- and anti-CD7-mAb (Figure 9A, Figure 10A). Wild type Jurkat E6.1 cells were equally homogeneously positive for CD2 and CD7 respectively, with no distinct CD2- or CD7-negative populations (Figure 9A, Figure 10A).

After CRISPR/Cas9-based knockout of CD2, the anti-CD2-mAb did not bind to 0.77 % of all used cells, thereby indicating a knockout efficiency of 0.77 % (Figure 9B). While there was a broader shift in anti-CD2-mAb binding, only 0.77 % fit the previously strictly set gate for CD2-negativity. Similarly, the knockout of CD7 resulted in a CD7-negative population of just 0.086 % of all analyzed cells (Figure 9B). A slight shift of a larger part of the population was visible, yet did not fit the set gate for CD7-negativity.

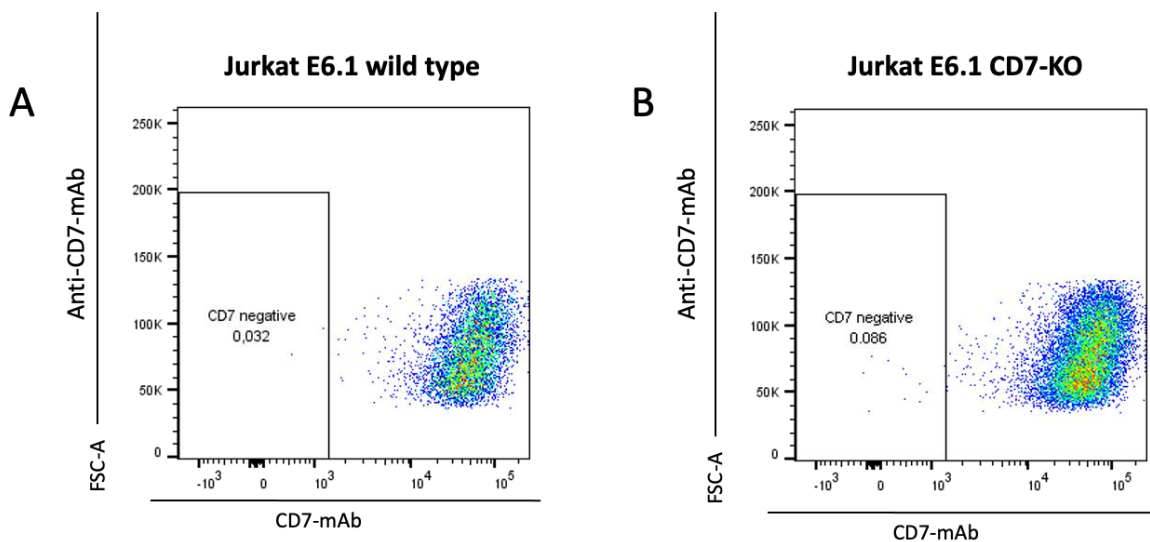


**Figure 10: CRISPR/Cas9-generated CD7-negative Jurkat E6.1 cells after lipofection.**

Flow cytometry analysis of Jurkat E6.1 cells before and after lipofection with RNP to knockout CD7. (A) Wild type CD7-positive Jurkat E6.1 cells were stained using a CD7-mAb and served as a negative control. (B) Jurkat E6.1 cells after lipofection (Jurkat E6.1 CD7-KO) were equally stained with CD7-mAb and showed a CD7-negative population of 0.086 %. Gates for a successful knockout were set based on unstained wild type Jurkat E6.1 cells.

These knockout-rates allowed for single-cell cloning to create a homogenous population of cells that are negative for CD2 or CD7, although the knockout rate of 0.086 % for the CD7-knockout needed a much extensive approach in regards to single-cell cloning. After dilution and seeding, single-cell-clones were grown for three weeks and then used for flow cytometric re-analysis of their respective CD2- or CD7-expression, to screen for a largely target-antigen-negative population. Analysis of CD2-knockout clones (Jurkat E6.1 CD2-KO\_sc) revealed a population which did not show any successful binding of either anti-CD2-mAb or -sAb and could

therefore be described as CD2-negative (Figure 11A). Moreover, since neither anti-CD2-mAb nor the anti-CD2-sdAb bound to the CD2-negative Jurkat E6.1 cells, it proved a distinct CD2-specificity of the analyzed CD2-sdAb.

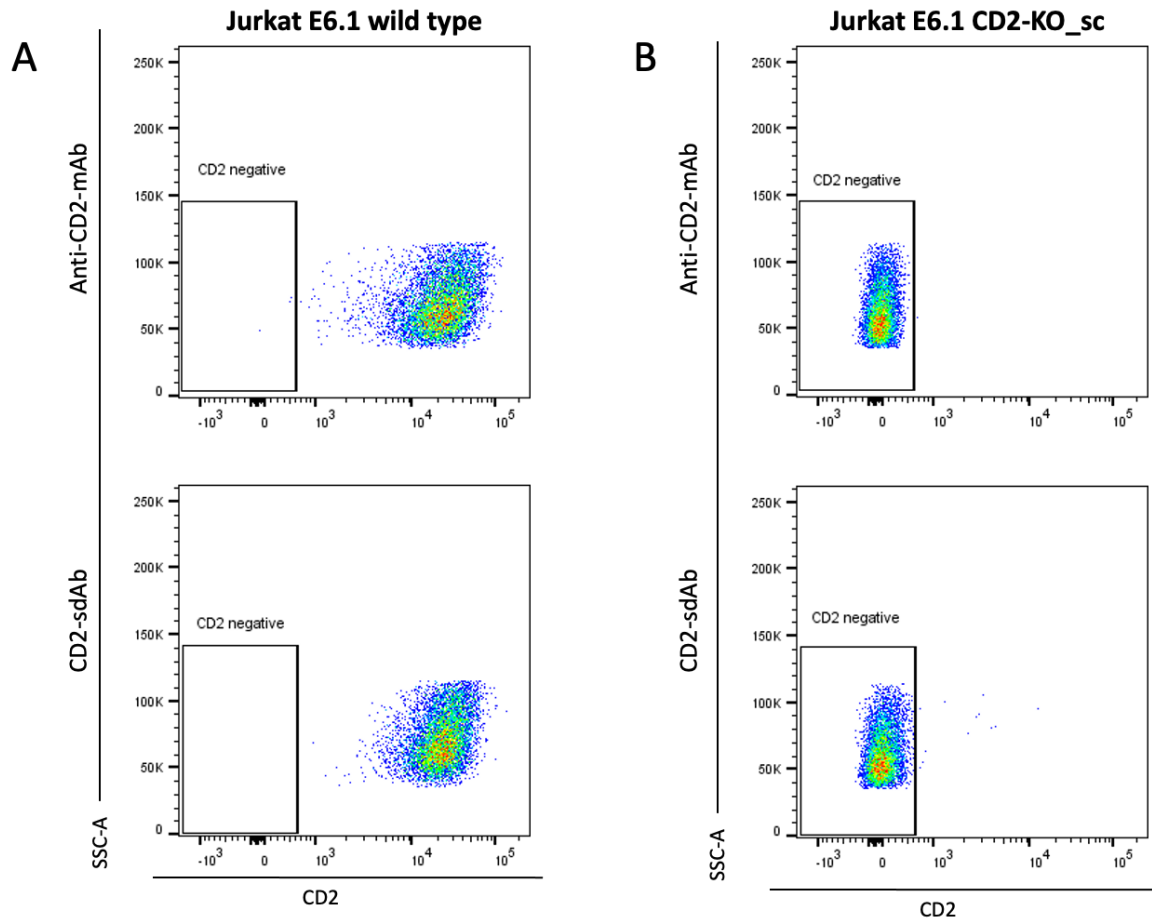


**Figure 11: Flow cytometry analysis of populations based of single-cell clones after CD2 knockout.**

Analysis of populations after single-cell cloning of previously CRISPR/Cas9-based CD2 knockout. Jurkat E.61 wild type cells were used as a positive control to confirm binding of a CD2-mAb and the characterized CD2-sdAb (A). A population based of single-cell cloning after CRISPR/Cas9-based CD2 knockout (Jurkat E6.1 CD2-KO\_sc) was stained with CD2-mAb and CD-sdAb to confirm CD2-binding specificity. (In cooperation with SB)

Equal analysis of clones from the CD7-knockout population revealed a population that was, however, not homogeneously negative for CD7, but only showed a CD7-negative population of 5.8 % (Figure 12). Repetition of single-cell cloning led to a very similar result, indicating that CD7 was not sufficiently knocked out.

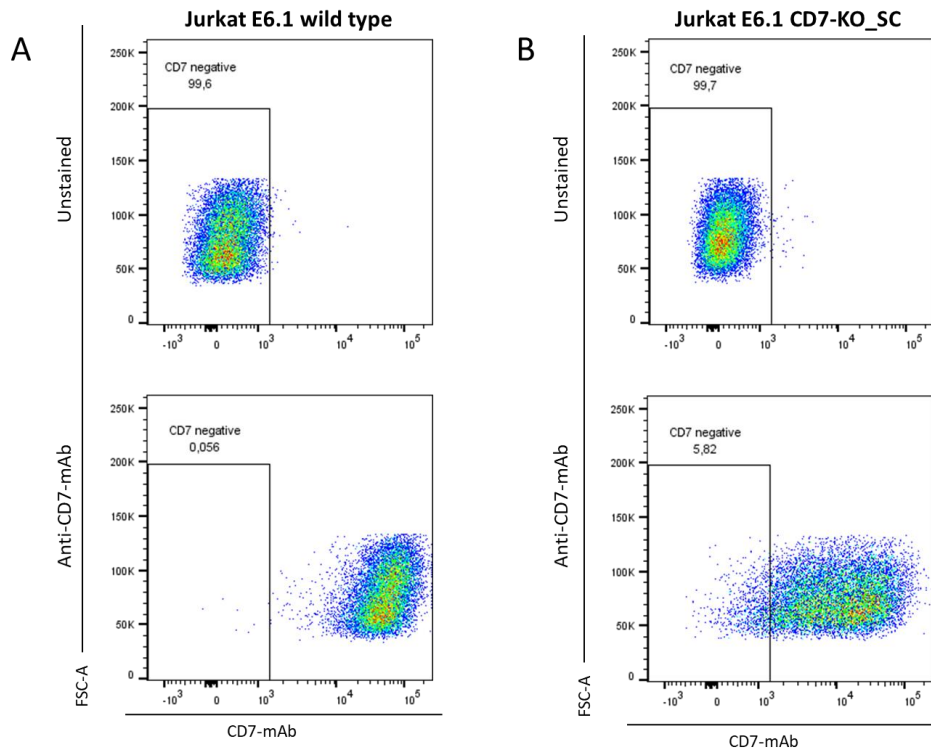


**Figure 12: Flow cytometry analysis of populations based of single-cell clones after CD7 knockout.**

Analysis of populations after single-cell cloning of previously CRISPR/Cas9-based CD7 knockout. Jurkat E.61 wild type cells were used as a positive control to confirm binding of a CD7-mAb and the characterized CD7-sdAb (A), and the population based of single-cell cloning after CRISPR/Cas9-based CD2 knockout (Jurkat E6.1 CD2-KO\_sc) was assessed identically.

To utilize the partially CD7-knocked-out Jurkat E6.1 cells to prove specificity of CD7-sdAb, a cell sort was performed to isolate CD7-negative cells from the partially knocked out population. As a control, Jurkat E6.1 wild type cells were analyzed using CD7-mAb (Figure 13A, top) and CD7-sdAb (Figure 13A, bottom) to show wild type expression of CD7 and functional binding of both constructs.

Immediate re-analysis of the sorted fraction by flow cytometry analysis using CD7-mAb (Figure 13B, top) and CD7-sdAb (Figure 13B, bottom) indicated that the Jurkat E6.1 cells did not express CD7 at the same level on its surface any longer. The CD7-mAb was not able to bind to 93 % of the assessed Jurkat E6.1 cells after previous sort, and the CD7-sdAb did not bind to 95 % of used cells. Therefore, the freshly sorted cells were eligible to conclusively proof

the CD7-binding specificity of CD7-sdAb. Flow cytometry analysis showed only marginal binding of CD7-sdAb to the Jurkat E6.1 CD7-KO\_sort cells, whereas CD7-sdAb was still able to bind over 99 % of wild type Jurkat E6.1 cells.

On top of binding-analysis using target antigen-transduced tumor cell line U698M, the CRISPR/Cas9-based knockout of CD2 and CD7 further supported a very distinct target-antigen specificity of both sdAb.

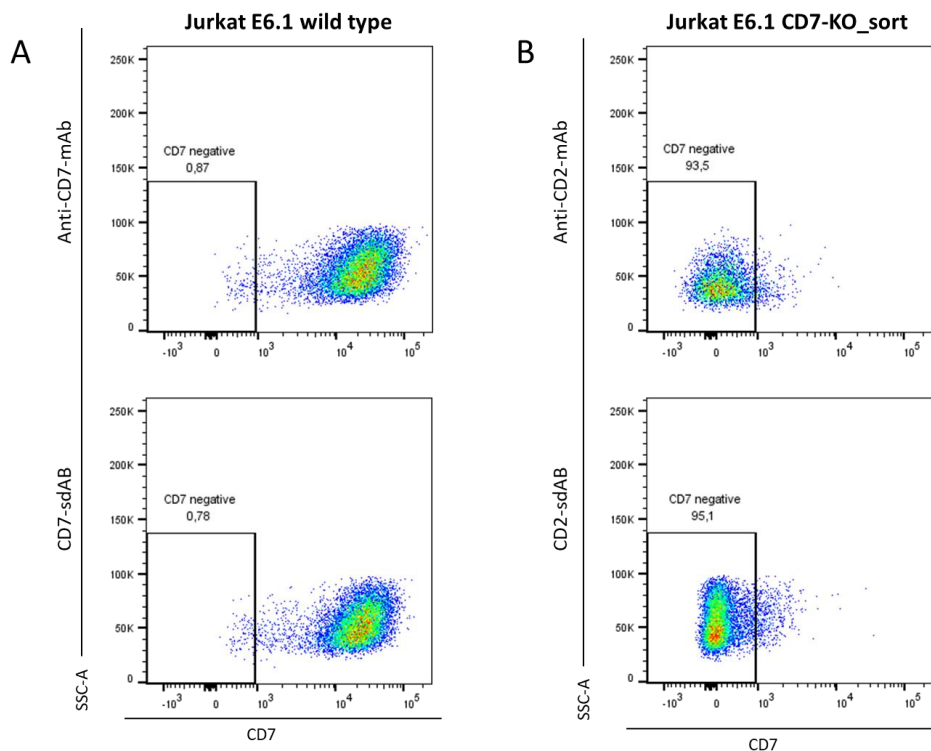


**Figure 13: Flow cytometry analysis of populations after sort for CD7-negative Jurkat E6.1 cells.**

Analysis of populations after CD7-negative based sort of previously CRISPR/Cas9-based CD7 knockout. Jurkat E.61 wild type cells were used as a positive control to confirm binding of a CD7-mAb and the characterized CD7-sdAb (A) and the population after CD7-negative based sort (Jurkat E6.1 CD7-KO\_sort) was assessed identically.

### 3.2.4 Dissociation constant and binding affinity of CD2- and CD7-sdAb

After in-depth characterization and confirmation of the binding specificity of both CD2- and CD7-sdAb, the binding affinity to their target antigens was evaluated and quantified by determination of the respective dissociation constants. Binding affinity was assessed by monitoring CD2- and CD7-sdAb binding to human CD8<sup>+</sup> T cells over the course of different sdAb-concentrations. As a result, both the CD2- and CD7-sdAb showed high-affinity binding. The dissociation constant, and by extension the corresponding binding affinity, was determined

to be  $6.34 \times 10^{-9}$  M for CD7-sdAb (Figure 14A) and  $2.30 \times 10^{-9}$  M for CD2-sdAb (Figure 14B). The irrelevant R3b23-sdAb was used as a negative control (Figure 14C).

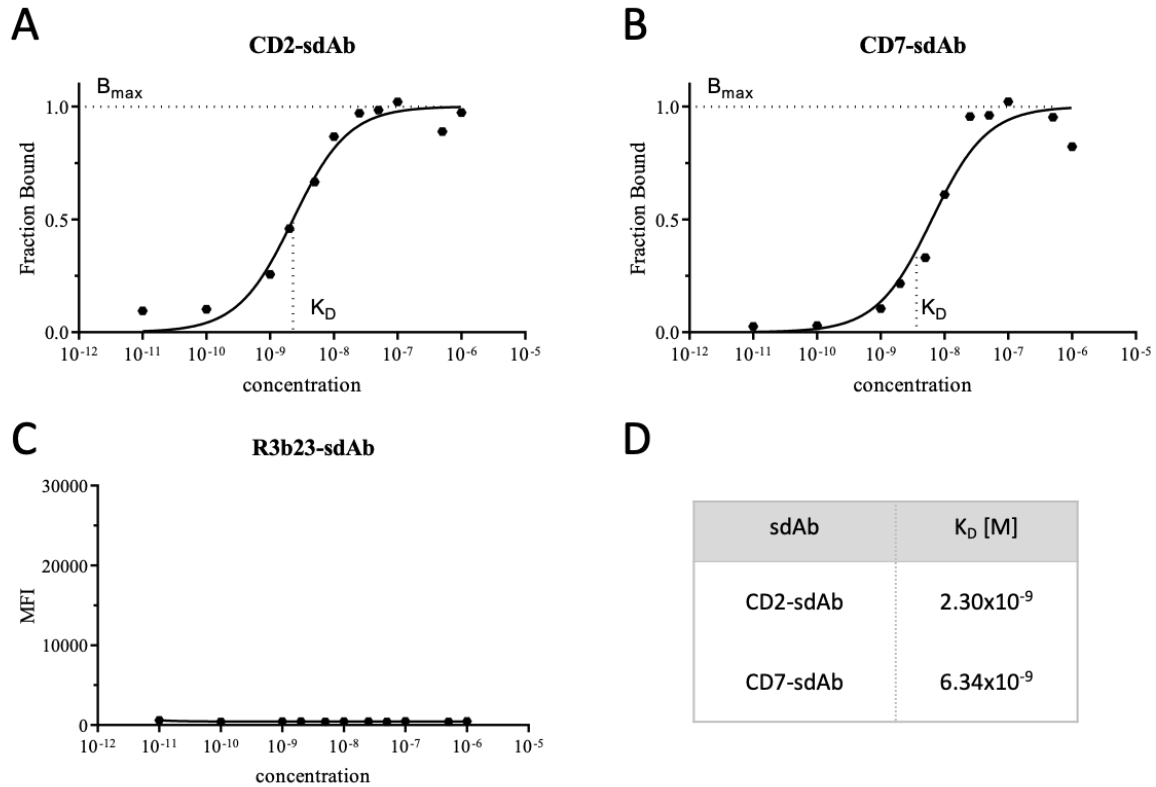


**Figure 14: Binding affinities of CD2- and CD7-sdAb on human CD8+ T cells.**

Determined affinity binding curves for CD2-sdAb (A) and CD7-sdAb (B) at different concentration on human CD8<sup>+</sup> T cells. R3b23-sdAb served as a negative control for unspecific binding (C). Binding of CD2-sdAb (A) and CD7-sdAb (B) is shown as a fraction of the maximum specific binding ( $B_{max}$ ) and the binding intensity of R3b23-sdAb (C) is shown via the MFI at the different concentrations. Measurements were performed in triplicates and data is depicted on a semi-logarithmic scale. The dissociation constants ( $K_D$ ) for CD2-sdAb and CD7-sdAb were calculated based of one-site specific binding and are depicted (D). (In cooperation with TK)

### 3.2.5 Evaluation of thermal stability of CD2- and CD7-sdAb

Besides specific and high-affinity binding to its target antigen, a high thermostability is a desired pharmaceutical property for antibody-binding fragments in regards to clinical translation. Favorable thermostability characteristics of sdAb increase the possibilities for storage, reduce the risk of aggregation and can be used to assess a protein's conformational stability. Thermostability for CD2-sdAb and CD7-sdAb was evaluated by exposing the sdAb to temperatures up to 90° C for as many as six hours, with subsequent binding analysis to human CD8<sup>+</sup> T cells. Both CD2- and CD7-sdAb showed a strong and consistent binding when kept on

either 37 or 60° C for up to six hours (Figure 15). The observed MFI for these temperatures was equal to or even surpassing the control condition that was kept at 4° C. However, the CD7-sdAb showed a reduced binding capability when kept at 90° C for 30 min, decreasing further over time until only a fraction of initial binding remains after six hours (Figure 15B).

Similarly, the CD2-sdAb exhibited stable binding to human CD8<sup>+</sup> T cells, and only when kept at 90° C for two hours onwards was a sharp decline in binding intensity visible (Figure 15A). Conclusively, CD2- and CD7-sdAb show thermal binding capabilities that remain resilient for up to 60° C for six hours. Taken together, the thermostability analysis, the data assessing the detailed binding specificity to their respective target antigens and the strong binding affinity characterize two sdAb with promising binding characteristics for in vivo T-cell tracking.

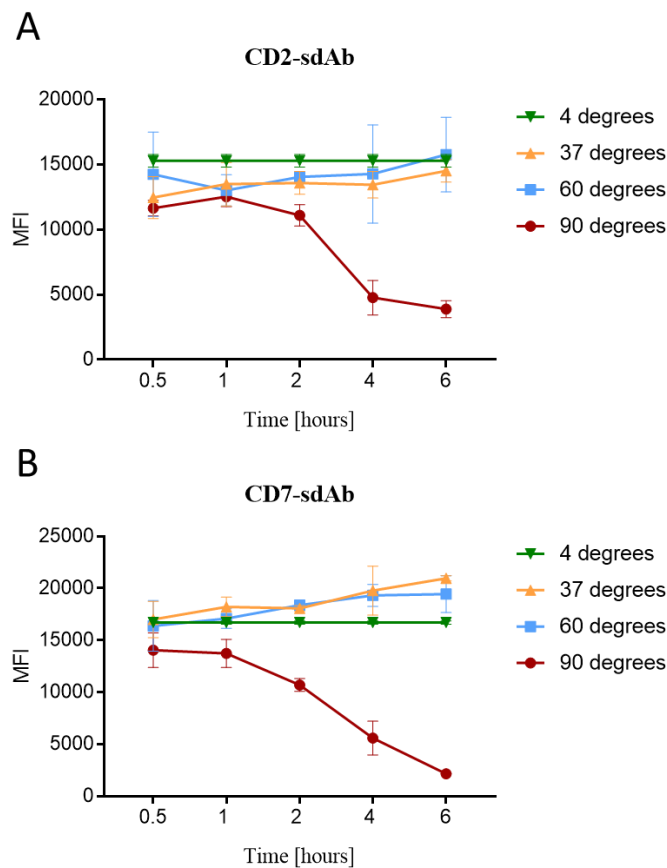


**Figure 15: Evaluation of thermostability of CD2- and CD7-sdAb binding to human CD8<sup>+</sup> T cells via flow cytometry analysis.**

CD2-sdAb (A) and CD7-sdAb (B) were kept at 4 °C, 37 °C, 60 °C or 90 °C for 0.5 h, 1 h, 2 h, 4 h or 6 h, after which their binding capabilities to human CD8<sup>+</sup> T cells were analyzed via flow cytometry. The temperatures of sdAb were kept steady by utilizing heating blocks for 37 °C, 60 °C and 90 °C and a fridge for 4° C. Measurements were performed in triplicates and flow cytometry data is depicted as MFI. (In cooperation with SB)

### 3.3 Impact of CD2- and CD7-sdAb binding on CD8<sup>+</sup> T cells in vitro

After evaluating the general characteristics of CD2-sdAb and CD7-sdAb in terms of binding properties and target-antigen specificity, the next step was to assess whether binding of each tested sdAb to T cells affects their functionality in any way. Ensuring that both tracers can be used to monitor T cells in the context of immunotherapies, without interfering in the therapy itself by influencing the complex immune response, was crucial for subsequent analysis.

#### 3.3.1 Effects of CD2- and CD7-sdAb binding on the dynamic cytotoxic activity of CD8<sup>+</sup> T cells in vitro

To investigate whether CD2- or CD7-sdAb binding results in functional impairment of T cells, the xCELLigence assay was used. This assay allowed for dynamic monitoring of T-cell functionality over the course of 24 h by observing the structure and characteristics of targeted tumor cells via parameters such as cell number, cell adhesion and cell morphology in the presence of T cells. For this experiment, the human melanoma cell line 624.38 Mel was used due to its adherent cell growth and expression of the HLA class I molecule HLA-B\*07:02. HLA-B\*07:02 enables the cell line to present the target antigen needed for T-cell recognition via the retrovirally transduced TCR2.5D6 T-cell receptor.

The used target antigen is myeloperoxidase MPO<sub>5</sub> (MPO) and was retrovirally transduced, coupled to the fluorescence marker DsRed, onto 624.38 Mel cells (Figure 16) to generate a cell line that fulfills the specific requirements needed to be used for the dynamic xCELLigence assay. Transduction efficiency of 624.38 Mel cells with MPO was confirmed by DsRed expression and assessed via flow cytometry, resulting in 77 % of cells expressing DsRed and consequently also the target antigen MPO (Figure 16B). Wild type 624.38 Mel served as a negative control (Figure 16A).

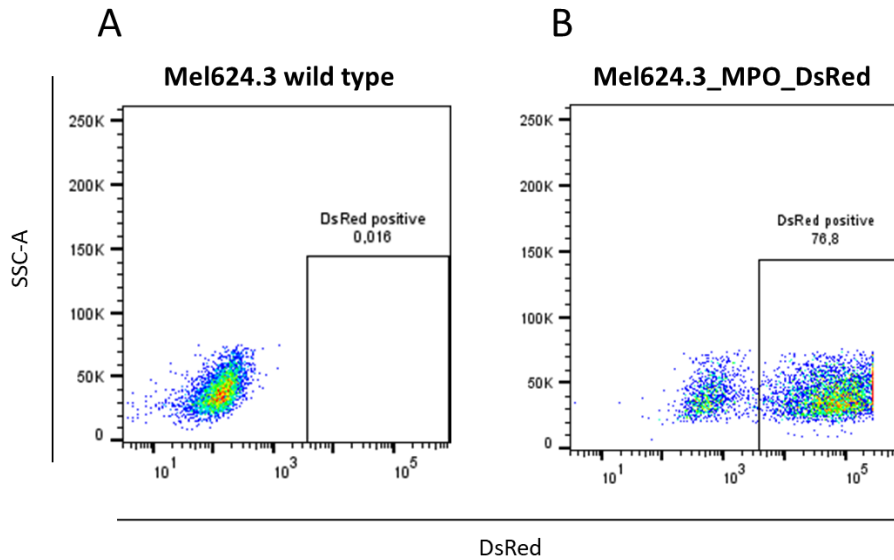


**Figure 16: Transduction efficiency analysis of retrovirally transduced 624.38 Mel cells with MPO.**

Flow cytometry analysis of Mel624.3 wild type cells (A) and Mel624.3 cells after retroviral transduction (B) with MPO coupled to the fluorescence marker DsRed (Mel624.3\_MPO\_DsRed). (In cooperation with TK)

To precisely evaluate the cytotoxic potential of T cells with and without addition of CD2-sdAb or CD7-sdAb, the parameters for the xCELLigence assay had to be defined. Therefore, different assortments of the number of used target tumor cells and effector T cells were tested. Firstly, a stable and consistent tumor growth had to be achieved using the defined number of cells per well. Therefore, various numbers of retrovirally transduced 624.38 Mel cells were grown for 48 h while their cell index was being monitored using the xCELLigence system. Since for subsequent experiments T cells needed to be added 24 h after target-cell growth, finding a cell number resulting in a swift and steady increase of the cell index up to 24 h, continuous growth for the following hours and an eventual plateau within the experimental time frame was essential.

Of the used cell numbers,  $7.5 \times 10^4$  624.38 Mel cells showed ideal progress of the cell index, with a linear trend after 24 h and continuing up until 45 h (Figure 17A, grey). Since T cells will be added for the dynamic cytotoxicity assay, a mixture of 50 % DMEM medium, normally used for cultivation of target cells, and 50 % T-cell medium (TCM) was used to determine ideal cell numbers. To ensure that this medium composition has no detrimental effects itself on tumor growth, it was compared to DMEM medium alone. Again,  $7.5 \times 10^4$  624.38 Mel cells were cultivated in either DMEM medium or a 50/50 mixture of DMEM- and T-cell medium. Observation of the cell index showed no major difference between both conditions (Figure 17B).

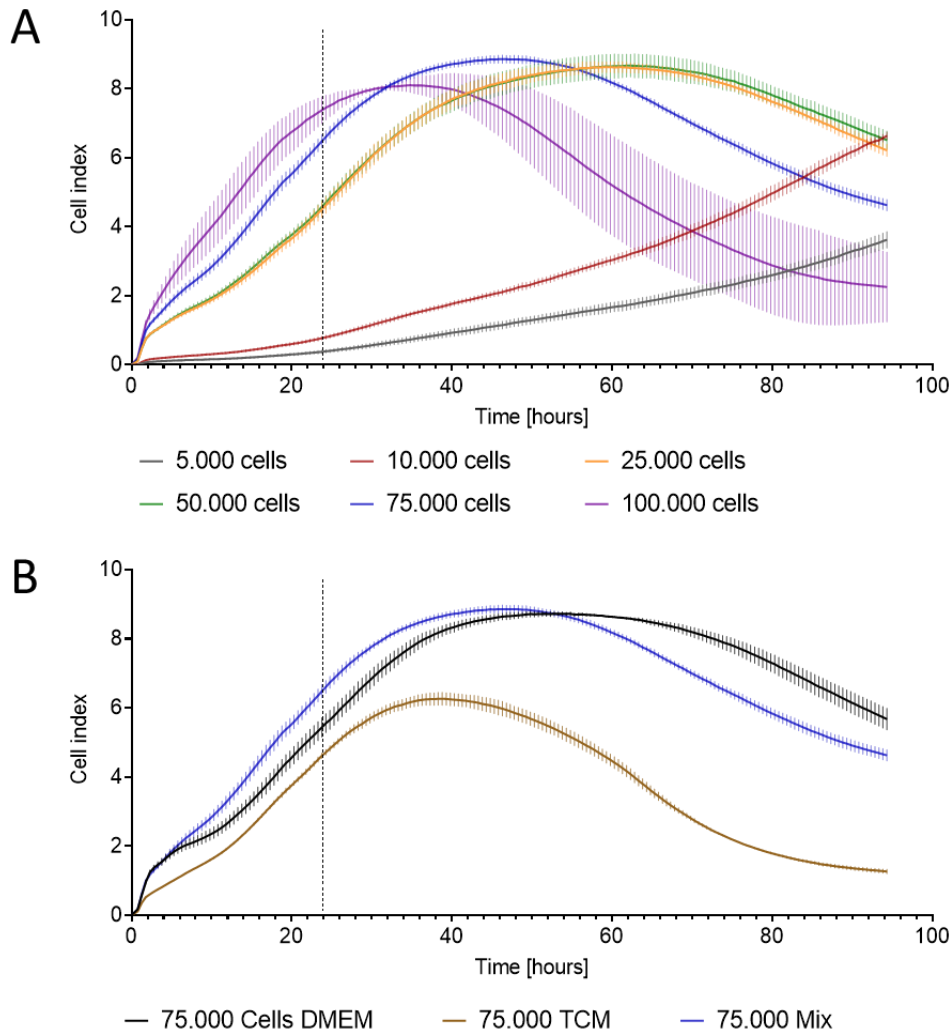


**Figure 17: Evaluation of parameters for utilizing the XCELLigence system to monitor dynamic T-cell cytotoxicity.**

Cell index of 624.38 Mel cells was monitored for 90 h at a measurement interval of 30 min using the XCELLigence system. Progression of cell index after seeding different 624.38 Mel cell numbers, ranging from 5.000 to 100.000 cells, were analyzed in a mixture of DMEM- and T-cell medium (A). Cell index comparison of 75.000 624.38 Mel cells for different media was analyzed over 90 h (B). Measurements were performed in triplicates with error bars representing SD. The dotted line at 24 h indicates the time point at which T cells would be added in subsequent experiments. (In cooperation with TK)

With the number of used tumor cells and the corresponding medium established, cytotoxicity of CD8<sup>+</sup> T cells could subsequently be assessed. Thus, after 24 h, TCR2.5D6 transduced human CD8<sup>+</sup> T cells were added to each well of  $7.5 \times 10^4$  624.38 Mel cells and the impact on the cell index was monitored for additional 24 h. As a control, tumor cells were used without the addition of T cells, to evaluate cell index of uninterrupted tumor growth. The analyzed effector to target ratios (E:T) used for this experiment were 1:10, 1:5, 1:2, 1:1 and 2:1.

To highlight the specific effect of the addition of T cells and exclude differences due to diverging target cell growth up to 24 h, the cell index readout was normalized at the time point of effector cell addition. By normalizing the cell index, the cell index at the chosen time is set as 1.0, thereby making this the time point of reference for each condition. By normalizing at the time point of T-cell addition, the variable of cell index before effector cell addition is excluded, resulting in a graph that represents the data on a comparable basis.

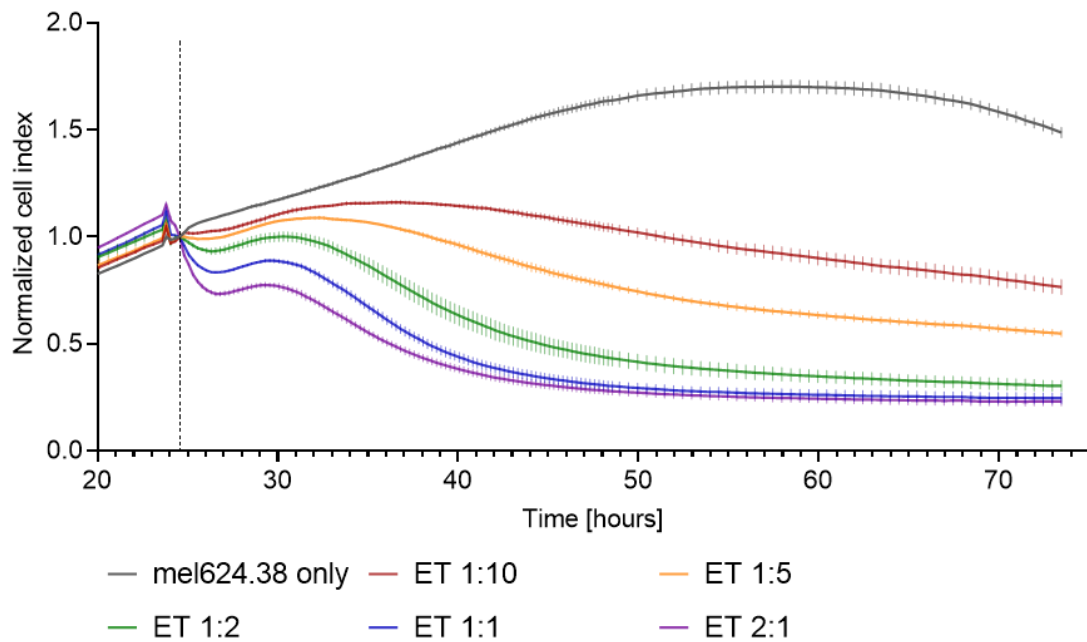


**Figure 18: Effects of different effector (E) to target (T) ratios on the cytotoxicity of 624.38 Mel by T cells.**

Cell indexes of 624.38 Mel cells and TCR-transduced CD8<sup>+</sup> T cells, added after 24 h at different ratios, were measured for 74 h at an interval of 30 min. Cell index values were normalized shortly after addition of T cells and measurements were performed in triplicates with error bars representing SD. The dotted line indicates the time point at which addition of T cells was complete and data was normalized. (In cooperation with TK)

The initial drop of the cell index after addition of T cells at 24 h is a known factor that is attributed to mechanical stress on the target cells by pipetting, movement of the experimental 96-well plate and re-positioning inside the machine. The positive control of only 624.38 Mel cells continued growing following the initial drop after addition of T cells to the other conditions, indicating that tumor cells grew as previously shown. Addition of T cells at an E:T ratio of 1:10 and 1:5 resulted in a shallow decline of the cell index and thus only in slight tumor cell lysis (Figure 18, red, orange). Increasing the number of T cells also expectedly increased the cytotoxic effect on target cells, with an E:T ratio of 1:2, 1:1 and 2:1 resulting in similarly strong cell lysis and eventual plateaus that were reached roughly 30 h after addition of T cells

(Figure 18, green, blue, purple). For subsequent analysis, an E:T ratio of 1:1 was used due to its fast cell lysis and small standard deviations.

The previously established parameters were then used to assess the influence that CD2- and CD7-sdAb binding has on the cytotoxicity of CD8<sup>+</sup> T cells. Therefore, after 24 h, TCR2.5D6 transduced human CD8<sup>+</sup> T cells were added to wells of  $7.5 \times 10^4$  624.38 Mel cells, together with either CD2-sdAb, CD7-sdAb, a CD2-derived Fab-fragment (CD2-F(ab')<sub>2</sub>) as a positive control or R3b23-sdAb as a negative control. The CD2-F(ab')<sub>2</sub> was used as a positive control, since it was previously shown that binding of CD2-F(ab')<sub>2</sub> resulted in a functional impairment of CD8<sup>+</sup> T cells, leading to failed tumor rejection in vivo (Mayer et al., 2018). Additionally, one condition did not receive any T cells and only contained 624.38 Mel cells, another condition did receive untransduced T cells to reveal any effects that the sole addition of T cells has on the cell index, and the final condition received TCR2.5D6 transduced T cells alone and served as the important baseline of un-affected cytotoxicity.

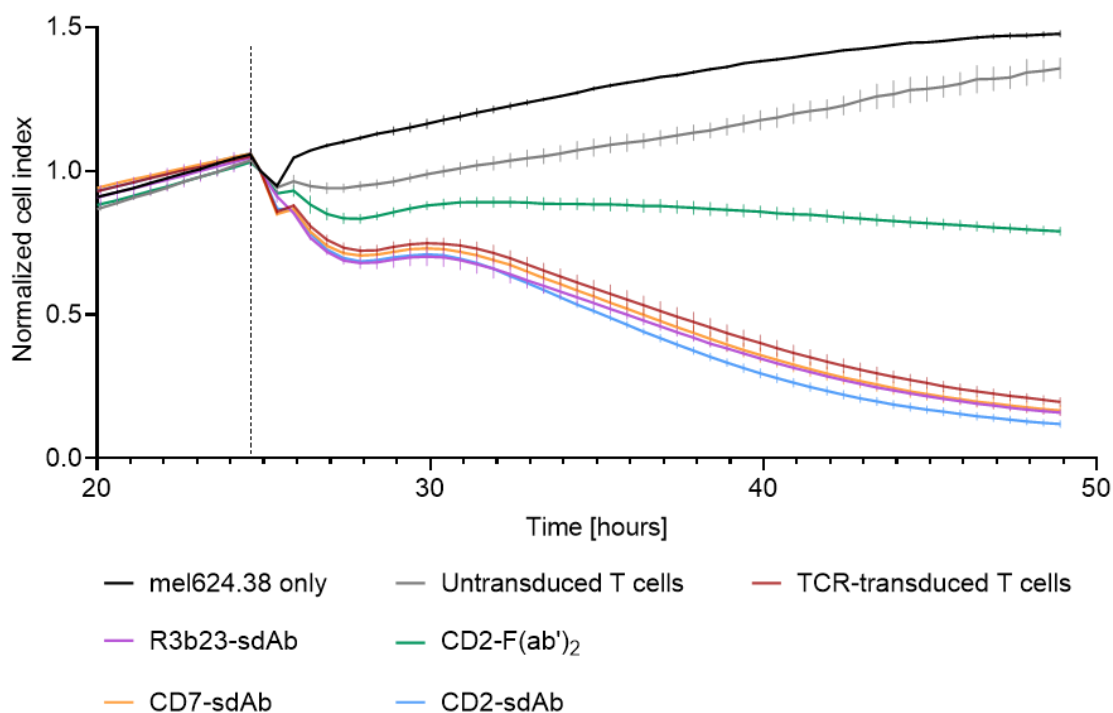


**Figure 19: Effect of CD2- and CD7-sdAb on T-cell cytotoxicity at a concentration of 100 nM.**

Cell indexes of 624.38 Mel cells, TCR-transduced CD8<sup>+</sup> T cells and added conditions were monitored for 74 h at a measurement interval of 30 min. Each condition was added at a concentration of 100 nM per well. R3b23-sdAb served as a negative control and CD2-F(ab')<sub>2</sub> served as positive control. Cell index values were normalized shortly after addition of T cells and measurements were performed in triplicates with error bars representing SD. The dotted line indicates the time point at which addition of T cells was complete and data was normalized. (In cooperation with TK)

The condition that contained only 624.38 Mel cells continued to grow unaffectedly up until 50 h (Figure 19, black). Similarly, the addition of untransduced T cells resulted in a largely unaffected growth of target cells (Figure 19, light grey). The slightly shallower growth is most likely attributed to the normal proliferation of T cells and the concomitant usage of medium and space in each well. Importantly, the wells that received the CD2-F(ab')<sub>2</sub> were considerably affected by CD2-F(ab')<sub>2</sub>-supplementation and demonstrated a very impaired and slowed tumor cell lysis (Figure 19, green). This confirmed previously reported *in vivo* data from Mayer & Mall et al. (Mayer et al., 2018), which showed a distinct functional impairment of T cells after intravenous injection of CD2-F(ab')<sub>2</sub>. Therefore, the normalized cell index of the CD2-F(ab')<sub>2</sub> condition can be used as a baseline of subsequent *in vivo* T-cell impairment.

The baseline for uninterrupted T-cell cytotoxicity on the other hand is the condition that received TCR2-5D6 transduced T cells (Figure 19, red). Here, tumor cell lysis set in after the first hour and consistently continued throughout the experiment. Addition of either CD2-sdAb (Figure 19, blue) or CD7-sdAb (Figure 19, orange) did not result in a distinct impairment of T-cell cytotoxicity and both conditions showed a dynamic cell lysis very similar to the added TCR2.5D6 transduced T cells alone. In this experiment, every component was added at a concentration of 100 nM per well.

To further exclude any possible effect of CD2- or CD7-sdAb that might only be visible at even higher concentrations, the same experimental setup was used with added CD2-F(ab')<sub>2</sub>, R3b23-sdAb, CD2- and CD7-sdAb at a concentration of 500 nM per well (Figure 20). The results from adding each component at a concentration of 500 nM were nearly identical to the results from using 100 nM. Neither CD2-sdAb nor CD7-sdAb did exhibit an impairing effect on T-cell functionality *in vitro* over the course of 24 h (Figure 20, blue, orange).

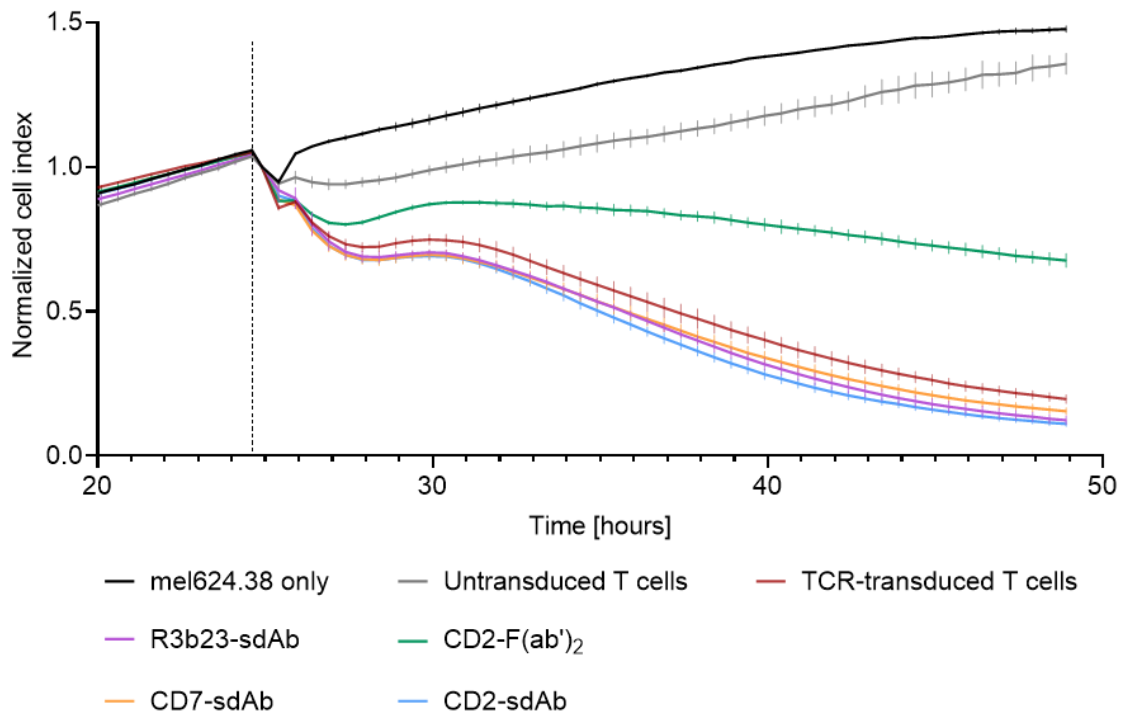


**Figure 20: Effect of CD2- and CD7-sdAb on T-cell cytotoxicity at a concentration of 500 nM.**

Cell indexes of 624.38 Mel cells, TCR-transduced CD8<sup>+</sup> T cells and added conditions were monitored for 74 h at a measurement interval of 30 min. Each condition was added at a concentration of 500 nM per well. R3b23-sdAb served as a negative control and CD2-F(ab')<sub>2</sub> served as positive control. Cell index values were normalized shortly after addition of T cells and measurements were performed in triplicates with error bars representing SD. The dotted line indicates the time point at which addition of T cells was complete and data was normalized. (In cooperation with TK)

The XCELLigence assay showed that there was no visible effect of T-cell impairment by addition of either CD2- or CD7-sdAb to a coculture of TCR2.5D6 transduced T cells and 624.38 Mel cells, while at the same time confirming previously published results of a CD2-derived Fab-fragment that does have a negative effect on T-cell cytotoxicity. While T-cell cytotoxicity is crucial as a readout to ensure the innate properties for a T-cell marker, another very important aspect is cytokine secretion of T cells.

### 3.3.2 Effects of CD2- and CD7-sdAb on cytokine-production of CD8<sup>+</sup> T cells in vitro

After assessing the effect of CD2- and CD7-sdAb binding on the cytotoxic capabilities of T cells, the subsequent step was to ensure that the cytokine production profile of T cells is not altered after CD2- or CD7-sdAb binding. To that end, three cell lines that have previously been established in the team were used as target cell lines for TCR2.5D6 transduced CD8<sup>+</sup> T cells: ML2 (acute myelomonocytic leukemia), NB4 (acute promyelocytic leukemia), and HL60 (acute myeloid leukemia). These cell lines were retrovirally transduced with the HLA class I molecule HLA-B\*07:02 (B7), which can present the target antigen (MPO<sub>5</sub>), essential for TCR2.5D6-based target recognition by CD8<sup>+</sup> transgenic T-cells (Klar et al., 2014).

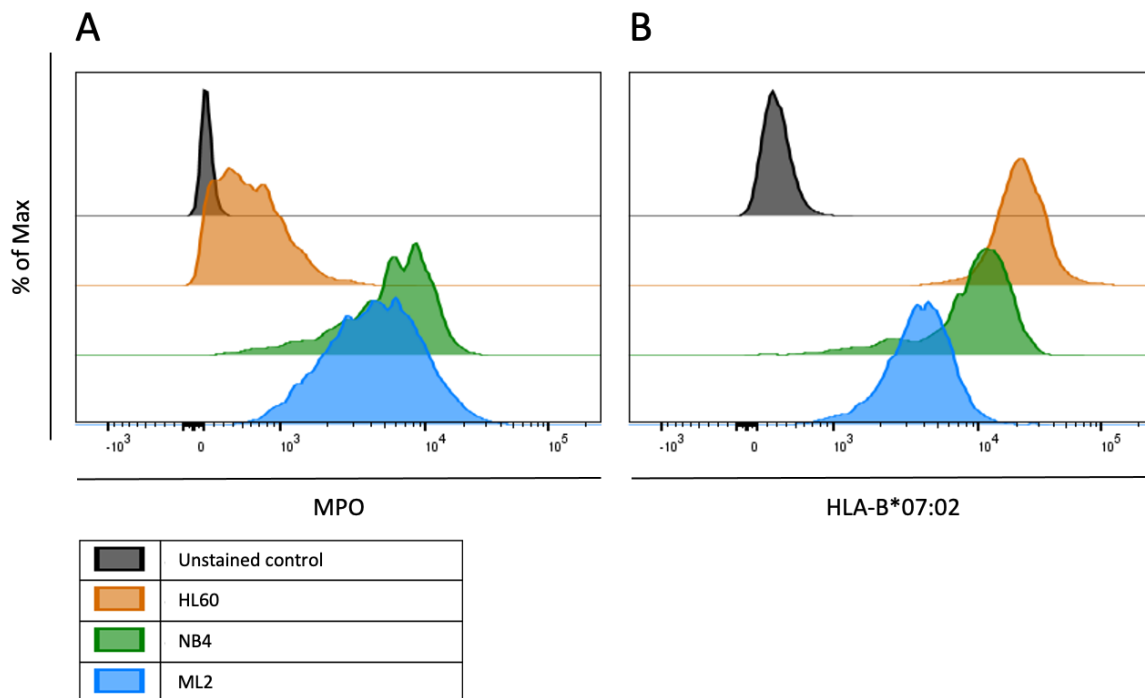


**Figure 21: Expression analysis of MPO and HLA-B\*07:02 on the cell lines HL60, NB4 and ML2.**

Half-offset depiction of flow cytometry analysis of expression intensities of MPO (A) and HLA-B\*07:02 (B) regarding the cell lines HL60, NB4 and ML2, with an unstained HL60-population serving as a negative control. (In cooperation with SB)

To characterize the used cell lines more precisely in terms of their suitability to serve as viable target cell lines, the expression of MPO (Figure 21A) and HLA-B\*07:02 (Figure 21B) was examined using flow cytometry analysis. All cell lines showed a distinct expression of HLA-B\*07:02 on their surface compared to the control (Figure 21B), while intracellular staining of the target antigen MPO showed a weaker signal compared to MPO-levels for NB4 and ML2 (Figure 21A).

After characterizing the parameters needed for successful TCR-mediated recognition of the target cell lines by TCR2.5D6 transduced CD8<sup>+</sup> T cells, the impact of CD2-sdAb and CD7-sdAb on T-cell cytokine secretion was evaluated. TCR2.5D6 transduced CD8<sup>+</sup> T cells and respective target cells were co-cultured for 4 h with the addition of either CD2-sdAb, CD7-sdAb, or R3b23-sdAb as a control. Supernatants were then evaluated by ELISA to analyze differences in IFN $\gamma$  secretion dependent on sdAb binding.

Over the course of 4 h neither CD2- nor CD7-sdAb did have a significant effect on IFN $\gamma$  secretion for any of the tested cell lines (Figure 22). While IFN $\gamma$  secretion of CD8<sup>+</sup> T cells in the presence of target cell line HL60-B7 was lower compared to ML2-B7 and NB4-B7, this can be attributed to the lower levels of MPO target antigens for the cell line HL60 cells compared to ML2 and NB4 (Figure 21A).

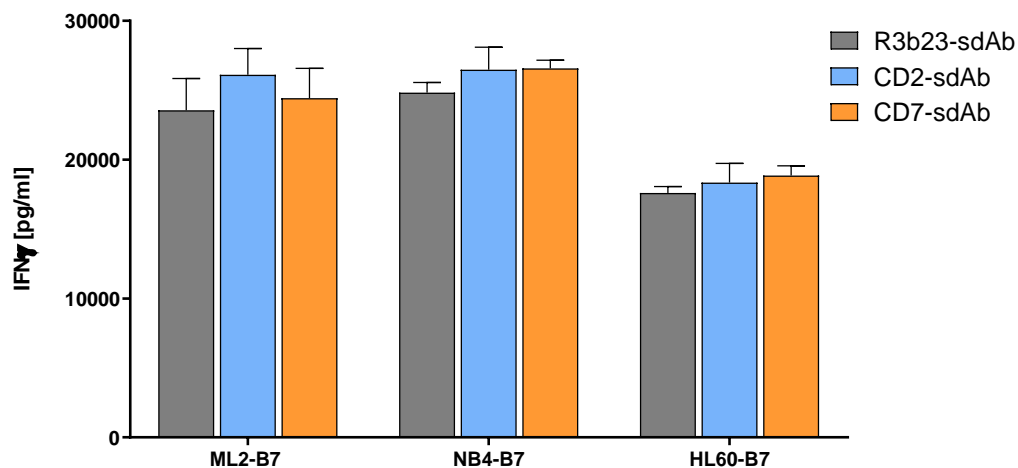


**Figure 22: IFN $\gamma$  cytokine secretion analysis of CD8<sup>+</sup> T cells by ELISA after coincubation with CD2- and CD7-sdAb.**

IFN $\gamma$  levels were determined by ELISA after 4 h coculture of human CD8<sup>+</sup> T cells, the respective target cell lines and CD2-sdAb, CD7-sdAb and R3b23-sdAb as a control. Measurements were performed in triplicates.

After showing that neither CD2-sdAb nor CD7-sdAb had a significant impact on IFN $\gamma$  secretion levels of CD8<sup>+</sup> T cells, the analysis was extended to additional cytokines, namely IL-2, GM-CSF and TNF- $\alpha$ . To reconfirm no cell line specific effects, the assessment was done utilizing the previously used cell lines ML2-B7 (Figure 23A), NB4-B7 (Figure 23B) and HL60-B7 (Figure 23C). The experimental setup was identical to the one used to determine IFN $\gamma$  secretion and cytokine levels were determined by ELISA.

The analysis showed differences in cytokine production between the cell lines themselves, however, the addition of CD2-sdAb and CD7-sdAb did not alter the cytokine profile in a

significant way compared to the R3b23-sdAb control. IL-2- and GM-CSF levels were unaffected and while the total values differed from cell line to cell line, the ratio remained consistent at roughly 2:1. TNF- $\alpha$  levels were expectedly very low and did not increase due to CD2- or CD7-sdAb binding to T cells.

Thorough evaluation of the effects of CD2- and CD7-sdAb on cytokine-production of CD8<sup>+</sup> T cells in vitro showed that coincubation with CD2- or CD7-sdAb did not result in an alteration in cytokine production profiles across multiple target cell lines. To further investigate the potential of CD2- and CD7-sdAb to act as inert T-cell tracers, the effect of both sdAb on T-cell cytotoxicity was subsequently tested in vivo.

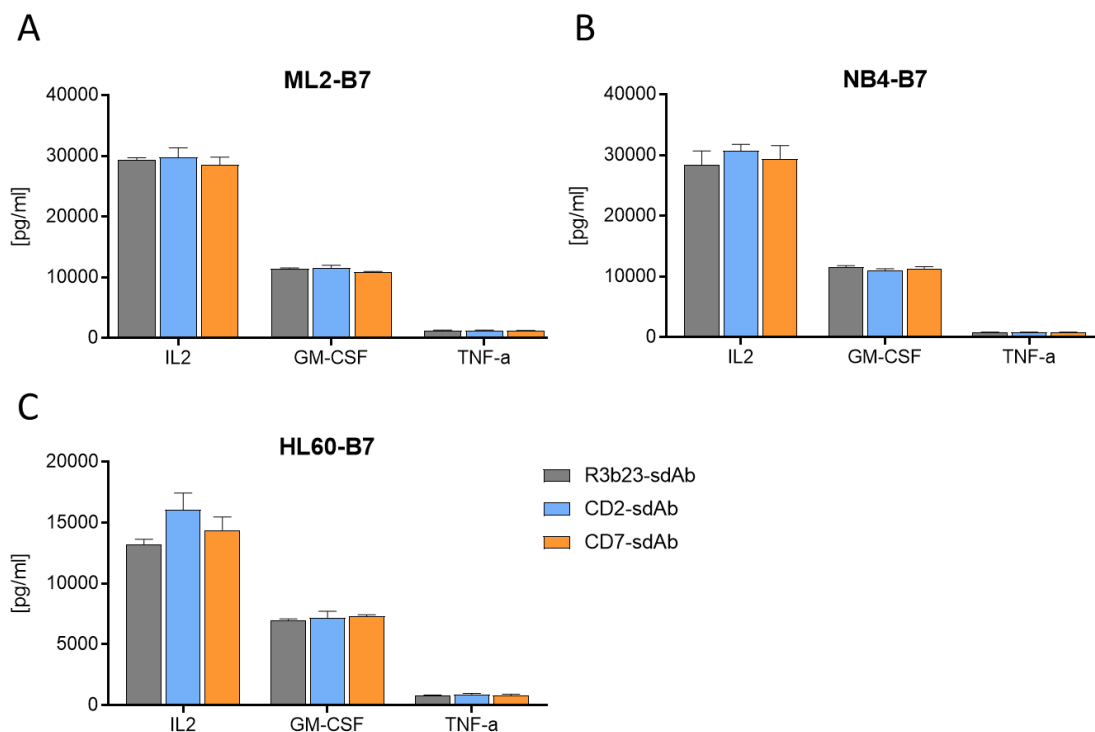


**Figure 23: Cytokine secretion analysis of IL2, GM-CSF and TNF- $\alpha$  by ELISA after coincubation with CD2- and CD7-sdAb.**

Cytokine secretion levels of IL-2, GM-CSF and TNF- $\alpha$  were determined by ELISA after 4 h coculture of human CD8<sup>+</sup> T cells, the respective target cell lines and CD2-sdAb, CD7-sdAb and R3b23-sdAb as a control. Used target cell lines were ML2-B7 (A), NB4-B7 (B) and HL60-B7 (C). Measurements were performed in triplicates.

### 3.4 Impact of CD2- and CD7-sdAb binding on cytotoxicity of CD8<sup>+</sup> T cells in vivo

In vitro analysis has shown that neither CD2-sdAb- nor CD7-sdAb-binding had an effect on human CD8<sup>+</sup> T cells in regards to their cytotoxic potential or cytokine production profile. Since previous results by Mayer & Mall et al. (Mayer et al., 2018) have shown that significant T-cell impairment of the tested CD2-F(ab')<sub>2</sub> was only visible in in vivo studies and not in vitro, confirming no altered T-cell cytotoxicity in vivo was a crucial next step in characterizing the CD2- and CD7-sdAb.

#### 3.4.1 Effect of CD2- and CD7-sdAb on cytotoxicity of TCR-transgenic CD8<sup>+</sup> T cells in vivo

To evaluate whether CD2- and CD7-sdAb effect the cytotoxic potential of CD8<sup>+</sup> T cells in vivo, a previously established mouse model was used. In short, severely immunodeficient NSG mice are subcutaneously injected with  $1 \times 10^7$  ML-B7 or -B15 tumor cells on day -8. ML2 cells expressing the HLA-molecule B7 are able to present the target antigen (MPO<sub>5</sub>) required for target recognition by TCR2.5D6-transgenic CD8<sup>+</sup> T-cells, while ML2 cells expressing the irrelevant HLA molecule B15 cannot present MPO<sub>5</sub> and therefore serve as a negative control. At day 0, TCR2.5D6-transgenic T cells are injected intravenously and at day 3 mice receive either PBS, R3-b23-sdAb, CD2-F(ab')<sub>2</sub> clone OKT11 (OKT11), CD2-F(ab')<sub>2</sub> clone RPA-2.10 (RPA), CD2-sdAb or CD7-sdAb. A schematic overview of the experimental setup is depicted in Figure 24.

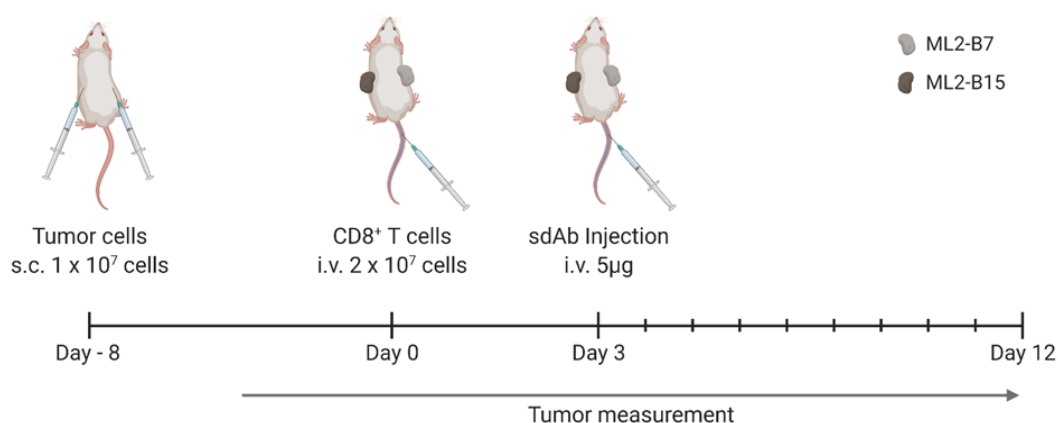


**Figure 24: Experimental setup of in vivo tumor rejection model for CD8<sup>+</sup> T cells.**

NSG mice were subcutaneously (s.c.) injected with ML2-B7 cells in the right flank and ML2-B15 cells in the left flank. After eight days, TCR-transgenic human CD8<sup>+</sup> T cells were injected intravenously (i.v.) through the tail vein, followed three days later by i.v. injection of R3-b23-sdAb, OKT11, RPA, CD2-sdAb or CD7-sdAb. Tumor growth was monitored from tumor onset until the end of experiment at day twelve. (Created with BioRender.com)

Mice did not exhibit any form of stress or decline of health as a result of any applied condition, including the characterized sdAb. Across all examined conditions, ML2-B15 tumors on the left flank were unaffected by the injected CD8<sup>+</sup> T cells and grew steadily until they reached a size of approximately 200 mm<sup>2</sup> at day twelve (Figure 25A). Therefore, TCR-transgenic CD8<sup>+</sup> T cells did not seem to attack irrelevant tumor cells in vivo in an unspecific way.

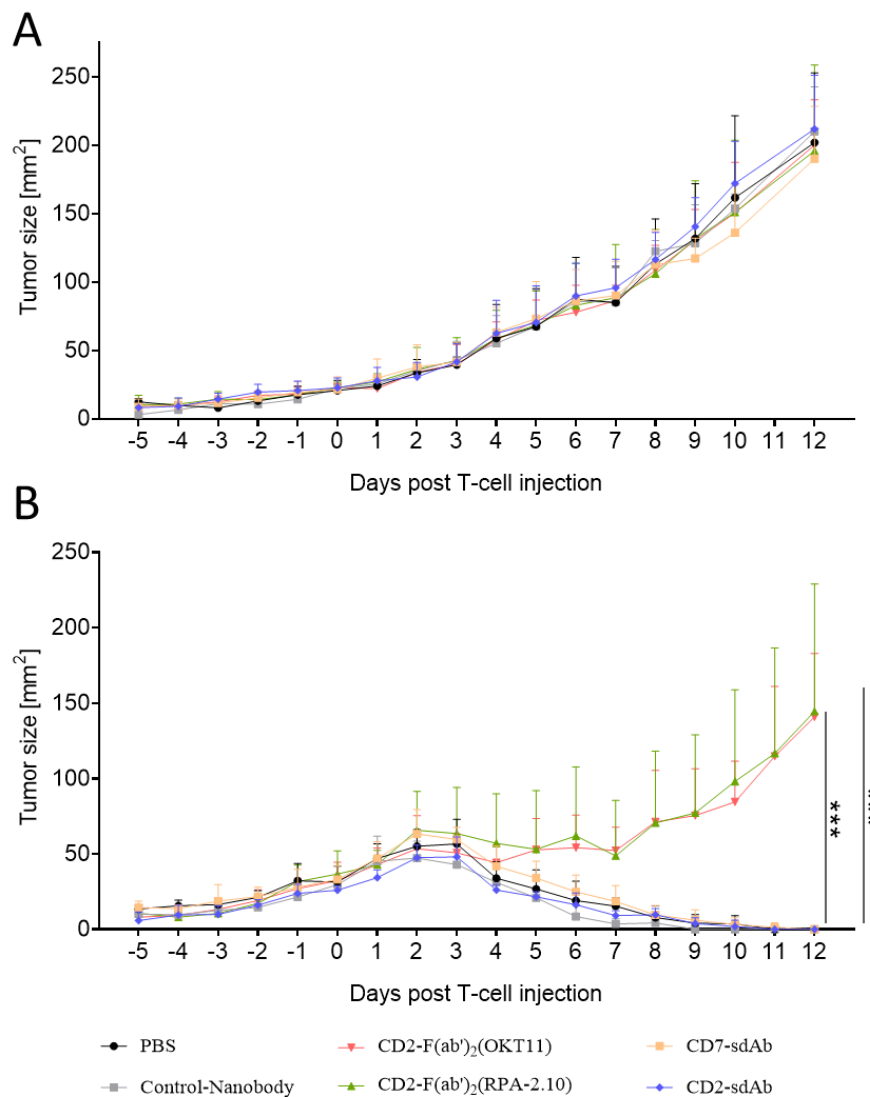


**Figure 25: Application of CD2-sdAb and CD7-sdAb did not impair T-cell cytotoxicity in vivo.**

Monitoring of tumor growth kinetics of ML2-B15 (A) and ML2-B7 tumors (B) in NSG mice. On day 0, eight days after subcutaneous tumor injection, mice were intravenously injected with TCR 2.5D6-transgenic CD8<sup>+</sup> T cells and three days later with either PBS, R3b23-sdAb, CD2-F(ab)<sup>2</sup> (OKT11), CD2-F(ab)<sup>2</sup> (RPA-2.10), CD2-sdAb or CD7-sdAb. Kinetics of tumor growth were monitored daily for twelve days post T-cell injection. The experiment was ended at day twelve, at which point all relevant non-control tumors had been fully rejected. Tumor sizes are shown in mm<sup>2</sup> and mean values and SDs are depicted for each group of mice. PBS n = 4, R3b23-sdAb n = 3, CD2-F(ab)<sup>2</sup> (OKT11) n = 6, CD2-F(ab)<sup>2</sup> (RPA-2.10) n = 4, CD2-sdAb n = 5, CD7-sdAb n = 5. Significance was calculated using Mann-Whitney test (\* p ≤ 0.05, \*\* p ≤ 0.01, \*\*\* p ≤ 0.001). (In cooperation with TK & SB)

ML2-B7 tumors in mice which received either PBS or R3b23-sdAb were rejected as expected starting from day three post T-cell injection (Figure 25B). At day twelve, ML2-B7 tumors from mice of both conditions were fully rejected and could no longer be quantified, showing that TCR-transgenic CD8<sup>+</sup> T cells were capable of specifically recognizing and rejecting ML-B7 tumors. Furthermore, application of R3b23-sdAb not impacting the strong tumor rejection shows that this sdAb-structure itself is not impairing T-cell functionality. Injection of the conditions used as a positive control, CD2-F(ab')<sub>2</sub> clone OKT11 and clone RPA, led to a distinct and significant impairment of T-cell functionality, resulting in a failed tumor rejection and consequently continued tumor growth until a size of approximately 150 mm<sup>2</sup> at day twelve was reached (Figure 25B).

Application of CD2- and CD7-sdAb did not have any impairing effects on T-cell mediated tumor rejection. ML2-B7 tumors of all mice from both groups were fully rejected twelve days after T-cell injection, equivalent to tumors of mice after PBS- or R3b23-sdAb application.

Additionally, to confirm presence of sdAb-binding to T cells in vivo, one mouse per group was euthanized 60 min after sdAb-injection. ML2-B7 and -B15 tumors, blood and spleen were analyzed by flow cytometry to identify T cells via CD3-staining, tumor cells via GFP-expression and sdAb-bound cells by using an anti-His-Tag mAb. Since only one mouse per group was analyzed, no statistical analyses were done and individual sample-fluctuation could not be compensated by a larger cohort.

CD3<sup>+</sup>, GFP<sup>-</sup> and 7-AAD<sup>-</sup> T cells were identified in large amounts in blood of R3b23-sdAb- and CD2-sdAb animals, but not in the animal following CD7-sdAb injection, most likely due to a technical error in the staining process. Of note, the number of T cells found in ML2-B7 tumors of all mice was distinctly higher compared to ML2-B15 tumors, confirming the established specific HLA-dependent T-cell infiltration in the used mouse model (Figure 26A).

Analysis of His-Tag<sup>+</sup> T cells showed that in ML2-B7 tumors more than 40 % of T cells were bound by CD7-sdAb and more than 60 % by CD2-sdAb (Figure 26B). In the mouse that received R3b23-sdAb, 8 % of T cells in ML2-B7 tumors correlated with anti-His-Tag binding, which is similar to ratio found in blood and spleen, indicating a degree of unspecific anti-His-Tag background.

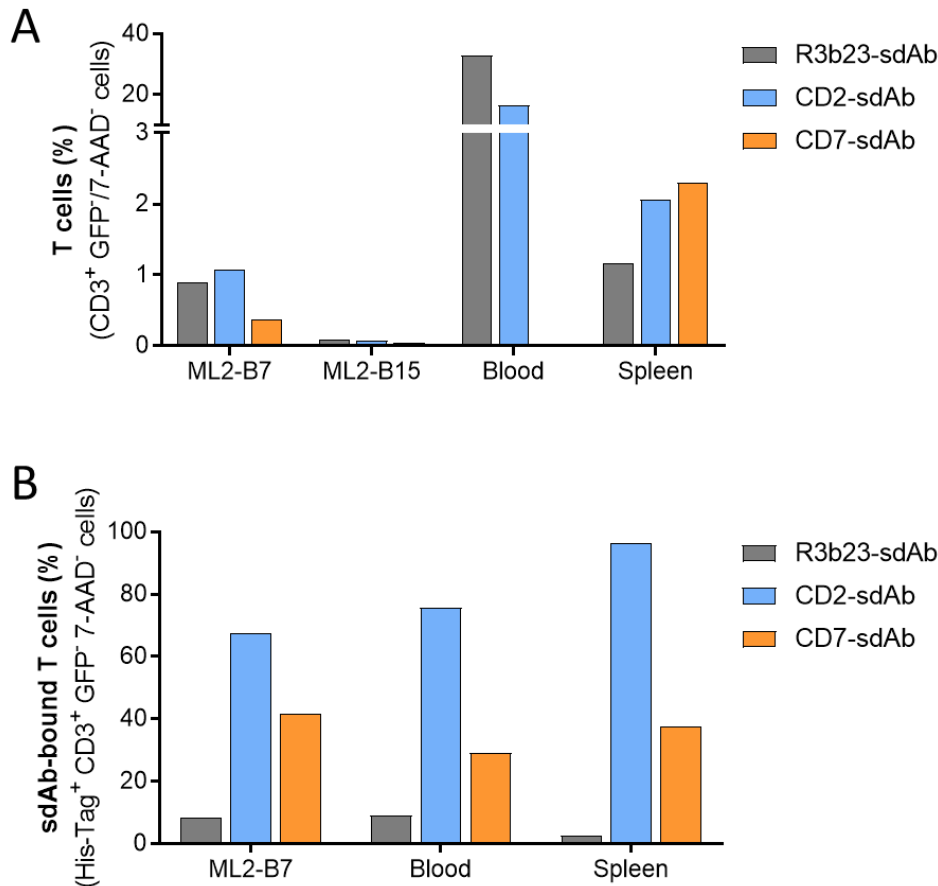


**Figure 26: Analysis of T-cell distribution following sdAb-injection.**

Exemplary flow cytometry analysis of one mouse per group 60 min after injection of the respective sdAb. Following single-cell suspension, analyzed cells were stained using CD3, 7-AAD and an anti-His-Tag mAb. ML2-B7 and -B15 tumor cells are retrovirally transduced to express GFP. The percentage of alive, GFP-negative and CD3-positive T cells was assessed in ML2-B7 and -B15 tumors, blood and spleen (A). This population was then additionally utilized to depict sdAb-bound T cells by analyzing anti-His-Tag mAb binding on alive, GFP-negative and CD3-positive T cells in ML2-B7 tumors, blood and spleen. (B) ML2-B15 tumors were not analyzed in this sub-analysis due to too low T-cell numbers. (In cooperation with TK & SB)

Taken together, this data confirmed previously shown *in vitro* effects demonstrated by the XCELLigence experiment to assess dynamic cytotoxicity, where OKT11 was also inhibiting T-cell mediated cytotoxicity (Figure 19). Additionally, Mayer & Mall et al. have previously shown that OKT11 F(ab')<sub>2</sub> did impair tumor rejection *in vivo*, which was confirmed in this experiment and supplemented with the similar CD2-F(ab')<sub>2</sub> clone RPA.

Injections of CD2-sdAb and CD7-sdAb did not result in any altered tumor cell rejection compared to either PBS or R3b23-sdAb, with all ML-B7 tumors being fully rejected on day twelve. Thus, these data demonstrate that neither CD2-sdAb nor CD7-sdAb affected T-cell functionality over the course of the experiment.

### 3.5 Using CD2- and CD7-sdAb to monitor tumor reactive TCR-transgenic CD8<sup>+</sup> T cells in vivo

After completion of the in-depth in vitro characterization and subsequent in vivo assessment of potential impairing effects on T-cell functionality, CD2- and CD7-sdAb were analyzed in terms of their tracer-capabilities to depict TCR-transgenic T cells in vivo.

#### 3.5.1 Intratumoral injections and PET/MRI-monitoring of CD8<sup>+</sup> T cells in vivo

To characterize CD2- and CD7-sdAb as T-cell tracers for PET/MRI imaging in vivo, a previously used experimental setup was adapted and used for an initial proof of concept experiment. The same NSG-mice based mouse model was used as in Figure 23 and CD2-sdAb was chosen as the candidate to reestablish the PET/MRI imaging pipeline and evaluate sdAb-handling in terms of radioactive-labeling and image acquisition.

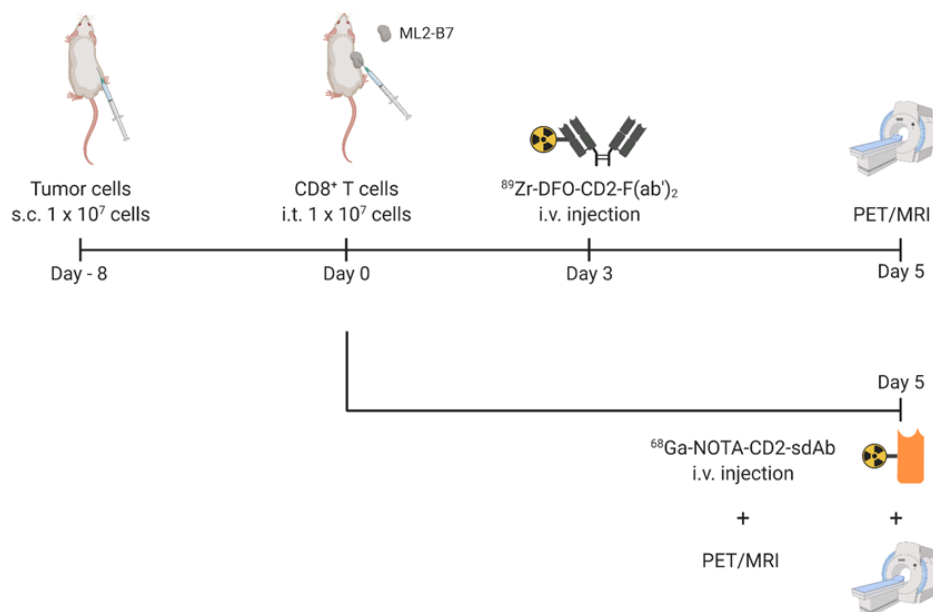


**Figure 27: Experimental setup of in vivo imaging for <sup>89</sup>Zr-DFO-CD2-F(ab')<sub>2</sub> and <sup>68</sup>Ga-NOTA-CD2-sdAb.** NSG mice were subcutaneously (s.c.) injected with ML2-B7 cells in the right shoulder. After eight days, TCR-transgenic human CD8<sup>+</sup> T cells were injected intratumorally (i.t.). One mouse was injected i.v. with <sup>89</sup>Zr-DFO-CD2-F(ab')<sub>2</sub> three days later, and PET/MRI images were acquired 48 h after F(ab')<sub>2</sub> injection (upper track). After i.t. T-cell injection on day zero, two mice were injected i.v. with <sup>68</sup>Ga-NOTA-CD2-sdAb on day five and used for PET/MRI imaging two hours after sdAb-injection (lower track). (Created with BioRender.com)

For CD2-sdAb to work as intended, ML-B7 tumors needed to be sufficiently infiltrated by previously injected TCR-transgenic T cells, to allow for a distinct and strong PET-signal. To guarantee T-cell presence in ML2-B7 tumors, these tumors were intratumorally injected with  $1 \times 10^7$  TCR-transgenic CD8<sup>+</sup> T cells. On day five after T-cell injections, animals were intravenously injected with approx.  $10.5 \pm 2$  MBq of Gallium-68 (<sup>68</sup>Ga)-labeled CD2-sdAb, utilizing NOTA as a chelator. Two hours after injection, mice were anesthetized and put into the PET/MRI for imaging acquisition. As a control, three days after T-cell application, a mouse was injected with CD2-F(ab')<sub>2</sub> clone OKT11, labeled with Zirconium-89 (<sup>89</sup>Zr) and DFO as a chelator. After 48 h, on day five, the mouse was scanned using the PET/MRI. An overview of the schematic experimental setup is depicted in Figure 27.

Acquisition of PET/MRI images 48 h after injection of <sup>89</sup>Zr-DFO-CD2-F(ab')<sub>2</sub> showed a distinct and clear PET-signal at the tumor-site (Figure 28A), with additional tracer uptake also seen in the kidneys, due to renal elimination. By successfully depicting T-cell infiltration in ML2-B7 tumors using <sup>89</sup>Zr-DFO-CD2-F(ab')<sub>2</sub>, previously published data could be reproduced using PET/MRI- instead of PET/CT imaging. Intravenous application of <sup>68</sup>Ga-NOTA-CD2-sdAb and subsequent PET/MRI acquisition 2 h post injection resulted in a high kidney uptake and a clear accumulation of tracer at the tumor site for both mice (Figure 28B). The experiment was therefore able to confirm the feasibility of the PET/MRI-imaging pipeline, reproduce previous <sup>89</sup>Zr-DFO-CD2-F(ab')<sub>2</sub> data and provide an estimation of the potential of <sup>68</sup>Ga-NOTA-CD2-sdAb as a T-cell tracer.

However, CD8<sup>+</sup> T cells were injected intratumorally instead of intravenously and images for the <sup>68</sup>Ga-NOTA-CD2-sdAb were acquired 2 h post injection based on literature research. Therefore, to further optimize workflow, time point of image-acquisition and utilize intravenous injection of T cells, the subsequent in vivo experiment was adapted.

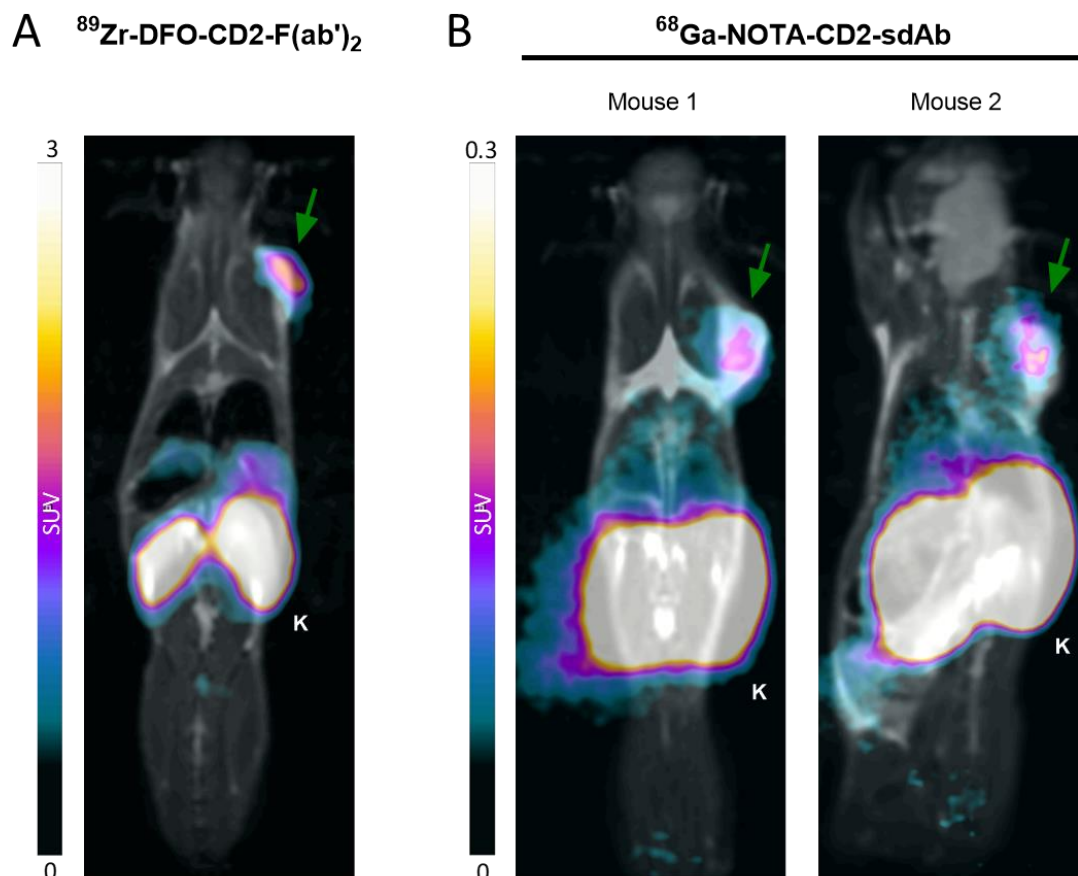


**Figure 28: Experimental setup of in vivo imaging for  $^{89}\text{Zr}$ -DFO-CD2-F(ab')<sub>2</sub> and  $^{68}\text{Ga}$ -NOTA-CD2-sdAb.** Coronal PET/MRI images (A) 48 h post intravenous injection of  $^{89}\text{Zr}$ -DFO-CD2-F(ab')<sub>2</sub> and (B) 2 h post intravenous injection of  $^{68}\text{Ga}$ -NOTA-CD2-sdAb in ML2-B7 tumor bearing mice.  $1 \times 10^7$  TCR-transgenic CD8+ T cells were injected intratumorally in the tumor on the right shoulder (green arrow). The injected dose of applied tracer was (A) 1.61 MBq of  $^{89}\text{Zr}$ -DFO-CD2-F(ab')<sub>2</sub> and (B)  $10.5 \pm 2$  MBq of  $^{68}\text{Ga}$ -NOTA-CD2-sdAb. Scale bar is represented as standardized uptake value (SUV), 0 – 3 SUV (A) and 0 – 0.3 SUV (B). K = Kidney. (In cooperation with SB)

### 3.5.2 Evaluation of image-acquisition time point for PET/MRI imaging using CD2- and CD7-sdAb

The ideal time point to acquire PET/MRI images for CD2- and CD7-sdAb is dependent on a variety of variables and specific for each tracer. Half-life of the used radioisotope, accumulation at the tissue of interest and subsequent detachment and clearance all influence the optimal time to obtain PET/MRI data. Assessment of the dynamic accumulation of the radioisotope-labeled CD2- and CD7sdAb was done by acquiring PET/MRI images at distinct time points after intravenous injection of the tracer.

In short, mice received ML2-B7 and –B15 tumors on either shoulder and after eight days mice were intravenously injected with  $2 \times 10^7$  CD8<sup>+</sup> T cells through the tail vein. Three days later, mice received  $12 \pm 1$ MBq <sup>68</sup>Ga-NOTA-CD2-sdAb and were sequentially scanned 1 h, 2 h, 3 h and 4 h post injection (Figure 29A).

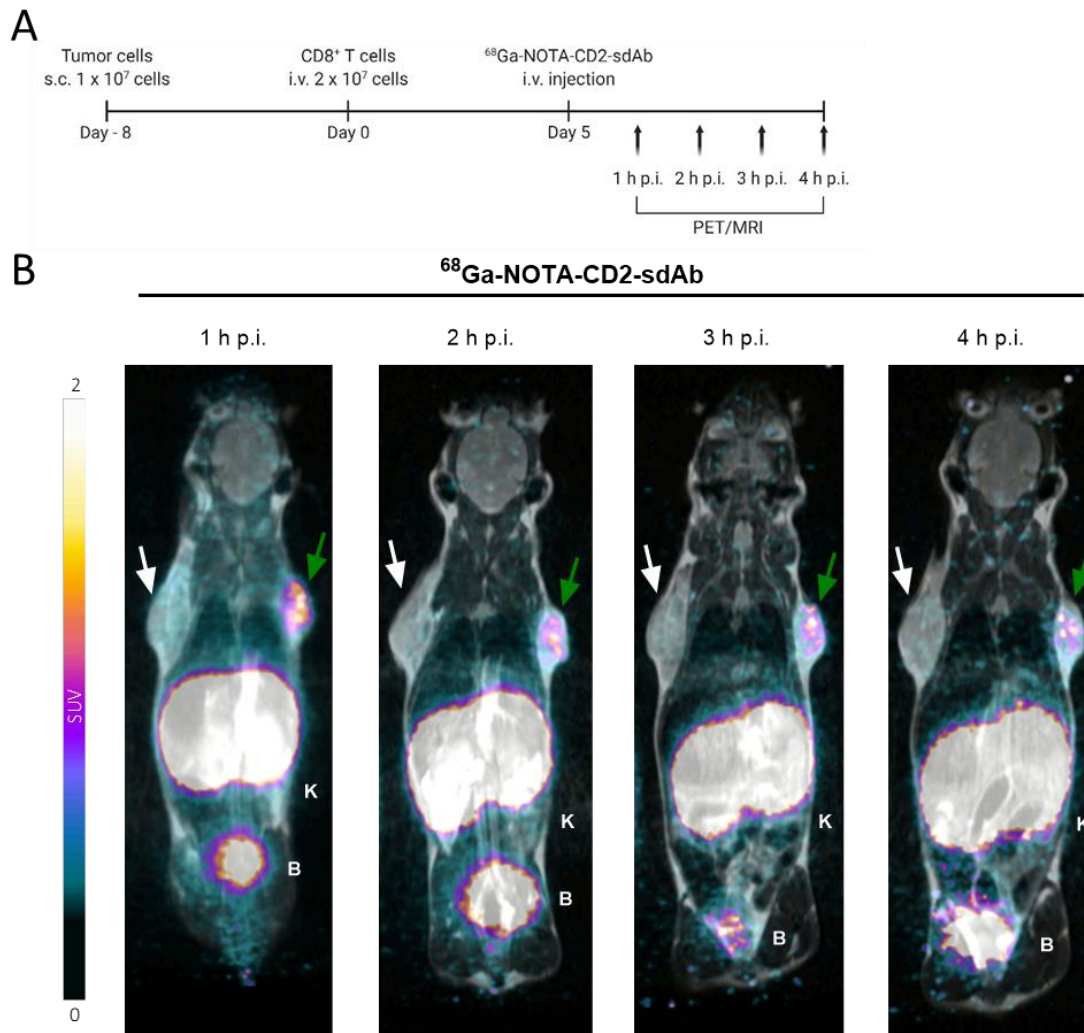


**Figure 29: Experimental setup and PET/MRI images of time point evaluation for in vivo imaging using <sup>68</sup>Ga-NOTA-CD2-sdAb.**

(A) Experimental layout of in vivo imaging study using intravenous injection of CD8<sup>+</sup> T cells and sequential PET/MRI acquisition. (B) Coronal PET/MRI images 1 h, 2 h, 3 h and 4 h post injection of <sup>68</sup>Ga-NOTA-CD2-sdAb.  $2 \times 10^7$  TCR-transgenic CD8<sup>+</sup> T cells were injected i.v. via the tail vein. The injected dose of applied tracer was  $12 \pm 1$ MBq. Scale bar is represented as standardized uptake value (SUV), 0 – 2 SUV. B = Bladder, K = Kidney. Green arrow = ML2-B7 tumor, white arrow = ML2-B15 tumor.

Across all imaging time points, there was no accumulation of tracer uptake at the irrelevant and not TCR-transgenic T-cells targeted control tumor ML2-B15, indicating no T-cell infiltration and no unspecific CD2-sdAb binding. In contrast, ML2-B7 tumors showed a distinct and specific PET-signal at the tumor site starting from 1 h p.i. and descending up until 4 h p.i. (Figure 29B). Tracer uptake in the kidneys (K) and bladder (B) was visible throughout the experiment. Due to the short half-life of the used radioisotope  $^{68}\text{Ga}$ , the overall signal intensity decreased over the course of the experiment but even at 4 h p.i. there was still a clear accumulation of  $^{68}\text{Ga}$ -NOTA-CD2-sdAb at the ML2-B7 tumors.

This experiment showed that after i.v. injection of  $2 \times 10^7$  CD8<sup>+</sup> T cells, application of  $^{68}\text{Ga}$ -NOTA-CD2-sdAb resulted in a specific ML2-B7 tumor uptake, indicating T-cell specific in vivo tracking of the immune response. The ideal time point for further imaging studies using  $^{68}\text{Ga}$ -NOTA-CD2-sdAb was determined to be 1 h p.i., at which time the strongest accumulation of tracer at the tumor site was detected (Figure 29B).

The experimental setup to determine the ideal time for PET/MRI acquisition for  $^{68}\text{Ga}$ -NOTA-CD7-sdAb was identical to the one used for CD2-sdAb and is depicted in Figure 30A. While the overall dynamic of the  $^{68}\text{Ga}$ -NOTA-CD7-sdAb is very similar to CD2-sdAb, the signal intensity for CD7-sdAb was noticeably lower compared to CD2-sdAb, which was accounted for by adapting the SUV-scale from 0 – 2 SUV for CD2-sdAb to 0 – 0.4 SUV for CD7-sdAb. However, accumulation of  $^{68}\text{Ga}$ -NOTA-CD7-sdAb was specific for the ML2-B7 tumor with no considerable tracer uptake in the ML2-B15 tumor, other than an overall background signal (Figure 30B). Accumulation in the kidneys was again seen throughout the experiment and additional bladder-uptake was visible at 2 h p.i. as indicated in the figure. Due to very similar, although weaker, tracer-uptake and –dynamics in the ML2-B7 tumor, the time point of 1 h p.i. was likewise chosen for subsequent imaging studies using  $^{68}\text{Ga}$ -NOTA-CD7-sdAb.

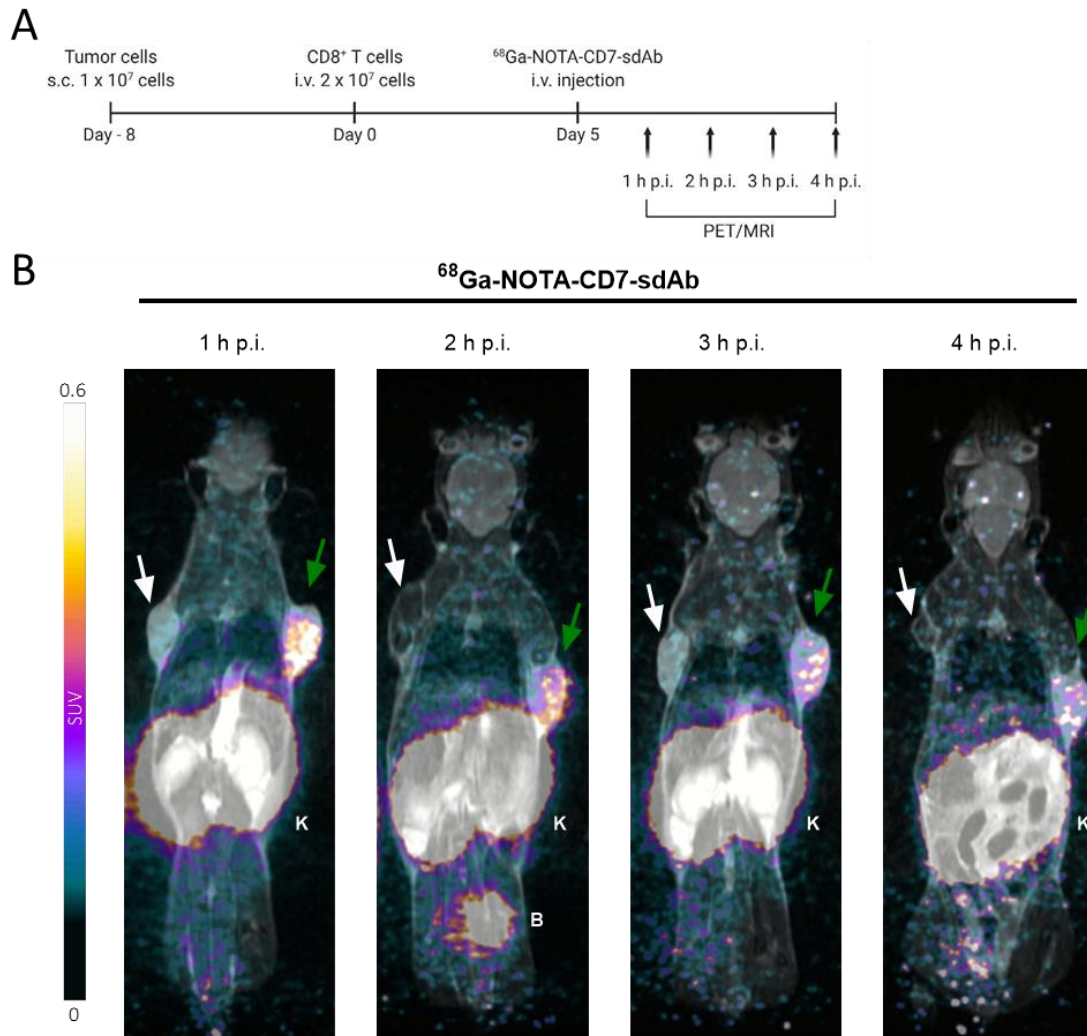


**Figure 30: Experimental setup and PET/MRI images of time point evaluation for in vivo imaging using <sup>68</sup>Ga-NOTA-CD7-sdAb.**

(A) Experimental layout of in vivo imaging study using intravenous injection of CD8<sup>+</sup> T cells and sequential PET/MRI acquisition. (B) Coronal PET/MRI images 1 h, 2 h, 3 h and 4 h post injection of <sup>68</sup>Ga-NOTA-CD7-sdAb.  $2 \times 10^7$  TCR-transgenic CD8<sup>+</sup> T cells were injected i.v. via the tail vein. The injected dose of applied tracer was  $12 \pm 1$  MBq. Scale bar is represented as standardized uptake value (SUV), 0 – 0.6 SUV. B = Bladder, K = Kidney. Green arrow = ML2-B7 tumor, white arrow = ML2-B15 tumor.

### 3.5.3 Monitoring of intravenously injected human CD8<sup>+</sup> T cells at the tumor site using <sup>68</sup>Ga-NOTA-CD2- and <sup>68</sup>Ga-NOTA-CD7-sdAb

To verify the previously assessed feasibility of CD2- and CD7-sdAb as promising T-cell tracers, the prior experimental setup was used with a PET/MRI acquisition time point of 1 h post injection of the respective tracer. As internal controls for specific T-cell accumulation, the irrelevant tumor ML2-B15 was subcutaneously injected in the left shoulder of NSG mice.

Furthermore, an additional control group of mice was injected with  $^{68}\text{Ga}$ -NOTA-labeled R3b23-sdAb to emphasize T-cell unspecific sdAb-accumulation in mice. An overview of the experimental setup can be seen in Figure 31.

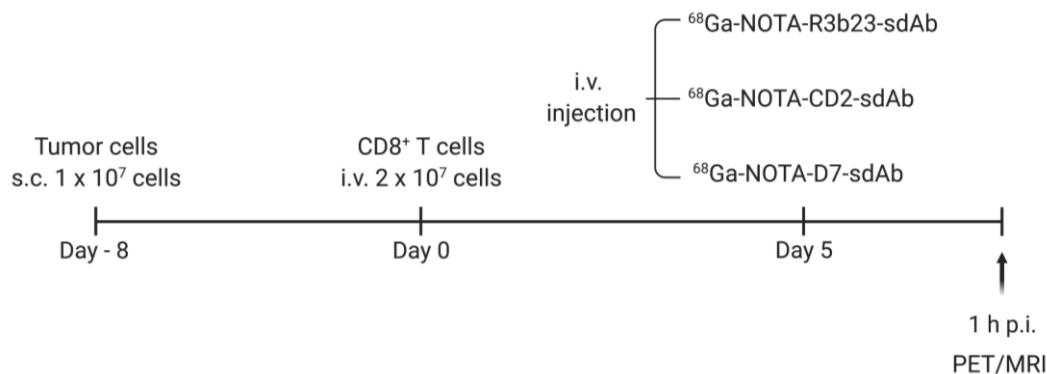


**Figure 31: Experimental setup for in vivo imaging using  $^{68}\text{Ga}$ -NOTA-labeled sdAb in NSG mice.**

Experimental layout of in vivo imaging study using intravenous injection of  $\text{CD8}^+$  T cells after ML2-B7 and -B15 tumor injection. Three groups of five mice per group were injected with each condition and 1 h p.i. scanned using PET/MRI.

PET/MRI imaging of mice that received  $^{68}\text{Ga}$ -NOTA-CD2-sdAb revealed a distinct accumulation of tracer at the relevant ML2-B7 tumor, while no considerable signal was visible at the irrelevant ML2-B15 control-tumor (Figure 32A). The strong accumulation at the ML2-B7 tumor was visible in coronal-, sagittal- and axial orientation, with the only other accumulation visible in the kidneys.

Mice that received  $^{68}\text{Ga}$ -NOTA-R3b23-sdAb as part of the control group showed only accumulation of tracer signal in the kidneys, with no visible tracer in either tumor after PET/MRI scan (Figure 32B). Ex vivo biodistribution of ML2-B7 tumors showed a significantly enhanced ratio of injected dose per gram tumor tissue (%ID/g) in mice that received  $^{68}\text{Ga}$ -NOTA-CD2-sdAb (mean 3.0 %ID/g) compared to  $^{68}\text{Ga}$ -NOTA-R3b23-sdAb (mean 1.2 %ID/g) (Figure 32C). Additionally, of mice that received  $^{68}\text{Ga}$ -NOTA-CD2-sdAb, tracer uptake in ML2-B7 tumors was significantly higher than in ML2-B15 tumors (0.3 %ID/g).

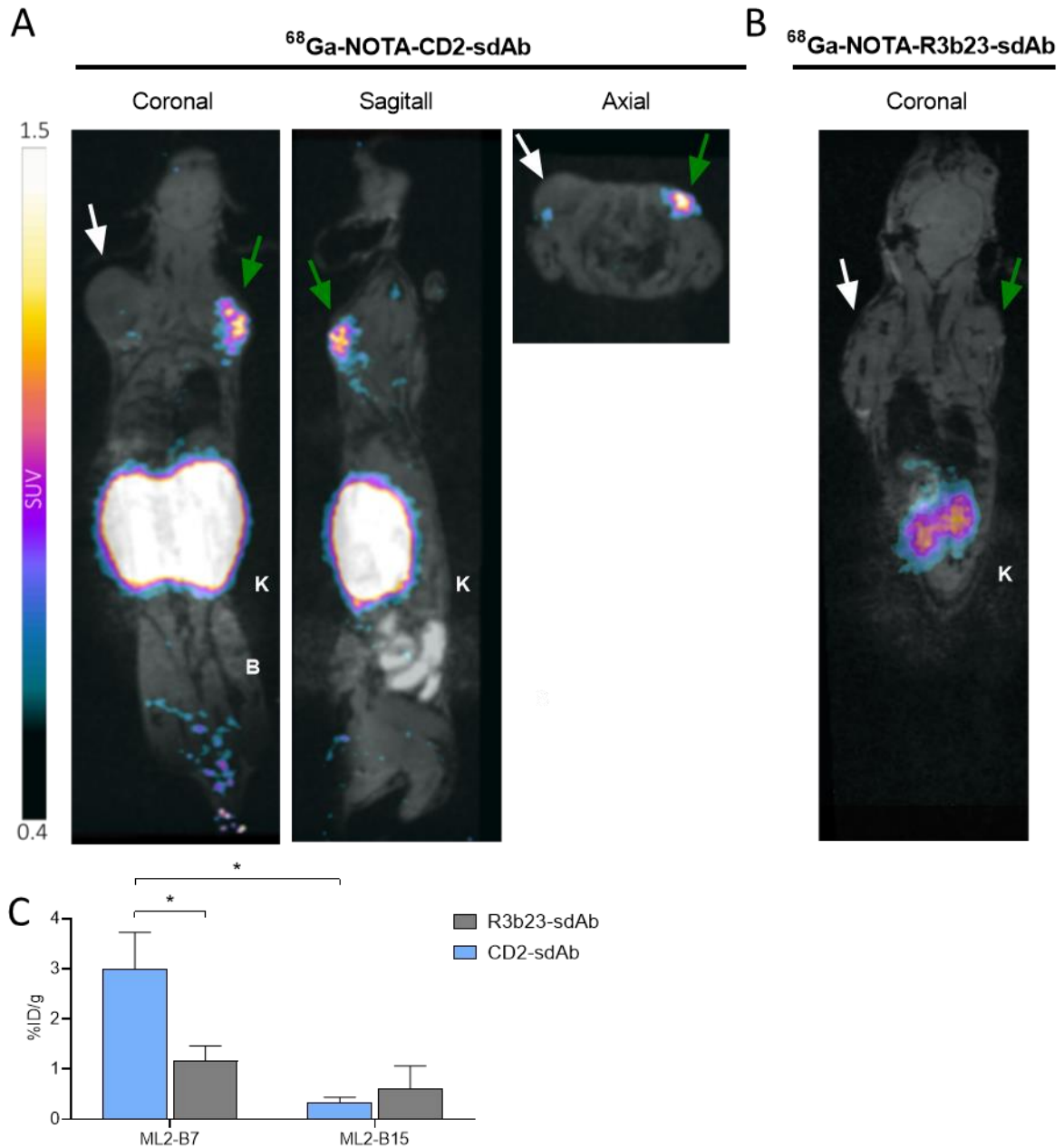


**Figure 32: In vivo tracking intravenously injected TCR-transgenic CD8<sup>+</sup> T cells in ML2-B7 tumors using  $^{68}\text{Ga-NOTA-CD2-sdAb}$ .**

PET/MRI images acquired 1 h p.i. of mice injected i.v. with  $^{68}\text{Ga-NOTA-CD2-sdAb}$  (A) or  $^{68}\text{Ga-NOTA-R3b23-sdAb}$  (B). Exemplary mice are shown in coronal, sagittal and axial orientation (A) or just in coronal orientation (B).  $2 \times 10^7$  TCR-transgenic CD8<sup>+</sup> T cells were injected i.v. and the injected dose of applied tracer was  $13 \pm 1\text{MBq}$  per mouse. Scale bar is represented as standardized uptake value (SUV), 0.4 – 1.5 SUV. B = Bladder, K = Kidney. Green arrow = ML2-B7 tumor, white arrow = ML2-B15 tumor. (C) Biodistribution of  $^{68}\text{Ga}$ -activity in ML2-B7 and -B15 tumors for mice receiving CD2-sdAb or R3b23-sdAb 1.5 h post injection and after previous PET/MRI image acquisition. Mean %ID/g  $\pm$  SD is depicted for each group of mice. R3b23-sdAb n = 4, CD2-sdAb n = 4. Significance was calculated using Mann-Whitney test (\* p  $\leq$  0.05).

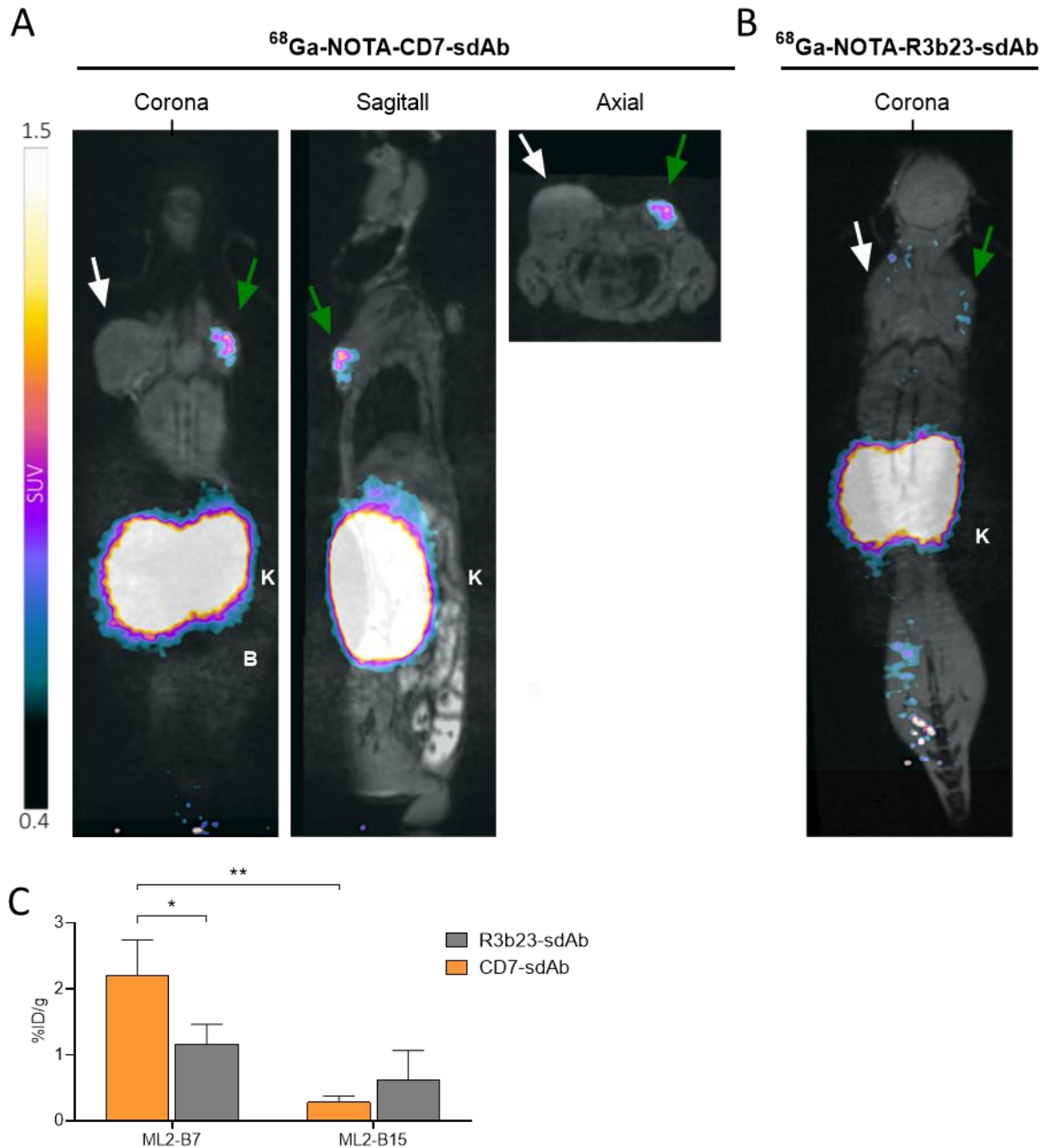


**Figure 33: In vivo tracking intravenously injected TCR-transgenic CD8<sup>+</sup> T cells in ML2-B7 tumors using  $^{68}\text{Ga-NOTA-CD7-sdAb}$ .**

PET/MRI images acquired 1 h p.i. of mice injected i.v. with  $^{68}\text{Ga-NOTA-CD7-sdAb}$  (A) or  $^{68}\text{Ga-NOTA-R3b23-sdAb}$  (B). Exemplary mice are shown in coronal, sagittal and axial orientation (A) or just in coronal orientation (B).  $2 \times 10^7$  TCR-transgenic CD8<sup>+</sup> T cells were injected i.v. and the injected dose of applied tracer was  $14 \pm 1\text{MBq}$  per mouse. Scale bar is represented as standardized uptake value (SUV), 0.4 – 1.5 SUV. B = Bladder, K = Kidney. Green arrow = ML2-B7 tumor, white arrow = ML2-B15 tumor. (C) Biodistribution of  $^{68}\text{Ga}$ -activity in ML2-B7 and -B15 tumors for mice receiving CD7-sdAb or R3b23-sdAb 1.5 h post injection and after previous PET/MRI image acquisition. Mean %ID/g  $\pm$  SD is depicted for each group of mice. R3b23-sdAb n = 4, CD7-sdAb n = 5. Significance was calculated using Mann-Whitney test (\* p  $\leq$  0.05, \*\* p  $\leq$  0.01).

Similarly, evaluation of  $^{68}\text{Ga}$ -NOTA-CD7-sdAb to track i.v. injected  $\text{CD8}^+$  T cells showed results that resembled the data from  $^{68}\text{Ga}$ -NOTA-CD2-sdAb, except slightly lower overall signal intensity. Acquisition of PET/MRI images showed that mice which received  $^{68}\text{Ga}$ -NOTA-CD7-sdAb exhibited strong and specific accumulation of tracer in ML2-B7 tumors compared to ML2-B15 tumors (Figure 33A). This specific signal in ML2-B7 tumors was seen in coronal-, sagittal- and axial orientation throughout the experiment. Ex vivo biodistribution of mice that received  $^{68}\text{Ga}$ -NOTA-CD7-sdAb showed a significantly enhanced activity in ML2-B7 tumors compared to ML2-B15 tumors (Figure 33C). Furthermore, biodistribution-analysis of tumors after  $^{68}\text{Ga}$ -NOTA-CD7-sdAb injection also confirmed previous PET/MRI data by showing a significantly higher accumulation of tracer in ML2-B7 tumors (mean 2.2 %ID/g) compared to ML2-B15 tumors (mean 0.3 %ID/g).

Additionally, biodistribution analysis of a variety of organs was conducted following PET/MRI image acquisition, depicting the expected high tracer-uptake in the kidney with minor tracer-uptakes in bladder in heterogeneous liver-uptake (Figure 34).

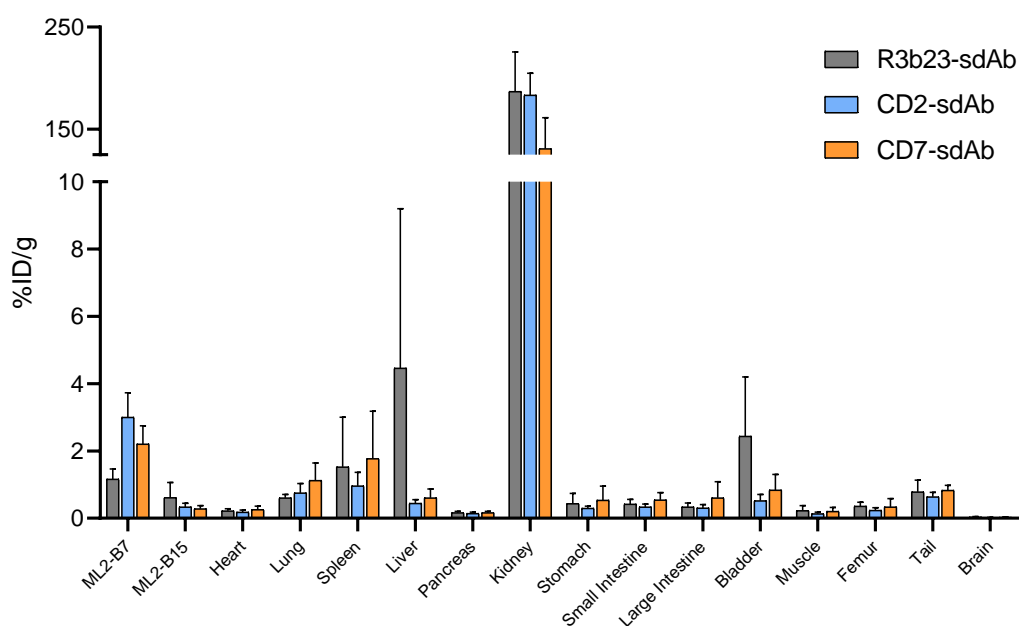


**Figure 34: Ex vivo biodistribution of  $^{68}\text{Ga}$ -radiolabeled CD2- and CD7-sdAb.**

Biodistribution of  $^{68}\text{Ga}$ -activity in various organs from mice 1.5 h post injection of the respective sdAb and following previously described PET/MRI analysis. Mean %ID/g  $\pm$  SD is depicted for each group of mice. R3b23-sdAb n = 4, CD2-sdAb n = 4, CD7-sdAb n = 5.

Taken as a whole, the data shows that  $^{68}\text{Ga}$ -radiolabeled CD2- and CD7-sdAb are promising candidates for clinical application to be utilized as PET/MRI tracers to specifically monitor human T cells in vivo.

## 4 Discussion

### 4.1 Evaluation of CD2 and CD7 as target antigens for immunoPET imaging

Establishment of a preclinical T-cell tracer with properties that allow for an attractive and advantageous possible clinical translation requires three main components: a suitable target antigen, a well-characterized probe and the matching, appropriate radionuclide (McCarthy, White, Viola, & Gibson, 2020). Since selection of the best suited radionuclide for CD2- and CD7-sdAb was done by our cooperation partners at the department of Nuclear Medicine, this discussion will focus on the first two mentioned subject areas.

Arguably the most impactful aspect, since it cannot be changed without necessitating the repetition of fundamental preclinical re-characterization, is the selection of a suitable T-cell target antigen. As described in the introduction, the key target-antigen of T-cell based immunoPET imaging over the past decade has been CD8, with numerous groups working preclinical approaches to specifically visualize and monitor CD8<sup>+</sup> T cells in regards to immunotherapy (Tavare et al., 2014).

As of this writing, a <sup>89</sup>Zr-labeled anti-CD8 minibody, termed <sup>89</sup>Zr-IAB22M2C, is the only T-cell specific tracer that was investigated in a first-in-humans clinical trial (NCT03107663). The study demonstrated that application of the tracer was safe and did not induce side effects, neither immediate nor delayed. Furthermore, the tracer was able to specifically depict CD8<sup>+</sup> T-cells rich tumor lesions 24 h post injection with off-target tracer-uptake in spleen, bone marrow, liver and kidney (Pandit-Taskar et al., 2020). While the study was a success and is currently followed up by a phase IIb study to analyze whether <sup>89</sup>Zr-IAB22M2C can predict responses of various tumor entities to immunotherapy (NCT05013099), the utilized tracer will only allow monitoring a part of the immune-response, restricted to CD8<sup>+</sup> T-cells.

However, a patients' response patterns as a consequence of immunotherapies can vary drastically (Borcoman et al., 2019) and encompass CD4<sup>+</sup> T-cells just as well as CD8<sup>+</sup> T-cells (Tran et al., 2014). Furthermore, newly developed immunotherapeutic approaches are increasingly utilizing the distinct role of CD4<sup>+</sup> T-cells for novel therapies. For example, using CD4<sup>+</sup> CAR T cells in a preclinical mouse model to treat acute lymphoblastic leukemia showed an equivalent cytotoxicity to CD8<sup>+</sup> CAR T cells while exhibiting an improved long-term tumor eradication (Yang et al., 2017). Additionally, the CD19-directed CAR T cell product lisocabtagene maraleucel, which has received FDA-approval in early 2021 for the treatment of adults with relapsed or refractory large B-cell lymphoma, is administered as a sequential

infusion of two components, CD8<sup>+</sup> and CD4<sup>+</sup> CD19-directed CAR T cells (Abramson et al., 2020).

Therefore, our study focused on harnessing the potential of an encompassing evaluation of T-cell immune responses by using the pan T-cell antigens CD2 and CD7.

#### 4.1.1 CD2

CD2 was first described as a pan T-cell antigen in 1982 by Sanchez-Madrid and colleagues (Sanchez-Madrid et al., 1982), and has since been used as a T-cell marker in flow cytometry (Cespedes et al., 2022) and immunohistochemistry (Tomita et al., 2015). Besides the previously discussed advantages of a pan T-cell antigen compared to a restricted subpopulation, CD2 has an added benefit, namely that it has been independently described by numerous groups to be more highly expressed on activated T cells (D. J. Lo et al., 2011; Rooney, Shukla, Wu, Getz, & Hacoen, 2015), with our group confirming these findings in 2018 (Mayer et al., 2018). This characteristic makes CD2 a highly attractive target to simultaneously depict the overarching T-cell population involved in the immune-response as well as specifically highlight activated T cells.

However, even though CD2 is most prominently expressed on T cells, it is also expressed on thymocytes (Reinherz, 1985) and both NK cells (Timonen et al., 1990) and dendritic cells (Matsui et al., 2009), which can therefore lead to binding of a CD2-targeted tracer to either of these cell populations, resulting in T-cell unspecific signal. While CD2 expression on cells other than T cells is not desirable, NK cells and dendritic cells both have been described to be important mediators in immunotherapy-responses and have been linked to improved patient survival or therapy response in tumors such as melanoma (Barry et al., 2018).

Therefore, although CD2 is expressed on all T cells, its simultaneous expression on NK cells (Tang et al., 2020) and dendritic cells (McArdel et al., 2016) can potentially still be linked to immunotherapeutic success and will likely not yield high-tracer binding unrelated to the patients' immune response. However, whether or not NK cells and dendritic cells affect the T-cell imaging capability of CD2-sdAb needs to be investigated, for instance in the context of a humanized mouse model.

#### 4.1.2 CD7

Expression of CD7 was, similarly to CD2, also described on thymocytes (Barcena et al., 1993) and NK cells (H. Rabinowich, L. Pricop, R. B. Herberman, & T. L. Whiteside, 1994), which leads to tracers targeting CD7 to be confronted with the same drawbacks. However, unlike CD2, expression of CD7 is only slightly increased on activated T cells (Mayer et al., 2018) and the highest expression levels were described on naïve- and memory T cells, while the lowest levels of CD7 were shown to be on effector T-cells (Aandahl et al., 2003).

While both CD2 and CD7 are expressed on thymocytes, expression of CD7 is present during all stages of T-cell development, while CD2 is not found on early T-cell precursor (ETP) cells and pro-T cells (Bayon-Calderon, Toribio, & Gonzalez-Garcia, 2020), thereby reducing the accumulation of tracer-signal in the thymus.

Taken together, while both CD2 and CD7 are primarily expressed on T cells, the fact that CD2 is more highly upregulated on specifically activated T cells than CD7 and less prominent on thymocytes makes CD2 the preferred target-antigen for non-invasive T-cell monitoring.

## 4.2 Specific binding site of CD2-sdAb and implications

Previous work of our group has used a CD2-targeted F(ab')<sub>2</sub>-fragment, radiolabeled with <sup>89</sup>Zr, to successfully track tumor-specific T cells in a xenograft mouse model (Mayer et al., 2018). While the used CD2-F(ab')<sub>2</sub> was able to specifically depict intravenously injected TCR-transduced T cells in vivo, its application resulted in severe T-cell depletion and subsequent failure of tumor rejection.

Importantly, the used CD2-F(ab')<sub>2</sub> was produced by enzymatic digestion of a full-size CD2-mAb, named OKT11, which targets the constantly expressed T11.1 epitope of CD2 (Warren & Parish, 1990). Of the three described epitopes of the CD2-protein, T11.1 and T11.2 are part of the adhesion domain needed for interaction between CD2 and CD58 and continuously expressed on T cells, while T11.3 is only increasingly expressed in the membrane-proximal domain after conformational changes of CD2 upon T-cell activation (J. Li, A. Smolyar, R. Sunder-Plassmann, & E. L. Reinherz, 1996).

As a result, most commercially available antibodies targeting CD2 are specifically developed to bind T11.1 or T11.2, to facilitate steady mAb-binding. This also enables the use of CD2-directed antibodies in therapeutic approaches for certain types of autoimmune conditions or organ transplantation, which can be characterized by excessive activation of CD2-positive T cells and NK cells (Sido et al., 1998).

While T-cell binding via OKT11-CD2-F(ab')<sub>2</sub> led to significant impairment of T-cell functionality, binding of CD2-sdAb did not affect cytokine secretion in vitro or cytotoxic abilities, neither in vitro or in vivo, of targeted T cells, suggesting that CD2-sdAb differs in terms of binding-specificity from OKT11.

The reason why CD2-sdAb binding differs from OKT11-CD2-F(ab')<sub>2</sub> binding and has no impairing effect on T-cell functionality could be because to the unique characteristics of sdAbs in terms of their antigen-binding capability. Due to its specific CDR3 region, which is able to form three distinct hypervariable loops (Desmyter et al., 2001), sdAbs are able to bind otherwise inaccessible epitopes in protein clefts that are otherwise not accessible by conventional mAbs (Huen et al., 2019). Therefore, CD2-sdAb could potentially bind either T11.1 or T11.2 in a way that is not accessible by OKT11-CD2-F(ab')<sub>2</sub>, and, importantly, does not result in T-cell depletion and –impairment. This would mean that CD2-sdAb is able to bind and depict T-cells irrespective of their activation status, since both T11.1 and T11.2 are also found on resting T cells.

Another hypothesis is that CD2-sdAb is not bypassing the effects that came with OKT11-CD2-F(ab')<sub>2</sub> binding to T11.1, but rather binding a different epitope altogether, namely T11.3. Since expression and availability of T11.3 is enhanced in activated T cells, this would allow CD2-sdAb to not just depict the overarching T-cell immune response via CD2, but to additionally increase the visibility and the impact of specifically activated T cells, irrespective of T-cell subpopulation.

To analyze both hypotheses simultaneously, binding of CD2-sdAb would need to be tested on rested, inactive T cells in comparison to specifically activated T cells. Commercially available kits allow the isolation of resting CD25<sup>-</sup> and CD4<sup>+</sup> T cells, which, compared to either activated CD4<sup>+</sup>- or CD8<sup>+</sup> T cells, would allow for a comparison of CD2-sdAb binding-intensity and quantity via flow cytometry analysis.

Another way to analyze whether CD2-sdAb binds CD2 via the T11.3 epitope would be to use a CRISPR/Cas9-based knockout of the specific T11.3 epitope on a CD2-positive cell population such as the naturally CD2- positive T cell leukemia cell line Jurkat E6.1. This would generate a CD2-positive but T11.3-negative control population that would facilitate specific binding analysis of CD2-sdAb via flow cytometry. However, only if a knockout of the T11.3 epitope would not change the conformation of CD2, thereby negating whether subsequent effects are due to T11.3-knockout or due to conformational changes of CD2 as a whole.

### 4.3 Impact of CD2- and CD7-sdAb binding on T-cell functionality

Investigating and correctly identifying potentially modulating effects of tracers is crucial in the context of immunoPET imaging, since mAb and its derivatives can have detrimental effects on T cells and other immune cells with a significant impact in therapeutic potential (Loubaki, Tremblay, & Bazin, 2013).

As briefly discussed beforehand, in previous work of our group we showed that in vivo application of a CD2-targeted F(ab')<sub>2</sub>-fragment resulted in severe T-cell depletion and failure of tumor rejection (Mayer et al., 2018). However, these T-cell impairing effects were not seen during in vitro studies where T-cell proliferation and –cytotoxic activity were analyzed by flow cytometry in response to CD2-F(ab')<sub>2</sub> binding. Cytotoxic efficacy of specifically activated T cells in the presence of CD2-targeted F(ab')<sub>2</sub> was analyzed by addition of CD2-targeted F(ab')<sub>2</sub> to a co-culture of TCR2.5D6 T cells and GFP-positive ML2-B7 tumor cells for 24 h. Afterwards, the percentage of GFP positive cells was assessed via flow cytometry to draw conclusions about T-cell efficacy over the preceding 24 h. This approach showed that while tumor-cell killing was slightly reduced in the presence of CD2-F(ab')<sub>2</sub> compared to T-cell mediated killing in the presence of an IgG1-isotype control.

To improve upon the previous workflow and to be able to identify T-cell impairing effects because of sdAb-binding before entering in vivo studies, we shifted from a static, flow cytometry-based way of analyzing T-cell cytotoxicity to a more sensitive, dynamic and real-time monitoring via the XCELLigence system. This assay enables a dynamic monitoring of T-cell functionality over the course of hours to even days by monitoring and analyzing structure and characteristics of targeted tumor cells via parameters such as cell number, cell adhesion and cell morphology in the presence of tumor-specific T cells. This allowed us to utilize cellular impedance to continuously evaluate real-time viability of target cells (624.38 Mel) in the presence of TCR2.5D6-transduced T cells and sdAb.

Using two different CD2-targeted F(ab')<sub>2</sub> fragments as positive controls, based on clones OKT11 and RPA-2.10, we evaluated T-cell mediated toxicity over the course of 24 h. The results confirmed effects that were previously only visible after in vivo studies, namely that addition of CD2-targeted F(ab')<sub>2</sub> fragments, independent of the used clone, leads to a significant reduction in T-cell mediated killing of targeted tumor cells (Figure 20). The T-cell impairing effects of CD2-targeted F(ab')<sub>2</sub> fragments that we have observed via the XCELLigence assay and that were shown in vivo in previous work by Mayer & Mall et al., could also be replicated in our subsequent in vivo study. While neither CD2- nor CD7-sdAb showed any effect on cytotoxic efficacy of T cells in vivo, both CD2-F(ab')<sub>2</sub>-(OKT11) and CD2-F(ab')<sub>2</sub> (RPA-2.10)

resulted in failed tumor rejection (Figure 25). Taken together and as a baseline for any future characterizations of potential imaging constructs, the XCELLigence assay will be implemented in the workflow to screen and assess any T-cell impairing effects in vitro.

Besides direct impairment of T-cell functionality, targeting a patient's T cells with a mAb or an antibody-derived construct can have an additional, less immediate but equally detrimental effect. Cytokine release syndrome (CRS) is a life-threatening condition that is characterized by heightened release of inflammatory cytokines such as IFN $\gamma$ , TNF $\alpha$ , IL6, GM-CSF, IL10, IL2, IL8, and IL5 (Brudno & Kochenderfer, 2016).

In the setting of adoptive T-cell therapy, the pathophysiology of CRS can be divided in two interconnecting phases. First, specifically activated TCR-T cells or CAR T cells produce large amounts of IFN $\gamma$  and TNF $\alpha$ , which are seen as the initiators of CRS (Karki et al., 2021). Next, IFN $\gamma$  and TNF $\alpha$  trigger the activation of other immune cells, especially monocytes and macrophages, which are thus themselves secreting cytokines such as IL1, IL6, and IL10 (Hunter & Jacobson, 2019; Mosser & Edwards, 2008). Early clinical manifestations of CRS are typically high fever (D. W. Lee et al., 2014) followed by a systemic inflammatory response, respiratory and cardiovascular insufficiency and, if left untreated, even death (Davila et al., 2014).

However, modification of secreted cytokines is rarely investigated in the context of T-cell imaging (Seo et al., 2018; Tavare et al., 2014) and excused by the claim that preclinical models are “not able to predict clinical response to immunotherapy”, including factors such as differences in cytokine release (Kasten et al., 2021). And while it is true that preclinical models are not able to represent the comprehensive and multifaceted clinical response to immunotherapy (Choi et al., 2018), preclinical research is able to evaluate whether addition of a T-cell targeting antibody or antibody derived construct will have an immediate and directly linked impact on T-cell based cytokine secretion. While this is only part of the immunotherapeutic response, it is still essential to minimize patient-risk as much as possible prior to clinical translation by assessing one of the most crucial consequences due to T-cell binding.

Therefore, to decrease the possibility of any effect that CD7-sdAb and CD2-sdAb might have on T-cell based cytokine secretion, we monitored the cytokine profiles of IFN $\gamma$ , GM-CSF, IL-2, and TNF $\alpha$  in the presence of both sdAbs. After 24 h, no significant alterations of cytokine levels were observed when comparing CD2-sdAb and CD7-sdAb to the control R3b23-sdAb (Figure 22 & 23). To gather as much information as possible, this analysis was repeated for three different cell lines, neither of which showed any cytokine-secretion alteration.

#### 4.4 Tracer-characteristics of CD2- and CD7-sdAb

Both CD2-sdAb and CD7-sdAb were extensively analyzed in terms of their specificity, binding affinity and thermal stability to describe relevant parameters for clinical-translation as early as possible.

##### 4.4.1 Target-antigen specificity

Evaluating target-antigen specificity for both CD2- and CD7-sdAb was an essential aspect of preclinical characterization. On the one hand, a distinct target-antigen specificity ensures the minimization of off-target binding and guarantees that a high accumulation of tracer, other than in clearance-related organs, is correlated to target-antigen density. On the other hand, by thoroughly investigating specificity, unwanted risks during subsequent preclinical toxicology-studies or clinical trials can be minimized (Starr & Tessier, 2019). Even though mAb and antibody-fragments are generally thought of as highly specific, there are still examples of detrimental off-target effects.

One such example was an antibody called PRO304186, which was targeting soluble IL17A and IL17F to be used as an anti-inflammatory therapeutic in regards to autoimmune- and inflammatory diseases (Pai et al., 2016). In a repeat-dose toxicology study where PRO304186 was administered to cynomolgus monkeys, its application led to adverse effects such as hypotension and gastrointestinal tract hemorrhage, which, in severe cases, could result in death of the animal. Investigation into the underlying reason for the unexpected adverse effects revealed that off-target binding of PRO304186 to vascular endothelial cells resulted in increased production of nitric oxide (NO), which enhanced vasodilation and ultimately led to hypotension.

Another example is the CD28-directed mAb TGN1412, which was originally intended to be used in the treatment of B cell chronic lymphocytic leukemia as well as rheumatoid arthritis (Luhder et al., 2003). The preliminary murine version of TGN1412 was extensively studied in both rats and mice for its therapeutic effects as well as safety, with beneficial therapeutic effects but no observable adverse effects (Dennehy et al., 2006). Additionally, a repeat dose study for toxicokinetic evaluation non-human primates (NHP) was conducted with doses as high as 50 mg/ml that were well tolerated and showed no adverse reactions (Hunig, 2016). However, a first-in-man clinical trial in which six healthy men received TGN1412 resulted in all volunteers experiencing cytokine release syndrome (CRS), leading to multiorgan failure and treatment in the intensive care unit (ICU) of the London hospital (Suntharalingam et al., 2006). Even though

all motifs critical for signal transduction in human and the used NHPs, cynomolgus and rhesus monkeys, are 100 % conserved, the toxicology-study was not able to predict the disastrous effects in human subjects (Hanke, 2006).

Therefore, a focus was put on ensuring that CD2- and CD7-sdAb show a high degree of binding specificity to their respective target antigens. To that end, binding-specificity was investigated twofold, once by transducing the CD2- and CD7-negative cell line U698M with CD2 and CD7 respectively (Figure 8), and once by using a CRISPR/Cas9-based knockout of each target-antigen on the naturally CD2- and CD7 positive T cell leukemia cell line Jurkat E6.1 (Figure 11,13).

The CD2- and CD7-positive U698M cell lines were analyzed via flow cytometry to assess whether CD2-sdAb and CD7-sdAb are specifically recognizing their target antigens and consequently only bind target-antigen transduced U698M cells compared to untransduced U698M control cells. While both sdAbs showed no binding to untransduced U698M cells, a distinct binding was observed for all CD2- or CD7-transduced U698M cells, confirming that both sdAb specifically recognize their respective target antigen on the surface of otherwise CD2- and CD7-negative tumor cells.

Next, it was evaluated whether CD2- and CD7-sdAb only bind to their respective target antigens on the surface of physiologically relevant target cells. To test this hypothesis, Jurkat E6.1 cells, which are an immortalized T-cell derived cell line, were used due to their high similarity to physiological T cells and because their immortality allows for the generation of a CD2- and CD7-negative T-cell derived cell line. After successfully depriving a large amount of Jurkat cells of CD2 and CD7 respectively, binding of CD2- and CD7-sdAb correspondingly decreased and no significant leftover binding on CD2- and CD7-negative Jurkat cells was observed.

Taken together, the specificity of both CD2- and CD7-sdAb to their respective target antigen was successfully proven and the likeliness of off-target T-cell binding was evaluated and considered to be very low.

#### 4.4.2 Binding affinity

Besides confirmation of target-antigen specificity for both CD2-sdAb and CD7-sdAb, binding affinity of each sdAb to their respective targets on T cells is equally important. The reason being, that high-affinity antibodies are able to bind the target-antigen quickly, allow for greater sensitivity and are crucial for in vivo binding under more challenging conditions (Bostrom, Lee,

Haber, & Fuh, 2009). Therefore, after in-depth characterization and confirmation of the binding specificity of both CD2- and CD7-sdAb, the binding affinity to their target antigens was evaluated and quantified by determination of the respective dissociation constants.

Binding of CD2- and CD7-sdAb to CD8<sup>+</sup> T cells was monitored over the course of using various sdAb-concentrations and quantifying the binding via flow cytometry analysis. Ultimately, the dissociation constants for each sdAb, and by extension their corresponding binding affinities, were observed to be  $2.30 \times 10^{-9}$  M for CD2-sdAb and  $6.34 \times 10^{-9}$  M for CD7-sdAb (Figure 14).

To evaluate the quantitative binding affinities of CD2- and CD7 and give them qualitative value, a literature comparison to other sdAb or T-cell targeting constructs currently in clinical trial was done.

In a preclinical study where 38 different anti-HER2-sdAb were investigated to find the candidate with the most promising characteristics in terms of an intended subsequent clinical trial, binding affinity was one of the key aspects when deciding on the best candidate (Vaneycken et al., 2011). Analysis of binding affinity, as determined via saturation binding, revealed a dissociation constant of the eventually decided upon candidate 2Rs15d of  $11.6 \times 10^{-9}$  M. The successive open-label phase I trial showed that the 2Rs15d-sdAb, coupled to <sup>68</sup>Ga, was able to successfully bind and visualize HER2-positive tissues in 20 women with primary or metastatic breast carcinoma (Keyaerts et al., 2016). Nonetheless, the requirements and challenges for a sdAb to bind antigen-specific tumor-tissue are different compared to tumor-infiltrating targets such as T cells.

Therefore, since there is no T-cell targeting sdAb currently in clinical trial, the anti-CD8-minibody that was successfully used in a phase I trial was used for comparison. While the clinical trial was a success and CD8<sup>+</sup> T-cell-rich tissues could be visualized in a safe manner in patients with solid tumors (Pandit-Taskar et al., 2020), preclinical investigation of the anti-CD8-minibody showed a binding affinity of  $33 \times 10^{-9}$  M (Tavare et al., 2014), thus 14x higher than CD2-sdAb and 5x higher than CD7-sdAb.

Taken together, the determined binding affinities of CD2- and CD7-sdAb are on par with an anti-HER2-sdAb and surpass an anti-CD8-minibody, both of which were successfully tested in clinical trials.

#### 4.4.3 Thermal stability

Evaluation of thermal stability is far less frequent in the preclinical characterization of antibodies or sdAb. While thermal stability is an important parameter to ensure robust *in vivo* binding (Ma, O'Fagain, & O'Kennedy, 2020), it is especially important for antibodies and sdAb that are being used in immunoPET imaging. Due to high temperatures used for radionuclide-labelling of up to 50 °C (Robu et al., 2021), it is crucial that the used constructs retain their binding capabilities in high temperatures.

While the previously discussed anti-CD8-minibody did not evaluate its thermal stability, the anti-HER2-sdAb was tested in terms of its melting temperature ( $T_m$ ) via monitoring the sdAb-unfolding with increasing temperatures (Vaneycken et al., 2011). It showed that up until 70 °C there was no significant sdAb-unfolding and the  $T_m$ , so the temperature at which half-maximal unfolding was observed, was determined to be 78.5 °C.

Compared to these results, the CD2- and CD7-sdAb were not just assessed in terms of unfolding at increasing temperatures, but whether or not they are still capable of effectively binding their target-antigens over the course of 6 hours, thereby including a functional aspect in the analysis. The data showed that at 37 °C and 60 °C, both CD2- and CD7-sdAb showed no impairment of their binding capabilities (Figure 15). Furthermore, incubation of both sdAbs at 90 °C did not immediately lead to reduced binding, but a decline in binding was observed after incubation for two hours, indicating that CD2- and CD7-sdAb are capable of retaining their binding abilities even at high temperatures.

#### 4.5 Suitability of sdAb for immunoPET imaging

Besides the choice of the appropriate and specific target antigen, the construct specifically binding the target-antigen and enabling the tissue-specific enrichment of tracer at the desired target site is equally as important.

As describes previously in the introduction, sdAb exhibit a great number of features that make them particularly advantageous as tracers during immunoPET imaging. To briefly summarize, sdAb stand out by exhibiting very low immunogenicity (Steeland et al., 2015), high affinity (Mitchell & Colwell, 2018) and specificity (Hassanzadeh-Ghassabeh et al., 2013), fast renal clearance (Xenaki et al., 2021) and, maybe most importantly, swift and thorough penetration of even dense tissue (Zottel et al., 2020). Taken together, sdAbs seem to be the ideal backbone for immunoPET imaging that aims to quickly visualize targets within hard to access tissues and minimize the radioactive burden to the patient due to fast clearance.

Yet, sdAbs also come with certain limitations, especially due to their small size. One such limitation is the high uptake of sdAb-based tracers in kidneys as well as the bladder (Movahedi et al., 2012). These accumulations are based on the small size and consequential rapid renal clearance via the kidneys (Asaadi, Jouneghani, Janani, & Rahbarizadeh, 2021).

However, the rapid renal clearance has a twofold impact on sdAb in terms of their imaging characteristics. For one thing, since it is rapidly cleared, the background signal during imaging reduces quickly after injection, which enables early monitoring of target areas not close to the kidney and simultaneously minimizes the risk as a result of lengthy off-target toxicity (Castelli, McGonigle, & Hornby, 2019). At the same time, imaging of lesions near the kidneys becomes more challenging and the radioactive burden at the kidneys increases (Hassanzadeh-Ghassabeh et al., 2013).

But there are several ways to minimize renal retention and therefore mitigate the possible adverse effects on the kidneys. Renal retention of sdAbs was shown to be primarily driven by the number of polar residues in the C-terminal amino acid tag (D'Huyvetter, Vincke, et al., 2014). The group that first described this, illustrated this finding by removing the Myc-His-Tag from a HER2-targeting sdAb and showed that renal accumulation was reduced by almost 90 % compared to the sdAb with the Myc-His-Tag still attached (D'Huyvetter, Vincke, et al., 2014). An additional strategy to further reduce kidney accumulation of sdAbs is based on blocking sdAb-binding to megalin, a protein involved in membrane-transportation and in large parts responsible for kidney reabsorption. A preclinical study showed that a <sup>99m</sup>Tc-radiolabeled sdAb exhibited a reduced renal uptake of 44 % in megalin-deficient mice compared to megalin-wild-type mice (Gainkam et al., 2011). To translate this approach to a feasible clinical setting, megalin-blocking could be achieved by simultaneous injection of lysine, monosium glutamate or gelofusine, which all can act as megalin-blockers and have been successfully tested in a preclinical setting (Rousseau et al., 2018).

An additional limitation that sdAbs face due to their small size, is the aspect that rapid clearance from the bloodstream via renal excretion might prevent sufficient and encompassing binding of sdAb to all epitopes at the target site. To overcome this issue, strategies were developed that are based on the modification of sdAbs by combining them with additional molecules to prolong the blood circulation of sdAbs.

One of the most promising approaches is the addition of polyethylene glycol (PEG), a hydrophilic polymer which has been shown to increase the blood circulation time of sdAbs in a preclinical setting (T. Wu et al., 2018). This approach, also called PEGylation, works by attaching PEG in a variety of possible sizes such as 5, 10 or 20 kDa to the sdAb, thereby

increasing their molecular weight and consequently their blood circulation time (Harmand, Islam, Pishesha, & Ploegh, 2021). A preclinical study, where a  $^{89}\text{Zr}$ -radiolabeled anti-CD8 sdAb was used to detect CD8<sup>+</sup> T cells in a melanoma mouse model, investigated the effects that addition PEG in a size of either 5, 10 or 20 kDa to the sdAb had on the blood circulation time (M. Rashidian et al., 2017). Mice were imaged via PET/CT 24 hours post injection of the tracer and kidney uptake was assessed for each group of mice. Kidney retention was inversely correlated to size of PEG-addition, with the 20-kDa PEGylated CD8-sdAb showing the least accumulation at the kidney, thereby indicating that addition of PEG is a feasible option to prolong the circulatory half-life of sdAbs in vivo.

While this approach is able to successfully extend sdAb blood-circulation, it simultaneously works against one of the biggest advantages of sdAb-imaging, namely their small size. By artificially increasing the molecular weight and by extension the size of the tracer, characteristics such as fast tissue penetration and the ability to enter dense tissues might be negatively impacted.

The importance of the advantaged presented the small size of a sdAb can be best illustrated by looking at an example of T-cell targeting construct that is larger in size. The already in the introduction of this dissertation described  $^{89}\text{Zr}$ -radiolabeled anti-CD8 minibody, with a molecular weight of ~ 80 kDa, was successfully used in a first-in-humans dose escalation phase clinical trial and declared to be safe in six patients suffering from solid malignancies (Pandit-Taskar et al., 2020). However, the  $^{89}\text{Zr}$ -radiolabeled anti-CD8 minibody was only able to visualize most CD8-positive lesions until after 24 hours post initial injection. This long delay can be attributed to the high molecular weight and size of the tracer and the ensuing limitations in regards to blood circulation time and velocity of tissue penetration.

This demonstrates the importance of choice when it comes to the tracer used in immunoPET imaging. The visualization of T cells in the context of immunotherapies requires fast and efficient in-depth tissue penetration, binding of the target-antigen within minutes instead of hours after injection and rapid clearance from the blood to ensure the highest degree of patient-safety. A sdAb is therefore estimated to have substantial advantages to address these characteristics and offer the widest range of advantages while facing the least number of limitations.

#### 4.6 CD2- and CD7-sdAb as immunoPET imaging tracers

After CD2- and CD7-sdAb were thoroughly characterized in terms of their target-antigen specificity, binding affinity and thermal stability and it was furthermore shown that, both in vitro and in vivo, the binding of each sdAb did not impair T-cell functionality, both tracers were evaluated for their aptness during PET/MRI imaging.

Initially, to establish a proof of concept, an imaging tumor model was used in which NSG mice were subcutaneously injected with ML2-B7 and -B15 tumor cells and after eight days,  $1 \times 10^7$  TCR-transgenic CD8<sup>+</sup> T cells were intratumorally injected. Intratumoral injection was done to guarantee T-cell presence in ML2-B7 tumors and to allow for a distinct and strong PET-signal as part of the proof of concept in vivo study. After five days, 1.61 MBq of <sup>68</sup>Ga-NOTA-CD2-sdAb was intravenously injected via tail vein and subsequent PET/MRI acquisition at 2 hours post injection showed a distinct accumulation of tracer at the tumor site, with additional, as expected for sdAb, tracer uptake at the kidneys (Figure 28). The time point of 2 hours post injection for the acquisition of the images was chosen based on literature research and based on the expected circulation time of the sdAb and the half-life of <sup>68</sup>Ga (Liu et al., 2021).

Further evaluation of the ideal timepoint of PET/MRI image acquisition was done by using one mouse per sdAb to sequentially monitor tracer uptake 1 h, 2 h, 3 h and 4 h post injection of intravenously injected with  $2 \times 10^7$  CD8<sup>+</sup> T cells (Figure 29, Figure 30). Since the optimal time point to acquire PET/MRI images is conditional on specifics such as half-life of the used radioisotope, accumulation at the tissue of interest and subsequent detachment and clearance of the sdAb, narrowing down the most suitable time point is essential. Both tracers showed no tracer accumulation at the irrelevant control tumor ML2-B15 at any time point, while clear and distinct tracer accumulation was seen in the ML2-B7 tumors starting from 1 hour post injection and steadily descending until 4 hours post injection.

Based on these results, 1 hour post injection was deemed the optimal time point due to strongest accumulation of tracer at the tumor site. However, these results were based on one mouse per group and therefore hold no statistical relevance and should be repeated to ensure that the time chosen for PET/MRI imaging is indeed the most suitable one for CD2- and CD7-sdAb.

Lastly, combining the previously generated framework parameters, utilizing CD2- and CD7-sdAb in an intravenously injected xenograft model with image acquisition 1 hour post injection, both tracers were evaluated via PET/MRI in comparison to R3b2-sdAb. Across all mice, four for CD2-sdAb and five for CD7-sdAb, no visible tracer uptake at the control tumor ML2-B15 was visible and no other off-target accumulation other than kidneys and bladder was seen (Figure 32, Figure 33). Tracer accumulation at ML2-B7 tumors on the other hand was

distinctly visible 1 hour post injection for all mice and showed clear T-cell infiltration of CD2- and CD7-targeted  $^{68}\text{Ga}$ -NOTA-sdAb. Additional biodistribution analysis of both tumors as well as of a variety of organs revealed a strong correlation between PET/MRI image accumulation and quantifiable tracer uptake, showing that ML2-B7 tumors had a significantly increased tracer uptake compared to control tumors and R3b2-sdAb controls.

## 5 Conclusion and outlook

We have established two novel sdAb-based tracers, CD2-sdAb and CD7-sdAb, targeting the pan T-cell markers CD2 and CD7 for immunoPET imaging of T cells in the context of immunotherapies. By targeting CD2 and CD7, we aim to overcome the limitations set by monitoring only a restricted population of T cells and instead encapsulate and visualize the whole spectrum of specific T-cell responses during immunotherapy. Expression profiles of both target antigens have been extensively studied and a large focus was put on ensuring CD2- and CD7-specificity to guarantee a high degree of specific tracer accumulation and reduce the chance for off-target target binding, thereby leading to an increased patient safety.

Additionally, we further developed and improved preclinical testing of T-cell impairment after tracer binding by implementing the XCELLigence assay in addition to monitoring of cytokine secretion profiles and in vivo tumor rejection studies. The effects of CD2- and CD7-sdAb binding on T cells were investigated by each assay and none of them showed any form of T-cell impairment or -modification, neither in vitro nor in vivo. We were therefore able to conclude that initial preclinical analysis shows that both tracers are safe and have no impact on T-cell functionality.

Besides analyses of purity, binding affinity, specificity, thermostability and possible T-cell affecting aspects, CD2- and CD7-sdAb were thoroughly assessed in regards to their capability to visualize adoptively transferred human T cells in a xenograft mouse model. Coupled to the radionuclide  $^{64}\text{Ga}$  via the chelator NOTA, injection of CD2- and CD7-sdAb resulted in highly specific PET/MRI signals one hour post injection at the tumor site of interest in a myeloid sarcoma mouse model, distinctly mapping therapeutic T-cell infiltration with no unexpected off-target accumulation.

Taken together, we have developed two pan T-cell tracers that were able to clearly differentiate between responding- and non-responding tumors while not impacting T-cell functionality. This would allow for this technology to be utilized as a T-cell tracer irrespective of T-cell subtype and be a vital tool in the decision-making process of immunotherapeutic approaches.

To bridge the gap between preclinical proof of concept and clinical translation, additional steps are required to guarantee patient safety as best as possible and minimize any risk posed by application of the tracer. Production and purification of both sdAbs would need to be more standardized and regulated to exclude the risk of contamination and build the foundation for eventual statutorily regulated good manufacturing practice (GMP)-production.

Additionally, in-depth safety studies regarding pharmacokinetic- and toxicology analyses are essential for clinical translation. Pharmacokinetic studies are needed to describe the absorption, distribution, metabolism and excretion of the administered CD2- or CD7-sdAb, while toxicology analyses aim to characterize the toxicity profile of both constructs by investigating the dose-related risks and their impact on organs structures.

Since toxicology studies require the selection of an appropriate and well-suited species for the studied application and we aim to specifically target human CD2- and CD7-positive T cells, rodents such as mice, rats or hamsters will not be a suitable species to adequately describe the toxicity profile. Instead, mice reconstituted with a human immune system, termed humanized mouse models, could provide an opportunity to appropriately detail the toxicological properties of CD2- and CD7-sdAb application.

## 6 References

- Aandahl, E. M., Sandberg, J. K., Beckerman, K. P., Tasken, K., Moretto, W. J., & Nixon, D. F. (2003). CD7 is a differentiation marker that identifies multiple CD8 T cell effector subsets. *J Immunol*, *170*(5), 2349-2355. doi:10.4049/jimmunol.170.5.2349
- Abbasi, A. W., Westerlaan, H. E., Holtman, G. A., Aden, K. M., van Laar, P. J., & van der Hoorn, A. (2018). Incidence of Tumour Progression and Pseudoprogression in High-Grade Gliomas: a Systematic Review and Meta-Analysis. *Clin Neuroradiol*, *28*(3), 401-411. doi:10.1007/s00062-017-0584-x
- Abou, D. S., Ku, T., & Smith-Jones, P. M. (2011). In vivo biodistribution and accumulation of <sup>89</sup>Zr in mice. *Nucl Med Biol*, *38*(5), 675-681. doi:10.1016/j.nucmedbio.2010.12.011
- Abramson, J. S., Palomba, M. L., Gordon, L. I., Lunning, M. A., Wang, M., Arnason, J., . . . Siddiqi, T. (2020). Lisocabtagene maraleucel for patients with relapsed or refractory large B-cell lymphomas (TRANSCEND NHL 001): a multicentre seamless design study. *Lancet*, *396*(10254), 839-852. doi:10.1016/S0140-6736(20)31366-0
- Agata, Y., Kawasaki, A., Nishimura, H., Ishida, Y., Tsubata, T., Yagita, H., & Honjo, T. (1996). Expression of the PD-1 antigen on the surface of stimulated mouse T and B lymphocytes. *Int Immunol*, *8*(5), 765-772. doi:10.1093/intimm/8.5.765
- Ahmadzadeh, M., Pasetto, A., Jia, L., Deniger, D. C., Stevanovic, S., Robbins, P. F., & Rosenberg, S. A. (2019). Tumor-infiltrating human CD4(+) regulatory T cells display a distinct TCR repertoire and exhibit tumor and neoantigen reactivity. *Sci Immunol*, *4*(31). doi:10.1126/sciimmunol.aao4310
- Aide, N., Hicks, R. J., Le Tourneau, C., Lheureux, S., Fanti, S., & Lopci, E. (2019). FDG PET/CT for assessing tumour response to immunotherapy : Report on the EANM symposium on immune modulation and recent review of the literature. *Eur J Nucl Med Mol Imaging*, *46*(1), 238-250. doi:10.1007/s00259-018-4171-4
- Alexandrov, L. B., Nik-Zainal, S., Wedge, D. C., Aparicio, S. A., Behjati, S., Biankin, A. V., . . . Stratton, M. R. (2013). Signatures of mutational processes in human cancer. *Nature*, *500*(7463), 415-421. doi:10.1038/nature12477
- Ansell, S. M., Lesokhin, A. M., Borrello, I., Halwani, A., Scott, E. C., Gutierrez, M., . . . Armand, P. (2015). PD-1 blockade with nivolumab in relapsed or refractory Hodgkin's lymphoma. *N Engl J Med*, *372*(4), 311-319. doi:10.1056/NEJMoa1411087
- Asaadi, Y., Jouneghani, F. F., Janani, S., & Rahbarizadeh, F. (2021). A comprehensive comparison between camelid nanobodies and single chain variable fragments. *Biomark Res*, *9*(1), 87. doi:10.1186/s40364-021-00332-6
- Ashmore-Harris, C., Iafrate, M., Saleem, A., & Fruhwirth, G. O. (2020). Non-invasive Reporter Gene Imaging of Cell Therapies, including T Cells and Stem Cells. *Mol Ther*, *28*(6), 1392-1416. doi:10.1016/j.ymthe.2020.03.016
- Ayati, N., Lee, S. T., Zakavi, S. R., Cheng, M., Lau, W. F. E., Parakh, S., . . . Scott, A. M. (2021). Response Evaluation and Survival Prediction After PD-1 Immunotherapy in Patients with Non-Small Cell Lung Cancer: Comparison of Assessment Methods. *J Nucl Med*, *62*(7), 926-933. doi:10.2967/jnumed.120.254508

## References

- Azimi, F., Scolyer, R. A., Rumcheva, P., Moncrieff, M., Murali, R., McCarthy, S. W., . . . Thompson, J. F. (2012). Tumor-infiltrating lymphocyte grade is an independent predictor of sentinel lymph node status and survival in patients with cutaneous melanoma. *J Clin Oncol*, *30*(21), 2678-2683. doi:10.1200/JCO.2011.37.8539
- Bailey, S. R., & Maus, M. V. (2019). Gene editing for immune cell therapies. *Nat Biotechnol*, *37*(12), 1425-1434. doi:10.1038/s41587-019-0137-8
- Banchereau, J., & Steinman, R. M. (1998). Dendritic cells and the control of immunity. *Nature*, *392*(6673), 245-252. doi:10.1038/32588
- Barcena, A., Muench, M. O., Galy, A. H., Cupp, J., Roncarolo, M. G., Phillips, J. H., & Spits, H. (1993). Phenotypic and functional analysis of T-cell precursors in the human fetal liver and thymus: CD7 expression in the early stages of T- and myeloid-cell development. *Blood*, *82*(11), 3401-3414. Retrieved from <https://www.ncbi.nlm.nih.gov/pubmed/7694684>
- Bardia, A., Hurvitz, S. A., Tolaney, S. M., Loirat, D., Punie, K., Oliveira, M., . . . Investigators, A. C. T. (2021). Sacituzumab Govitecan in Metastatic Triple-Negative Breast Cancer. *N Engl J Med*, *384*(16), 1529-1541. doi:10.1056/NEJMoa2028485
- Barry, K. C., Hsu, J., Broz, M. L., Cueto, F. J., Binnewies, M., Combes, A. J., . . . Krummel, M. F. (2018). A natural killer-dendritic cell axis defines checkpoint therapy-responsive tumor microenvironments. *Nat Med*, *24*(8), 1178-1191. doi:10.1038/s41591-018-0085-8
- Bayon-Calderon, F., Toribio, M. L., & Gonzalez-Garcia, S. (2020). Facts and Challenges in Immunotherapy for T-Cell Acute Lymphoblastic Leukemia. *Int J Mol Sci*, *21*(20). doi:10.3390/ijms21207685
- Beckford Vera, D. R., Smith, C. C., Bixby, L. M., Glatt, D. M., Dunn, S. S., Saito, R., . . . Parrott, M. C. (2018). Immuno-PET imaging of tumor-infiltrating lymphocytes using zirconium-89 radiolabeled anti-CD3 antibody in immune-competent mice bearing syngeneic tumors. *PLoS One*, *13*(3), e0193832. doi:10.1371/journal.pone.0193832
- Borcoman, E., Kanjanapan, Y., Champiat, S., Kato, S., Servois, V., Kurzrock, R., . . . Le Tourneau, C. (2019). Novel patterns of response under immunotherapy. *Ann Oncol*, *30*(3), 385-396. doi:10.1093/annonc/mdz003
- Borghaei, H., Paz-Ares, L., Horn, L., Spigel, D. R., Steins, M., Ready, N. E., . . . Brahmer, J. R. (2015). Nivolumab versus Docetaxel in Advanced Nonsquamous Non-Small-Cell Lung Cancer. *N Engl J Med*, *373*(17), 1627-1639. doi:10.1056/NEJMoa1507643
- Bostrom, J., Lee, C. V., Haber, L., & Fuh, G. (2009). Improving antibody binding affinity and specificity for therapeutic development. *Methods Mol Biol*, *525*, 353-376, xiii. doi:10.1007/978-1-59745-554-1\_19
- Brentjens, R. J., Davila, M. L., Riviere, I., Park, J., Wang, X., Cowell, L. G., . . . Olszewska, M. (2013). CD19-targeted T cells rapidly induce molecular remissions in adults with chemotherapy-refractory acute lymphoblastic leukemia. *Science translational medicine*, *5*(177), 177ra138-177ra138.
- Brocker, T. (2000). Chimeric Fv-zeta or Fv-epsilon receptors are not sufficient to induce activation or cytokine production in peripheral T cells. *Blood*, *96*(5), 1999-2001. Retrieved from <https://www.ncbi.nlm.nih.gov/pubmed/10961908>

- Brocker, T., & Karjalainen, K. (1995). Signals through T cell receptor-zeta chain alone are insufficient to prime resting T lymphocytes. *J Exp Med*, *181*(5), 1653-1659. doi:10.1084/jem.181.5.1653
- Brown, J. R., Cymbalista, F., Sharman, J., Jacobs, I., Nava-Parada, P., & Mato, A. (2018). The Role of Rituximab in Chronic Lymphocytic Leukemia Treatment and the Potential Utility of Biosimilars. *Oncologist*, *23*(3), 288-296. doi:10.1634/theoncologist.2017-0150
- Brudno, J. N., & Kochenderfer, J. N. (2016). Toxicities of chimeric antigen receptor T cells: recognition and management. *Blood, The Journal of the American Society of Hematology*, *127*(26), 3321-3330.
- Brunet, J. F., Denizot, F., Luciani, M. F., Roux-Dosseto, M., Suzan, M., Mattei, M. G., & Golstein, P. (1987). A new member of the immunoglobulin superfamily--CTLA-4. *Nature*, *328*(6127), 267-270. doi:10.1038/328267a0
- Burugu, S., Dancsok, A. R., & Nielsen, T. O. (2018). Emerging targets in cancer immunotherapy. *Semin Cancer Biol*, *52*(Pt 2), 39-52. doi:10.1016/j.semcancer.2017.10.001
- Busch, W. (1868). Aus der Sitzung der medicinischen Section vom 13 November 1867. *Berl Klin Wochenschr*, *5*(5), 137.
- Butterfield, L. H., Ribas, A., Dissette, V. B., Amarnani, S. N., Vu, H. T., Oseguera, D., . . . Economou, J. S. (2003). Determinant spreading associated with clinical response in dendritic cell-based immunotherapy for malignant melanoma. *Clin Cancer Res*, *9*(3), 998-1008. Retrieved from <https://www.ncbi.nlm.nih.gov/pubmed/12631598>
- Butts, C., Socinski, M. A., Mitchell, P. L., Thatcher, N., Havel, L., Krzakowski, M., . . . team, S. t. (2014). Tecemotide (L-BLP25) versus placebo after chemoradiotherapy for stage III non-small-cell lung cancer (START): a randomised, double-blind, phase 3 trial. *Lancet Oncol*, *15*(1), 59-68. doi:10.1016/S1470-2045(13)70510-2
- Campana, D., van Dongen, J. J., Mehta, A., Coustan-Smith, E., Wolvers-Tettero, I. L., Ganeshaguru, K., & Janossy, G. (1991). Stages of T-cell receptor protein expression in T-cell acute lymphoblastic leukemia. *Blood*, *77*(7), 1546-1554.
- Capelan, M., Pugliano, L., De Azambuja, E., Bozovic, I., Saini, K. S., Sotiriou, C., . . . Piccart-Gebhart, M. J. (2013). Pertuzumab: new hope for patients with HER2-positive breast cancer. *Ann Oncol*, *24*(2), 273-282. doi:10.1093/annonc/mds328
- Cardillo, T. M., Govindan, S. V., Sharkey, R. M., Trisal, P., Arrojo, R., Liu, D., . . . Goldenberg, D. M. (2015). Sacituzumab Govitecan (IMMU-132), an Anti-Trop-2/SN-38 Antibody-Drug Conjugate: Characterization and Efficacy in Pancreatic, Gastric, and Other Cancers. *Bioconjug Chem*, *26*(5), 919-931. doi:10.1021/acs.bioconjchem.5b00223
- Carey, L. A., Loirat, D., Punie, K., Bardia, A., Diéras, V., Dalenc, F., . . . Cortés, J. (2022). Sacituzumab govitecan as second-line treatment for metastatic triple-negative breast cancer—phase 3 ASCENT study subanalysis. *npj Breast Cancer*, *8*(1), 72. doi:10.1038/s41523-022-00439-5
- Cascone, T., William, W. N., Jr., Weissferdt, A., Leung, C. H., Lin, H. Y., Pataer, A., . . . Sepesi, B. (2021). Neoadjuvant nivolumab or nivolumab plus ipilimumab in operable non-small cell lung cancer: the phase 2 randomized NEOSTAR trial. *Nat Med*, *27*(3), 504-514. doi:10.1038/s41591-020-01224-2

## References

- Castelli, M. S., McGonigle, P., & Hornby, P. J. (2019). The pharmacology and therapeutic applications of monoclonal antibodies. *Pharmacol Res Perspect*, 7(6), e00535. doi:10.1002/prp2.535
- Cescato, R., Schulz, S., Waser, B., Eltschinger, V., Rivier, J. E., Wester, H. J., . . . Reubi, J. C. (2006). Internalization of sst2, sst3, and sst5 receptors: effects of somatostatin agonists and antagonists. *J Nucl Med*, 47(3), 502-511. Retrieved from <https://www.ncbi.nlm.nih.gov/pubmed/16513620>
- Cespedes, P. F., Jainarayanan, A., Fernandez-Messina, L., Valvo, S., Saliba, D. G., Kurz, E., . . . Dustin, M. L. (2022). T-cell trans-synaptic vesicles are distinct and carry greater effector content than constitutive extracellular vesicles. *Nat Commun*, 13(1), 3460. doi:10.1038/s41467-022-31160-3
- Chakravarty, R., Goel, S., & Cai, W. (2014). Nanobody: the "magic bullet" for molecular imaging? *Theranostics*, 4(4), 386-398. doi:10.7150/thno.8006
- Chan, A., Mobley, J. L., Fields, G. B., & Shimizu, Y. (1997). CD7-mediated regulation of integrin adhesiveness on human T cells involves tyrosine phosphorylation-dependent activation of phosphatidylinositol 3-kinase. *The Journal of Immunology*, 159(2), 934-942.
- Chari, R. V., Martell, B. A., Gross, J. L., Cook, S. B., Shah, S. A., Blattler, W. A., . . . Goldmacher, V. S. (1992). Immunoconjugates containing novel maytansinoids: promising anticancer drugs. *Cancer Res*, 52(1), 127-131. Retrieved from <https://www.ncbi.nlm.nih.gov/pubmed/1727373>
- Charoenphun, P., Meszaros, L. K., Chuamsaamarkkee, K., Sharif-Paghaleh, E., Ballinger, J. R., Ferris, T. J., . . . Blower, P. J. (2015). [(89)Zr]oxinate4 for long-term in vivo cell tracking by positron emission tomography. *Eur J Nucl Med Mol Imaging*, 42(2), 278-287. doi:10.1007/s00259-014-2945-x
- Chau, C. H., Steeg, P. S., & Figg, W. D. (2019). Antibody-drug conjugates for cancer. *Lancet*, 394(10200), 793-804. doi:10.1016/S0140-6736(19)31774-X
- Chen, L., & Flies, D. B. (2013). Molecular mechanisms of T cell co-stimulation and co-inhibition. *Nat Rev Immunol*, 13(4), 227-242. doi:10.1038/nri3405
- Chick, R. C., Faries, M. B., Hale, D. F., Kemp Bohan, P. M., Hickerson, A., Vreeland, T. J., . . . Hynstrom, J. R. (2020). Multi-institutional, prospective, randomized, double-blind, placebo-controlled phase IIb trial of the tumor lysate, particle-loaded, dendritic cell (TLPLDC) vaccine to prevent recurrence in high-risk melanoma patients: A subgroup analysis. In: American Society of Clinical Oncology.
- Chiou, V. L., & Burotto, M. (2015). Pseudoprogression and Immune-Related Response in Solid Tumors. *J Clin Oncol*, 33(31), 3541-3543. doi:10.1200/JCO.2015.61.6870
- Choi, Y., Lee, S., Kim, K., Kim, S. H., Chung, Y. J., & Lee, C. (2018). Studying cancer immunotherapy using patient-derived xenografts (PDXs) in humanized mice. *Exp Mol Med*, 50(8), 1-9. doi:10.1038/s12276-018-0115-0
- Chung, J., Kang, J., & Kang, K. (2010). Molecular Imaging With Reporter Genes.
- Cohen, R. B., Johnson, M., Twardowski, P., Stein, M., Vaishampayan, U., Gillison, M., . . . Agnihotri, P. (2019). Broad immunogenicity from GEN-009, a neoantigen vaccine using ATLASTM, an autologous immune assay, to identify immunogenic and inhibitory tumor neoantigens. *J Immunother. Cancer*, 7(Suppl. 1), P420.

## References

- Couzin-Frankel, J. (2013). Breakthrough of the year 2013. Cancer immunotherapy. *Science*, *342*(6165), 1432-1433. doi:10.1126/science.342.6165.1432
- Cummings, J., Aisen, P., Lemere, C., Atri, A., Sabbagh, M., & Salloway, S. (2021). Aducanumab produced a clinically meaningful benefit in association with amyloid lowering. *Alzheimers Res Ther*, *13*(1), 98. doi:10.1186/s13195-021-00838-z
- Curigliano, G., Gelderblom, H., Mach, N., Doi, T., Tai, W. M. D., Forde, P., . . . Hodi, S. (2019). Abstract CT183: Phase (Ph) I/II study of MBG453±spartalizumab (PDR001) in patients (pts) with advanced malignancies. *Cancer Research*, *79*(13\_Supplement), CT183-CT183.
- Curran, K. J., Riviere, I., Silverman, L. B., Kobos, R., Shukla, N., Steinherz, P. G., . . . Margossian, S. P. (2015). Multi-center clinical trial of car t cells in pediatric/young adult patients with relapsed B-cell all. *Blood*, *126*(23), 2533.
- D'Huyvetter, M., Vincke, C., Xavier, C., Aerts, A., Impens, N., Baatout, S., . . . Lahoutte, T. (2014). Targeted radionuclide therapy with A 177Lu-labeled anti-HER2 nanobody. *Theranostics*, *4*(7), 708-720. doi:10.7150/thno.8156
- D'Huyvetter, M., Xavier, C., Caveliers, V., Lahoutte, T., Muyldermans, S., & Devoogdt, N. (2014). Radiolabeled nanobodies as theranostic tools in targeted radionuclide therapy of cancer. *Expert Opin Drug Deliv*, *11*(12), 1939-1954. doi:10.1517/17425247.2014.941803
- Damato, B. E., Dukes, J., Goodall, H., & Carvajal, R. D. (2019). Tebentafusp: T Cell Redirection for the Treatment of Metastatic Uveal Melanoma. *Cancers (Basel)*, *11*(7). doi:10.3390/cancers11070971
- Das, M., Zhu, C., & Kuchroo, V. K. (2017). Tim-3 and its role in regulating anti-tumor immunity. *Immunol Rev*, *276*(1), 97-111. doi:10.1111/imr.12520
- Davila, M. L., Riviere, I., Wang, X., Bartido, S., Park, J., Curran, K., . . . Brentjens, R. (2014). Efficacy and toxicity management of 19-28z CAR T cell therapy in B cell acute lymphoblastic leukemia. *Sci Transl Med*, *6*(224), 224ra225. doi:10.1126/scitranslmed.3008226
- Demaimay, F., Dazard, L., Roucoux, A., Noiret, N., Patin, H., & Moisan, A. (1997). Rhenium-188 and technetium-99m nitridobis(N-ethoxy-N-ethylthiocarbamate) leucocyte labelling radiopharmaceuticals: [188ReN(NOET)2] and [99mTcN(NOET)2], NOET = Et(EtO)NCS2: their in vitro localization and chemical behaviour. *Nucl Med Biol*, *24*(8), 701-705. doi:10.1016/s0969-8051(97)00096-6
- Demetriou, P., Abu-Shah, E., McCuaig, S., Mayya, V., Valvo, S., Korobchevskaya, K., . . . Dustin, M. L. (2019). CD2 expression acts as a quantitative checkpoint for immunological synapse structure and T-cell activation. *bioRxiv*, 589440. doi:10.1101/589440
- Dennehy, K. M., Elias, F., Zeder-Lutz, G., Ding, X., Altschuh, D., Luhder, F., & Hunig, T. (2006). Cutting edge: monovalency of CD28 maintains the antigen dependence of T cell costimulatory responses. *J Immunol*, *176*(10), 5725-5729. doi:10.4049/jimmunol.176.10.5725
- Derby, M., Alexander-Miller, M., Tse, R., & Berzofsky, J. (2001). High-avidity CTL exploit two complementary mechanisms to provide better protection against viral infection than low-avidity CTL. *J Immunol*, *166*(3), 1690-1697. doi:10.4049/jimmunol.166.3.1690

- Desmyter, A., Decanniere, K., Muyldermans, S., & Wyns, L. (2001). Antigen specificity and high affinity binding provided by one single loop of a camel single-domain antibody. *J Biol Chem*, *276*(28), 26285-26290. doi:10.1074/jbc.M102107200
- Di Gaetano, N., Cittera, E., Nota, R., Vecchi, A., Grieco, V., Scanziani, E., . . . Golay, J. (2003). Complement activation determines the therapeutic activity of rituximab in vivo. *J Immunol*, *171*(3), 1581-1587. doi:10.4049/jimmunol.171.3.1581
- Di Giacomo, A. M., Danielli, R., Guidoboni, M., Calabro, L., Carlucci, D., Miracco, C., . . . Maio, M. (2009). Therapeutic efficacy of ipilimumab, an anti-CTLA-4 monoclonal antibody, in patients with metastatic melanoma unresponsive to prior systemic treatments: clinical and immunological evidence from three patient cases. *Cancer Immunol Immunother*, *58*(8), 1297-1306. doi:10.1007/s00262-008-0642-y
- Dong, H., Zhu, G., Tamada, K., & Chen, L. (1999). B7-H1, a third member of the B7 family, co-stimulates T-cell proliferation and interleukin-10 secretion. *Nat Med*, *5*(12), 1365-1369. doi:10.1038/70932
- Drago, J. Z., Modi, S., & Chandarlapaty, S. (2021). Unlocking the potential of antibody-drug conjugates for cancer therapy. *Nat Rev Clin Oncol*, *18*(6), 327-344. doi:10.1038/s41571-021-00470-8
- Dranitsaris, G., Molassiotis, A., Clemons, M., Roeland, E., Schwartzberg, L., Dielenseger, P., . . . Apro, M. (2017). The development of a prediction tool to identify cancer patients at high risk for chemotherapy-induced nausea and vomiting. *Ann Oncol*, *28*(6), 1260-1267. doi:10.1093/annonc/mdx100
- Ducry, L., & Stump, B. (2010). Antibody-drug conjugates: linking cytotoxic payloads to monoclonal antibodies. *Bioconjug Chem*, *21*(1), 5-13. doi:10.1021/bc9002019
- Dumont, C., Déas, O., Mollereau, B., Hebib, C., Giovino-Barry, V., Bernard, A., . . . Senik, A. (1998). Potent apoptotic signaling and subsequent unresponsiveness induced by a single CD2 mAb (BTI-322) in activated human peripheral T cells. *The Journal of Immunology*, *160*(8), 3797-3804.
- Dumoulin, M., Conrath, K., Van Meirhaeghe, A., Meersman, F., Heremans, K., Frenken, L. G., . . . Matagne, A. (2002). Single-domain antibody fragments with high conformational stability. *Protein Sci*, *11*(3), 500-515. doi:10.1110/ps.34602
- Ehlerding, E. B., England, C. G., McNeel, D. G., & Cai, W. (2016). Molecular Imaging of Immunotherapy Targets in Cancer. *J Nucl Med*, *57*(10), 1487-1492. doi:10.2967/jnumed.116.177493
- Elliott, D. E., Li, J., Blum, A. M., Metwali, A., Patel, Y. C., & Weinstock, J. V. (1999). SSTR2A is the dominant somatostatin receptor subtype expressed by inflammatory cells, is widely expressed and directly regulates T cell IFN-gamma release. *Eur J Immunol*, *29*(8), 2454-2463. doi:10.1002/(SICI)1521-4141(199908)29:08<2454::AID-IMMU2454>3.0.CO;2-H
- Fang, J., Nakamura, H., & Maeda, H. (2011). The EPR effect: Unique features of tumor blood vessels for drug delivery, factors involved, and limitations and augmentation of the effect. *Adv Drug Deliv Rev*, *63*(3), 136-151. doi:10.1016/j.addr.2010.04.009
- Fehleisen, F. (1882). Ueber die Züchtung der Erysipelkokken auf künstlichem Nährboden und ihre Übertragbarkeit auf den Menschen. *Dtsch Med Wochenschr*, *8*(31), 553-554.

## References

- Ferris, R. L., Blumenschein, G., Jr., Fayette, J., Guigay, J., Colevas, A. D., Licitra, L., . . . Gillison, M. L. (2016). Nivolumab for Recurrent Squamous-Cell Carcinoma of the Head and Neck. *N Engl J Med*, *375*(19), 1856-1867. doi:10.1056/NEJMoa1602252
- Finney, H. M., Akbar, A. N., & Lawson, A. D. (2004). Activation of resting human primary T cells with chimeric receptors: costimulation from CD28, inducible costimulator, CD134, and CD137 in series with signals from the TCR zeta chain. *J Immunol*, *172*(1), 104-113. doi:10.4049/jimmunol.172.1.104
- Fisher, B., Packard, B. S., Read, E. J., Carrasquillo, J. A., Carter, C. S., Topalian, S. L., . . . Rosenberg, S. A. (1989). Tumor localization of adoptively transferred indium-111 labeled tumor infiltrating lymphocytes in patients with metastatic melanoma. *J Clin Oncol*, *7*(2), 250-261. doi:10.1200/JCO.1989.7.2.250
- Friedlaender, A., Addeo, A., & Banna, G. (2019). New emerging targets in cancer immunotherapy: the role of TIM3. *ESMO Open*, *4*(Suppl 3), e000497. doi:10.1136/esmoopen-2019-000497
- Fu, R., Carroll, L., Yahiolglu, G., Aboagye, E. O., & Miller, P. W. (2018). Antibody Fragment and Affibody ImmunoPET Imaging Agents: Radiolabelling Strategies and Applications. *ChemMedChem*, *13*(23), 2466-2478. doi:10.1002/cmdc.201800624
- Fu, Z., Li, S., Han, S., Shi, C., & Zhang, Y. (2022). Antibody drug conjugate: the "biological missile" for targeted cancer therapy. *Signal Transduct Target Ther*, *7*(1), 93. doi:10.1038/s41392-022-00947-7
- Gabrilovich, D. I., Chen, H. L., Girgis, K. R., Cunningham, H. T., Meny, G. M., Nadaf, S., . . . Carbone, D. P. (1996). Production of vascular endothelial growth factor by human tumors inhibits the functional maturation of dendritic cells. *Nat Med*, *2*(10), 1096-1103. doi:10.1038/nm1096-1096
- Gabrilovich, D. I., Ciernik, I. F., & Carbone, D. P. (1996). Dendritic cells in antitumor immune responses. I. Defective antigen presentation in tumor-bearing hosts. *Cell Immunol*, *170*(1), 101-110. doi:10.1006/cimm.1996.0139
- Gainkam, L. O., Caveliers, V., Devoogdt, N., Vanhove, C., Xavier, C., Boerman, O., . . . Lahoutte, T. (2011). Localization, mechanism and reduction of renal retention of technetium-99m labeled epidermal growth factor receptor-specific nanobody in mice. *Contrast Media Mol Imaging*, *6*(2), 85-92. doi:10.1002/cmimi.408
- Gambhir, S. S., Barrio, J. R., Phelps, M. E., Iyer, M., Namavari, M., Satyamurthy, N., . . . Herschman, H. R. (1999). Imaging adenoviral-directed reporter gene expression in living animals with positron emission tomography. *Proc Natl Acad Sci U S A*, *96*(5), 2333-2338. doi:10.1073/pnas.96.5.2333
- Gandhi, L., Rodriguez-Abreu, D., Gadgeel, S., Esteban, E., Felip, E., De Angelis, F., . . . Investigators, K.-. (2018). Pembrolizumab plus Chemotherapy in Metastatic Non-Small-Cell Lung Cancer. *N Engl J Med*, *378*(22), 2078-2092. doi:10.1056/NEJMoa1801005
- Gardner, R., Wu, D., Cherian, S., Fang, M., Hanafi, L. A., Finney, O., . . . Turtle, C. J. (2016). Acquisition of a CD19-negative myeloid phenotype allows immune escape of MLL-rearranged B-ALL from CD19 CAR-T-cell therapy. *Blood*, *127*(20), 2406-2410. doi:10.1182/blood-2015-08-665547
- Gawne, P., Man, F., Fonslet, J., Radia, R., Bordoloi, J., Cleveland, M., . . . de Rosales, R. T. M. (2018). Manganese-52: applications in cell radiolabelling and liposomal nanomedicine PET imaging

- using oxine (8-hydroxyquinoline) as an ionophore. *Dalton Trans*, 47(28), 9283-9293. doi:10.1039/c8dt00100f
- Gettinger, S. N., Horn, L., Gandhi, L., Spigel, D. R., Antonia, S. J., Rizvi, N. A., . . . Brahmer, J. R. (2015). Overall Survival and Long-Term Safety of Nivolumab (Anti-Programmed Death 1 Antibody, BMS-936558, ONO-4538) in Patients With Previously Treated Advanced Non-Small-Cell Lung Cancer. *J Clin Oncol*, 33(18), 2004-2012. doi:10.1200/JCO.2014.58.3708
- Golay, J., Zaffaroni, L., Vaccari, T., Lazzari, M., Borleri, G. M., Bernasconi, S., . . . Introna, M. (2000). Biologic response of B lymphoma cells to anti-CD20 monoclonal antibody rituximab in vitro: CD55 and CD59 regulate complement-mediated cell lysis. *Blood*, 95(12), 3900-3908. Retrieved from <https://www.ncbi.nlm.nih.gov/pubmed/10845926>
- Grupp, S. A., Kalos, M., Barrett, D., Aplenc, R., Porter, D. L., Rheingold, S. R., . . . June, C. H. (2013). Chimeric antigen receptor-modified T cells for acute lymphoid leukemia. *N Engl J Med*, 368(16), 1509-1518. doi:10.1056/NEJMoa1215134
- Gückel, B., Berek, C., Lutz, M., Altevogt, P., Schirmacher, V., & Kyewski, B. (1991). Anti-CD2 antibodies induce T cell unresponsiveness in vivo. *The Journal of experimental medicine*, 174(5), 957-967.
- Haddad, R., Concha-Benavente, F., Blumenschein, G., Jr., Fayette, J., Guigay, J., Colevas, A. D., . . . Ferris, R. L. (2019). Nivolumab treatment beyond RECIST-defined progression in recurrent or metastatic squamous cell carcinoma of the head and neck in CheckMate 141: A subgroup analysis of a randomized phase 3 clinical trial. *Cancer*, 125(18), 3208-3218. doi:10.1002/cncr.32190
- Hahn, W. C., & Bierer, B. E. (1993). Separable portions of the CD2 cytoplasmic domain involved in signaling and ligand avidity regulation. *J Exp Med*, 178(5), 1831-1836. doi:10.1084/jem.178.5.1831
- Hammond, S. A., Fuhrmann, S., Roff, S., Kiener, P. A., Coats, S., & Kinch, M. S. (2006). Mechanistic Evaluation of Siplizumab (MEDI-507) Activity on Normal and Malignant T-Lymphocytes. In: American Society of Hematology.
- Hanke, T. (2006). Lessons from TGN1412. *Lancet*, 368(9547), 1569-1570; author reply 1570. doi:10.1016/S0140-6736(06)69651-7
- Harari, A., Graciotti, M., Bassani-Sternberg, M., & Kandalaft, L. E. (2020). Antitumour dendritic cell vaccination in a priming and boosting approach. *Nat Rev Drug Discov*, 19(9), 635-652. doi:10.1038/s41573-020-0074-8
- Harmand, T. J., Islam, A., Pishesha, N., & Ploegh, H. L. (2021). Nanobodies as in vivo, non-invasive, imaging agents. *RSC Chem Biol*, 2(3), 685-701. doi:10.1039/d1cb00023c
- Harris, D. T., & Kranz, D. M. (2016). Adoptive T Cell Therapies: A Comparison of T Cell Receptors and Chimeric Antigen Receptors. *Trends Pharmacol Sci*, 37(3), 220-230. doi:10.1016/j.tips.2015.11.004
- Hassanzadeh-Ghassabeh, G., Devoogdt, N., De Pauw, P., Vincke, C., & Muyldermans, S. (2013). Nanobodies and their potential applications. *Nanomedicine (Lond)*, 8(6), 1013-1026. doi:10.2217/nnm.13.86

## References

- Haynes, B. F., Eisenbarth, G. S., & Fauci, A. S. (1979). Human lymphocyte antigens: production of a monoclonal antibody that defines functional thymus-derived lymphocyte subsets. *Proceedings of the National Academy of Sciences*, *76*(11), 5829-5833.
- He, X., & Xu, C. (2020). Immune checkpoint signaling and cancer immunotherapy. *Cell Res*, *30*(8), 660-669. doi:10.1038/s41422-020-0343-4
- He, Y., Cao, J., Zhao, C., Li, X., Zhou, C., & Hirsch, F. R. (2018). TIM-3, a promising target for cancer immunotherapy. *Onco Targets Ther*, *11*, 7005-7009. doi:10.2147/OTT.S170385
- Hegi-Johnson, F., Rudd, S., Hicks, R. J., De Ruyscher, D., Trapani, J. A., John, T., . . . MacManus, M. P. (2022). Imaging immunity in patients with cancer using positron emission tomography. *NPJ Precis Oncol*, *6*(1), 24. doi:10.1038/s41698-022-00263-x
- Hellmann, M. D., Ciuleanu, T. E., Pluzanski, A., Lee, J. S., Otterson, G. A., Audigier-Valette, C., . . . Paz-Ares, L. (2018). Nivolumab plus Ipilimumab in Lung Cancer with a High Tumor Mutational Burden. *N Engl J Med*, *378*(22), 2093-2104. doi:10.1056/NEJMoa1801946
- Herbert, G. S., Vreeland, T. J., Clifton, G. T., Greene, J. M., Jackson, D. O., Hardin, M. O., . . . Peoples, G. E. (2018). Initial phase I/IIa trial results of an autologous tumor lysate, particle-loaded, dendritic cell (TLPLDC) vaccine in patients with solid tumors. *Vaccine*, *36*(23), 3247-3253. doi:10.1016/j.vaccine.2018.04.078
- Herbst, R. S., Soria, J. C., Kowanetz, M., Fine, G. D., Hamid, O., Gordon, M. S., . . . Hodi, F. S. (2014). Predictive correlates of response to the anti-PD-L1 antibody MPDL3280A in cancer patients. *Nature*, *515*(7528), 563-567. doi:10.1038/nature14011
- Hess, S., Blomberg, B. A., Zhu, H. J., Hoiland-Carlsen, P. F., & Alavi, A. (2014). The pivotal role of FDG-PET/CT in modern medicine. *Acad Radiol*, *21*(2), 232-249. doi:10.1016/j.acra.2013.11.002
- Heusch, P., Nensa, F., Schaarschmidt, B., Sivanesapillai, R., Beiderwellen, K., Gomez, B., . . . Buchbender, C. (2015). Diagnostic accuracy of whole-body PET/MRI and whole-body PET/CT for TNM staging in oncology. *Eur J Nucl Med Mol Imaging*, *42*(1), 42-48. doi:10.1007/s00259-014-2885-5
- Hickerson, A., Clifton, G. T., Brown, T. A., Campf, J., Myers, J. W., Vreeland, T. J., . . . Yu, X. (2019). Clinical efficacy of vaccination with the autologous tumor lysate particle loaded dendritic cell (TLPLDC) vaccine in metastatic melanoma. In: American Society of Clinical Oncology.
- Hirano, F., Kaneko, K., Tamura, H., Dong, H., Wang, S., Ichikawa, M., . . . Chen, L. (2005). Blockade of B7-H1 and PD-1 by monoclonal antibodies potentiates cancer therapeutic immunity. *Cancer Res*, *65*(3), 1089-1096. Retrieved from <https://www.ncbi.nlm.nih.gov/pubmed/15705911>
- Hodi, F. S., Hwu, W. J., Kefford, R., Weber, J. S., Daud, A., Hamid, O., . . . Wolchok, J. D. (2016). Evaluation of Immune-Related Response Criteria and RECIST v1.1 in Patients With Advanced Melanoma Treated With Pembrolizumab. *J Clin Oncol*, *34*(13), 1510-1517. doi:10.1200/JCO.2015.64.0391
- Hodi, F. S., O'Day, S. J., McDermott, D. F., Weber, R. W., Sosman, J. A., Haanen, J. B., . . . Urba, W. J. (2010). Improved survival with ipilimumab in patients with metastatic melanoma. *N Engl J Med*, *363*(8), 711-723. doi:10.1056/NEJMoa1003466
- Holland, J. P., Sheh, Y., & Lewis, J. S. (2009). Standardized methods for the production of high specific-activity zirconium-89. *Nuclear medicine and biology*, *36*(7), 729-739.

## References

- Hong, S. G., Sato, N., Legrand, F., Gadkari, M., Makiya, M., Stokes, K., . . . Franco, L. M. (2020). Glucocorticoid-induced eosinopenia results from CXCR4-dependent bone marrow migration. *Blood*, *136*(23), 2667-2678. doi:10.1182/blood.2020005161
- Hou, A. J., Chen, L. C., & Chen, Y. Y. (2021). Navigating CAR-T cells through the solid-tumour microenvironment. *Nat Rev Drug Discov*, *20*(7), 531-550. doi:10.1038/s41573-021-00189-2
- Howard, F. D., Ledbetter, J. A., Wong, J., Bieber, C. P., Stinson, E. B., & Herzenberg, L. A. (1981). A human T lymphocyte differentiation marker defined by monoclonal antibodies that block E-rosette formation. *J Immunol*, *126*(6), 2117-2122. Retrieved from <https://www.ncbi.nlm.nih.gov/pubmed/6785348>
- Hu, Y., Liu, C., & Muyldermans, S. (2017). Nanobody-Based Delivery Systems for Diagnosis and Targeted Tumor Therapy. *Front Immunol*, *8*, 1442. doi:10.3389/fimmu.2017.01442
- Hubert, P., & Amigorena, S. (2012). Antibody-dependent cell cytotoxicity in monoclonal antibody-mediated tumor immunotherapy. *Oncoimmunology*, *1*(1), 103-105. doi:10.4161/onci.1.1.17963
- Huen, J., Yan, Z., Iwashkiw, J., Dubey, S., Gimenez, M. C., Ortiz, M. E., . . . Shahinas, D. (2019). A Novel Single Domain Antibody Targeting FliC Flagellin of Salmonella enterica for Effective Inhibition of Host Cell Invasion. *Front Microbiol*, *10*, 2665. doi:10.3389/fmicb.2019.02665
- Hui, E., Cheung, J., Zhu, J., Su, X., Taylor, M. J., Wallweber, H. A., . . . Vale, R. D. (2017). T cell costimulatory receptor CD28 is a primary target for PD-1-mediated inhibition. *Science*, *355*(6332), 1428-1433. doi:10.1126/science.aaf1292
- Hunig, T. (2016). The rise and fall of the CD28 superagonist TGN1412 and its return as TAB08: a personal account. *FEBS J*, *283*(18), 3325-3334. doi:10.1111/febs.13754
- Hunter, B. D., & Jacobson, C. A. (2019). CAR T-Cell Associated Neurotoxicity: Mechanisms, Clinicopathologic Correlates, and Future Directions. *J Natl Cancer Inst*, *111*(7), 646-654. doi:10.1093/jnci/djz017
- Iafrate, M., & Fruhwirth, G. O. (2020). How Non-invasive in vivo Cell Tracking Supports the Development and Translation of Cancer Immunotherapies. *Front Physiol*, *11*, 154. doi:10.3389/fphys.2020.00154
- Imai, C., Mihara, K., Andreansky, M., Nicholson, I. C., Pui, C. H., Geiger, T. L., & Campana, D. (2004). Chimeric receptors with 4-1BB signaling capacity provoke potent cytotoxicity against acute lymphoblastic leukemia. *Leukemia*, *18*(4), 676-684. doi:10.1038/sj.leu.2403302
- Ishida, Y., Agata, Y., Shibahara, K., & Honjo, T. (1992). Induced expression of PD-1, a novel member of the immunoglobulin gene superfamily, upon programmed cell death. *EMBO J*, *11*(11), 3887-3895. doi:10.1002/j.1460-2075.1992.tb05481.x
- Iwai, Y., Ishida, M., Tanaka, Y., Okazaki, T., Honjo, T., & Minato, N. (2002). Involvement of PD-L1 on tumor cells in the escape from host immune system and tumor immunotherapy by PD-L1 blockade. *Proc Natl Acad Sci U S A*, *99*(19), 12293-12297. doi:10.1073/pnas.192461099
- Jackson, H. J., Rafiq, S., & Brentjens, R. J. (2016). Driving CAR T-cells forward. *Nat Rev Clin Oncol*, *13*(6), 370-383. doi:10.1038/nrclinonc.2016.36

## References

- Jacoby, E., Nguyen, S. M., Fountaine, T. J., Welp, K., Gryder, B., Qin, H., . . . Fry, T. J. (2016). CD19 CAR immune pressure induces B-precursor acute lymphoblastic leukaemia lineage switch exposing inherent leukaemic plasticity. *Nat Commun*, *7*, 12320. doi:10.1038/ncomms12320
- Jayaraman, J., Mellody, M. P., Hou, A. J., Desai, R. P., Fung, A. W., Pham, A. H. T., . . . Zhao, W. (2020). CAR-T design: Elements and their synergistic function. *EBioMedicine*, *58*, 102931. doi:10.1016/j.ebiom.2020.102931
- Jefferson, R. A., Burgess, S. M., & Hirsh, D. (1986). beta-Glucuronidase from *Escherichia coli* as a gene-fusion marker. *Proc Natl Acad Sci U S A*, *83*(22), 8447-8451. doi:10.1073/pnas.83.22.8447
- Johnson, D. B., Peng, C., & Sosman, J. A. (2015). Nivolumab in melanoma: latest evidence and clinical potential. *Ther Adv Med Oncol*, *7*(2), 97-106. doi:10.1177/1758834014567469
- Jones, R. G., & Thompson, C. B. (2007). Revving the engine: signal transduction fuels T cell activation. *Immunity*, *27*(2), 173-178. doi:10.1016/j.immuni.2007.07.008
- Junttila, T. T., Akita, R. W., Parsons, K., Fields, C., Lewis Phillips, G. D., Friedman, L. S., . . . Sliwkowski, M. X. (2009). Ligand-independent HER2/HER3/PI3K complex is disrupted by trastuzumab and is effectively inhibited by the PI3K inhibitor GDC-0941. *Cancer Cell*, *15*(5), 429-440. doi:10.1016/j.ccr.2009.03.020
- Jurtz, V., Paul, S., Andreatta, M., Marcatili, P., Peters, B., & Nielsen, M. (2017). NetMHCpan-4.0: Improved Peptide-MHC Class I Interaction Predictions Integrating Eluted Ligand and Peptide Binding Affinity Data. *J Immunol*, *199*(9), 3360-3368. doi:10.4049/jimmunol.1700893
- Kantoff, P. W., Higano, C. S., Shore, N. D., Berger, E. R., Small, E. J., Penson, D. F., . . . Investigators, I. S. (2010). Sipuleucel-T immunotherapy for castration-resistant prostate cancer. *N Engl J Med*, *363*(5), 411-422. doi:10.1056/NEJMoa1001294
- Karki, R., Sharma, B. R., Tuladhar, S., Williams, E. P., Zalduondo, L., Samir, P., . . . Kanneganti, T. D. (2021). Synergism of TNF-alpha and IFN-gamma Triggers Inflammatory Cell Death, Tissue Damage, and Mortality in SARS-CoV-2 Infection and Cytokine Shock Syndromes. *Cell*, *184*(1), 149-168 e117. doi:10.1016/j.cell.2020.11.025
- Kasten, B. B., Houson, H. A., Coleman, J. M., Leavenworth, J. W., Markert, J. M., Wu, A. M., . . . Sorace, A. G. (2021). Positron emission tomography imaging with (89)Zr-labeled anti-CD8 cys-diabody reveals CD8(+) cell infiltration during oncolytic virus therapy in a glioma murine model. *Sci Rep*, *11*(1), 15384. doi:10.1038/s41598-021-94887-x
- Keene, J. A., & Forman, J. (1982). Helper activity is required for the in vivo generation of cytotoxic T lymphocytes. *J Exp Med*, *155*(3), 768-782. doi:10.1084/jem.155.3.768
- Keu, K. V., Witney, T. H., Yaghoubi, S., Rosenberg, J., Kurien, A., Magnusson, R., . . . Gambhir, S. S. (2017). Reporter gene imaging of targeted T cell immunotherapy in recurrent glioma. *Sci Transl Med*, *9*(373). doi:10.1126/scitranslmed.aag2196
- Keyaerts, M., Xavier, C., Heemskerk, J., Devoogdt, N., Everaert, H., Ackaert, C., . . . Lahoutte, T. (2016). Phase I Study of 68Ga-HER2-Nanobody for PET/CT Assessment of HER2 Expression in Breast Carcinoma. *J Nucl Med*, *57*(1), 27-33. doi:10.2967/jnumed.115.162024
- Kimby, E. (2005). Tolerability and safety of rituximab (MabThera). *Cancer Treat Rev*, *31*(6), 456-473. doi:10.1016/j.ctrv.2005.05.007

## References

- Kircher, M. F., Gambhir, S. S., & Grimm, J. (2011). Noninvasive cell-tracking methods. *Nat Rev Clin Oncol*, *8*(11), 677-688. doi:10.1038/nrclinonc.2011.141
- Klar, R., Schober, S., Rami, M., Mall, S., Merl, J., Hauck, S. M., . . . Krackhardt, A. M. (2014). Therapeutic targeting of naturally presented myeloperoxidase-derived HLA peptide ligands on myeloid leukemia cells by TCR-transgenic T cells. *Leukemia*, *28*(12), 2355-2366. doi:10.1038/leu.2014.131
- Koehne, G., Doubrovin, M., Doubrovina, E., Zanzonico, P., Gallardo, H. F., Ivanova, A., . . . Tjuvajev, J. G. (2003). Serial in vivo imaging of the targeted migration of human HSV-TK-transduced antigen-specific lymphocytes. *Nat Biotechnol*, *21*(4), 405-413. doi:10.1038/nbt805
- Kohler, G., & Milstein, C. (1975). Continuous cultures of fused cells secreting antibody of predefined specificity. *Nature*, *256*(5517), 495-497. doi:10.1038/256495a0
- Kreiter, S., Vormehr, M., van de Roemer, N., Diken, M., Lower, M., Diekmann, J., . . . Sahin, U. (2015). Mutant MHC class II epitopes drive therapeutic immune responses to cancer. *Nature*, *520*(7549), 692-696. doi:10.1038/nature14426
- Krekorian, M., Fruhwirth, G. O., Srinivas, M., Figdor, C. G., Heskamp, S., Witney, T. H., & Aarntzen, E. (2019). Imaging of T-cells and their responses during anti-cancer immunotherapy. *Theranostics*, *9*(25), 7924-7947. doi:10.7150/thno.37924
- Krensky, A. M., Sanchez-Madrid, F., Robbins, E., Nagy, J. A., Springer, T. A., & Burakoff, S. J. (1983). The functional significance, distribution, and structure of LFA-1, LFA-2, and LFA-3: cell surface antigens associated with CTL-target interactions. *The Journal of Immunology*, *131*(2), 611-616.
- Kristensen, L. K., Frohlich, C., Christensen, C., Melander, M. C., Poulsen, T. T., Galler, G. R., . . . Kjaer, A. (2019). CD4(+) and CD8a(+) PET imaging predicts response to novel PD-1 checkpoint inhibitor: studies of Sym021 in syngeneic mouse cancer models. *Theranostics*, *9*(26), 8221-8238. doi:10.7150/thno.37513
- Krummel, M. F., & Allison, J. P. (1995). CD28 and CTLA-4 have opposing effects on the response of T cells to stimulation. *J Exp Med*, *182*(2), 459-465. doi:10.1084/jem.182.2.459
- Kuhn, N. F., Purdon, T. J., van Leeuwen, D. G., Lopez, A. V., Curran, K. J., Daniyan, A. F., & Brentjens, R. J. (2019). CD40 Ligand-Modified Chimeric Antigen Receptor T Cells Enhance Antitumor Function by Eliciting an Endogenous Antitumor Response. *Cancer Cell*, *35*(3), 473-488 e476. doi:10.1016/j.ccell.2019.02.006
- Kuwana, Y., Asakura, Y., Utsunomiya, N., Nakanishi, M., Arata, Y., Itoh, S., . . . Kurosawa, Y. (1987). Expression of chimeric receptor composed of immunoglobulin-derived V regions and T-cell receptor-derived C regions. *Biochem Biophys Res Commun*, *149*(3), 960-968. doi:10.1016/0006-291x(87)90502-x
- Labrecque, N., Whitfield, L. S., Obst, R., Waltzinger, C., Benoist, C., & Mathis, D. (2001). How much TCR does a T cell need? *Immunity*, *15*(1), 71-82. doi:10.1016/s1074-7613(01)00170-4
- Labun, K., Montague, T. G., Krause, M., Torres Cleuren, Y. N., Tjeldnes, H., & Valen, E. (2019). CHOPCHOP v3: expanding the CRISPR web toolbox beyond genome editing. *Nucleic Acids Res*, *47*(W1), W171-W174. doi:10.1093/nar/gkz365

## References

- Laing, R. E., Nair-Gill, E., Witte, O. N., & Radu, C. G. (2010). Visualizing cancer and immune cell function with metabolic positron emission tomography. *Curr Opin Genet Dev*, *20*(1), 100-105. doi:10.1016/j.gde.2009.10.008
- Larimer, B. M., Wehrenberg-Klee, E., Caraballo, A., & Mahmood, U. (2016). Quantitative CD3 PET Imaging Predicts Tumor Growth Response to Anti-CTLA-4 Therapy. *J Nucl Med*, *57*(10), 1607-1611. doi:10.2967/jnumed.116.173930
- Larkin, J., Chiarion-Sileni, V., Gonzalez, R., Grob, J. J., Cowey, C. L., Lao, C. D., . . . Wolchok, J. D. (2015). Combined Nivolumab and Ipilimumab or Monotherapy in Untreated Melanoma. *N Engl J Med*, *373*(1), 23-34. doi:10.1056/NEJMoa1504030
- Le, D. T., Pardoll, D. M., & Jaffee, E. M. (2010). Cellular vaccine approaches. *Cancer J*, *16*(4), 304-310. doi:10.1097/PPO.0b013e3181eb33d7
- Leach, D. R., Krummel, M. F., & Allison, J. P. (1996). Enhancement of antitumor immunity by CTLA-4 blockade. *Science*, *271*(5256), 1734-1736. doi:10.1126/science.271.5256.1734
- Lechermann, L. M., Manavaki, R., Attili, B., Lau, D., Jarvis, L. B., Fryer, T. D., . . . Gallagher, F. A. (2020). Detection limit of (89)Zr-labeled T cells for cellular tracking: an in vitro imaging approach using clinical PET/CT and PET/MRI. *EJNMMI Res*, *10*(1), 82. doi:10.1186/s13550-020-00667-5
- Ledford, H. (2011). Melanoma drug wins US approval. *Nature*, *471*(7340), 561. doi:10.1038/471561a
- Lee, D. M., Staats, H. F., Sundy, J. S., Patel, D. D., Sempowski, G. D., Scarce, R. M., . . . Haynes, B. F. (1998). Immunologic characterization of CD7-deficient mice. *The Journal of Immunology*, *160*(12), 5749-5756.
- Lee, D. W., Gardner, R., Porter, D. L., Louis, C. U., Ahmed, N., Jensen, M., . . . Mackall, C. L. (2014). Current concepts in the diagnosis and management of cytokine release syndrome. *Blood*, *124*(2), 188-195. doi:10.1182/blood-2014-05-552729
- Lee, S. H., Soh, H., Chung, J. H., Cho, E. H., Lee, S. J., Ju, J. M., . . . Ryu, J. S. (2020). Feasibility of real-time in vivo 89Zr-DFO-labeled CAR T-cell trafficking using PET imaging. *PLoS One*, *15*(1), e0223814. doi:10.1371/journal.pone.0223814
- Li, J., Smolyar, A., Sunder-Plassmann, R., & Reinherz, E. L. (1996). Ligand-induced conformational change within the CD2 ectodomain accompanies receptor clustering: implication for molecular lattice formation. *Journal of molecular biology*, *263*(2), 209-226.
- Li, J., Smolyar, A., Sunder-Plassmann, R., & Reinherz, E. L. (1996). Ligand-induced conformational change within the CD2 ectodomain accompanies receptor clustering: implication for molecular lattice formation. *J Mol Biol*, *263*(2), 209-226. doi:10.1006/jmbi.1996.0570
- Li, M., Wang, Y., Liu, M., & Lan, X. (2018). Multimodality reporter gene imaging: Construction strategies and application. *Theranostics*, *8*(11), 2954-2973. doi:10.7150/thno.24108
- Liu, Q., Jiang, L., Li, K., Li, H., Lv, G., Lin, J., & Qiu, L. (2021). Immuno-PET imaging of (68)Ga-labeled nanobody Nb109 for dynamic monitoring the PD-L1 expression in cancers. *Cancer Immunol Immunother*, *70*(6), 1721-1733. doi:10.1007/s00262-020-02818-y
- Lo, D. J., Weaver, T. A., Stempora, L., Mehta, A. K., Ford, M. L., Larsen, C. P., & Kirk, A. D. (2011). Selective targeting of human alloresponsive CD8+ effector memory T cells based on CD2 expression. *American Journal of Transplantation*, *11*(1), 22-33.

- Lo, D. J., Weaver, T. A., Stempora, L., Mehta, A. K., Ford, M. L., Larsen, C. P., & Kirk, A. D. (2011). Selective targeting of human alloresponsive CD8+ effector memory T cells based on CD2 expression. *Am J Transplant*, *11*(1), 22-33. doi:10.1111/j.1600-6143.2010.03317.x
- Long, D., Skoberne, M., Gierahn, T. M., Larson, S., Price, J. A., Clemens, V., . . . Flechtner, J. B. (2014). Identification of novel virus-specific antigens by CD4(+) and CD8(+) T cells from asymptomatic HSV-2 seropositive and seronegative donors. *Virology*, *464-465*, 296-311. doi:10.1016/j.virol.2014.07.018
- Lopez, J. S., Camidge, R., Iafora, M., Rottey, S., Schuler, M., Hellmann, M., . . . Sullivan, R. (2020). Abstract CT301: A phase Ib study to evaluate RO7198457, an individualized Neoantigen Specific immunoTherapy (iNeST), in combination with atezolizumab in patients with locally advanced or metastatic solid tumors. In: AACR.
- Loubaki, L., Tremblay, T., & Bazin, R. (2013). In vivo depletion of leukocytes and platelets following injection of T cell-specific antibodies into mice. *J Immunol Methods*, *393*(1-2), 38-44. doi:10.1016/j.jim.2013.04.004
- Lu, D., Wang, Y., Zhang, T., Wang, F., Li, K., Zhou, S., . . . Liu, Z. (2021). Metabolic radiolabeling and in vivo PET imaging of cytotoxic T lymphocytes to guide combination adoptive cell transfer cancer therapy. *J Nanobiotechnology*, *19*(1), 175. doi:10.1186/s12951-021-00924-2
- Luhder, F., Huang, Y., Dennehy, K. M., Guntermann, C., Muller, I., Winkler, E., . . . Hunig, T. (2003). Topological requirements and signaling properties of T cell-activating, anti-CD28 antibody superagonists. *J Exp Med*, *197*(8), 955-966. doi:10.1084/jem.20021024
- Ma, H., O'Fagain, C., & O'Kennedy, R. (2020). Antibody stability: A key to performance - Analysis, influences and improvement. *Biochimie*, *177*, 213-225. doi:10.1016/j.biochi.2020.08.019
- MacCallum, R. M., Martin, A. C., & Thornton, J. M. (1996). Antibody-antigen interactions: contact analysis and binding site topography. *J Mol Biol*, *262*(5), 732-745. doi:10.1006/jmbi.1996.0548
- Maher, J., Brentjens, R. J., Gunset, G., Riviere, I., & Sadelain, M. (2002). Human T-lymphocyte cytotoxicity and proliferation directed by a single chimeric TCRzeta /CD28 receptor. *Nat Biotechnol*, *20*(1), 70-75. doi:10.1038/nbt0102-70
- Man, F., Lim, L., Volpe, A., Gabizon, A., Shmeeda, H., Draper, B., . . . R, T. M. d. R. (2019). In Vivo PET Tracking of (89)Zr-Labeled Vgamma9Vdelta2 T Cells to Mouse Xenograft Breast Tumors Activated with Liposomal Alendronate. *Mol Ther*, *27*(1), 219-229. doi:10.1016/j.ymthe.2018.10.006
- Mariani, M., Camagna, M., Tarditi, L., & Seccamani, E. (1991). A new enzymatic method to obtain high-yield F(ab)2 suitable for clinical use from mouse IgG1. *Mol Immunol*, *28*(1-2), 69-77. doi:10.1016/0161-5890(91)90088-2
- Marin-Acevedo, J. A., Kimbrough, E. O., & Lou, Y. (2021). Next generation of immune checkpoint inhibitors and beyond. *J Hematol Oncol*, *14*(1), 45. doi:10.1186/s13045-021-01056-8
- Maruhashi, T., Sugiura, D., Okazaki, I. M., & Okazaki, T. (2020). LAG-3: from molecular functions to clinical applications. *J Immunother Cancer*, *8*(2). doi:10.1136/jitc-2020-001014
- Mastelic-Gavillet, B., Balint, K., Boudousquie, C., Gannon, P. O., & Kandalaft, L. E. (2019). Personalized Dendritic Cell Vaccines-Recent Breakthroughs and Encouraging Clinical Results. *Front Immunol*, *10*, 766. doi:10.3389/fimmu.2019.00766

- Matsui, T., Connolly, J. E., Michnevitz, M., Chaussabel, D., Yu, C. I., Glaser, C., . . . Palucka, A. K. (2009). CD2 distinguishes two subsets of human plasmacytoid dendritic cells with distinct phenotype and functions. *J Immunol*, *182*(11), 6815-6823. doi:10.4049/jimmunol.0802008
- Maxwell, C. A., Fleisch, M. C., Costes, S. V., Erickson, A. C., Boissiere, A., Gupta, R., . . . Barcellos-Hoff, M. H. (2008). Targeted and nontargeted effects of ionizing radiation that impact genomic instability. *Cancer Res*, *68*(20), 8304-8311. doi:10.1158/0008-5472.CAN-08-1212
- Mayer, K. E., Mall, S., Yusufi, N., Gosmann, D., Steiger, K., Russelli, L., . . . Krackhardt, A. M. (2018). T-cell functionality testing is highly relevant to developing novel immuno-tracers monitoring T cells in the context of immunotherapies and revealed CD7 as an attractive target. *Theranostics*, *8*(21), 6070-6087. doi:10.7150/thno.27275
- McArdel, S. L., Terhorst, C., & Sharpe, A. H. (2016). Roles of CD48 in regulating immunity and tolerance. *Clin Immunol*, *164*, 10-20. doi:10.1016/j.clim.2016.01.008
- McCarthy, C. E., White, J. M., Viola, N. T., & Gibson, H. M. (2020). In vivo Imaging Technologies to Monitor the Immune System. *Front Immunol*, *11*, 1067. doi:10.3389/fimmu.2020.01067
- Meidenbauer, N., Marienhagen, J., Laumer, M., Vogl, S., Heymann, J., Andreesen, R., & Mackensen, A. (2003). Survival and tumor localization of adoptively transferred Melan-A-specific T cells in melanoma patients. *J Immunol*, *170*(4), 2161-2169. doi:10.4049/jimmunol.170.4.2161
- Meuer, S. C., Hussey, R. E., Fabbi, M., Fox, D., Acuto, O., Fitzgerald, K. A., . . . Reinherz, E. L. (1984). An alternative pathway of T-cell activation: a functional role for the 50 kd T11 sheep erythrocyte receptor protein. *Cell*, *36*(4), 897-906. doi:10.1016/0092-8674(84)90039-4
- Middleton, M. R., McAlpine, C., Woodcock, V. K., Corrie, P., Infante, J. R., Steven, N. M., . . . Sznol, M. (2020). Tebentafusp, A TCR/Anti-CD3 Bispecific Fusion Protein Targeting gp100, Potently Activated Antitumor Immune Responses in Patients with Metastatic Melanoma. *Clin Cancer Res*, *26*(22), 5869-5878. doi:10.1158/1078-0432.CCR-20-1247
- Mitchell, L. S., & Colwell, L. J. (2018). Comparative analysis of nanobody sequence and structure data. *Proteins*, *86*(7), 697-706. doi:10.1002/prot.25497
- Moingeon, P., Lucich, J. L., McConkey, D. J., Letourneur, F., Malissen, B., Kochan, J., . . . Reinherz, E. L. (1992). CD3 zeta dependence of the CD2 pathway of activation in T lymphocytes and natural killer cells. *Proc Natl Acad Sci U S A*, *89*(4), 1492-1496. doi:10.1073/pnas.89.4.1492
- Monney, L., Sabatos, C. A., Gaglia, J. L., Ryu, A., Waldner, H., Chernova, T., . . . Kuchroo, V. K. (2002). Th1-specific cell surface protein Tim-3 regulates macrophage activation and severity of an autoimmune disease. *Nature*, *415*(6871), 536-541. doi:10.1038/415536a
- Mosser, D. M., & Edwards, J. P. (2008). Exploring the full spectrum of macrophage activation. *Nature reviews immunology*, *8*(12), 958-969.
- Motzer, R. J., Escudier, B., McDermott, D. F., George, S., Hammers, H. J., Srinivas, S., . . . CheckMate, I. (2015). Nivolumab versus Everolimus in Advanced Renal-Cell Carcinoma. *N Engl J Med*, *373*(19), 1803-1813. doi:10.1056/NEJMoa1510665
- Motzer, R. J., Tannir, N. M., McDermott, D. F., Aren Frontera, O., Melichar, B., Choueiri, T. K., . . . CheckMate, I. (2018). Nivolumab plus Ipilimumab versus Sunitinib in Advanced Renal-Cell Carcinoma. *N Engl J Med*, *378*(14), 1277-1290. doi:10.1056/NEJMoa1712126

## References

- Movahedi, K., Schoonooghe, S., Laoui, D., Houbracken, I., Waelput, W., Breckpot, K., . . . Van Ginderachter, J. A. (2012). Nanobody-based targeting of the macrophage mannose receptor for effective in vivo imaging of tumor-associated macrophages. *Cancer Res*, *72*(16), 4165-4177. doi:10.1158/0008-5472.CAN-11-2994
- Mullard, A. (2017). FDA approves first CAR T therapy. *Nat Rev Drug Discov*, *16*(10), 669. doi:10.1038/nrd.2017.196
- Mullard, A. (2021). FDA approves 100th monoclonal antibody product. *Nat Rev Drug Discov*, *20*(7), 491-495. doi:10.1038/d41573-021-00079-7
- Mullard, A. (2022a). Antibody-oligonucleotide conjugates enter the clinic. *Nat Rev Drug Discov*, *21*(1), 6-8. doi:10.1038/d41573-021-00213-5
- Mullard, A. (2022b). FDA approval of Immunocore's first-in-class TCR therapeutic broadens depth of the T cell engager platform. *Nat Rev Drug Discov*, *21*(3), 170. doi:10.1038/d41573-022-00031-3
- Muruganandam, A., Tanha, J., Narang, S., & Stanimirovic, D. (2002). Selection of phage-displayed llama single-domain antibodies that transmigrate across human blood-brain barrier endothelium. *FASEB J*, *16*(2), 240-242. doi:10.1096/fj.01-0343fje
- Nadler, L. M., Anderson, K. C., Marti, G., Bates, M., Park, E., Daley, J. F., & Schlossman, S. F. (1983). B4, a human B lymphocyte-associated antigen expressed on normal, mitogen-activated, and malignant B lymphocytes. *J Immunol*, *131*(1), 244-250. Retrieved from <https://www.ncbi.nlm.nih.gov/pubmed/6408173>
- Nadler, L. M., Korsmeyer, S. J., Anderson, K. C., Boyd, A. W., Slaughenhaupt, B., Park, E., . . . et al. (1984). B cell origin of non-T cell acute lymphoblastic leukemia. A model for discrete stages of neoplastic and normal pre-B cell differentiation. *J Clin Invest*, *74*(2), 332-340. doi:10.1172/JCI111428
- Nagarsheth, N., Wicha, M. S., & Zou, W. (2017). Chemokines in the cancer microenvironment and their relevance in cancer immunotherapy. *Nat Rev Immunol*, *17*(9), 559-572. doi:10.1038/nri.2017.49
- Nagasaki, J., Togashi, Y., Sugawara, T., Itami, M., Yamauchi, N., Yuda, J., . . . Nishikawa, H. (2020). The critical role of CD4+ T cells in PD-1 blockade against MHC-II-expressing tumors such as classic Hodgkin lymphoma. *Blood Adv*, *4*(17), 4069-4082. doi:10.1182/bloodadvances.2020002098
- Nathan, P., Hassel, J. C., Rutkowski, P., Baurain, J. F., Butler, M. O., Schlaak, M., . . . Investigators, I. M.-. (2021). Overall Survival Benefit with Tebentafusp in Metastatic Uveal Melanoma. *N Engl J Med*, *385*(13), 1196-1206. doi:10.1056/NEJMoa2103485
- Niiranen, L., Makela, K. A., Mutt, S. J., Viitanen, R., Kaisanlahti, A., Vicente, D., . . . Herzig, K. H. (2021). Role of Brown and Beige Adipose Tissues in Seasonal Adaptation in the Raccoon Dog (*Nyctereutes procyonoides*). *Int J Mol Sci*, *22*(17). doi:10.3390/ijms22179623
- Nishimura, H., Nose, M., Hiai, H., Minato, N., & Honjo, T. (1999). Development of lupus-like autoimmune diseases by disruption of the PD-1 gene encoding an ITIM motif-carrying immunoreceptor. *Immunity*, *11*(2), 141-151. doi:10.1016/s1074-7613(00)80089-8
- Nishino, M., Giobbie-Hurder, A., Manos, M. P., Bailey, N., Buchbinder, E. I., Ott, P. A., . . . Hodi, F. S. (2017). Immune-Related Tumor Response Dynamics in Melanoma Patients Treated with

- Pembrolizumab: Identifying Markers for Clinical Outcome and Treatment Decisions. *Clin Cancer Res*, 23(16), 4671-4679. doi:10.1158/1078-0432.CCR-17-0114
- Oiseth, S. J., & Aziz, M. S. (2017). Cancer immunotherapy: a brief review of the history, possibilities, and challenges ahead. *Journal of cancer metastasis and treatment*, 3, 250-261.
- Okada, H., Weller, M., Huang, R., Finocchiaro, G., Gilbert, M. R., Wick, W., . . . Brandes, A. A. (2015). Immunotherapy response assessment in neuro-oncology: a report of the RANO working group. *The Lancet Oncology*, 16(15), e534-e542.
- Olafsen, T., & Wu, A. M. (2010). Antibody vectors for imaging. *Semin Nucl Med*, 40(3), 167-181. doi:10.1053/j.semnuclmed.2009.12.005
- Oldham, R. K. (2017). Cancer Biotherapy: More Than Immunotherapy. *Cancer Biother Radiopharm*, 32(4), 111-114. doi:10.1089/cbr.2017.28999.old
- Ott, P. A., Hu, Z., Keskin, D. B., Shukla, S. A., Sun, J., Bozym, D. J., . . . Wu, C. J. (2017). An immunogenic personal neoantigen vaccine for patients with melanoma. *Nature*, 547(7662), 217-221. doi:10.1038/nature22991
- Ovacik, M., & Lin, K. (2018). Tutorial on Monoclonal Antibody Pharmacokinetics and Its Considerations in Early Development. *Clin Transl Sci*, 11(6), 540-552. doi:10.1111/cts.12567
- Padilla-Galo, A., Garcia-Ruiz, A. J., Levy Abitbol, R. C., Oliveira, C., Rivas-Ruiz, F., Garcia-Agua Soler, N., . . . Levy-Naon, A. (2021). Real-life cost-effectiveness of benralizumab in patients with severe asthma. *Respir Res*, 22(1), 163. doi:10.1186/s12931-021-01758-0
- Pages, F., Berger, A., Camus, M., Sanchez-Cabo, F., Costes, A., Molidor, R., . . . Galon, J. (2005). Effector memory T cells, early metastasis, and survival in colorectal cancer. *N Engl J Med*, 353(25), 2654-2666. doi:10.1056/NEJMoa051424
- Pai, R., Ma, N., Connor, A. V., Danilenko, D. M., Tarrant, J. M., Salvail, D., . . . Dambach, D. M. (2016). Therapeutic Antibody-Induced Vascular Toxicity Due to Off-Target Activation of Nitric Oxide in Cynomolgus Monkeys. *Toxicol Sci*, 151(2), 245-260. doi:10.1093/toxsci/kfw037
- Pan, J., Niu, Q., Deng, B., Liu, S., Wu, T., Gao, Z., . . . Tong, C. (2019). CD22 CAR T-cell therapy in refractory or relapsed B acute lymphoblastic leukemia. *Leukemia*, 33(12), 2854-2866. doi:10.1038/s41375-019-0488-7
- Pandit-Taskar, N., Postow, M. A., Hellmann, M. D., Harding, J. J., Barker, C. A., O'Donoghue, J. A., . . . Wolchok, J. D. (2020). First-in-Humans Imaging with (89)Zr-Df-IAB22M2C Anti-CD8 Minibody in Patients with Solid Malignancies: Preliminary Pharmacokinetics, Biodistribution, and Lesion Targeting. *J Nucl Med*, 61(4), 512-519. doi:10.2967/jnumed.119.229781
- Pardi, N., Hogan, M. J., Porter, F. W., & Weissman, D. (2018). mRNA vaccines - a new era in vaccinology. *Nat Rev Drug Discov*, 17(4), 261-279. doi:10.1038/nrd.2017.243
- Pardoll, D. M. (2012). The blockade of immune checkpoints in cancer immunotherapy. *Nat Rev Cancer*, 12(4), 252-264. doi:10.1038/nrc3239
- Peng, M., Mo, Y., Wang, Y., Wu, P., Zhang, Y., Xiong, F., . . . Zeng, Z. (2019). Neoantigen vaccine: an emerging tumor immunotherapy. *Mol Cancer*, 18(1), 128. doi:10.1186/s12943-019-1055-6

## References

- Peters, B., Nielsen, M., & Sette, A. (2020). T Cell Epitope Predictions. *Annu Rev Immunol*, 38, 123-145. doi:10.1146/annurev-immunol-082119-124838
- Phan, H. T., Jager, P. L., Paans, A. M., Plukker, J. T., Sturkenboom, M. G., Sluiter, W. J., . . . Links, T. P. (2008). The diagnostic value of 124I-PET in patients with differentiated thyroid cancer. *Eur J Nucl Med Mol Imaging*, 35(5), 958-965. doi:10.1007/s00259-007-0660-6
- Pires da Silva, I., Lo, S., Quek, C., Gonzalez, M., Carlino, M. S., Long, G. V., & Menzies, A. M. (2020). Site-specific response patterns, pseudoprogression, and acquired resistance in patients with melanoma treated with ipilimumab combined with anti-PD-1 therapy. *Cancer*, 126(1), 86-97. doi:10.1002/cncr.32522
- Polakis, P. (2016). Antibody Drug Conjugates for Cancer Therapy. *Pharmacol Rev*, 68(1), 3-19. doi:10.1124/pr.114.009373
- Poon, M., Dennis, K., DeAngelis, C., Chung, H., Stinson, J., Zhang, L., . . . Chow, E. (2015). Symptom clusters of gastrointestinal cancer patients undergoing radiotherapy using the Functional Living Index-Emesis (FLIE) quality-of-life tool. *Support Care Cancer*, 23(9), 2589-2598. doi:10.1007/s00520-015-2617-9
- Porter, D. L., Levine, B. L., Kalos, M., Bagg, A., & June, C. H. (2011). Chimeric antigen receptor-modified T cells in chronic lymphoid leukemia. *N Engl J Med*, 365(8), 725-733. doi:10.1056/NEJMoa1103849
- Rabinowich, H., Pricop, L., Herberman, R. B., & Whiteside, T. L. (1994). Expression and function of CD7 molecule on human natural killer cells. *J Immunol*, 152(2), 517-526. Retrieved from <https://www.ncbi.nlm.nih.gov/pubmed/7506726>
- Rabinowich, H., Pricop, L., Herberman, R. B., & Whiteside, T. L. (1994). Expression and function of CD7 molecule on human natural killer cells. *The Journal of Immunology*, 152(2), 517-526.
- Rafiq, S., Hackett, C. S., & Brentjens, R. J. (2020). Engineering strategies to overcome the current roadblocks in CAR T cell therapy. *Nat Rev Clin Oncol*, 17(3), 147-167. doi:10.1038/s41571-019-0297-y
- Rashidian, M., Ingram, J. R., Dougan, M., Dongre, A., Whang, K. A., LeGall, C., . . . Ploegh, H. L. (2017). Predicting the response to CTLA-4 blockade by longitudinal noninvasive monitoring of CD8 T cells. *J Exp Med*, 214(8), 2243-2255. doi:10.1084/jem.20161950
- Rashidian, M., LaFleur, M. W., Verschoor, V. L., Dongre, A., Zhang, Y., Nguyen, T. H., . . . Ploegh, H. L. (2019). Immuno-PET identifies the myeloid compartment as a key contributor to the outcome of the antitumor response under PD-1 blockade. *Proc Natl Acad Sci U S A*, 116(34), 16971-16980. doi:10.1073/pnas.1905005116
- Rashidian, M., & Ploegh, H. (2020). Nanobodies as non-invasive imaging tools. *Immuno-Oncology Technology*, 7, 2-14.
- Reardon, D. A., & Weller, M. (2018). Pseudoprogression: fact or wishful thinking in neuro-oncology? *The Lancet Oncology*, 19(12), 1561-1563.
- Reddy, S., & Robinson, M. K. (2010). Immuno-positron emission tomography in cancer models. *Semin Nucl Med*, 40(3), 182-189. doi:10.1053/j.semnuclmed.2009.12.004

- Rege, S., Maass, A., Chaiken, L., Hoh, C. K., Choi, Y., Lufkin, R., . . . Phelps, M. E. (1994). Use of positron emission tomography with fluorodeoxyglucose in patients with extracranial head and neck cancers. *Cancer*, *73*(12), 3047-3058. doi:10.1002/1097-0142(19940615)73:12<3047::aid-cncr2820731225>3.0.co;2-#
- Reinherz, E. L. (1985). A molecular basis for thymic selection: regulation of T11 induced thymocyte expansion by the T3-Ti antigen/MHC receptor pathway. *Immunol Today*, *6*(3), 75-79. doi:10.1016/0167-5699(85)90019-2
- Rinde, M. (2019). Sipuleucel-T shows potential with new trial data, but questions regarding clinical relevance remain. *Targeted Therapies Oncol*, *8*.
- Robu, S., Richter, A., Gosmann, D., Seidl, C., Leung, D., Hayes, W., . . . Weber, W. A. (2021). Synthesis and Preclinical Evaluation of a (68)Ga-Labeled Adnectin, (68)Ga-BMS-986192, as a PET Agent for Imaging PD-L1 Expression. *J Nucl Med*, *62*(9), 1228-1234. doi:10.2967/jnumed.120.258384
- Rogers, O. C., Rosen, D. M., Antony, L., Harper, H. M., Das, D., Yang, X., . . . Denmeade, S. R. (2021). Targeted delivery of cytotoxic proteins to prostate cancer via conjugation to small molecule urea-based PSMA inhibitors. *Sci Rep*, *11*(1), 14925. doi:10.1038/s41598-021-94534-5
- Rooney, M. S., Shukla, S. A., Wu, C. J., Getz, G., & Hachohen, N. (2015). Molecular and genetic properties of tumors associated with local immune cytolytic activity. *Cell*, *160*(1-2), 48-61. doi:10.1016/j.cell.2014.12.033
- Rosenberg, J. E., Hoffman-Censits, J., Powles, T., van der Heijden, M. S., Balar, A. V., Necchi, A., . . . Dreicer, R. (2016). Atezolizumab in patients with locally advanced and metastatic urothelial carcinoma who have progressed following treatment with platinum-based chemotherapy: a single-arm, multicentre, phase 2 trial. *Lancet*, *387*(10031), 1909-1920. doi:10.1016/S0140-6736(16)00561-4
- Rosenberg, S. A., Yang, J. C., Sherry, R. M., Kammula, U. S., Hughes, M. S., Phan, G. Q., . . . Dudley, M. E. (2011). Durable complete responses in heavily pretreated patients with metastatic melanoma using T-cell transfer immunotherapy. *Clin Cancer Res*, *17*(13), 4550-4557. doi:10.1158/1078-0432.CCR-11-0116
- Rossin, R., Versteegen, R. M., Wu, J., Khasanov, A., Wessels, H. J., Steenbergen, E. J., . . . Robillard, M. S. (2018). Chemically triggered drug release from an antibody-drug conjugate leads to potent antitumour activity in mice. *Nat Commun*, *9*(1), 1484. doi:10.1038/s41467-018-03880-y
- Rousseau, E., Lau, J., Kuo, H. T., Zhang, Z., Merkens, H., Hundal-Jabal, N., . . . Benard, F. (2018). Monosodium Glutamate Reduces (68)Ga-PSMA-11 Uptake in Salivary Glands and Kidneys in a Preclinical Prostate Cancer Model. *J Nucl Med*, *59*(12), 1865-1868. doi:10.2967/jnumed.118.215350
- Sachpekidis, C., Larribere, L., Pan, L., Haberkorn, U., Dimitrakopoulou-Strauss, A., & Hassel, J. C. (2015). Predictive value of early 18F-FDG PET/CT studies for treatment response evaluation to ipilimumab in metastatic melanoma: preliminary results of an ongoing study. *Eur J Nucl Med Mol Imaging*, *42*(3), 386-396. doi:10.1007/s00259-014-2944-y
- Sahin, U., Derhovanessian, E., Miller, M., Kloke, B. P., Simon, P., Lower, M., . . . Tureci, O. (2017). Personalized RNA mutanome vaccines mobilize poly-specific therapeutic immunity against cancer. *Nature*, *547*(7662), 222-226. doi:10.1038/nature23003

- Sahin, U., & Tureci, O. (2018). Personalized vaccines for cancer immunotherapy. *Science*, *359*(6382), 1355-1360. doi:10.1126/science.aar7112
- Sanchez-Madrid, F., Krensky, A. M., Ware, C. F., Robbins, E., Strominger, J. L., Burakoff, S. J., & Springer, T. A. (1982). Three distinct antigens associated with human T-lymphocyte-mediated cytotoxicity: LFA-1, LFA-2, and LFA-3. *Proc Natl Acad Sci U S A*, *79*(23), 7489-7493. doi:10.1073/pnas.79.23.7489
- Sanders, M. E., Makgoba, M., Sharrow, S., Stephany, D., Springer, T., Young, H., & Shaw, S. (1988). Human memory T lymphocytes express increased levels of three cell adhesion molecules (LFA-3, CD2, and LFA-1) and three other molecules (UCHL1, CDw29, and Pgp-1) and have enhanced IFN-gamma production. *The Journal of Immunology*, *140*(5), 1401-1407.
- Sarkizova, S., Klaeger, S., Le, P. M., Li, L. W., Oliveira, G., Keshishian, H., . . . Keskin, D. B. (2020). A large peptide dataset improves HLA class I epitope prediction across most of the human population. *Nat Biotechnol*, *38*(2), 199-209. doi:10.1038/s41587-019-0322-9
- Sato, N., Stringaris, K., Davidson-Moncada, J. K., Reger, R., Adler, S. S., Dunbar, C., . . . Childs, R. W. (2020). In Vivo Tracking of Adoptively Transferred Natural Killer Cells in Rhesus Macaques Using (89)Zirconium-Oxine Cell Labeling and PET Imaging. *Clin Cancer Res*, *26*(11), 2573-2581. doi:10.1158/1078-0432.CCR-19-2897
- Savas, P., Virassamy, B., Ye, C., Salim, A., Mintoff, C. P., Caramia, F., . . . Loi, S. (2018). Single-cell profiling of breast cancer T cells reveals a tissue-resident memory subset associated with improved prognosis. *Nat Med*, *24*(7), 986-993. doi:10.1038/s41591-018-0078-7
- Sayre, P. H., Hussey, R. E., Chang, H. C., Ciardelli, T. L., & Reinherz, E. L. (1989). Structural and binding analysis of a two domain extracellular CD2 molecule. *J Exp Med*, *169*(3), 995-1009. doi:10.1084/jem.169.3.995
- Schadendorf, D., Hodi, F. S., Robert, C., Weber, J. S., Margolin, K., Hamid, O., . . . Wolchok, J. D. (2015). Pooled Analysis of Long-Term Survival Data From Phase II and Phase III Trials of Ipilimumab in Unresectable or Metastatic Melanoma. *J Clin Oncol*, *33*(17), 1889-1894. doi:10.1200/JCO.2014.56.2736
- Schechter, A. L., Stern, D. F., Vaidyanathan, L., Decker, S. J., Drebin, J. A., Greene, M. I., & Weinberg, R. A. (1984). The neu oncogene: an erb-B-related gene encoding a 185,000-Mr tumour antigen. *Nature*, *312*(5994), 513-516. doi:10.1038/312513a0
- Scott, A. M., Wolchok, J. D., & Old, L. J. (2012). Antibody therapy of cancer. *Nat Rev Cancer*, *12*(4), 278-287. doi:10.1038/nrc3236
- Scott, S. D. (1998). Rituximab: a new therapeutic monoclonal antibody for non-Hodgkin's lymphoma. *Cancer Pract*, *6*(3), 195-197. doi:10.1046/j.1523-5394.1998.006003195.x
- Selvaraj, P., Plunkett, M. L., Dustin, M., Sanders, M. E., Shaw, S., & Springer, T. A. (1987). The T lymphocyte glycoprotein CD2 binds the cell surface ligand LFA-3. *Nature*, *326*(6111), 400-403. doi:10.1038/326400a0
- Seo, J. W., Tavare, R., Mahakian, L. M., Silvestrini, M. T., Tam, S., Ingham, E. S., . . . Ferrara, K. W. (2018). CD8(+) T-Cell Density Imaging with (64)Cu-Labeled Cys-Diobody Informs Immunotherapy Protocols. *Clin Cancer Res*, *24*(20), 4976-4987. doi:10.1158/1078-0432.CCR-18-0261

## References

- Seymour, L., Bogaerts, J., Perrone, A., Ford, R., Schwartz, L. H., Mandrekar, S., . . . group, R. w. (2017). iRECIST: guidelines for response criteria for use in trials testing immunotherapeutics. *Lancet Oncol*, *18*(3), e143-e152. doi:10.1016/S1470-2045(17)30074-8
- Sezer, A., Kilickap, S., Gumus, M., Bondarenko, I., Ozguroglu, M., Gogishvili, M., . . . Rietschel, P. (2021). Cemiplimab monotherapy for first-line treatment of advanced non-small-cell lung cancer with PD-L1 of at least 50%: a multicentre, open-label, global, phase 3, randomised, controlled trial. *Lancet*, *397*(10274), 592-604. doi:10.1016/S0140-6736(21)00228-2
- Sharma, P., & Allison, J. P. (2015). Immune checkpoint targeting in cancer therapy: toward combination strategies with curative potential. *Cell*, *161*(2), 205-214. doi:10.1016/j.cell.2015.03.030
- Sharma, P., Wagner, K., Wolchok, J. D., & Allison, J. P. (2011). Novel cancer immunotherapy agents with survival benefit: recent successes and next steps. *Nat Rev Cancer*, *11*(11), 805-812. doi:10.1038/nrc3153
- Sido, B., Dengler, T. J., Otto, G., Zimmermann, R., Muller, P., & Meuer, S. C. (1998). Differential immunosuppressive activity of monoclonal CD2 antibodies on allograft rejection versus specific antibody production. *Eur J Immunol*, *28*(4), 1347-1357. doi:10.1002/(SICI)1521-4141(199804)28:04<1347::AID-IMMU1347>3.0.CO;2-L
- Singh, N., Orlando, E., Xu, J., Xu, J., Binder, Z., Collins, M. A., . . . Melenhorst, J. J. (2020). *Mechanisms of resistance to CAR T cell therapies*. Paper presented at the Seminars in cancer biology.
- Slamon, D. J., Clark, G. M., Wong, S. G., Levin, W. J., Ullrich, A., & McGuire, W. L. (1987). Human breast cancer: correlation of relapse and survival with amplification of the HER-2/neu oncogene. *Science*, *235*(4785), 177-182. doi:10.1126/science.3798106
- Slamon, D. J., Godolphin, W., Jones, L. A., Holt, J. A., Wong, S. G., Keith, D. E., . . . et al. (1989). Studies of the HER-2/neu proto-oncogene in human breast and ovarian cancer. *Science*, *244*(4905), 707-712. doi:10.1126/science.2470152
- Small, E. J., Schellhammer, P. F., Higano, C. S., Redfern, C. H., Nemunaitis, J. J., Valone, F. H., . . . Hershberg, R. M. (2006). Placebo-controlled phase III trial of immunologic therapy with sipuleucel-T (APC8015) in patients with metastatic, asymptomatic hormone refractory prostate cancer. *J Clin Oncol*, *24*(19), 3089-3094. doi:10.1200/JCO.2005.04.5252
- Sotillo, E., Barrett, D. M., Black, K. L., Bagashev, A., Oldridge, D., Wu, G., . . . Thomas-Tikhonenko, A. (2015). Convergence of Acquired Mutations and Alternative Splicing of CD19 Enables Resistance to CART-19 Immunotherapy. *Cancer Discov*, *5*(12), 1282-1295. doi:10.1158/2159-8290.CD-15-1020
- Spain, L., Larkin, J., & Turajlic, S. (2020). New survival standards for advanced melanoma. *Br J Cancer*, *122*(9), 1275-1276. doi:10.1038/s41416-020-0738-5
- Spick, C., Herrmann, K., & Czernin, J. (2016). 18F-FDG PET/CT and PET/MRI Perform Equally Well in Cancer: Evidence from Studies on More Than 2,300 Patients. *J Nucl Med*, *57*(3), 420-430. doi:10.2967/jnumed.115.158808
- Spitzer, M. H., Carmi, Y., Reticker-Flynn, N. E., Kwek, S. S., Madhireddy, D., Martins, M. M., . . . Engleman, E. G. (2017). Systemic Immunity Is Required for Effective Cancer Immunotherapy. *Cell*, *168*(3), 487-502 e415. doi:10.1016/j.cell.2016.12.022

- Starr, C. G., & Tessier, P. M. (2019). Selecting and engineering monoclonal antibodies with drug-like specificity. *Curr Opin Biotechnol*, *60*, 119-127. doi:10.1016/j.copbio.2019.01.008
- Stashenko, P., Nadler, L. M., Hardy, R., & Schlossman, S. F. (1980). Characterization of a human B lymphocyte-specific antigen. *J Immunol*, *125*(4), 1678-1685. Retrieved from <https://www.ncbi.nlm.nih.gov/pubmed/6157744>
- Steeland, S., Puimege, L., Vandenbroucke, R. E., Van Hauwermeiren, F., Haustraete, J., Devoogdt, N., . . . Libert, C. (2015). Generation and characterization of small single domain antibodies inhibiting human tumor necrosis factor receptor 1. *J Biol Chem*, *290*(7), 4022-4037. doi:10.1074/jbc.M114.617787
- Steiner, M., & Neri, D. (2011). Antibody-radionuclide conjugates for cancer therapy: historical considerations and new trends. *Clin Cancer Res*, *17*(20), 6406-6416. doi:10.1158/1078-0432.CCR-11-0483
- Stepan, L. P., Trueblood, E. S., Hale, K., Babcook, J., Borges, L., & Sutherland, C. L. (2011). Expression of Trop2 cell surface glycoprotein in normal and tumor tissues: potential implications as a cancer therapeutic target. *J Histochem Cytochem*, *59*(7), 701-710. doi:10.1369/0022155411410430
- Sullivan, D. C., Schwartz, L. H., & Zhao, B. (2013). The imaging viewpoint: how imaging affects determination of progression-free survival. *Clin Cancer Res*, *19*(10), 2621-2628. doi:10.1158/1078-0432.CCR-12-2936
- Sullivan, R., Alatishe, O. I., Anderson, B. O., Audisio, R., Autier, P., Aggarwal, A., . . . Purushotham, A. (2015). Global cancer surgery: delivering safe, affordable, and timely cancer surgery. *Lancet Oncol*, *16*(11), 1193-1224. doi:10.1016/S1470-2045(15)00223-5
- Sung, H., Ferlay, J., Siegel, R. L., Laversanne, M., Soerjomataram, I., Jemal, A., & Bray, F. (2021). Global Cancer Statistics 2020: GLOBOCAN Estimates of Incidence and Mortality Worldwide for 36 Cancers in 185 Countries. *CA Cancer J Clin*, *71*(3), 209-249. doi:10.3322/caac.21660
- Suntharalingam, G., Perry, M. R., Ward, S., Brett, S. J., Castello-Cortes, A., Brunner, M. D., & Panoskaltsis, N. (2006). Cytokine storm in a phase 1 trial of the anti-CD28 monoclonal antibody TGN1412. *N Engl J Med*, *355*(10), 1018-1028. doi:10.1056/NEJMoa063842
- Tan, M. P., Gerry, A. B., Brewer, J. E., Melchiori, L., Bridgeman, J. S., Bennett, A. D., . . . Sewell, A. K. (2015). T cell receptor binding affinity governs the functional profile of cancer-specific CD8+ T cells. *Clin Exp Immunol*, *180*(2), 255-270. doi:10.1111/cei.12570
- Tang, J. J., Sung, A. P., Guglielmo, M. J., Navarrete-Galvan, L., Redelman, D., Smith-Gagen, J., & Hudig, D. (2020). Natural Killer (NK) Cell Expression of CD2 as a Predictor of Serial Antibody-Dependent Cell-Mediated Cytotoxicity (ADCC). *Antibodies (Basel)*, *9*(4). doi:10.3390/antib9040054
- Tanizaki, J., Hayashi, H., Kimura, M., Tanaka, K., Takeda, M., Shimizu, S., . . . Nakagawa, K. (2016). Report of two cases of pseudoprogression in patients with non-small cell lung cancer treated with nivolumab-including histological analysis of one case after tumor regression. *Lung Cancer*, *102*, 44-48. doi:10.1016/j.lungcan.2016.10.014
- Tavare, R., Escuin-Ordinas, H., Mok, S., McCracken, M. N., Zettlitz, K. A., Salazar, F. B., . . . Wu, A. M. (2016). An Effective Immuno-PET Imaging Method to Monitor CD8-Dependent Responses to Immunotherapy. *Cancer Res*, *76*(1), 73-82. doi:10.1158/0008-5472.CAN-15-1707

## References

- Tavare, R., McCracken, M. N., Zettlitz, K. A., Knowles, S. M., Salazar, F. B., Olafsen, T., . . . Wu, A. M. (2014). Engineered antibody fragments for immuno-PET imaging of endogenous CD8+ T cells in vivo. *Proc Natl Acad Sci U S A*, *111*(3), 1108-1113. doi:10.1073/pnas.1316922111
- Tawbi, H. A., Schadendorf, D., Lipson, E. J., Ascierto, P. A., Matamala, L., Castillo Gutierrez, E., . . . Investigators, R.-. (2022). Relatlimab and Nivolumab versus Nivolumab in Untreated Advanced Melanoma. *N Engl J Med*, *386*(1), 24-34. doi:10.1056/NEJMoa2109970
- Tazdait, M., Mezquita, L., Lahmar, J., Ferrara, R., Bidault, F., Ammari, S., . . . Caramella, C. (2018). Patterns of responses in metastatic NSCLC during PD-1 or PDL-1 inhibitor therapy: Comparison of RECIST 1.1, irRECIST and iRECIST criteria. *Eur J Cancer*, *88*, 38-47. doi:10.1016/j.ejca.2017.10.017
- Thaxton, J. E., & Li, Z. (2014). To affinity and beyond: harnessing the T cell receptor for cancer immunotherapy. *Hum Vaccin Immunother*, *10*(11), 3313-3321. doi:10.4161/21645515.2014.973314
- Thurber, G. M., Schmidt, M. M., & Wittrup, K. D. (2008). Antibody tumor penetration: transport opposed by systemic and antigen-mediated clearance. *Adv Drug Deliv Rev*, *60*(12), 1421-1434. doi:10.1016/j.addr.2008.04.012
- Thust, S. C., van den Bent, M. J., & Smits, M. (2018). Pseudoprogression of brain tumors. *J Magn Reson Imaging*. doi:10.1002/jmri.26171
- Tian, T., & Li, Z. (2021). Targeting Tim-3 in Cancer With Resistance to PD-1/PD-L1 Blockade. *Front Oncol*, *11*, 731175. doi:10.3389/fonc.2021.731175
- Till, B. G., Jensen, M. C., Wang, J., Chen, E. Y., Wood, B. L., Greisman, H. A., . . . Press, O. W. (2008). Adoptive immunotherapy for indolent non-Hodgkin lymphoma and mantle cell lymphoma using genetically modified autologous CD20-specific T cells. *Blood*, *112*(6), 2261-2271. doi:10.1182/blood-2007-12-128843
- Timonen, T., Gahmberg, C. G., & Patarroyo, M. (1990). Participation of CD11a-c/CD18, CD2 and RGD-binding receptors in endogenous and interleukin-2-stimulated NK activity of CD3-negative large granular lymphocytes. *Int J Cancer*, *46*(6), 1035-1040. doi:10.1002/ijc.2910460615
- Tjuvajev, J. G., Doubrovin, M., Akhurst, T., Cai, S., Balatoni, J., Alauddin, M. M., . . . Blasberg, R. G. (2002). Comparison of radiolabeled nucleoside probes (FIAU, FHBG, and FHPG) for PET imaging of HSV1-tk gene expression. *J Nucl Med*, *43*(8), 1072-1083. Retrieved from <https://www.ncbi.nlm.nih.gov/pubmed/12163634>
- Tomita, S., Kikuti, Y. Y., Carreras, J., Kojima, M., Ando, K., Takasaki, H., . . . Nakamura, N. (2015). Genomic and immunohistochemical profiles of enteropathy-associated T-cell lymphoma in Japan. *Mod Pathol*, *28*(10), 1286-1296. doi:10.1038/modpathol.2015.85
- Tran, E., Turcotte, S., Gros, A., Robbins, P. F., Lu, Y. C., Dudley, M. E., . . . Rosenberg, S. A. (2014). Cancer immunotherapy based on mutation-specific CD4+ T cells in a patient with epithelial cancer. *Science*, *344*(6184), 641-645. doi:10.1126/science.1251102
- Tumeh, P. C., Harview, C. L., Yearley, J. H., Shintaku, I. P., Taylor, E. J., Robert, L., . . . Ribas, A. (2014). PD-1 blockade induces responses by inhibiting adaptive immune resistance. *Nature*, *515*(7528), 568-571. doi:10.1038/nature13954

## References

- Tumeh, P. C., Radu, C. G., & Ribas, A. (2008). PET imaging of cancer immunotherapy. *J Nucl Med*, *49*(6), 865-868. doi:10.2967/jnumed.108.051342
- Uckun, F. M., Jaszcz, W., Ambrus, J. L., Fauci, A. S., Gajl-Peczalska, K., Song, C. W., . . . Ledbetter, J. A. (1988). Detailed studies on expression and function of CD19 surface determinant by using B43 monoclonal antibody and the clinical potential of anti-CD19 immunotoxins. *Blood*, *71*(1), 13-29. Retrieved from <https://www.ncbi.nlm.nih.gov/pubmed/3257143>
- UniProt, C. (2019). UniProt: a worldwide hub of protein knowledge. *Nucleic Acids Res*, *47*(D1), D506-D515. doi:10.1093/nar/gky1049
- Urquhart, L. (2022). FDA new drug approvals in Q1 2022. *Nat Rev Drug Discov*, *21*(5), 329. doi:10.1038/d41573-022-00063-9
- van Dongen, G. A., Visser, G. W., Lub-de Hooge, M. N., de Vries, E. G., & Perk, L. R. (2007). Immuno-PET: a navigator in monoclonal antibody development and applications. *Oncologist*, *12*(12), 1379-1389. doi:10.1634/theoncologist.12-12-1379
- Vaneycken, I., Devoogdt, N., Van Gassen, N., Vincke, C., Xavier, C., Wernery, U., . . . Caveliers, V. (2011). Preclinical screening of anti-HER2 nanobodies for molecular imaging of breast cancer. *FASEB J*, *25*(7), 2433-2446. doi:10.1096/fj.10-180331
- Vansteenkiste, J., Zielinski, M., Linder, A., Dahabreh, J., Gonzalez, E. E., Malinowski, W., . . . Brichard, V. G. (2013). Adjuvant MAGE-A3 immunotherapy in resected non-small-cell lung cancer: phase II randomized study results. *J Clin Oncol*, *31*(19), 2396-2403. doi:10.1200/JCO.2012.43.7103
- Vedvyas, Y., McCloskey, J. E., Yang, Y., Min, I. M., Fahey, T. J., Zarnegar, R., . . . Jin, M. M. (2019). Manufacturing and preclinical validation of CAR T cells targeting ICAM-1 for advanced thyroid cancer therapy. *Sci Rep*, *9*(1), 10634. doi:10.1038/s41598-019-46938-7
- Vollger, L. W., Tuck, D., Springer, T., Haynes, B., & Singer, K. (1987). Thymocyte binding to human thymic epithelial cells is inhibited by monoclonal antibodies to CD-2 and LFA-3 antigens. *The Journal of Immunology*, *138*(2), 358-363.
- Wagner, S., Mullins, C. S., & Linnebacher, M. (2018). Colorectal cancer vaccines: Tumor-associated antigens vs neoantigens. *World J Gastroenterol*, *24*(48), 5418-5432. doi:10.3748/wjg.v24.i48.5418
- Wang, D., Aguilar, B., Starr, R., Alizadeh, D., Brito, A., Sarkissian, A., . . . Brown, C. E. (2018). Glioblastoma-targeted CD4+ CAR T cells mediate superior antitumor activity. *JCI Insight*, *3*(10). doi:10.1172/jci.insight.99048
- Wang, J., Day, R., Dong, Y., Weintraub, S. J., & Michel, L. (2008). Identification of Trop-2 as an oncogene and an attractive therapeutic target in colon cancers. *Mol Cancer Ther*, *7*(2), 280-285. doi:10.1158/1535-7163.MCT-07-2003
- Ward, S. G., Parry, R., Lefevre, C., Sansom, D. M., Westwick, J., & Lazarovits, A. I. (1995). Antibody ligation of CD7 leads to association with phosphoinositide 3-kinase and phosphatidylinositol 3, 4, 5-trisphosphate formation in T lymphocytes. *European journal of immunology*, *25*(2), 502-507.
- Warren, H. S., & Parish, C. R. (1990). Mapping the dextran sulfate binding site on CD2. *Immunol Cell Biol*, *68* ( Pt 3), 199-205. doi:10.1038/icb.1990.28

## References

- Weekes, M. P., Antrobus, R., Lill, J. R., Duncan, L. M., Hor, S., & Lehner, P. J. (2010). Comparative analysis of techniques to purify plasma membrane proteins. *J Biomol Tech*, *21*(3), 108-115. Retrieved from <https://www.ncbi.nlm.nih.gov/pubmed/20808639>
- Weiner, L. M., Beldegrun, A. S., Crawford, J., Tolcher, A. W., Lockbaum, P., Arends, R. H., . . . Figlin, R. A. (2008). Dose and schedule study of panitumumab monotherapy in patients with advanced solid malignancies. *Clin Cancer Res*, *14*(2), 502-508. doi:10.1158/1078-0432.CCR-07-1509
- Weiner, L. M., Surana, R., & Wang, S. (2010). Monoclonal antibodies: versatile platforms for cancer immunotherapy. *Nat Rev Immunol*, *10*(5), 317-327. doi:10.1038/nri2744
- Weiskopf, K., Ring, A. M., Ho, C. C., Volkmer, J. P., Levin, A. M., Volkmer, A. K., . . . Garcia, K. C. (2013). Engineered SIRPalpha variants as immunotherapeutic adjuvants to anticancer antibodies. *Science*, *341*(6141), 88-91. doi:10.1126/science.1238856
- Weist, M. R., Starr, R., Aguilar, B., Chea, J., Miles, J. K., Poku, E., . . . Shively, J. E. (2018). PET of Adoptively Transferred Chimeric Antigen Receptor T Cells with (89)Zr-Oxine. *J Nucl Med*, *59*(10), 1531-1537. doi:10.2967/jnumed.117.206714
- Wesolowski, J., Alzogaray, V., Reyelt, J., Unger, M., Juarez, K., Urrutia, M., . . . Koch-Nolte, F. (2009). Single domain antibodies: promising experimental and therapeutic tools in infection and immunity. *Med Microbiol Immunol*, *198*(3), 157-174. doi:10.1007/s00430-009-0116-7
- Wherry, E. J., & Kurachi, M. (2015). Molecular and cellular insights into T cell exhaustion. *Nat Rev Immunol*, *15*(8), 486-499. doi:10.1038/nri3862
- Wolf, Y., Anderson, A. C., & Kuchroo, V. K. (2020). TIM3 comes of age as an inhibitory receptor. *Nat Rev Immunol*, *20*(3), 173-185. doi:10.1038/s41577-019-0224-6
- Wu, A. M. (2014). Engineered antibodies for molecular imaging of cancer. *Methods*, *65*(1), 139-147. doi:10.1016/j.ymeth.2013.09.015
- Wu, T., Huang, H., Sheng, Y., Shi, H., Min, Y., & Liu, Y. (2018). Transglutaminase mediated PEGylation of nanobodies for targeted nano-drug delivery. *J Mater Chem B*, *6*(7), 1011-1017. doi:10.1039/c7tb03132g
- Xenaki, K. T., Dorrestijn, B., Muns, J. A., Adamzek, K., Doukeridou, S., Houthoff, H., . . . van Bergen En Henegouwen, P. M. (2021). Homogeneous tumor targeting with a single dose of HER2-targeted albumin-binding domain-fused nanobody-drug conjugates results in long-lasting tumor remission in mice. *Theranostics*, *11*(11), 5525-5538. doi:10.7150/thno.57510
- Xu, Y., Yang, Z., Horan, L. H., Zhang, P., Liu, L., Zimdahl, B., . . . Liu, C. (2018). A novel antibody-TCR (AbTCR) platform combines Fab-based antigen recognition with gamma/delta-TCR signaling to facilitate T-cell cytotoxicity with low cytokine release. *Cell Discov*, *4*, 62. doi:10.1038/s41421-018-0066-6
- Yaghoubi, S. S., Campbell, D. O., Radu, C. G., & Czernin, J. (2012). Positron emission tomography reporter genes and reporter probes: gene and cell therapy applications. *Theranostics*, *2*(4), 374-391. doi:10.7150/thno.3677
- Yaghoubi, S. S., Jensen, M. C., Satyamurthy, N., Budhiraja, S., Paik, D., Czernin, J., & Gambhir, S. S. (2009). Noninvasive detection of therapeutic cytolytic T cells with 18F-FHBG PET in a patient with glioma. *Nat Clin Pract Oncol*, *6*(1), 53-58. doi:10.1038/ncponc1278

- Yamada, Y., Post, S. R., Wang, K., Tager, H. S., Bell, G. I., & Seino, S. (1992). Cloning and functional characterization of a family of human and mouse somatostatin receptors expressed in brain, gastrointestinal tract, and kidney. *Proc Natl Acad Sci U S A*, *89*(1), 251-255. doi:10.1073/pnas.89.1.251
- Yang, Y., Kohler, M. E., Chien, C. D., Sauter, C. T., Jacoby, E., Yan, C., . . . Fry, T. J. (2017). TCR engagement negatively affects CD8 but not CD4 CAR T cell expansion and leukemic clearance. *Sci Transl Med*, *9*(417). doi:10.1126/scitranslmed.aag1209
- Yang, Y., McCloskey, J. E., Yang, H., Puc, J., Alcaina, Y., Vedvyas, Y., . . . Jin, M. M. (2021). Bispecific CAR T Cells against EpCAM and Inducible ICAM-1 Overcome Antigen Heterogeneity and Generate Superior Antitumor Responses. *Cancer Immunol Res*, *9*(10), 1158-1174. doi:10.1158/2326-6066.CIR-21-0062
- Yarchoan, M., Johnson, B. A., 3rd, Lutz, E. R., Laheru, D. A., & Jaffee, E. M. (2017). Targeting neoantigens to augment antitumor immunity. *Nat Rev Cancer*, *17*(4), 209-222. doi:10.1038/nrc.2016.154
- Ying, Z., Huang, X. F., Xiang, X., Liu, Y., Kang, X., Song, Y., . . . Chen, S. Y. (2019). A safe and potent anti-CD19 CAR T cell therapy. *Nat Med*, *25*(6), 947-953. doi:10.1038/s41591-019-0421-7
- Zah, E., Nam, E., Bhuvan, V., Tran, U., Ji, B. Y., Gosliner, S. B., . . . Chen, Y. Y. (2020). Systematically optimized BCMA/CS1 bispecific CAR-T cells robustly control heterogeneous multiple myeloma. *Nat Commun*, *11*(1), 2283. doi:10.1038/s41467-020-16160-5
- Zamora, A. E., Crawford, J. C., & Thomas, P. G. (2018). Hitting the target: how T cells detect and eliminate tumors. *The Journal of Immunology*, *200*(2), 392-399.
- Zeh, H. J., 3rd, Perry-Lalley, D., Dudley, M. E., Rosenberg, S. A., & Yang, J. C. (1999). High avidity CTLs for two self-antigens demonstrate superior in vitro and in vivo antitumor efficacy. *J Immunol*, *162*(2), 989-994. Retrieved from <https://www.ncbi.nlm.nih.gov/pubmed/9916724>
- Zhang, X., Huang, H., Han, L., Li, T., Wang, Z., & Gao, Q. (2021). Advanced Renal-Cell Carcinoma Pseudoprogression After Combined Immunotherapy: Case Report and Literature Review. *Front Oncol*, *11*, 640447. doi:10.3389/fonc.2021.640447
- Zhao, H., Wang, C., Yang, Y., Sun, Y., Wei, W., Wang, C., . . . Liu, J. (2021). ImmunoPET imaging of human CD8(+) T cells with novel (68)Ga-labeled nanobody companion diagnostic agents. *J Nanobiotechnology*, *19*(1), 42. doi:10.1186/s12951-021-00785-9
- Zhong, S., Malecek, K., Johnson, L. A., Yu, Z., Vega-Saenz de Miera, E., Darvishian, F., . . . Krosgaard, M. (2013). T-cell receptor affinity and avidity defines antitumor response and autoimmunity in T-cell immunotherapy. *Proc Natl Acad Sci U S A*, *110*(17), 6973-6978. doi:10.1073/pnas.1221609110
- Zinkernagel, R. M., & Doherty, P. C. (1974). Restriction of in vitro T cell-mediated cytotoxicity in lymphocytic choriomeningitis within a syngeneic or semiallogeneic system. *Nature*, *248*(5450), 701-702. doi:10.1038/248701a0
- Zottel, A., Jovcevska, I., Samec, N., Mlakar, J., Sribar, J., Krizaj, I., . . . Komel, R. (2020). Anti-vimentin, anti-TUFM, anti-NAP1L1 and anti-DPYSL2 nanobodies display cytotoxic effect and reduce glioblastoma cell migration. *Ther Adv Med Oncol*, *12*, 1758835920915302. doi:10.1177/1758835920915302



## 7 Appendix

### 7.1 List of figures

FIGURE 1: OVERVIEW OF IMMUNOTHERAPEUTIC APPROACHES. (CREATED WITH BIORENDER.COM) .....	8
FIGURE 2: SCHEMATIC OVERVIEW OF RESPONSE-PATTERNS FOR IMMUNOTHERAPIES. ....	20
FIGURE 3: KEY CHARACTERISTICS OF ANTIBODY-BASED CONSTRUCTS WITH REGARDS TO IMMUNOPET BASED IMAGING. ....	24
FIGURE 4: SCHEME OF THE GENERATION AND IDENTIFICATION OF SDAB SPECIFIC FOR CD2 AND CD7. ....	63
FIGURE 5: SIZE-VALIDATION AND -CHARACTERIZATION OF CD2- AND CD7-SDAB AFTER HIS-TAG BASED PURIFICATION. ....	65
FIGURE 6: ANALYSIS OF THE CAPABILITY OF CD2-SDAB AND CD7-SDAB TO BIND HUMAN CD8+ T CELLS. ....	67
FIGURE 7: TRANSDUCTIONS OF B CELL LYMPHOMA TUMOR CELL LINE U698M WITH HUMAN CD2 OR CD7. ....	68
FIGURE 8: ANALYSIS OF CD2- AND CD7-SDAB BINDING TO RETROVIRALLY TRANSDUCED U698M CELLS. ....	69
FIGURE 9: CRISPR/Cas9-GENERATED CD2-NEGATIVE JURKAT E6.1 CELLS AFTER LIPOFECTION. ....	70
FIGURE 10: CRISPR/Cas9-GENERATED CD7-NEGATIVE JURKAT E6.1 CELLS AFTER LIPOFECTION. ....	71
FIGURE 11: FLOW CYTOMETRY ANALYSIS OF POPULATIONS BASED OF SINGLE-CELL CLONES AFTER CD2 KNOCKOUT. ....	72
FIGURE 12: FLOW CYTOMETRY ANALYSIS OF POPULATIONS BASED OF SINGLE-CELL CLONES AFTER CD7 KNOCKOUT. ....	73
FIGURE 13: FLOW CYTOMETRY ANALYSIS OF POPULATIONS AFTER SORT FOR CD7-NEGATIVE JURKAT E6.1 CELLS. ....	74
FIGURE 14: BINDING AFFINITIES OF CD2- AND CD7-SDAB ON HUMAN CD8+ T CELLS. ....	75
FIGURE 15: EVALUATION OF THERMOSTABILITY OF CD2- AND CD7-SDAB BINDING TO HUMAN CD8+ T CELLS VIA FLOW CYTOMETRY ANALYSIS.....	76
FIGURE 16: TRANSDUCTION EFFICIENCY ANALYSIS OF RETROVIRALLY TRANSDUCED 624.38 MEL CELLS WITH MPO. ....	78
FIGURE 17: EVALUATION OF PARAMETERS FOR UTILIZING THE XCELLIGENCE SYSTEM TO MONITOR DYNAMIC T-CELL CYTOTOXICITY. ....	79
FIGURE 18: EFFECTS OF DIFFERENT EFFECTOR (E) TO TARGET (T) RATIOS ON THE CYTOLYSIS OF 624.38 MEL BY T CELLS. ....	80
FIGURE 19: EFFECT OF CD2- AND CD7-SDAB ON T-CELL CYTOTOXICITY AT A CONCENTRATION OF 100 NM. ....	81
FIGURE 20: EFFECT OF CD2- AND CD7-SDAB ON T-CELL CYTOTOXICITY AT A CONCENTRATION OF 500 NM. ....	83
FIGURE 21: EXPRESSION ANALYSIS OF MPO AND HLA-B*07:02 ON THE CELL LINES HL60, NB4 AND ML2. ....	84
FIGURE 22: IFNY CYTOKINE SECRETION ANALYSIS OF CD8+ T CELLS BY ELISA AFTER COINCUBATION WITH CD2- AND CD7-SDAB... ..	85
FIGURE 23: CYTOKINE SECRETION ANALYSIS OF IL2, GM-CSF AND TNF-A BY ELISA AFTER COINCUBATION WITH CD2- AND CD7-SDAB. ....	86
FIGURE 24: EXPERIMENTAL SETUP OF IN VIVO TUMOR REJECTION MODEL FOR CD8+ T CELLS.....	87
FIGURE 25: APPLICATION OF CD2-SDAB AND CD7-SDAB DID NOT IMPAIR T-CELL CYTOTOXICITY IN VIVO.....	88
FIGURE 26: ANALYSIS OF T-CELL DISTRIBUTION FOLLOWING SDAB-INJECTION. ....	90
FIGURE 27: EXPERIMENTAL SETUP OF IN VIVO IMAGING FOR <sup>89</sup> Zr-DFO-CD2-F(ab') <sub>2</sub> AND <sup>68</sup> Ga-NOTA-CD2-SDAB.....	91
FIGURE 28: EXPERIMENTAL SETUP OF IN VIVO IMAGING FOR <sup>89</sup> Zr-DFO-CD2-F(ab') <sub>2</sub> AND <sup>68</sup> Ga-NOTA-CD2-SDAB.....	93
FIGURE 29: EXPERIMENTAL SETUP AND PET/MRI IMAGES OF TIME POINT EVALUATION FOR IN VIVO IMAGING USING <sup>68</sup> Ga-NOTA-CD2-SDAB.....	94
FIGURE 30: EXPERIMENTAL SETUP AND PET/MRI IMAGES OF TIME POINT EVALUATION FOR IN VIVO IMAGING USING <sup>68</sup> Ga-NOTA-CD7-SDAB.....	96
FIGURE 31: EXPERIMENTAL SETUP FOR IN VIVO IMAGING USING <sup>68</sup> Ga-NOTA-LABELED SDAB IN NSG MICE.....	97

FIGURE 32: IN VIVO TRACKING INTRAVENOUSLY INJECTED TCR-TRANSGENIC CD8+ T CELLS IN ML2-B7 TUMORS USING <sup>68</sup>GA-NOTA-CD2-SDAB..... 98

FIGURE 33: IN VIVO TRACKING INTRAVENOUSLY INJECTED TCR-TRANSGENIC CD8+ T CELLS IN ML2-B7 TUMORS USING <sup>68</sup>GA-NOTA-CD7-SDAB..... 99

FIGURE 34: EX VIVO BIODISTRIBUTION OF <sup>68</sup>GARADIOLABELED CD2- AND CD7-SDAB..... 100

## 7.2 List of tables

TABLE 1: TECHNICAL EQUIPMENT.....	33
TABLE 2: CONSUMABLES .....	36
TABLE 3: REAGENTS AND CHEMICALS .....	37
TABLE 4: KITS.....	39
TABLE 5: BUFFERS.....	40
TABLE 6: MEDIA .....	41
TABLE 7: CYTOKINES.....	41
TABLE 8: ANTIBODIES FOR FLOW CYTOMETRY .....	42
TABLE 9: VECTORS .....	43
TABLE 10: CRRNA SEQUENCES.....	43
TABLE 11: PRIMERS.....	44
TABLE 12: CELL LINES AND PRIMARY CELLS.....	45
TABLE 13: MOUSE MODEL.....	46
TABLE 14: SOFTWARE.....	46
TABLE 15: PREPARATION OF RNP COMPLEX .....	51
TABLE 16: LIPOFECTION MIX .....	51
TABLE 17: PCR REACTION MIX .....	55
TABLE 18: PCR REACTION PROGRAM.....	55
TABLE 19: REACTION MIXTURE FOR THE DIGESTION OF AMPLIFIED SDAB GENES.....	56
TABLE 20: REACTION MIXTURE FOR THE DIGESTION OF PHEN6C VECTOR.....	56
TABLE 21: REACTION MIX FOR LIGATION.....	57
TABLE 22: PROTEIN SEQUENCES AND CDR3 ALLOCATION OF CD2- AND CD7-SDAB.....	64

## 7.3 Abbreviations

%ID	Percent injected dose
%ID/g	Percent injected dose per gram
<sup>18</sup> F	Fluorine-18
<sup>18</sup> F-FDG	Fluor-18-Fluorodesoxyglucose
<sup>64</sup> Cu	Copper-64
<sup>68</sup> Ga	Gallium-68
7-AAD	7-aminoactinomycine-D
<sup>89</sup> Zr	Zirconium-89
ADC	Antibody-drug conjugate
ADCC	Antibody-dependent cellular cytotoxicity
ADCP	Antibody-dependent cellular phagocytosis
ALL	Acute lymphoblastic leukemia
APC	Antigen-presenting cell
B-ALL	B-cell acute lymphoblastic leukemia
BCMA	B-cell maturation antigen
CAR	Chimeric antigen receptor
cDb	Cys-diabodies
CDC	Complement-dependent cytotoxicity
CDR3	Complementarity determination region-3
CEACAM1	Carcinoembryonic antigen-related cell adhesion molecule 1
cHL	Classic Hodgkin Lymphoma
CLL	Chronic lymphocytic leukemia
crRNA	Crispr RNA
CT	Computed tomography
CTL	Cytotoxic T cell
CTLA-4	Cytotoxic T-lymphocyte antigen number 4

DC	Dendritic cell
DCR	Disease control rate
DNA	Deoxyribonucleic acid
dsRed	Discosoma sp. red fluorescent protein
EPR	Enhanced permeability and retention
FDA	US Food and Drug Administration
GAL-9	Galectin-9
GFP	Green fluorescent protein
GLUT	Glucose transporters
GM-CSF	Granulocyte-macrophage colony-stimulating factor
gp100	Glycoprotein 100
gRNA	Guide RNA
HER2	Human epidermal growth factor receptor 2
HPLC	High-performance liquid chromatography
HSV1-tk	Herpes simplex virus type-1 thymidine kinase
i.t.	Intratumoral
i.v.	Intravenous
ICB	Immune checkpoint blockade
ICI	Immune checkpoint inhibitor
IgG	Immunoglobuline G
IL	Interleukin
IMAC	Immobilized metal affinity chromatography
ImmTAC	Immune-mobilizing monoclonal TCRs against cancer
ImmunoPET	Immuno-positron emission tomography
IPTG	Isopropyl- $\beta$ -D-thiogalactopyranosid
iRFP	Near-infrared fluorescent protein
kDa	Kilodalton

LAG3	Lymphocyte activation gene 3
LFA3	Lymphocyte-associated antigen 3
mAb	Monoclonal antibody
MFI	Mean fluorescence intensity
MHC	Major histocompatibility complex
MPO	Myeloperoxidase
MRI	Magnetic resonance imaging
MS	Mass spectrometry
mTNBC	Metastatic triple-negative breast cancer
NGS	Next-generation sequencing
NHEJ	Non-homologous end joining
NSCLC	Non-small cell lung cancer
NSG	NOD scid gamma
ORR	Overall response rate
OS	Overall survival
p.i.	Post injection
PAP	Prostatic acid phosphatase
PCR	Polymerase chain reaction
PD-1	Programmed cell death 1 protein
PD-L1	Programmed cell death 1 protein ligand
PET	Positron emission tomography
PFS	Progression-free survival
PR	Partial response
PSMA	Human prostate specific membrane antigen
RNA	Ribonucleic acid
RNP	Ribonucleoproteins
ROI	Region of interest

scFv	Single-chain variable fragment
sdab	Single-domain antibody
SG	Sacituzumab govitecan
SLAMF7	SLAM family member 7
SSTR2	Somatostatin receptor subtype 2
SUV	Standardized uptake value
$t_{1/2}$	Half-life
TAA	Tumor-associated antigen
TCR	T-cell receptor
TIM-3	T cell immunoglobulin 3
TME	Tumor microenvironment
tracrRNA	Trans-activating crRNA
TSA	Tumor-specific antigens
VH3	Type 3 VH domain
YCWP	Yeast cell wall particles
$\gamma\delta$ T cells	Gamma delta T cells

## 8 Danksagung

In erster Linie gilt mein herzlicher Dank Prof. Dr. Angela Krackhardt für die Möglichkeit, an diesem spannenden Thema zu arbeiten, für ihre kreative und hilfsbereite Betreuung und für die hervorragende Unterstützung während der gesamten Zeit meiner Arbeit. Ihre Begeisterung für die Forschung und das Thema meiner Dissertation haben mich zu jeder Zeit inspiriert.

Weiterhin möchte ich mich bei PD Dr. Calogero D`Alessandria, Prof. Dr. Wolfgang Weber, Prof Dr. Florian Bassermann, Prof Dr. Hans-Jürgen Wester und Prof. Dr. Robert Oostendorp für die exzellente wissenschaftliche Betreuung bedanken, ohne die das Projekt nicht möglich gewesen wäre.

Ein großer Dank gilt allen Mitgliedern der AG Krackhardt, die meine Promotionszeit durch ihre Begeisterung an der Forschung und viel Positivität erst zu dem gemacht haben was sie war. Besonders möchte ich mich bei Theresa, Philipp, Gaia und Lisa bedanken, nicht nur für die Zeit im Labor, sondern vor allem für die Freundschaften die außerhalb davon entstanden sind.

Des Weiteren möchte ich meinem ganzen Freundeskreis, der mich während der Promotion immer unterstützt hat, großen Dank aussprechen.

Mein innigster Dank gilt meinen Eltern, Lorena, John, Karla und Doro. Für eure uneingeschränkte Unterstützung und eure liebevolle Art, die mich immer motiviert und aufgemuntert haben, danke ich euch von ganzem Herzen.